Condition Assessment of In-Service Pendulum Tuned Mass Dampers

by

Aaron J. Roffel

A thesis
presented to the University of Waterloo
in fulfillment of the
thesis requirement for the degree of
Doctor of Philosophy
in
Civil Engineering

Waterloo, Ontario, Canada, 2012

I hereby declare that I am the sole author of this thesis. This is a true copy of the thesis, including any required final revisions, as accepted by my examiners.

I understand that my thesis may be made electronically available to the public.

Abstract

Tuned mass dampers (TMDs) are auxiliary damping devices installed within tall structures to reduce undesirable wind-induced vibrations and to enhance the overall system damping and hence, the dissipative capacity. The design of TMDs involves the selection of optimal auxiliary mass, frequency, and damping, based on the main structure's mass, natural frequency and damping properties. TMDs are inherently susceptible to detuning, where the auxiliary parameters are no longer optimal due to deterioration or changes within the system, resulting in a degradation in their performance. In order to correct for this detuning, it is necessary to perform a condition assessment while the TMDs are in service. The main goal of this thesis is to present a methodology to conduct condition assessment while the TMDs are in service. The proposed methodology does not involve either restraining the TMD or providing controlled external excitation to the structure, and relies on ambient measurements only. The first phase in the condition assessment is to estimate the bare structure's modal properties using acceleration measurements obtained from the structure while the TMDs are unrestrained. The present work accomplishes this goal within the framework of parametric identification using Kalman filtering, where the unknown parameters (bare modal properties) are appended to the state vector and estimated. Unlike most of the literature on this subject, the noise statistics for the filter are not assumed to be known *a priori*. They are estimated from the measurements and incorporated into the filter equations. This filter involves direct feedthrough of the process noise in the measurement equation and the appropriate filter is derived and used following the noise covariance estimation step. In the next phase, criteria to assess the condition of the TMD are developed. They include optimal tuning parameters established using simulated experiments and measured equivalent viscous damping. The research considered pendulum tuned mass dampers (PTMDs), which presently account for a large fraction of full-scale applications. Results were demonstrated using numerical investigations, a bench-scale model equipped with an adaptive mechanism for adjusting auxiliary damper parameters, and a full-scale PTMD-equipped structure. The main contributions of this thesis are: (a) a broader understanding of the coupled biaxial behaviour of PTMDs has been developed; (b) a systematic procedure for estimating the underlying modal characteristics of the structure

from ambient vibration measurements within the framework of Kalman filtering has been achieved; (c) a comprehensive framework to undertake condition assessment of TMDs has been presented, integrating parametric identification from measured response data and performance prediction for design period wind events using boundary layer wind tunnel studies. The work provided new insight into the design and behaviour of PTMDs and presented a comprehensive approach to quantify their performance. The Kalman filtering framework also provides an efficient platform to build adaptive passive tuned mass dampers (APTMDs) that can be tuned in place and adjusted to correct for detuning and accommodate various operating conditions.

Acknowledgements

I am grateful to Dr. Sriram Narasimhan for his encouragement, guidance, and insight throughout the development of this research and the expertise he has shared with me on this subject.

I would like to sincerely thank my co-supervisor Dr. Mahesh Pandey, and the committee members, Dr. Ahsan Kareem, Dr. Serhiy Yarusevych, Dr. Scott Walbridge, and Dr. Giovanni Cascante.

I would also like to recognize the assistance of various members of the Structural Dynamics, Control, and Identification research group; Mr. Paul Paquet, for his assistance in instrumenting the full-scale structure and assessing various reduced-order modelling techniques; Mr. Richard Lourenco, for developing an impressive laboratory model with an adaptive tuning mechanism; Dr. Budhaditya Hazra and Mr. Ayan Sadhu for their collaboration on analyzing the output data from the full-scale measurement program and laboratory model and providing results for comparison; and Mr. Chad Van der Woude, for his assistance in full-scale data collection and assistance with generating synthetic wind time histories.

I would like to recognize the Greater Toronto Airport Authority (GTAA) for partnering to collect full-scale field data from a structure equipped with a pendulum tuned mass damper and Rowan Williams Davies and Irwin Inc. (RWDI) for providing wind tunnel data to be used in my analysis. Several insightful observations with Trevor Haskett, Scott Gamble, and Greg Thompson are gratefully acknowledged. This work was made possible by the facilities of the Shared Hierarchical Academic Research Computing Network (SHARCNET) and Compute/Calcul Canada [5].

I owe my deepest gratitude to my wife, Ashley, and our dear children, Ashton and Anna. Their love, support, and encouragement have been my primary motivation.

Dedication

To Ashley, Ashton and Anna.

Table of Contents

List of Tables

List of Figures

Nomenclature

$\mathbf{0}$ matrix with all elements equal to zero

$\mathbf{A}_c$ continuous time $\tilde{n}\times\tilde{n}$ state matrix

$\mathbf{A}_k$ discrete time $\tilde{n}\times\tilde{n}$ state matrix for the k^{th} time step

$\bar{\mathbf{A}}_{k-1}$ Jacobian matrix of partial derivatives of the non-linear transition equation, $f(\mathbf{x}, \mathbf{0})$, with respect to $\mathbf{x}$, evaluated at the previous *a posteriori* state estimate, $\hat{\mathbf{x}}_{k-1|k-1}$

$\mathbf{B}_c$ continuous time $\tilde{n}\times s$ input matrix corresponding to the control force, $\mathbf{u}(t)$

$\mathbf{C}$ damping matrix for a multi-degree-of-freedom (MDOF) system (N s/m)

c main structure damping coefficient (N s/m)

c_a auxiliary damping coefficient (N s/m)

c_α velocity-squared proportional auxiliary damping coefficient (N s^2/m^2)

c_{eq} equivalent linear auxiliary damping coefficient (N s/m)

c_x auxiliary damping coefficient in the x-direction (N s/m)

c_y auxiliary damping coefficient in the y-direction (N s/m)

$\hat{\mathbf{C}}$ diagonal classical modal damping matrix

$\mathbf{C}_c$ continuous time $p \times \tilde{n}$ output matrix

C_j modal or generalized damping for the j^{th} mode

$\mathbf{C}_k$ discrete time $\tilde{n} \times \tilde{n}$ state matrix for the k^{th} time step

$\bar{\mathbf{C}}_k$ Jacobian matrix of partial derivatives of the non-linear measurement equation, $h(\mathbf{x}, \mathbf{0})$, with respect to $\mathbf{x}$, evaluated at the current *a priori* state estimate, $\hat{\mathbf{x}}_{k|k-1}$

$\bar{\mathbf{C}}_{k-1}$ Jacobian matrix of partial derivatives of the non-linear measurement equation, $h(\mathbf{x}, \mathbf{0})$, with respect to $\mathbf{x}$, evaluated at the previous *a priori* state estimate, $\hat{\mathbf{x}}_{k-1|k-2}$

$C_{r,j}$ modal damping for the j^{th} mode

$\hat{c}_v$ coefficient of variation, ratio of the standard deviation to the the mean (%)

$\mathbf{D}_c$ continuous time $p \times s$ direct feedthrough matrix corresponding to the control force, $\mathbf{u}(t)$

$\mathbf{D}_k$ discrete time $p \times r$ direct feedthrough matrix corresponding to the known deterministic external disturbance vector $\mathbf{u}_k$ for the k^{th} time step

$\mathbf{d}_k$ discrete time $q \times 1$ zero mean unknown stochastic external disturbance vector with covariance $\mathbf{S}_k$ for the k^{th} time step

$\mathbf{E}_c$ continuous time $\tilde{n} \times m$ input matrix corresponding to the unknown stochastic external disturbance force, $\mathbf{w}(t)$

$\mathbf{E}_k$ discrete time $\tilde{n} \times q$ input matrix corresponding to a unknown stochastic external disturbance vector $\mathbf{d}_k$ for the k^{th} time step

$\bar{\mathbf{E}}_{k-1}$ Jacobian matrix of partial derivatives of $f(\mathbf{x}, \mathbf{d})$ with respect to $\mathbf{d}$ evaluated at the previous *a posterior* state estimate, $\hat{\mathbf{x}}_{k-1|k-1}$

$\mathbf{F}_c$ continuous time $p \times q$ direct feedthrough matrix corresponding to the unknown stochastic external disturbance force, $\mathbf{w}(t)$

$\mathbf{F}_k$ discrete time $p \times q$ direct feedthrough matrix corresponding to the unknown stochastic external disturbance vector $\mathbf{d}_k$ for the k^{th} time step

$\bar{\mathbf{F}}_k$ Jacobian matrix of partial derivatives of the non-linear measurement equation, $h(\mathbf{x}, \mathbf{d})$, with respect to $\mathbf{d}$, evaluated at the current *a priori* state estimate, $\hat{\mathbf{x}}_{k|k-1}$

$\bar{\mathbf{F}}_{k-1}$ Jacobian matrix of partial derivatives of the non-linear measurement equation, $h(\mathbf{x}, \mathbf{d})$, with respect to $\mathbf{d}$, evaluated at the previous *a priori* state estimate, $\hat{\mathbf{x}}_{k-1|k-2}$

$f_{n,j}$ main structure natural frequency for the j^{th} mode (Hz)

$\hat{f}_{n,j}$ estimate of the main structure natural frequency for the j^{th} mode (Hz)

$F_{r,j}(t)$ modal applied force for the j^{th} mode

f_r auxiliary system to main structure ratio of natural frequencies

$f_{r,opt}$ optimal auxiliary system to main structure ratio of natural frequencies

g acceleration due to gravity, equal to $g = 9.807$ m/s^2 at the earth's surface

$\mathbf{G}_c$ continuous time $\tilde{n} \times r$ input matrix corresponding to the input force, $\mathbf{u}(t)$

$\mathbf{G}_k$ discrete time $\tilde{n} \times r$ input matrix corresponding to a known deterministic external disturbance vector $\mathbf{u}_k$ for the k^{th} time step

h distance from the suspension point to the connection point of the auxiliary spring and viscous damper along the suspended length (m)

h_n overall height of the structure (m)

h_x distance from the suspension point to the connection point of the x-direction auxiliary spring and viscous damper along the suspended length (m)

h_y distance from the suspension point to the connection point of the y-direction auxiliary spring and viscous damper along the suspended length (m)

$\mathbf{I}$ identity matrix

I_a moment of inertia of the auxiliary mass about the suspension point (kg m^2)

$\mathbf{J}_k$ One-step predictor gain matrix selected to eliminate the correlation between the transition and measurement equation for the k^{th} time step

$\mathbf{K}$ stiffness matrix for a MDOF system (N/m)

k main structure stiffness (N/m); or, integer discrete time index

k_a auxiliary stiffness (N/m)

k_x auxiliary stiffness in the x-direction (N/m)

k_y auxiliary stiffness in the y-direction (N/m)

K_j modal or generalized stiffness for the j^{th} mode

$\mathbf{K}_k$ Kalman gain matrix for the k^{th} time step

$K_{r,j}$ modal stiffness for the j^{th} mode

L pendulum length, measured from the suspension point to the centre of mass for a point mass (m)

$\mathbf{M}$ mass matrix for a MDOF system (kg)

m main mass (kg)

m_a auxiliary mass (kg)

$\mathbf{M}_r$ diagonal modal mass matrix

M_{xx} high frequency base balance (HFBB) measured base moment about the x-axis (N m)

M_{yy} HFBB measured base moment about the z-axis (N m)

M_{zz} HFBB measured base moment about the z-axis (N m)

$M_{r,j}$ modal mass for the j^{th} mode to be controlled; the modal matrix is normalized such that the mode shape coordinate at the degree-of-freedom (DOF) where the tuned mass damper (TMD) is located is unity

n number of DOFs

$\hat{N}$ number of components of the unknown noise covariance estimation parameter, α to be estimated

$\bar{n}$ number of measured or retained DOFs in the reduced order model of the main system

$\hat{n}$ number of retained modes of vibration in the reduced order model of the main structure

$\tilde{n}$ number of states in the state space model

p number of outputs in the state space model

$\mathbf{P}_{k|k}$ *a posteriori* state estimate error covariance matrix

$\mathbf{P}_0$ initial state estimate error covariance matrix

$\mathbf{P}_{k|k-1}$ *a priori* state estimate error covariance matrix

$\mathbf{P}(t)$ arbitrary main mass time-varying force vector (N)

q number of unknown stochastic inputs in the state space model

$\mathbf{Q}_k$ discrete time $\tilde{n}\times\tilde{n}$ process noise covariance matrix for the k^{th} time step

Q_r generalized force

q_r generalized coordinate or displacement

$\dot{q}_r$ generalized velocity

r number of known deterministic inputs in the state space model

$\mathbf{R}_k$ discrete time $p \times p$ measurement noise covariance matrix for the k^{th} time step

s number of control forces in the state space model

$S_{wj}(\omega)$ power spectral density of the generalized wind forces

$\mathbf{S}_k$ discrete time $q \times q$ unknown stochastic disturbance noise covariance matrix for the k^{th} time step

T discrete time sampling rate (s)

t continuous time (s)

$\mathbf{u}(t)$ continuous time $s \times 1$ control force vector; or continuous time $r \times 1$ known input force vector

$\ddot{\mathbf{u}}_r(t)$ acceleration response for the retained DOFs of the MDOF main structure

$\ddot{\mathbf{u}}_t(t)$ acceleration response for the truncated DOFs of the MDOF main structure

$\dot{\mathbf{u}}_r(t)$ velocity response for the retained DOFs of the MDOF main structure

$\dot{\mathbf{u}}_t(t)$ velocity response for the truncated DOFs of the MDOF main structure

$u_j(t)$ continuous time control force in the modal domain

$\mathbf{u}_k$ discrete time $r \times 1$ known deterministic external disturbance vector for the k^{th} time step

$\mathbf{u}_r(t)$ displacement response for the retained DOFs of the MDOF main structure

$\mathbf{u}_t(t)$ displacement response for the truncated DOFs of the MDOF main structure

$\mathbf{v}_k$ discrete time $p \times 1$ zero mean measurement noise vector with covariance $\mathbf{R}_k$ for the k^{th} time step

$\mathbf{w}(t)$ continuous time $q\times 1$ unknown external disturbance vector

$w_j(t)$ generalized wind force for the j^{th} mode

$\mathbf{w}_k$ discrete time $\tilde{n}\times 1$ zero mean process or disturbance noise vector with covariance $\mathbf{Q}_k$ for the k^{th} time step

$\mathbf{x}(t)$ continuous time $\tilde{n}\times 1$ state vector

$\mathbf{x}_k$ discrete time $\tilde{n}\times 1$ state vector for the k^{th} time step

$\hat{\mathbf{x}}_{k|k}$ *a posteriori* estimate of $\mathbf{x}_k$; that is, estimate of $\mathbf{x}_k$ when all the measurements up to and including k are available

$\hat{\mathbf{x}}_{k|k-1}$ *a priori* estimate of $\mathbf{x}_k$; that is, estimate of $\mathbf{x}_k$ when all the measurements before (but not including) time k are available

$\ddot{\mathbf{y}}(t)$ modal acceleration response vector

$\dot{\mathbf{y}}(t)$ modal velocity response vector

$\mathbf{y}(t)$ modal displacement response vector

$\mathbf{y}_r(t)$ modal displacement response for the retained modes of the MDOF main structure

$\mathbf{y}_t(t)$ modal displacement response for the truncated modes of the MDOF main structure

$\mathbf{z}(t)$ continuous time $p\times 1$ measurement vector

$\mathbf{z}_k$ discrete time $p\times 1$ measurement vector for the k^{th} time step

α $1\times\hat{N}$ noise covariance parameter to be estimated from the residual sequence

$\delta_{k,j}$ Kronecker delta function; $\delta_{k,j}=1$ when $k=j$ and 0 otherwise

$\epsilon_{k|k}$ *a posteriori* state estimate error

$\epsilon_{k|k-1}$ *a priori* state estimate error

$\mathbf{\Gamma}$ influence vector, assigning the base-excited force to the DOFs of the structure or assigning the TMD control force the DOF to which the TMD is coupled

$\mathbf{\Lambda}$ spectral matrix

μ ratio of the auxiliary mass m_a to the main mass m of the structure for a single-degree-of-freedom (SDOF) system or ratio of the auxiliary mass m_a to the modal mass $M_{r,j}$ for the mode of vibration to be controlled for a MDOF system

ν_k discrete time $p\times 1$ measurement residual or innovation for the k^{th} time step

ω forcing frequency (rad/s)

ω_n bare main structure circular natural frequency (rad/s)

ω_a auxiliary system circular natural frequency (rad/s)

$\omega_{n,j}$ main structure circular natural frequency for the j^{th} mode (rad/s)

$\hat{\omega}_{n,j}$ estimate of the main structure circular natural frequency for the j^{th} mode (rad/s)

$\mathbf{\Phi}$ modal matrix

$\varphi(t)$ spherical angle (angle of rotation about the vertical) of the auxiliary mass

ϕ_{ij} mode shape coefficient of the modal matrix, $\mathbf{\Phi}$, at the i^{th} DOF for the j^{th} mode of vibration

$\hat{\phi}_{ij}$ estimate of the mode shape coefficient at the i^{th} DOF for the j^{th} mode of vibration

$\mathbf{\Phi}_{rr}$ reduced order modal matrix corresponding to the retained DOFs and retained modes

$\mathbf{\Phi}_{rr}^{+}$ Moore-Penrose generalized inverse or pseudoinverse of the reduced order modal matrix, $\mathbf{\Phi}_{rr}$, given by $\left(\mathbf{\Phi}_{rr}^T\mathbf{\Phi}_{rr}\right)^{-1}\mathbf{\Phi}_{rr}^T$

$\mathbf{\Phi}_{rt}$ reduced order modal matrix corresponding to the retained DOFs and truncated modes

$\mathbf{\Phi}_{tr}$ reduced order modal matrix corresponding to the truncated DOFs and retained modes

$\mathbf{\Phi}_{tt}$ reduced order modal matrix corresponding to the truncated DOFs and truncated modes

ϕ forcing frequency ratio

$\theta(t)$ planar angle (angle of swing away from the vertical) of the auxiliary mass

ζ main structure damping ratio

ζ_a auxiliary system damping ratio

$\zeta_{a,opt}$ optimal auxiliary system damping ratio

ζ_e effective damping introduced by a TMD

ζ_j main structure modal damping ratio for the j^{th} mode

$\hat{\zeta}_j$ estimate of the main structure modal damping ratio for the j^{th} mode

Acronyms

APTMD adaptive passive tuned mass damper

ATMD active tuned mass damper

BSS Blind Source Separation

COV coefficient of variation

DOF degree-of-freedom

EKF extended Kalman filter

HFBB high frequency base balance

IRS Improved Reduction System

MDOF multi-degree-of-freedom

MTMD multiple tuned mass damper

PTMD pendulum tuned mass damper

RMS root mean squared

SDOF single-degree-of-freedom

SEREP System Equivalent Reduction Expansion Process

SNR signal-to-noise ratio

STMD semi-active tuned mass damper

TMD tuned mass damper

UKF unscented Kalman filter

Chapter 1

Introduction

Wind-induced vibrations impose large demands on structural components and connections for tall structures. Taller, lighter, and more slender modern construction is a consequence of the advances in structural materials, design efficiencies and technologies. Tall structures are susceptible to vibrations due to their flexibility, lack of sufficient inherent structural damping, and the larger wind loads these structures are subjected to due to their height. These demands in many cases lead to considerable discomfort to the occupants, particularly at upper floors.

Since the designer has little control over the wind loads, aside from optimization the shape of the structure, the available options to minimize the vibrations include reducing the building's flexibility or enhancing the vibrational dissipation capacity through increased damping. The flexibility of a structure can be reduced by increasing its stiffness, using larger or a greater number of structural components, resulting in structures with increased weight. Heavier structures consume more materials, require increased construction effort and time, necessitate larger foundations, and are generally more costly.

Methods to increase damping in structures are an active area of research. The basic concept of damping is to dissipate vibrational energy through heat, thus reducing the impact of the imposed forces on the structure. One method of mitigating the effects of wind-induced vibrations is through the use of auxiliary damping devices, known as tuned

mass dampers (TMDs). A TMD consists of a relatively small mass, spring, and viscous damper, or a pendulum mass and viscous damper, attached to the main structure. The schematic geometry of a TMD is shown in Fig. 1.1a. An alternative to the conventional translational mass is a cable supported mass (Fig. 1.1b), where the suspended length determines the auxiliary operating frequency; this is known as a pendulum tuned mass damper (PTMD). When properly designed, that is, when the auxiliary parameters are properly selected, the TMD is effective in reducing the structural response and enhancing the intrinsic damping of the system.

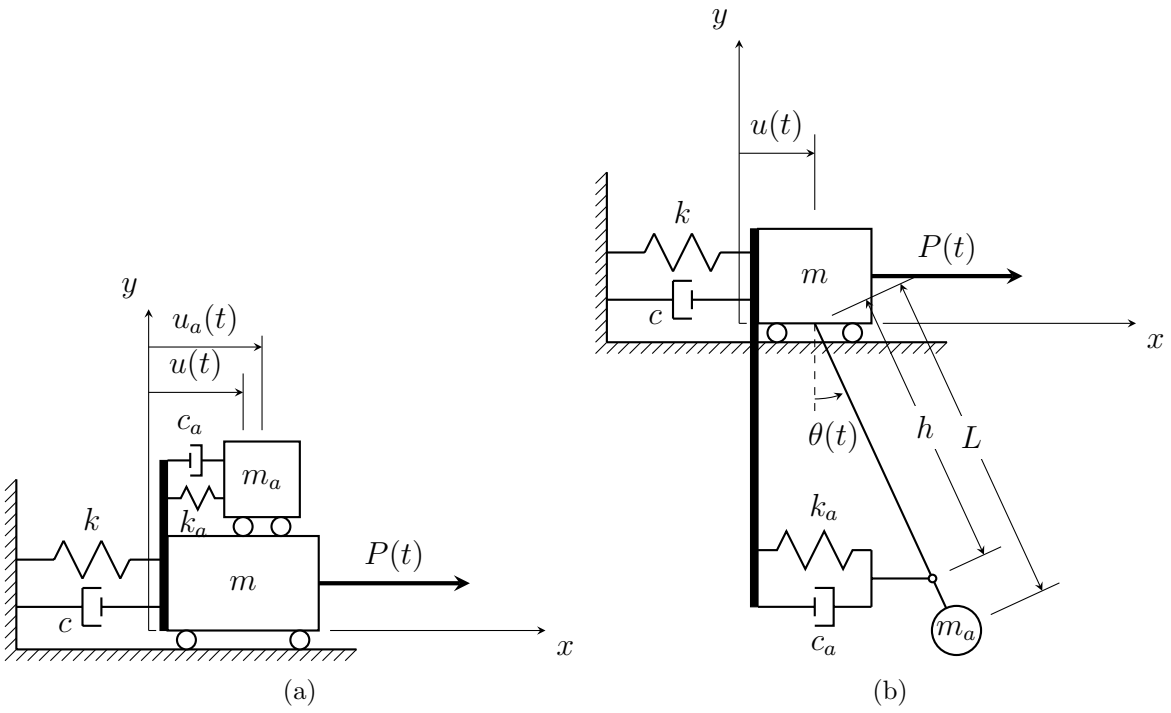

Figure 1.1: Schematic geometry of a (a) translational- and (b) pendulum-type TMD

The main parameters of a typical TMD at the discretion of the designer are: (i) the mass, (ii) frequency, and (iii) damping. The mass is selected based on the main structure's mass, generally between a ratio of 0.1% and 5%. The selection of the TMD's frequency and damping parameters are based on the main structure's natural frequencies. The optimal

values of the parameters are typically obtained using a combination of numerical simulations and wind tunnel experiments. Analytical expressions are possible for simplified cases. When the actual versus optimal values drift apart, the TMD is said to be detuned. Detuning can result from a variety of different factors, but primarily due to changes in the operating environment such as structural deterioration or damage, inadvertent or intentional structural changes, varying mass, or differing loading events. Other causes of detuning include forecasting, where the designers tune the TMD to an estimated future structural condition for the dominant frequency [42], or for a particular design event.

There are several configurations of TMDs based on a particular application. However, they are also common in the sense that the three design parameters are of concern in all of them. PTMDs are perhaps the most simple and commonly employed TMDs today and also constitute the focus of this thesis. The three-dimensional behaviour of PTMDs and their optimal design are studied in this research. Novel methods to identify when detuning has occurred in a structure are developed, along with a framework to perform the condition assessment while they are in service with little or no disruption to their operations. The methodology can be directly extended to semi-active tuned mass dampers (STMDs) or adaptive passive tuned mass dampers (APTMDs) with little or no modification to the algorithms.

1.1 Damping in structures

Damping is a measure of energy dissipation in a vibrating system. In the context of structural dynamics, kinetic energy is converted into another form of energy that can be removed from the system. Generally, the energy is converted into heat, though the form to which the energy is converted is dependant on the damping mechanism. Unlike stiffness and mass, inherent damping in structures is difficult to quantify precisely, as it does not relate to a single physical phenomenon. Damping in structures is a result of primarily three different mechanisms: material damping, interfacial damping, and aerodynamic damping [50].

Material damping results from complex interactions within the material at the microscopic scale. Material damping differs between materials, but also between samples of the same materials. It also varies with stress states of the structural element. Interfacial damping is Coulomb friction damping between structural members and their connections, as well as between structural components such as façades, exterior cladding, and partition walls. For example, bolted connections have a larger contribution to interfacial damping than their welded counterparts [50]. Structure-soil interactions are also a source of interfacial damping. Aerodynamic damping is the effective damping experienced by a structure as it is being buffeted by wind, introducing a restoring force that opposes the wind response, and has a relatively low contribution to the overall inherent damping of a structure [50].

In design, structural damping is estimated based on data available from other structures of similar size, material, and a comparable structural system. However, these estimates are difficult to predict closer than accuracies of $\pm 30\%$ [51]. It is difficult to engineer additional inherent damping in a structure; however, a known level of damping can be added to a structure through auxiliary damping devices such as TMDs, thus providing a more predictable, adaptable, and reliable method of damping [51].

1.2 Tuned mass dampers

The precursor to the TMD was the dynamic vibration absorber, first proposed in 1883 by Watts [98], and further described in a patent submitted by Frahm in 1909 [22]. It was in 1928 when Ormondroyd and den Hartog [72] first presented the theory of the dynamic vibration absorber.

A TMD typically consists of an inertial mass—relatively small when compared to the mass of the structure—attached to the structure near the location where the responses are largest, generally at the top. The mass exerts an inertial force on the main system to reduce its motion, through a stiffness and damping mechanism. For typical translational TMDs, auxiliary stiffness is provided through springs, and damping using viscous or viscoelastic dampers. The performance of the TMD is related to its dynamic characteristics, that is,

the auxiliary stiffness and damping, ratio of the auxiliary mass to main mass, and the stroke of the mass [51]. The TMD's damping effect is based on the premise that the TMD's response is out of phase with the structure's response. Thus, in order to develop good performance of the TMDs, the stiffness parameter must be selected such that the absorber's natural frequency is tuned to a ratio of the main structure's mode of vibration that is to be controlled; the auxiliary damping device will operate at nearly the same frequency of the structure but with a phase shift. This ratio is known as the frequency ratio, and is generally related to the mass ratio (ratio of the auxiliary to main mass), and the type of excitation. A schematic of a single-degree-of-freedom (SDOF) main structure equipped with a typical translational TMD is shown in Fig. 1.1a. The performance of TMDs can be expressed as the reduction in acceleration or dynamic deflection of the main system at a particular location on the structure, or equivalently, the amount of additional damping the TMD provides to the structure (as a ratio of the critical damping of the structure). Typically this is in the range of 0.5-2.5% [80].

One of the earliest applications of the TMD for the mitigation of vibrations in tall buildings can be found in the John Hancock Tower, a 60 storey, 241 m tall building in Boston. Occupants of the upper floors were complaining of motion sickness, caused by wind-induced torsional motion in the structure. To mitigate the effects, two 272 tonne lead masses were installed at each end of the 58^{th} floor, attached to the structure using shock absorbers. The masses slide on oil-lubricated steel plates for motions exceeding 3 milli-g ($g = 9.807$ m/s^2 is the acceleration due to gravity at the earth's surface) [51]. A second early application was a TMD design as part of the original structural design for the Citigroup Center (formerly Citicorp Building), a 59 storey, 278 m tall building in New York City. A 372 tonne concrete TMD was installed with spring and damping mechanisms in both directions. It is activated by a computer, hydraulically raising the mass after the 3 milli-g threshold motion in the main structure is exceeded. The system reduced the overall response of the structure by up to 40% [101], as evidenced by several events since its installation.

1.3 Pendulum tuned mass dampers

Perhaps the most simple TMD configuration is a suspended mass. When augmented with viscous damping elements, they provide an effective means of suppressing structural vibrations. Such TMDs are called pendulum-type TMDs, or PTMDs. The typical schematic geometry is shown in Fig. 1.1b. PTMDs are generally suggested for tall structures with large masses and low natural frequencies [80]. The frequency of the PTMD can be adjusted in the field by changing the pendulum suspended length. This is accomplished by changing the pivot point of the suspended mass using a sliding clamp [55] or by changing the height along the auxiliary mass where the cable connects. Fine frequency tuning can also be performed by augmenting the mass with springs that can be adjusted along the suspended length [26].

The Chifley Tower in Sydney is a 52 storey, 209 m tall office building constructed in 1992 and equipped with a 400 tonne PTMD, complete with a tuning frame hanging below the upper suspension point of the mass. The tuning frame allows the pivot to be moved along the length of the cable, thereby changing the effective pendulum length. The natural frequency of the structure was determined through forced vibration tests, in which the tower was excited by driving the damper mass using actuators. The structure was found to have varying natural frequencies depending on the amplitude of the forced vibration; therefore, the PTMD was tuned to the most frequently occurring mode of vibration. The structural damping was increased from 1% to 2-4% depending on the level of vibration [55]. Park Tower in Chicago is another example of a PTMD system where an upper tuning frame was incorporated. The damper consists of a 272 tonne mass with pendulum length up to 7.46 m (34.5 ft). The auxiliary system uses non-linear viscous dampers, where the damping force is proportional to the velocity squared. The damper constants are also adjustable and rotation about the vertical axis is prevented by an anti-yaw device [42]. The measured frequencies of the structure at the time of commissioning the PTMD were in error by 10-20% [42], demonstrating the necessity of adjustable systems.

The most eminent PTMD installation is on the 509 m tall, 101 storey Taipei 101 in Taipei, Taiwan. A 660 tonne pendulum mass, currently the largest installation, is

suspended from the 91st floor and occupies five storeys. During the strongest expected wind for a six month return period, the PTMD reduces the acceleration response from 7.9 to 5.0 milli-g [29]. The PTMD was integrated as an architectural feature of the structure, as seen in Fig. 1.2.

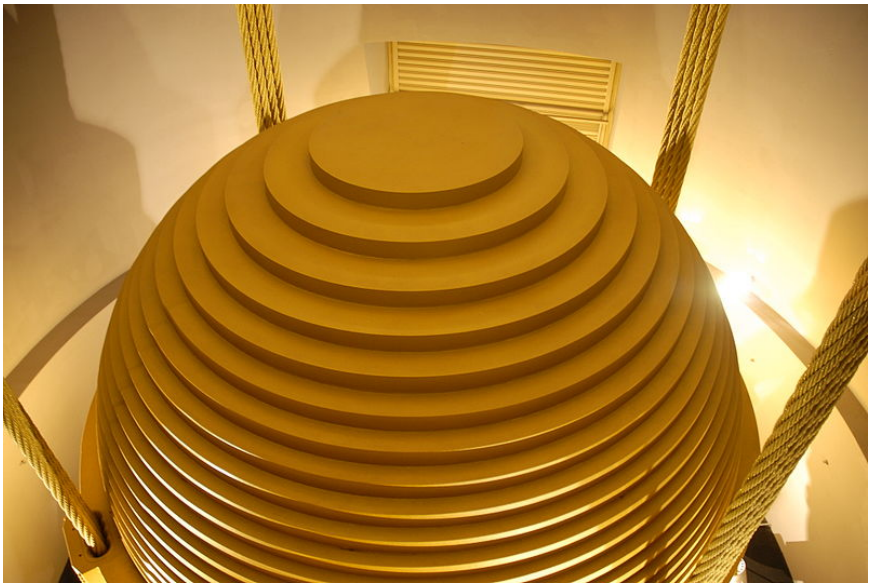

Figure 1.2: A 660 tonne PTMD installed in Taipei 101 as an architectural feature (Courtesy Guillaume Paumier / Wikimedia Commons, CC-by-sa-3.0)

The Apron Control Tower at Toronto's Pearson International Airport in Mississauga, Ontario, Canada is a 68.5 m tall structure equipped with a pair of PTMDs to attenuate undesirable wind-induced vibrations, primarily because the structure is susceptible to vortex induced vibrations in the across-wind direction due to its circular shape. This structure is used in the current research as the testbed for condition assessment of in-service PTMDs. The combined mass of the PTMDs is $50,000$ kg, representing a high mass ratio in comparison to other applications of TMDs in flexible structures [79]. The CN Tower, a signature structure in Toronto, Ontario, Canada, is a 553 m tall tower equipped with two PTMDs to attenuate the antenna responses. The effectiveness of the PTMDs has been found to be quite poor due to the issue of detuning [43], which provides one of the motivations for the present work.

1.4 Motivation

The issue of detuning, where the auxiliary system parameters (frequency and damping) move away from their optimal values, is the motivation for condition assessment of TMDs. Causes of detuning include structural deterioration or damage, changes to the structure's use or occupancy, or inaccurate design forecasting (where a future structural condition is predicted and the TMD tuned to that condition). Detuning results in a loss of performance of the TMD. Current methodologies to overcome this issue include routine maintenance, where the motion of the TMD is arrested and the structure's modal characteristics are identified from either ambient measurements or force vibration tests. The frequency and damping are adjusted to better conform to the main structure's dynamic characteristics. This demonstrates the need for TMD systems to have adjustable mechanisms for changing their frequency and damping parameters [80]. For typical translational-type TMDs, frequency adjustment is accomplished using a variety of adjustable stiffness materials, such as adjustable stiffness springs [70]. For example, the aforementioned Citigroup Center TMD was equipped with pneumatic springs for frequency adjustment on-site [101]. Suspended mass applications usually employ a tuning frame to adjust the pendulum length, such as in the aforementioned Chifley Tower in Sydney or the Toronto Pearson International Airport Apron Tower.

Manual routine maintenance is costly, uses trained technicians, and requires arresting TMD motion, potentially sacrificing user comfort and safety. Therefore, the present work seeks to develop a systematic methodology of identifying the main structure's modal characteristics without restraining the TMD. Once the underlying structure's modal characteristics are known, the response of the structure can be simulated using an updated finite element model. Using optimal design equations or a numerical search algorithm, the optimal damper parameters can be determined and compared with the current in-service values. A comprehensive condition assessment includes benchmarking the performance of the TMD against the uncontrolled structure, using realistic wind input excitations.

The algorithms developed for the purpose of condition assessment could be directly integrated into adaptive mechanisms to adjust the damper parameters in response to their

operating environment. Therefore, an ideal identification approach would be easily adaptable to online implementation. These systems are known as STMDs or APTMDs.

1.5 Gap areas in the current understanding of PTMDs

TMDs are a relatively mature area of research; however, several important issues related to their design and performance assessment remain unaddressed, or only partially addressed, in the literature. These gap areas are first identified, followed by a brief description of the procedure undertaken in present work to address them. The following gap areas present the motivation for the current study.

- Despite many full-scale applications [35], few works have explicitly considered the design and performance of pendulum-type devices for mitigating vibrations in tall structures [79, 78, 26, 25, 29, 80]. Previous studies of PTMDs have considered linear planar pendulum models coupled with a SDOF main system described using modal coordinates to find the optimal auxiliary stiffness and damping, and to determine the main structural response [26]. Such models are adequate, for example, in analyzing the response of flexible structures where the dominant response is believed to be primarily in one direction. When the responses in both along-wind and across-wind directions are of concern, then it is important to quantify the effect of the PTMD in both directions. There is a lack of understanding of the inherent bi-axial nature of the PTMD and its effect on the design equations [26].

- Performing condition assessments for in-service TMDs has not been studied comprehensively. Specifically, algorithms to determine the bare structure's modal characteristics are scarce [59, 99]. A few studies have addressed this issue [30, 77] using *ad hoc*, experiential, or approximate methods; however, a comprehensive method is not available. These approaches require some knowledge of the degree of detuning

present in the auxiliary system and rely on relatively smooth response spectra. Alternatively, the motion of the auxiliary damping device can be arrested to prevent it from contaminating the responses, and the structure's modal characteristics can be identified by conventional approaches [78]. Harnessing the auxiliary mass causes it to be lumped with the main structure, underestimating the structure's natural frequency, particularly for high auxiliary masses. To the author's knowledge, there is no prior research where the bare structure properties have been identified using measurements obtained from a structure with an in-service TMD, using ambient vibration measurements.

- Parametric identification by Kalman filtering (and the related extended Kalman filter (EKF) and unscented Kalman filter (UKF)), has been widely applied to structural engineering applications, such as damage detection [62, 107, 106], system identification [36, 63, 53, 27, 84, 95, 109, 102], and input estimation [39]. Many of these studies involve parameter estimation in addition to state estimation [36, 63, 53, 27, 84, 62, 95, 109, 107, 106, 102]. Two issues regarding parameter identification remain unaddressed, which are critical for wind engineering applications. First, for the case where only acceleration response measurements are available–true for the majority of full-scale measurements–there is feedthrough of the external disturbance in the measurement equation. The majority of studies have assumed the availability of displacement or velocity (direct state) measurements [109, 95, 61, 36] or have considered base-excited structures [102, 60, 86] where the feedthrough term is not present. Direct feedthrough of the disturbance in the measurement equations has been considered in the context of input estimation [39, 38, 64], but these studies have focused only on that one aspect and parameter estimation has not been attempted. Second, *a priori* estimates for the process and measurement noise covariances are not available in practical situations. Most studies have overlooked this issue and have assumed arbitrary values. While possible in numerical studies, this poses a significant practical hurdle in implementing online identification and for condition assessment. Studies that have addressed input estimation have done so outside the context of parameter estimation, assuming perfect knowledge of the model and any additive process or

measurement noise covariances [39, 38, 64]. Finally, the issues of detuning, online retuning, and bare structure system identification from TMD attenuated response data using parametric identification approaches have not been reported thus far.

- The concept of effective or equivalent damping introduced by a TMD is routinely quantified in the literature [66, 55, 88, 94, 25, 26]. It refers to an equivalent level of viscous damping in a SDOF system that produces the same root mean squared (RMS) displacement response of the combined main and auxiliary system, operating at the same natural frequency as the controlled mode of vibration. Though theoretically simple to calculate, it requires precise knowledge of the main structure's natural frequency and measured displacement responses. The former is difficult to determine from TMD attenuated response measurements of full-scale structures, due to the issues discussed earlier. The latter is generally not available, as structural responses are often measured using accelerometers. Therefore, its use has been predominantly in parametric studies involving numerical models; to the knowledge of the author, quantifications from actual measurement data have not been reported.

- Finally, there lacks a comprehensive method to compare the response of a structure equipped with TMDs subjected to a variety of return period wind events to the response of the structure as if there were no TMD. Limited full-scale studies of TMDs have demonstrated that their performance can only be approximately quantified over a period of time through a number of wind events [51]. To compare to the uncontrolled structure, the TMD motion must be arrested, sacrificing occupant comfort and possibly structural safety. Even so, it isn't feasible to compare the responses to the exact same event. Therefore, numerical models are predominantly studied in the literature in order to evaluate TMD performance, excited using harmonic inputs [75], white noise [3, 28], or synthetic wind time histories [77, 105]. Alternatively, scale models of structures equipped with TMDs have been studied using a wind tunnel [88, 104]. These analyses are performed in the design stage and lack precise knowledge of the as-constructed modal characteristics. A limited number of studies considering synthetic wind excitations have shown that white noise or harmonically

excited models generally overstate TMD performance [77, 105], demonstrating a need to accurately model excitations when assessing TMD effectiveness. The author is unaware of a comprehensive study that compares the TMD-equipped structure to its uncontrolled counterpart using a numerical model based on identified modal characteristics, and excited by reliability-based excitations from a wind tunnel study.

1.6 Objectives of the proposed research

Having outlined the gap areas, the main objectives of the proposed research are summarized as follows:

- Develop a mathematical framework and conduct numerical studies to understand and quantify the three-dimensional behavior of PTMDs.
- Develop an estimation procedure to enable the extraction of bare structural modes from ambient acceleration responses attenuated by the TMD.
- Develop a comprehensive approach to perform condition assessment of in-service TMDs.

1.7 General methodology

Given a structure equipped with a TMD and assuming the ability to collect attenuated acceleration response measurements of the main and auxiliary system, the primary steps in performing a condition assessment of a TMD as undertaken in this thesis are summarized as follows:

- Develop equations of motion for the dynamic response of a multi-degree-of-freedom (MDOF) flexible structure coupled with a PTMD from the principles of analytical dynamics. Integrate the equations of motion with the finite element representation of a structure and simulate the response to harmonic and white noise excitations.

- Quantify the effect of detuning, where the auxiliary damper parameters move away from their optimal values, using a numerical model that considers the biaxial motion of the auxiliary mass. Evaluate the effect of considering the combined planar and spherical motions of the PTMD on the optimal auxiliary damper parameters through parametric studies and contrast these findings to those presented in the literature for simple linear planar PTMD models.

- Develop a model framework using standard finite element models to establish an initial estimate of the modal parameters to be identified in the identification step. Study issues related to reduced-order models and computational burden.

- Collect acceleration response measurements of the PTMDs and main structure at a sufficiently fast sampling rate. The selection of the measurement locations should be informed by any *a priori* knowledge of the mode shapes for the modes of vibration of interest.

- Establish the auxiliary damper parameters (auxiliary mass, frequency, and damping) by field measurement.

- Using the measured response data, field measurement of the auxiliary parameters, and the initial estimate of the model parameters from the finite element model, identify the underlying structure's natural frequency, modal damping ratios, and mode shape vectors. The method should not require *a priori* knowledge of the wind excitation statistics.

- Create an updated dynamic model of the system using the identified modal properties. The dynamic model of the combined main-auxiliary system can then be studied using loading information established by boundary layer wind tunnel results for various return period wind events and compared to the uncontrolled system. The performance improvement is quantified as a percent reduction in the RMS displacement or acceleration response.

- Using a numerical search of the auxiliary parameters with the updated model and realistic wind excitations, the optimal parameters can be established and compared

with measured values. Alternatively, the identified underlying structure's modal characteristics can be used in established TMD design equations and compared with the measured values; however, these are primarily based on simplifying assumptions and do not necessarily account for the uniqueness of the particular structural system or the input.

- Similar to the parametric identification step, identify the effective damping introduced by the TMD using the measured responses.

- Validate the identification algorithm through experimentation on a bench-scale laboratory model as well as using full-scale acceleration response measurement from a PTMD-equipped structure.

1.8 Organization

The thesis is organized as follows:

- **Chapter 2** presents a brief background of the historical development of TMDs, including various adaptations to improve their performance and reduce their susceptibility to detuning. The issues associated with detuning of the auxiliary system are introduced.

- Motivated by the limitations of using simplified SDOF dynamic models for PTMD parameter optimization and performance assessment, **Chapter 3** presents the formulation, using Lagrangian dynamics [68], of a system of equations for modelling the response of a flexible MDOF structure coupled with the dynamics of a PTMD. Establishing the auxiliary mass position using spherical (L, $\theta(t)$, and $\varphi(t)$) and Cartesian coordinates are both considered. The case of both nonlinear auxiliary damping and equivalent linear viscous damping are presented. The model is extended to accept high frequency base balance (HFBB) measurements from wind tunnel studies as inputs.

- Using the developed model, a parametric study is undertaken in **Chapter 4** in order to establish the optimal damper parameters. These results are compared with equations found using a simplified planar model presented in the literature. The effects of detuning and increasing the auxiliary to main mass ratio of the damping device are considered.

- **Chapter 5** introduces the concept of parametric identification using the EKF. The algorithm is presented and a simple example is first considered for the case of a known base excitation. The method is demonstrated for both known and unknown main mass excitations, the latter requiring the algorithm be adapted for the case where the process noise appears in the measurement equations when using acceleration response measurements. Finally, the case of unknown noise statistics is considered and the complete procedure is demonstrated using a numerical example.

- The EKF modal identification is then proposed in the context of estimating the bare structure's modal properties in **Chapter 6**. The concept of equivalent or effective damping introduced by a TMD is investigated. The algorithm for identifying the structure's modal properties is extended for the estimation of effective damping. This overcomes the challenges associated with quantifying the performance of in-service TMDs using this measure when only acceleration response measurements are available and the bare structure's controlled frequency is not known precisely. The algorithms are demonstrated using a numerical model of a 5-degree-of-freedom (DOF) structure.

- **Chapter 7** demonstrates the effectiveness of the identification algorithm for identifying modal properties of the bare structure from PTMD attenuated acceleration response measurements from a bench-scale laboratory model and a full-structure structure, both equipped with PTMDs with known auxiliary parameters. The condition assessment of an actual in-service PTMD is presented subsequently. A numerical search is performed using the updated model and realistic wind excitations to determine the optimal parameters. These are compared against typical design equations. The effect of using simplified models of the main-auxiliary system is considered as

well.

- Finally, a number of conclusions resulting from the present work are discussed in **Chapter 8**. Several recommendations for extending the present work are also discussed. The significant contributions resulting from this work to the study of TMDs and parametric identification are summarized.

Chapter 2

Background

A review of the background and evolution of tuned mass dampers (TMDs) is presented, including relevant research in the area of design of TMDs and pendulum tuned mass dampers (PTMDs) and previous work on adaptive mechanisms to enhance the performance of TMDs. The concepts of detuning and assessing the performance of TMDs are introduced. Finally, a brief background on full-scale studies of TMDs is presented.

2.1 Tuned mass damper theory

The basic formulation and design parameters of conventional translational-type TMDs are presented. The historical development of the TMD is introduced, with a particular emphasis on the development of optimal TMD parameters together with the various adaptations to improve performance.

The equations of motion for the single-degree-of-freedom (SDOF) system equipped with a translational-type TMD and subjected to an external force, $P(t)$ (Fig. 1.1a), are

$$m\ddot{u}(t) + c\dot{u}(t) + ku(t) + k_a\left[u(t) - u_a(t)\right] + c_a\left[\dot{u}(t) - \dot{u}_a(t)\right] = P(t) \tag{2.1a}$$

$$m_a\ddot{u}_a(t) + k_a\left[u_a(t) - u(t)\right] + c_a\left[\dot{u}_a(t) - \dot{u}(t)\right] = 0 \tag{2.1b}$$

where m, c, and k are the mass, damping coefficient, and stiffness of the main system, respectively; m_a, k_a, and c_a are the mass, damping coefficient, and stiffness of the TMD. $u(t)$ and $u_a(t)$ are the displacement responses of the main system and the TMD, respectively; $\dot{u}(t)$ and $\ddot{u}(t)$ denote the velocity and acceleration responses of the main system; $\dot{u}_a(t)$ and $\ddot{u}_a(t)$ are the velocity and acceleration responses of the TMD. The equations of motion can be cast in matrix format as

$$\begin{aligned}\begin{bmatrix} m & 0 \\ 0 & m_a \end{bmatrix} \begin{Bmatrix} \ddot{u}(t) \\ \ddot{u}_a(t) \end{Bmatrix} + \begin{bmatrix} c + c_a & -c_a \\ -c_a & c_a \end{bmatrix} \begin{Bmatrix} \dot{u}(t) \\ \dot{u}_a(t) \end{Bmatrix} \\ + \begin{bmatrix} k + k_a & -k_a \\ -k_a & k_a \end{bmatrix} \begin{Bmatrix} u(t) \\ u_a(t) \end{Bmatrix} = \begin{Bmatrix} P(t) \\ 0 \end{Bmatrix}\end{aligned} \tag{2.2}$$

Several important quantities related to the study of TMDs are introduced. The main structure's circular natural frequency, ω_n, is defined as

$$\omega_n = \sqrt{\frac{k}{m}} \tag{2.3}$$

Similarly, the auxiliary system circular natural frequency, ω_a, is given by

$$\omega_a = \sqrt{\frac{k_a}{m_a}} \tag{2.4}$$

The frequency ratio, f_r, is defined as the auxiliary natural frequency to main structure's natural frequency.

$$f_r = \frac{\omega_a}{\omega_n} \tag{2.5}$$

The mass ratio, μ, is an important design parameter for the TMD, given by

$$\mu = \frac{m_a}{m} \tag{2.6}$$

for a SDOF system or

$$\mu = \frac{m_a}{M_{r,j}} \tag{2.7}$$

for a multi-degree-of-freedom (MDOF), where $M_{r,j}$ is the modal mass for the j^{th} mode of vibration to be controlled. Finally, the damping ratio of the main mass, ζ, is

$$\zeta = \frac{c}{2\omega_n m} \tag{2.8}$$

The damping ratio of the TMD, ζ_a, is

$$\zeta_a = \frac{c_a}{2\omega_a m_a} \tag{2.9}$$

In both instances, the denominator term is known as the critical damping, corresponding to the primary and auxiliary system, respectively.

Gerges and Vickery [26] presented the equations of motion for a mixed translational primary structure and PTMD (Fig. 1.1b) under both force and base acceleration excitations. They modelled the primary structure as a SDOF system and assumed the mode shapes of the structure were not significantly impacted by the addition of the auxiliary damping device. The presentation also makes the assumption that the pendulum rotations are small. Motion was only considered in the planar pendulum direction; that is, the spherical motion was neglected. The equations of motion can be expanded to the following form for the case of main mass excitation:

$$m\ddot{u}(t) + c\dot{u}(t) + ku(t) + m_a\ddot{u}(t) + m_a L\ddot{\theta}(t) = P(t) \tag{2.10}$$

$$m_a L^2\ddot{\theta}(t) + c_a h^2\dot{\theta}(t) + \left(m_a gL + k_a h^2\right)\theta(t) + m_a L\ddot{u}(t) = 0 \tag{2.11}$$

The auxiliary circular natural frequency is given by

$$\omega_{n,a} = \sqrt{\frac{m_a gL + k_a h^2}{m_a L^2}} \tag{2.12}$$

for the case of a point mass. When there is no auxiliary spring ($k_a = 0$), this simplifies to $\omega_{n,a} = \sqrt{\frac{g}{L}}$.

2.2 Optimal design parameters

The TMD is one of the earliest devices developed to control structural vibrations [75]. They are based on a concept first proposed in 1883 by Watts [98], and subsequently in a patent filing in 1909 by Hermann Frahm [22], called a dynamic vibration absorber. Frahm's original damping device had several inherent limitations. It was only effective when the natural frequency of the absorber was very close to the excitation frequency, deteriorating rapidly when the excitation frequency moved outside this narrow band. Therefore, the dynamic vibration absorber had to be designed to attenuate a known excitation frequency.

Ormondroyd and den Hartog enhanced Frahm's absorber by incorporating auxiliary damping [72]. They showed that the performance deterioration was less severe when the excitation frequency moved away from the absorber's natural frequency. They were the first to formally present the theory of the damped vibration absorber, assuming no main mass damping in order to simplify the derivation. Using this approach, closed-form expressions for the optimal damper parameters were derived by den Hartog [18].

The optimal design parameters for a TMD consist of the optimal mass ratio, μ_{opt}, frequency ratio, $f_{r,opt}$, and auxiliary damping ratio $\zeta_{a,opt}$. Research in this area began with den Hartog's [18] optimal damper parameters for the undamped main system ($c = 0$) using harmonic main mass excitation.

$$f_{r,opt} = \frac{1}{1+\mu} \tag{2.13a}$$

$$\zeta_{a,opt} = \sqrt{\frac{3\mu}{8\,(1+\mu)}} \tag{2.13b}$$

When the structure is excited using a harmonic base excitation, the optimal parameters

are [75]

$$f_{r,opt} = \frac{1}{1+\mu}\left(\sqrt{\frac{2-\mu}{2}}\right) \tag{2.14a}$$

$$\zeta_{2,opt} = \sqrt{\frac{3\mu}{8\left(1+\mu\right)}}\left(\sqrt{\frac{2}{2-\mu}}\right) \tag{2.14b}$$

The optimal auxiliary stiffness and damping can then be calculated as

$$f_{r,opt} = \frac{\omega_{a,opt}}{\omega_n} = \frac{\sqrt{\frac{k_{a,opt}}{m_a}}}{\omega_n} \tag{2.15}$$

which can be rearranged to find

$$k_{a,opt} = f_{r,opt}^2 \omega_n^2 m_a \tag{2.16}$$

Similarly, the optimal auxiliary damping can be found by rearranging the following equation

$$\zeta_{a,opt} = \frac{c_{a,opt}}{2\omega_a m_a} \tag{2.17}$$

which gives

$$c_{a,opt} = 2\zeta_{a,opt} f_{opt} \omega_n m_a \tag{2.18}$$

Warburton [96] extended this work to derive closed-form optimal damping equations for white-noise excitation as well. This work was extended in order to incorporate damping in the main structure, where closed-form solutions are no longer available. Falcon *et al* [20] optimized the absorber parameters for an idealized main structure with a restricted level of damping. Using a light main mass damping assumption, Ioi and Ikeda [41] developed empirical relationships for the optimal spring constant and damping factor that minimized the structural response. Warburton and Ayorinde [97] minimized various response measures for a TMD attached to a damped main structure model using a numerical search approach for various levels of main and auxiliary damping. McNamara [66] and Vickery

et al [93] introduced the concept of effective damping added to the structure by a TMD. Vickery *et al* developed design charts to quantify this value for various tuning ratios, f_r, and auxiliary damping ratio, ζ_a, for a fixed mass ratio. Lee *et al* [58] proposed a numerical method which seeks to find the optimal damper parameters by minimizing the mean square value of the structural responses in the frequency domain for a structure with no model reduction, which allows for more extensive applications of the TMD.

Optimum tuning parameters for pendulum-type TMDs are presented by Gerges and Vickery [26], similar to those developed by den Hartog [18], for the case of the undamped primary system. An equivalent structural damping for the combined main and rotational auxiliary system was also presented. The optimal frequency ratio for force excited main mass is

$$f_{opt} = \frac{\omega_{2_{opt}}}{\omega_1} = \frac{\sqrt{1 + \mu\left(1 - \frac{3}{2r_a}\right)}}{1 + \mu} \tag{2.19}$$

where

$$r_a = \frac{I_a}{m_a L^2} \tag{2.20}$$

and I_a is the moment of inertia of the mass about the suspension point. For a point mass, $I_a = m_a L^2$ ($r_a = 1$). The optimal auxiliary damping ratio is

$$\zeta_{a,opt} = \sqrt{\frac{\mu + \mu^2\left(1 - \frac{1}{4r_a}\right)}{4r_a + 2\mu\left(4r_a - 1\right) + 2\mu^2\left(2r_a - 1\right)}} \tag{2.21}$$

Tabulated results for optimal tuning ratio and auxiliary damping ratio for various choices of r_a and μ for a damped primary system were determined numerically. They concluded that negligible errors between the undamped and damped primary systems existed for optimal damping, and slightly different optimal tuning ratios. Two main conclusions drawn from this study were: PTMDs are more effective under wind loading than earthquake loading, requiring larger frequency ratios; and increasing the auxiliary damping above its optimal value is effective in reducing the PTMD motion if larger mass ratios are not possible. The aforementioned models are adequate, for example, in analyzing the response of flexible

structures where the dominant response is believed to be primarily in one direction. When the responses in both along-wind and across-wind directions are of concern, then it is important to quantify the effect of the PTMD in both directions.

Rana and Soong [75] performed a parametric study of a passive TMD in order to better understand its important characteristics. Since no closed-form solutions for the optimal damper parameters can be obtained for a system with main mass damping, a numerical search was performed for a damped main mass system. An investigation into the effect of detuning was also performed using a base excited steady-state harmonic analysis. It was concluded that frequency detuning is more severe than auxiliary damping detuning, and with increasing auxiliary damping or mass ratio, the effect of detuning was less severe. The detuning effect was considered using a base excited time-history analysis; the optimal damping and frequency ratios were found to be similar to the harmonic analysis results, but the detuning effect was less severe. It was also established that increasing the inherent damping of the main structure caused the optimal frequency and damping ratios to also increase. The same was observed for large mass ratios.

The following key points are summarized based on the literature of TMDs:

- If the main mass inherent damping is considered, closed-form solutions for optimal damper parameters cannot be obtained and numerical search methods must be used. The approach relies on the presence of "fixed-point" frequencies, where the transmissibility of vibration is independent of the auxiliary damping; for structures that exhibit main mass damping, these frequencies no longer exist [3], though close agreement with numerical results for low to moderate main mass damping in structures has been demonstrated by approximating the"fixed-point" frequencies [28].

- Optimal auxiliary damping and stiffness parameters are different depending on whether the TMD is optimized for base excitation, such as earthquake loading, or main mass excitation, as is the case for wind loading.

- Increasing the mass ratio increases the robustness of TMDs to detuning effects, and improves their performance [75, 79]. However, practical considerations often limit

and decide this parameter. Considering the mass ratio as a parameter to be optimized has been considered by other researchers [65]. More recent studies into more unconventional mass ratios up to 20% have been considered, such as using segmented upper stories and sliding roof systems [16, 9, 10, 90, 111, 21]. However, in a majority of applications, it is practical to target mass ratios as low as possible, which means they are likely to be susceptible to detuning.

2.3 Multiple, active, semi-active, and adaptive tuned mass dampers

Thus far, the discussion of TMDs has focussed on passive systems, whose damper parameters are generally fixed. While the passive mass damper is an effective and inexpensive means to reduce structural vibrations, their limitations are well documented in the literature [75, 77]. Narrowband suppression frequency, sensitivity to detuning, and inability to effectively reduce both wind- and earthquake-induced vibrations are inherent limitations of passive TMDs [74]. Several enhancements to the passive TMD are described next.

2.3.1 Multiple tuned mass dampers

A number of researchers have investigated the effect of multiple tuned mass dampers (MTMDs) [103, 1, 52, 13, 75, 7, 33], with concentrated or distributed masses vibrating at various frequencies corresponding to the modes of the primary structure or tuned about the primary mode of vibration. Rana and Soon found that TMDs tuned to the higher modes of vibration may deteriorate the performance of the first [75], generally dominant, mode. Kareem and Kline investigated MTMDs tuned to various frequencies about a dominant mode, and found that distributing the mass across the MTMDs resulting in improved performance over a single TMD [52]. It was also concluded that the main parameter of interest in the design of MTMDs for the purpose of attenuating the primary mode was the range of frequencies of the TMDs, with a narrow range generally producing better

results. Hoang and Warnitchai demonstrated an increased robustness of MTMDs to errors in the main system parameters and an enhanced robustness when the frequency range of the MTMD was increased [33].

2.3.2 Active tuned mass dampers

The active tuned mass damper (ATMD) is considered a superior alternative to the passive TMD. ATMDs use a control system to monitor the response of the structure and then introduce a control force operating on a auxiliary mass to counteract the motion of the structure. The ATMD generally requires a smaller auxiliary mass, and in all reported cases has superior performance than its passive counterpart [55, 51, 74].

ATMDs consist of a feedback control system, including [55]:

- Sensors that monitor external excitations or responses of the structure (accelerations, velocities, or displacements)
- A computer which collects and processes the sensor information and determines the necessary control force using classic control theory methods
- Actuators to generate the required control force on the auxiliary mass

ATMDs are reported to increase the structural damping to 10% critical and reduce the acceleration response of the structure by up to two thirds [55], as compared to the 3-5% damping ratio increase and 30-50% structural response reductions reported for conventional TMDs [51].

Although ATMDs demonstrate better performance, they are more expensive to design, implement, and operate, require careful maintenance, and are therefore less reliable. ATMDs also require a considerable amount of electrical energy to operate [55], which may not be available during the storms they are designed to mitigate against [37].

2.3.3 Semi-active tuned mass dampers

Recognizing the inherent limitations of both passive and active systems, and the added benefit of active damping, the concept of a semi-active tuned mass damper (STMD), originally proposed by Hrovat *et al* in 1983 [37], has been studied extensively in the literature [74, 77, 87]. STMDs are passive devices enhanced with mechanisms to adjust the auxiliary damping in real-time, based on the response of the structure. Only a small amount of active energy is required to change the auxiliary stiffness and damping, thus eliminating the need for the large energy supply required by active mass damping systems [74].

The study of STMDs with adjustable damping mechanisms has been motivated in the literature as follows. In practical applications of TMDs, the displacement necessary to provide adequate performance of the TMD is quite large; therefore over-damped auxiliary systems are selected to limit the stroke of the TMD, which results in a larger response of the main system and a reduced efficiency of the device [77]. The larger displacements are only likely to occur during extreme events; therefore, it is desirable to have adjustable damping in order to improve the performance of the TMD during routine loading. There is also a propensity for the structure's frequency to vary over time; real-time adjustment of the auxiliary frequency mitigates against such detuning effects.

Due to the uncertainties in the excitation and the structural parameters, the properties of the STMD are only changed based on the measured response of the structure [77]. A concept similar to the STMD, called an adaptive passive tuned mass damper (APTMD), was developed by the author and his colleagues. While the basic idea of the adaptation is the same between the APTMD and STMDs, the tuning algorithm is not real-time. This is discussed in more detail in Chapter 7. There are several advantages of STMDs over passive TMDs due to the following reasons:

- Structures are quite complex, and the use of simplified models to represent their response may result in significant inaccuracies in their response predictions. In finding the primary structure's natural frequencies, the contribution of non-structural elements to the stiffness of the structure is generally ignored; also, the mass is overestimated for the purpose of a conservative static design. The structural properties

of a structure are only known with a limited degree of certainty. This results in incorrect estimation of the optimal auxiliary damping parameters, and though this can be rectified during the commissioning of the TMD, it still requires a considerable accuracy during the design phase. STMDs can be made robust to such uncertainties.

- Structural properties vary over time, generally arising from either a deterioration of the structure, inadvertent or deliberate modification of the structure, or through the variation of mass related to the loads carried by the structure (occupants or equipment, for example). STMDs can easily overcome such detuning effects.

- The excitation of the structure can be from a variety of sources, such as wind or seismic loading. Also, it is neither harmonic nor white noise [77], so closed-form solutions presented in the literature for the optimal selection of auxiliary damping parameters [26, 74, 75] may not be applicable for all conditions. Also, wind and seismic loading vary with time and direction, and may excite modes [77] other than the single mode response the TMD is designed to control [75]. This is especially true in lightweight structures such as pedestrian bridges where the live load magnitude and pattern can excite different modes. STMDs can be tuned to counteract such effects.

STMDs have been studied extensively in the literature. Several algorithms and configurations have been proposed and evaluated. Pinkaew and Fujino [74] demonstrated that a STMD with variable damping was effective in reducing the displacement response of the structure beyond the reduction a passive TMD provides. The study involved various frequencies of harmonic excitations, and noted a particularly good improvement near the resonant frequency of the structure. They demonstrated that the STMD requires sufficient amplitude before effectively reducing the structural vibrations. The STMD with variable damping provides adequate flexibility to handle the variation in the excitation. While the STMD cannot provide a sufficient control force during the transient period, it provides the equivalent effect of increasing the auxiliary mass by four times in the steady-state region of the response.

Ricciardelli *et al* [77] investigated STMDs for the control of wind-excited structures, using a numerical model of a tall, slender structure equipped with a TMD. The complement of the ratio of the root mean squared (RMS) response between the controlled and uncontrolled cases were used as a measure of the TMDs's efficiency. For the ideal case of white noise excitation, the efficiency parameter was 0.53. When a more realistic wind load input excitation was used, the efficiency fell to 0.33. Finally, when a 21% error in the estimation of the stiffness and mass of the main structure were used, subsequently effecting the optimal tuning parameter selection, the efficiency of the TMD fell to 0.12 and 0.08, respectively. For the case of the error in stiffness, the peak displacement of the main structure was only reduced by 3%, and no reduction in peak displacement occurred when the mass was incorrectly estimated. A STMD was proposed, whose frequency and damping can be varied with time to keep the performance close to optimal. This accommodates three weaknesses in TMDs design: the uncertainties in the main structural parameters, the variation of the structural parameters with time, and the variation in the excitation. Ricciardelli *et al* proposed pneumatic springs and hydraulic dampers, which can be integrated with control mechanism to automatically adjust stiffness and damping with time. Since the RMS response of the structure doesn't directly contain any information on the performance of auxiliary damping devices, Riccardelli *et al* used a iterative trial-and-error approach, where the frequency response of the structure was measured and the auxiliary damper parameters were adjusted until the frequency response curve became similar to optimal response curves found using numerical parameter studies. Explicit determination of the primary structural frequencies was not performed. The optimization algorithm did not result in a reduction in the main structural response, but instead reduced the stroke of the TMD with the same effectiveness of the passive TMD.

Setareh [83] studied the ground hook TMD, where the auxiliary damping level is related to the absolute velocity of the main mass. The application of a harmonic base excited structure was considered, and the results of a numerical study concluded the following:

- The semi-active system achieved up to 12% better performance than the passive counterpart

- The system is more sensitive to frequency detuning than auxiliary damping detuning
- The system's mass ratio should be selected as large as attainable, as a system with higher mass ratios is less susceptible to detuning
- The auxiliary damping should be selected such that detuning does not result in the parameters being less than optimal, as there is a more dramatic performance reduction when auxiliary damping is suboptimal

A summary of various adaptive mechanisms for enhancing TMDs, including STMDs, together with example applications has been provided by Kareem and Kijewski [51]. Several variable stiffness and damping mechanisms, including full-scale applications, have been summarized by Nagarajaiah [69].

The ensuing study will primarily investigate adaptive passive PTMDs, as they are common in the application of reducing the response of tall structures and offer a simple means of stiffness adjustment by varying the effective pendulum length. Particular emphasis will be on design aspect of three-dimensional PTMDs, an area that has so far been neglected in the literature.

2.4 Pendulum-type tuned mass dampers

Much of this thesis is devoted to the study and condition assessment of PTMDs. The parameters (stiffness, damping, and mass ratio) in translational TMDs have direct equivalents in PTMDs; however, the fundamental dynamics of the PTMDs are considerably different, are nonlinear, and require separate treatment. Sacks and Swallow [80] suggested several design factors that must be considered in the design of a TMD.

- A TMD must allow for the natural frequency and damping to be easily adjustable, primarily to allow for variations in the structural properties, particularly as they differ from those forecasted during the design stage.

- A TMD should function in all directions.
- A TMD should be operational at all times, but also incorporate a mechanism for arresting their motion when it becomes necessary to do so.

When viewed with respect to the above list of specifications, PTMDs offer a naturally simple design. For example, PTMDs are intrinsically three-dimensional in nature; that is, they can respond in all directions (lateral and rotational). Furthermore, their natural frequency is easily adjustable, as it depends only on the suspended length of the mass, and not on other properties such as the magnitude of the mass or the properties of the suspension material. Frequency adjustment in a PTMD can be accomplished by changing the location of the pivot point, such as using an adjustable tuning frame below the upper support, as in the Chifley Tower in Sydney [55] or Park Tower in Chicago [42]. Fine frequency tuning can also be performed by augmenting the mass with springs that can be adjusted along the height [26]. In contrast, adjustments in translational-type TMDs [70] and introducing multi-directional behaviour [51] can sometimes be cumbersome to obtain.

The first aspect in the study of PTMDs is their mathematical models. Surprisingly, this aspect has not been fully studied in the literature. Most studies on the subject have either linearized the system of equations or considered motion in only in the planar direction, or both [26]. Studies of pendulum motion have been considered in the context of its own nonlinear motion [82].

The work is proposed in the context of improving occupant comfort in upper floors of tall buildings using PTMDs, by reducing the peak or RMS acceleration response to within acceptable levels for various return period events. Assessing occupant comfort in tall buildings subjected to wind excitation is difficult, due to the subjectiveness of quantifying perception of motion. A recent paper on this topic [56] reviewed an extensive database of studies aimed at understanding and unifying comfort guidelines, and presented an excellent overview of current standards in use today. It is generally accepted that within the lower frequency range of less than 1 Hz, human perception threshold reduces with increasing frequency [56]. For structures with well-separated lateral frequencies, a PTMD designed to satisfy comfort performance requirements in one direction may have a significant impact

in the other direction. As a consequence, it may not meet the overall performance objectives in a given situation. Hence, it is critical that the response for structures equipped with PTMDs be estimated with a good degree of accuracy in order to ascertain its overall performance.

To the knowledge of the author, none have considered structures coupled with nonlinear bi-axial pendulums in the framework of PTMDs. The closest study in this regard has been in the context of tower cranes. The coupled equations of motion for structural dynamics and pendulum motion involve complex nonlinear dynamical phenomena [11, 82], which have not been adequately addressed. Acknowledging that many recent studies of the dynamics and control of cranes have been based on simplified models [11], Ju *et al* [44] concluded that when the dynamic response of the crane structure was of interest, more detailed models of the main structure are required. Their study involved deriving the integrated finite element formulations to analyze the coupled dynamics of the tower crane structure and pendulum motion of the payload. Using Lagrange's equation, including the dissipation function, the governing equations for the dynamic response of the tower cranes coupled with pendulum motion were derived. The tower crane itself was modelled using the finite element method. The result is a set of coupled differential equations with nonlinear excitation loads, which are difficult to solve analytically or numerically. The present work differs from the study of tower cranes in that it considers the addition of an auxiliary spring for fine frequency adjustment and auxiliary viscous and non-linear damping for energy dissipation. Also, the aforementioned study considered three simplifications including rigid main structure, pure planar motion, and pure spherical motion. The combined planar-spherical response was not considered.

Considering the biaxial motion of the PTMD is important for several reasons. First, the lateral coupling effect introduced by a three-dimensional pendulum has the potential to transfer energy between lateral modes, potentially producing a increased response for an uncontrolled mode orthogonal to the controlled lateral mode of vibration. Second, a comparison of the optimal design equations for a three-dimensional and planar PTMD has not been presented in the literature; the effect of increasing mass ratio on the coupling effect has also been unexplored. Third, it is not clear from the literature whether the

planar assumption and linearized model produces conservative response estimates when compared to the three-dimensional PTMD model.

2.5 Detuning in tuned mass dampers

Generally, the research in the area of TMDs has focused on evaluating the performance of TMDs [52, 50, 54, 55, 74], finding optimal damper parameters [58, 26, 33, 59, 83, 75, 1, 97, 96, 20], with little attention on determining if an in-service TMD is optimally tuned or not[77, 30].

Current methods of detuning detection involve periodically arresting the motion of the TMD and finding the natural modes of the structure [78] as part of the routine maintenance of the TMD. The TMD parameters are manually adjusted, subsequently. This method is labour intensive, time consuming, costly, and involves removing the TMD from service, potentially sacrificing safety or comfort of the occupants of the structure. Furthermore, this process cannot be integrated into adaptive control systems to incorporate automated adjustments.

Identifying the main structural modes while a TMD is in-service is difficult, caused by the effective change the TMD has on the structural parameters [75, 30, 99]. Estimating the main structural modal parameters (natural frequency, modal damping ratios, and mode shapes) is key to identify detuning. The main theoretical challenge in the estimation of bare structure modal properties using TMD attenuated response measurements is that the presence of a TMD alters the overall dynamics of the system [30], and hence contaminates the measurements at all the degrees of freedom. This issue has been considered in a few studies [77, 59, 99]. They employ traditional system identification algorithms such as the random decrement and Ibrahim time-domain techniques [59], or a combination of heuristic and design inference rules [47, 99, 30, 77]. However, these studies did not demonstrate the effectiveness of their algorithms to address the issues of detuning and on-line adaptive control of TMDs for wind engineering applications. Hazra *et al* [30] presented a non-parametric identification method based on time frequency analysis to estimate the bare

structure modal properties from TMD attenuated responses. However, significant user judgment is required, which makes the method non-ideal for online control applications. Weber and Feltrin performed a system identification of two pedestrian bridges equipped with TMDs and documented the challenges associated with identifying the underlying structure's properties while the absorber was enabled [99]. To overcome this challenge, several model parameter were fixed to their known values based on identification results (while the absorber was disabled) and *a priori* knowledge of the auxiliary parameters, and the remaining unknown parameters were identified. To the knowledge of the author, prior to this study, a framework consisting of online identification of bare structural model properties from TMD attenuated response measurements, and their utilization in the condition assessment and tuning in PTMDs, has not yet been addressed.

2.6 Full-scale condition assessment of tuned mass dampers

Kareem and Kijewski [51], Kwok and Samali [55], and Irwin and Breukelman [42] presented several recent applications of TMDs, PTMDs, and STMDs. Kwok and Samali [55] demonstrated the effectiveness of the auxiliary damping devices by presenting the results from several extensive full-scale measurement studies on a number of tall buildings and structures, reporting reductions of 40% to 50% in the RMS response of the structure during wind loading and an increase in effective structural damping between 3% to 5%. Kwok and Macdonald [54] presented the results of a full-sale study of the Sydney Tower before and after the installation of a secondary TMD on the structure. Sydney Tower is a 250 m tall structure, originally fitted with 180 tonne TMD to increase the damping level. Later, a 40 tonne damper was installed to reduce wind-induced vibrations, primarily in the second mode. Kwok and Macdonald reported a "significant reduction in both peak along-wind and peak cross-wind acceleration responses after the installation of the secondary TMD [54].

Beyond the aforementioned full-scale studies, few results of full-scale studies are pre-

sented in the literature. In order to more fully understand the applicability of STMDs in practical applications, further investigation into the effects of detuning on full-scale structures is required. This lack of information is further exemplified for the case of PTMDs, despite many full-scale applications in use today [35].

Chapter 3

Dynamic response of a flexible structure coupled with a PTMD

In the process of condition assessment, a key step is to develop a system of equations that couples the dynamics of a flexible structure with the motion of the pendulum tuned mass damper (PTMD). This model will eventually enable the development of design parameters that can be checked with the as-built values and the PTMD can be retuned, if necessary, in the subsequent steps. Most studies have developed the design parameters based on simplified models of the coupled dynamic system. The following effort is to compare, quantify, and understand the effects of such simplifications on the structural dynamics and the resulting design equations.

A five-degree-of-freedom (DOF) system is considered, combining a pendulum mass with a main structure capable of translation in three directions. The three dimensional behaviour of the PTMD is modelled using two generalized coordinates representing the planar rotation and the spherical motion. The system equations include auxiliary damping and stiffness. The equations of motion are then extended to a PTMD attached to a multi-degree-of-freedom (MDOF) flexible structure. The equations of motion are cast into state space form to aid in the simulation of the structural response. An alternate formulation is presented (in Appendix A), where the auxiliary system is described using a Cartesian

coordinate system. Finally, the effect of using a non-linear auxiliary damper, such as a velocity-squared proportional damper, is presented.

3.1 5DOF system modeling

A five-DOF system is considered first, as shown in Fig. 3.1a. The origin of the system is set up to coincide with the suspension point of the pendulum mass. The vectors $u(t)$, $v(t)$, and $w(t)$ are the displacements of the suspension point in the x-, y-, and z-directions, respectively. The angle $\theta(t)$ is the angle of swing away from the vertical line passing through the origin, also known as the planar angle. The angle $\varphi(t)$ is the angle of the auxiliary mass rotating about the vertical line, also known as the spherical angle. All of the aforementioned parameters vary with time. L is the length of the pendulum and m_a is the auxiliary pendulum mass.

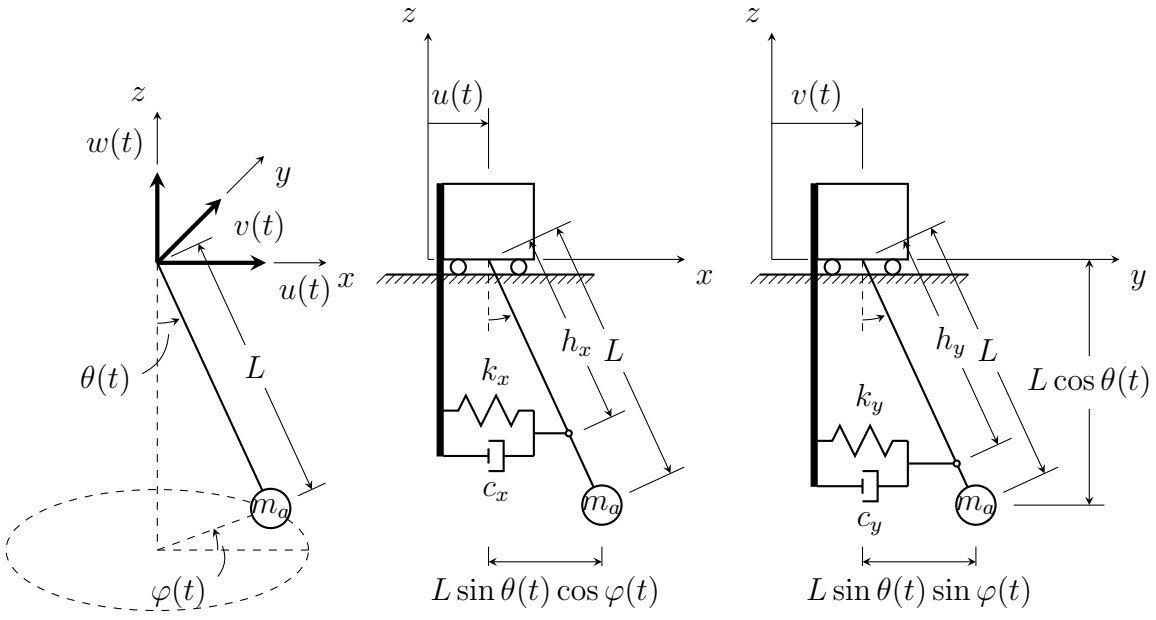

(a) (b) x-direction (c) y-direction

Figure 3.1: Schematic geometry of the PTMD mass with auxiliary damper and spring

The position vector, in three-dimensional space, where the rows corresponds to the x-, y-, and z-directions, respectively, of the auxiliary mass, m_a is

$$\mathbf{r}(t) = \left\{ \begin{array}{c} u(t) + L\sin\theta(t)\cos\varphi(t) \\ v(t) + L\sin\theta(t)\sin\varphi(t) \\ w(t) - L\cos\theta(t) \end{array} \right\} \tag{3.1}$$

The velocity of the auxiliary mass is found by taking the first time derivative of the position.

$$\mathbf{v}(t) = \left\{ \begin{array}{c} \dot{u}(t) + L\cos\theta(t)\cos\varphi(t)\dot{\theta}(t) - L\sin\theta(t)\sin\varphi(t)\dot{\varphi}(t) \\ \dot{v}(t) + L\cos\theta(t)\sin\varphi(t)\dot{\theta}(t) + L\sin\theta(t)\cos\varphi(t)\dot{\varphi}(t) \\ \dot{w}(t) + L\sin\theta(t)\dot{\theta}(t) \end{array} \right\} \tag{3.2}$$

3.1.1 Kinetic energy, potential energy, and dissipation functions

The next step is to calculate the kinetic energy. The notion of time, (t), is implicit wherever applicable in the ensuing equations. The kinetic energy is given by

$$\begin{aligned} \mathcal{T}_a &= \frac{1}{2}\mathbf{v}m_a\mathbf{v}^T \\ &= \frac{1}{2}m_a\Big[\Big(\dot{u} + L\cos\theta\cos\varphi\dot{\theta} - L\sin\theta\sin\varphi\dot{\varphi}\Big)^2 \\ &\quad + \Big(\dot{v} + L\cos\theta\sin\varphi\dot{\theta} + L\sin\theta\cos\varphi\dot{\varphi}\Big)^2 \\ &\quad + \Big(\dot{w} + L\sin\theta\dot{\theta}\Big)^2\Big] \\ &= \frac{1}{2}m_a\Big[\dot{u}^2 + \dot{v}^2 + \dot{w}^2 + L^2\dot{\theta}^2 + L^2\dot{\varphi}^2\sin^2\theta + 2\dot{u}L\cos\theta\cos\varphi\dot{\theta} \\ &\quad - 2\dot{u}L\sin\theta\sin\varphi\dot{\varphi} + 2\dot{v}L\cos\theta\sin\varphi\dot{\theta} + 2\dot{v}L\sin\theta\cos\varphi\dot{\varphi} \\ &\quad + 2L\dot{w}\dot{\theta}\sin\theta\Big] \end{aligned} \tag{3.3}$$

The potential energy of the auxiliary mass, measured with respect to the arbitrarily selected origin, is

$$\mathcal{V}_a = m_a g \left(w - L \cos\theta \right) \tag{3.4}$$

where g is the acceleration due to gravity. The kinetic energy of the main structure is

$$\mathcal{T}_m = \frac{1}{2} \dot{\mathbf{\Delta}}^T \mathbf{M} \dot{\mathbf{\Delta}} = \frac{1}{2} \left\{ \begin{array}{c} \dot{u} \\ \dot{v} \\ \dot{w} \end{array} \right\}^T \left[\begin{array}{ccc} m_{uu} & m_{uv} & m_{uw} \\ m_{vu} & m_{vv} & m_{vw} \\ m_{wu} & m_{wv} & m_{ww} \end{array} \right] \left\{ \begin{array}{c} \dot{u} \\ \dot{v} \\ \dot{w} \end{array} \right\} \tag{3.5}$$

where $\mathbf{M}$ is the 3×3 mass matrix corresponding to the pendulum suspension point, in the x-, y-, and z-direction. The potential (strain) energy of the main mass is

$$\mathcal{V}_m = \frac{1}{2} \mathbf{\Delta}^T \mathbf{K} \mathbf{\Delta} = \frac{1}{2} \left\{ \begin{array}{c} u \\ v \\ w \end{array} \right\}^T \left[\begin{array}{ccc} k_{uu} & k_{uv} & k_{uw} \\ k_{vu} & k_{vv} & k_{vw} \\ k_{wu} & k_{wv} & k_{ww} \end{array} \right] \left\{ \begin{array}{c} u \\ v \\ w \end{array} \right\} \tag{3.6}$$

where $\mathbf{K}$ is the 3×3. The Raleigh dissipation function for the main mass is

$$\mathcal{F}_m = \frac{1}{2} \dot{\mathbf{\Delta}}^T \mathbf{C} \dot{\mathbf{\Delta}} = \frac{1}{2} \left\{ \begin{array}{c} \dot{u} \\ \dot{v} \\ \dot{w} \end{array} \right\}^T \left[\begin{array}{ccc} c_{uu} & c_{uv} & c_{uw} \\ c_{vu} & c_{vv} & c_{vw} \\ c_{wu} & c_{wv} & c_{ww} \end{array} \right] \left\{ \begin{array}{c} \dot{u} \\ \dot{v} \\ \dot{w} \end{array} \right\} \tag{3.7}$$

where $\mathbf{C}$ is the 3×3 damping matrix.

3.1.2 Lagrange's Equation

The kinetic energy, potential energy, and dissipation factor for the combined main system and PTMD are

$$\mathcal{T} = \mathcal{T}_m + \mathcal{T}_a \tag{3.8a}$$

$$\mathcal{V} = \mathcal{V}_m + \mathcal{V}_a \tag{3.8b}$$

$$\mathcal{F} = \mathcal{F}_m \tag{3.8c}$$

Lagrange's equation for the case of free vibration is [68]

$$\frac{d}{dt}\frac{\partial \mathcal{T}}{\partial \dot{q}_r} - \frac{\partial \mathcal{T}}{\partial q_r} + \frac{\partial \mathcal{V}}{\partial q_r} + \frac{\partial \mathcal{F}}{\partial \dot{q}_r} = 0 \tag{3.9}$$

where q_r and $\dot{q}_r$ are the generalized coordinates and velocities of the system. For the combined main structure and PTMD system, the generalized coordinates are u, v, w, θ, and φ and the generalized velocities are $\dot{u}$, $\dot{v}$, $\dot{w}$, $\dot{\theta}$, and $\dot{\varphi}$.

3.1.3 Equations of motion

Substituting Eq. 3.8 into Eq. 3.9 produces the following system of equations for a 5-DOF system, including the motion of a PTMD, for free vibration:

$$\left[\mathbf{M} + \begin{bmatrix} m_a & 0 & 0 \\ 0 & m_a & 0 \\ 0 & 0 & m_a \end{bmatrix}\right] \begin{Bmatrix} \ddot{u} \\ \ddot{v} \\ \ddot{w} \end{Bmatrix} + \mathbf{C} \begin{Bmatrix} \dot{u} \\ \dot{v} \\ \dot{w} \end{Bmatrix} + \mathbf{K} \begin{Bmatrix} u \\ v \\ w \end{Bmatrix} = m_a L$$
$$\times \begin{Bmatrix} -\cos\theta\cos\varphi\ddot{\theta} + \sin\theta\cos\varphi\dot{\theta}^2 + 2\cos\theta\sin\varphi\dot{\theta}\dot{\varphi} + \sin\theta\sin\varphi\ddot{\varphi} + \sin\theta\cos\varphi\dot{\varphi}^2 \\ -\cos\theta\sin\varphi\ddot{\theta} + \sin\theta\sin\varphi\dot{\theta}^2 - 2\cos\theta\cos\varphi\dot{\theta}\dot{\varphi} - \sin\theta\cos\varphi\ddot{\varphi} + \sin\theta\sin\varphi\dot{\varphi}^2 \\ -\sin\theta\ddot{\theta} - \cos\theta\dot{\theta}^2 - \dfrac{g}{L} \end{Bmatrix} \tag{3.10}$$

The equation of motion corresponding to planar pendulum motion (θ-DOF) is

$$L\ddot{\theta} - L\sin\theta\cos\theta\dot{\varphi}^2 + \cos\theta\cos\varphi\ddot{u} + \cos\theta\sin\varphi\ddot{v} + \sin\theta\ddot{w} + g\sin\theta = 0 \tag{3.11}$$

The equation of motion corresponding to spherical pendulum motion (φ-DOF) is

$$L\sin\theta\ddot{\varphi} + 2L\cos\theta\dot{\theta}\dot{\varphi} - \sin\varphi\ddot{u} + \cos\varphi\ddot{v} = 0 \tag{3.12}$$

3.2 Auxiliary damping and stiffness

A linear auxiliary viscous damper and linear spring are introduced, as shown in Figs. 3.1b and 3.1c. The viscous damper has a damping coefficient c_x in the x-direction and c_y in the y-direction. The linear spring has a spring constant k_x in the x-direction and k_y in the y-direction. The damper and spring are connected to the pendulum length at a distance h_x and h_y from the suspension point, in the x- and y-directions, respectively. Assuming the auxiliary damper and spring remain horizontal, the relative position of the attachment point is

$$r_{p,x} = h_x\sin\theta\cos\varphi \tag{3.13a}$$

$$r_{p,y} = h_y\sin\theta\sin\varphi \tag{3.13b}$$

The velocity of the suspension point in the x- and y-directions can be found by taking the first time derivative of the position.

$$v_{p,x} = h_x\cos\theta\cos\varphi\dot{\theta} - h_x\sin\theta\sin\varphi\dot{\varphi} \tag{3.14a}$$

$$v_{p,y} = h_y\cos\theta\sin\varphi\dot{\theta} + h_y\sin\theta\cos\varphi\dot{\varphi} \tag{3.14b}$$

The kinetic energy of the auxiliary mass remains the same, as in Eq. 3.3. The potential energy becomes

$$\begin{aligned}\mathcal{V}_a &= \frac{1}{2}k_x r_{p,x}^2 + \frac{1}{2}k_y r_{p,y}^2 + m_a g\left(w - L\cos\theta\right) \\ &= \frac{1}{2}k_x h_x^2 \sin^2\theta\cos^2\varphi + \frac{1}{2}k_y h_y^2 \sin^2\theta\sin^2\varphi + m_a g\left(w - L\cos\theta\right)\end{aligned} \tag{3.15}$$

A Raleigh dissipation function for the auxiliary system is introduced. The auxiliary dissipation factor is

$$\begin{aligned}\mathcal{F}_a &= \frac{1}{2}c_x v_{p,x}^2 + \frac{1}{2}c_y v_{p,y}^2 \\ &= \frac{1}{2}c_x\left(h_x^2\cos^2\theta\cos^2\varphi\dot{\theta}^2 - 2h_x^2\cos\theta\cos\varphi\dot{\theta}\sin\theta\sin\varphi\dot{\varphi} + h_x^2\sin^2\theta\sin^2\varphi\dot{\varphi}^2\right) \\ &\quad + \frac{1}{2}c_y\left(h_y^2\cos^2\theta\sin^2\varphi\dot{\theta}^2 + 2h_y^2\cos\theta\cos\varphi\dot{\theta}\sin\theta\sin\varphi\dot{\varphi} + h_y^2\sin^2\theta\cos^2\varphi\dot{\varphi}^2\right)\end{aligned} \tag{3.16}$$

The kinetic energy, potential energy, and dissipation function for the main structure are unchanged. The dissipation function for the combined main and auxiliary system is

$$\mathcal{F} = \mathcal{F}_m + \mathcal{F}_a \tag{3.17}$$

These results are then used in Lagrange's equation (Eq. 3.9) and the system of equations are found for the simple 5DOF system including a linear viscous damper and linear spring connected to the auxiliary system. Eq. 3.10 corresponding to the translational DOF of the suspension point remains unchanged.

The equation of motion corresponding to the planar (θ-DOF) motion of the pendulum

(Eq. 3.11) becomes

$$\begin{aligned} & L\ddot{\theta} - L\sin\theta\cos\theta\dot{\varphi}^2 + \cos\theta\cos\varphi\ddot{u} + \cos\theta\sin\varphi\ddot{v} + \sin\theta\ddot{w} + g\sin\theta \\ & + \frac{k_x h_x^2}{m_a L}\sin\theta\cos\theta\cos^2\varphi + \frac{k_y h_y^2}{m_a L}\sin\theta\cos\theta\sin^2\varphi \\ & + \frac{c_x h_x^2}{m_a L}\left(\cos^2\theta\cos^2\varphi\dot{\theta} - \cos\theta\cos\varphi\sin\theta\sin\varphi\dot{\varphi}\right) \\ & + \frac{c_y h_y^2}{m_a L}\left(\cos^2\theta\sin^2\varphi\dot{\theta} + \cos\theta\cos\varphi\sin\theta\sin\varphi\dot{\varphi}\right) = 0 \end{aligned} \tag{3.18}$$

The equation of motion corresponding to spherical (φ-DOF) motion of the pendulum (Eq. 3.12) becomes

$$\begin{aligned} & L\sin\theta\ddot{\varphi} + 2L\cos\theta\dot{\theta}\dot{\varphi} - \sin\varphi\ddot{u} + \cos\varphi\ddot{v} - \frac{k_x h_x^2 - k_y h_y^2}{m_a L}\left(\sin\theta\sin\varphi\cos\varphi\right) \\ & + \frac{c_x h_x^2}{m_a L}\left(-\cos\theta\cos\varphi\sin\varphi\dot{\theta} + \sin\theta\sin^2\varphi\dot{\varphi}\right) \\ & + \frac{c_y h_y^2}{m_a L_a}\left(\cos\theta\cos\varphi\sin\varphi\dot{\theta} + \sin\theta\cos^2\varphi\dot{\varphi}\right) = 0 \end{aligned} \tag{3.19}$$

3.3 Pendulum dynamics coupled with MDOF structure

Consider a flexible MDOF main structure with three translational degrees of freedom in each orthogonal direction for each floor mass, as shown in Fig. 3.2. $\mathbf{M}_{n\times n}$ is the global mass matrix, $\mathbf{C}_{n\times n}$ is the global damping matrix, and $\mathbf{K}_{n\times n}$ is the global stiffness matrix, where n is the number of degrees of freedom. The upper-left 3×3 matrix of the $\mathbf{M}$, $\mathbf{C}$, and $\mathbf{K}$ matrices corresponds to the DOF from which the PTMD is suspended. This is typically the top floor, though the equations can be modified to account for a PTMD suspended at a different location.

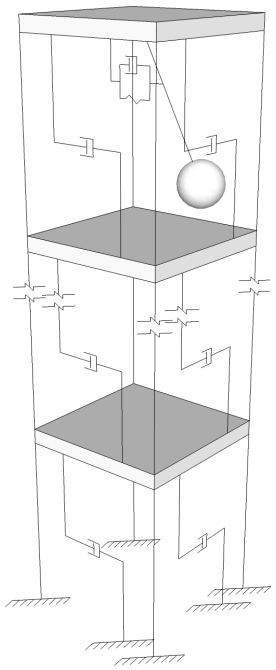

Figure 3.2: Schematic of a MDOF flexible main structure equipped with a PTMD

The kinetic energy of the main system is [44]

$$\mathcal{T}_m = \frac{1}{2}\dot{\mathbf{\Delta}}^T\mathbf{M}\dot{\mathbf{\Delta}} = \frac{1}{2}\begin{Bmatrix} \dot{u} \\ \dot{v} \\ \dot{w} \\ \dot{\mathbf{\Delta}}_r \end{Bmatrix}^T \begin{bmatrix} m_{uu} & m_{uv} & m_{uw} & \mathbf{M}_{ur} \\ m_{vu} & m_{vv} & m_{vw} & \mathbf{M}_{vr} \\ m_{wu} & m_{wv} & m_{ww} & \mathbf{M}_{wr} \\ \mathbf{M}_{ru} & \mathbf{M}_{rv} & \mathbf{M}_{rw} & \mathbf{M}_{rr} \end{bmatrix} \begin{Bmatrix} \dot{u} \\ \dot{v} \\ \dot{w} \\ \dot{\mathbf{\Delta}}_r \end{Bmatrix} \tag{3.20}$$

Here $\dot{\mathbf{\Delta}} = \begin{Bmatrix} \dot{u} & \dot{v} & \dot{w} & \dot{\mathbf{\Delta}}_r \end{Bmatrix}^T$ is the velocity vector of the main system, where $\dot{u}$, $\dot{v}$, and $\dot{w}$ are the nodal velocities of the suspension point, and $\dot{\mathbf{\Delta}}_r$ are the velocities of the remainder of the DOFs for the main structure. Similarly, the subscript r in the global mass matrix represents the remainder of the rows or columns of the mass matrix.

The potential (strain) energy of the main system is [44]

$$\mathcal{V}_m = \frac{1}{2}\mathbf{\Delta}^T\mathbf{K}\mathbf{\Delta} = \frac{1}{2}\begin{Bmatrix} u \\ v \\ w \\ \mathbf{\Delta_r} \end{Bmatrix}^T \begin{bmatrix} k_{uu} & k_{uv} & k_{uw} & \mathbf{K}_{ur} \\ k_{vu} & k_{vv} & k_{vw} & \mathbf{K}_{vr} \\ k_{wu} & k_{wv} & k_{ww} & \mathbf{K}_{wr} \\ \mathbf{K}_{ru} & \mathbf{K}_{rv} & \mathbf{K}_{rw} & \mathbf{K}_{rr} \end{bmatrix} \begin{Bmatrix} u \\ v \\ w \\ \mathbf{\Delta}_r \end{Bmatrix} \tag{3.21}$$

Here $\mathbf{\Delta} = \begin{Bmatrix} u & v & w & \mathbf{\Delta}_r \end{Bmatrix}^T$ is the displacement vector of the main system, where u, v, and w are the nodal displacements of the suspension point, and $\mathbf{\Delta}_r$ are the displacements of the remainder of the DOFs for the main structure. Similarly, the subscript r in the global stiffness matrix represents the remainders of the rows or columns of the stiffness matrix.

The Raleigh dissipation function for the main mass is

$$\mathcal{F}_m = \frac{1}{2}\dot{\mathbf{\Delta}}^T\mathbf{C}\dot{\mathbf{\Delta}} = \frac{1}{2}\begin{Bmatrix} \dot{u} \\ \dot{v} \\ \dot{w} \\ \dot{\mathbf{\Delta}}_r \end{Bmatrix}^T \begin{bmatrix} c_{uu} & c_{uv} & c_{uw} & \mathbf{C}_{ur} \\ c_{vu} & c_{vv} & c_{vw} & \mathbf{C}_{vr} \\ c_{wu} & c_{wv} & c_{ww} & \mathbf{C}_{wr} \\ \mathbf{C}_{ru} & \mathbf{C}_{rv} & \mathbf{C}_{rw} & \mathbf{C}_{rr} \end{bmatrix} \begin{Bmatrix} \dot{u} \\ \dot{v} \\ \dot{w} \\ \dot{\mathbf{\Delta}}_r \end{Bmatrix} \tag{3.22}$$

Lagrange's equation including the generalized forces [68] is given by

$$\frac{d}{dt}\frac{\partial \mathcal{T}}{\partial \dot{q}_r} - \frac{\partial \mathcal{T}}{\partial q_r} + \frac{\partial \mathcal{V}}{\partial q_r} + \frac{\partial \mathcal{F}}{\partial \dot{q}_r} = Q_r \tag{3.23}$$

where Q_r is the generalized force. For the MDOF system, the generalized forces are $\mathbf{Q} = \begin{bmatrix} P_u & P_v & P_w & \mathbf{P}_r & 0 & 0 \end{bmatrix}$, where P_u, P_v, and P_w are the arbitrary forces applied to the main structure at the location of the suspended mass in the $x-$, $y-$, and $z-$directions, respectively; $\mathbf{P}_r$ is the arbitrary force excitation for the remainder of the DOF of the main structure.

This result is substituted into Eq. 3.23 where the generalized coordinates are u, v, w, $\mathbf{\Delta}$, θ, and φ and the generalized velocities are $\dot{u}$, $\dot{v}$, $\dot{w}$, $\dot{\mathbf{\Delta}}$, $\dot{\theta}$, and $\dot{\varphi}$. The equations of

motion corresponding to the translational DOFs of the main MDOF structure for forced vibration are

$$\left[\mathbf{M}+\left[\begin{array}{cccc} m_a & 0 & 0 & \mathbf{0} \\ 0 & m_a & 0 & \mathbf{0} \\ 0 & 0 & m_a & \mathbf{0} \\ \mathbf{0} & \mathbf{0} & \mathbf{0} & \mathbf{0} \end{array}\right]\right]\left\{\begin{array}{c} \ddot{u} \\ \ddot{v} \\ \ddot{w} \\ \ddot{\mathbf{\Delta}}_r \end{array}\right\}+\mathbf{C}\left\{\begin{array}{c} \dot{u} \\ \dot{v} \\ \dot{w} \\ \dot{\mathbf{\Delta}}_r \end{array}\right\}+\mathbf{K}\left\{\begin{array}{c} u \\ v \\ w \\ \mathbf{\Delta}_r \end{array}\right\}=m_a L_a$$
$$\times\left\{\begin{array}{c} -\cos\theta\cos\varphi\ddot{\theta}+\sin\theta\cos\varphi\dot{\theta}^2+2\cos\theta\sin\varphi\dot{\theta}\dot{\varphi}+\sin\theta\sin\varphi\ddot{\varphi}+\sin\theta\cos\varphi\dot{\varphi}^2 \\ -\cos\theta\sin\varphi\ddot{\theta}+\sin\theta\sin\varphi\dot{\theta}^2-2\cos\theta\cos\varphi\dot{\theta}\dot{\varphi}-\sin\theta\cos\varphi\ddot{\varphi}+\sin\theta\sin\varphi\dot{\varphi}^2 \\ -\sin\theta\ddot{\theta}-\cos\theta\dot{\theta}^2-\dfrac{g}{L} \\ \mathbf{0} \end{array}\right\}+\left\{\begin{array}{c} P_u \\ P_v \\ P_w \\ \mathbf{P}_r \end{array}\right\} \tag{3.24}$$

where $\mathbf{M}$, $\mathbf{C}$, and $\mathbf{K}$ are described in Eqs. 3.20 through 3.22. The matrix $\mathbf{0}$ is a matrix with all elements equal to zero. The equation of motion corresponding to planar ($\theta(t)$-DOF) and spherical ($\varphi(t)$-DOF) motion of the pendulum are the same as given in Eqs. 3.18 and 3.19. Eqs. 3.24, 3.18, and 3.19 are the integrated finite element representation of a MDOF flexible structure with coupled dynamics of a PTMD for forced vibration.

3.3.1 Uniaxial response of the combined system

If the motion of the primary structure is restricted to the x-direction and the PTMD begins from at-rest initial conditions, then $\varphi=\dot{\varphi}=\ddot{\varphi}=0$, $v=\dot{v}=\ddot{v}=0$, and $w=\dot{w}=\ddot{w}=0$. For small angle displacements, $\sin\theta$ and $\cos\theta$ can be approximated by θ and 1, respectively. Neglecting the nonlinear term $\theta\dot{\theta}^2$, the equations of motion reduce to

$$\left(\mathbf{M}_x+\left[\begin{array}{cc} m_a & \mathbf{0} \\ \mathbf{0} & \mathbf{0} \end{array}\right]\right)\left\{\begin{array}{c} \ddot{u} \\ \ddot{\mathbf{\Delta}}_{r,x} \end{array}\right\}+\mathbf{C}_x\left\{\begin{array}{c} \dot{u} \\ \dot{\mathbf{\Delta}}_{r,x} \end{array}\right\}+\mathbf{K}_x\left\{\begin{array}{c} u \\ \mathbf{\Delta}_{r,x} \end{array}\right\}=\left\{\begin{array}{c} P_u-m_a L_a\ddot{\theta} \\ \mathbf{P}_{r,x} \end{array}\right\} \tag{3.25a}$$

$$m_a L_a^2\ddot{\theta}+c_x h_x^2\dot{\theta}+\left(m_a g L_a+k_x h_x^2\right)\theta+m_a L_a\ddot{u}=0 \tag{3.25b}$$

where $\mathbf{M}_x$, $\mathbf{C}_x$, and $\mathbf{K}_x$, are the mass, damping, and stiffness matrices when all but the terms corresponding to translation in the x-direction are removed.

3.4 State-space representation

The state-space representation provides an efficient framework to evaluate the responses of a dynamic system. State-space relates the input, output, and state variables using first-order differential equations. There are several advantages of using state space models. First, the equations of motion are expressed as first-order differential equations. Second, it provides a direct time-domain solution, which is of primary interest, and also accommodates general (non-proportional) damping. Third, the auxiliary system can easily be expressed in terms of a control force or feedback loop. Finally, the system can easily be implemented within the Kalman framework for state and parameter estimation. The general form of the state-space model is

$$\dot{\mathbf{x}}(t) = \mathbf{A_c}\mathbf{x}(t) + \mathbf{B_c}\mathbf{u}(t) + \mathbf{E_c}\mathbf{w}(t) \tag{3.26a}$$

$$\mathbf{z}(t) = \mathbf{C_c}\mathbf{x}(t) + \mathbf{D_c}\mathbf{u}(t) + \mathbf{F_c}\mathbf{w}(t) \tag{3.26b}$$

where $\mathbf{A}_c$ is the $\tilde{n}\times\tilde{n}$ state matrix, $\mathbf{B}_c$ is the $\tilde{n}\times s$ input matrix corresponding to the control force, $\mathbf{u}(t)$, $\mathbf{E}_c$ is the $\tilde{n}\times q$ input matrix corresponding to the external excitation, $\mathbf{w}(t)$, $\mathbf{C}_c$ is the output matrix, $\mathbf{D}_c$ is the $p\times s$ feedthrough matrix corresponding to the control force, $\mathbf{u}(t)$, and $\mathbf{F}_c$ is the $p\times q$ direct feedthrough matrix corresponding to the unknown external disturbance force vector, $\mathbf{w}(t)$. The vector $\mathbf{x}(t)$ is the state vector of dimension $\tilde{n}$ and $\mathbf{z}(t)$ is the output vector of dimension p. In order to express Eqs. 3.24, 3.18, and 3.19 in state-space form, Eq. 3.24 can be rewritten as in the following equation, with the known disturbance $\mathbf{P}(t)$ replaced with the unknown external disturbance force, $\mathbf{w}(t)$.

$$\hat{\mathbf{M}}\ddot{\mathbf{\Delta}}(t) + \mathbf{C}\dot{\mathbf{\Delta}}(t) + \mathbf{K}\mathbf{\Delta}(t) = \mathbf{u}(t) + \mathbf{w}(t) \tag{3.27}$$

where $\hat{\mathbf{M}}$ is an augmented mass matrix, determined by including the auxiliary mass at the DOFs from which it is suspended.

$$\hat{\mathbf{M}} = \mathbf{M} + \begin{bmatrix} m_a & 0 & 0 & \mathbf{0} \\ 0 & m_a & 0 & \mathbf{0} \\ 0 & 0 & m_a & \mathbf{0} \\ \mathbf{0} & \mathbf{0} & \mathbf{0} & \mathbf{0} \end{bmatrix} \tag{3.28}$$

and the control force vector is

$$\mathbf{u}(t) = m_a L_a \begin{Bmatrix} -\cos\theta\cos\varphi\ddot{\theta} + \sin\theta\cos\varphi\dot{\theta}^2 + 2\cos\theta\sin\varphi\dot{\theta}\dot{\varphi} + \sin\theta\sin\varphi\ddot{\varphi} + \sin\theta\cos\varphi\dot{\varphi}^2 \\ -\cos\theta\sin\varphi\ddot{\theta} + \sin\theta\sin\varphi\dot{\theta}^2 - 2\cos\theta\cos\varphi\dot{\theta}\dot{\varphi} - \sin\theta\cos\varphi\ddot{\varphi} + \sin\theta\sin\varphi\dot{\varphi}^2 \\ -\sin\theta\ddot{\theta} - \cos\theta\dot{\theta}^2 - \dfrac{g}{L_a} \\ \mathbf{0} \end{Bmatrix} \tag{3.29}$$

The input vector is

$$\mathbf{w}(t) = \begin{Bmatrix} P_u(t) \\ P_v(t) \\ P_w(t) \\ \mathbf{P}_r(t) \end{Bmatrix} \tag{3.30}$$

Eq. 3.27 can be rewritten as

$$\ddot{\boldsymbol{\Delta}}(t) = -\hat{\mathbf{M}}^{-1}\mathbf{C}\dot{\boldsymbol{\Delta}}(t) - \hat{\mathbf{M}}^{-1}\mathbf{K}\boldsymbol{\Delta}(t) + \hat{\mathbf{M}}^{-1}\mathbf{u}(t) + \hat{\mathbf{M}}^{-1}\mathbf{w}(t) \tag{3.31}$$

The displacements and velocities of the main structure are chosen as the states of the

system, as follows:

$$
\begin{aligned}
x_1 &= u_1 && && \text{top floor displacement in the } x\text{-direction} \\
x_2 &= v_1 && && \text{top floor displacement in the } y\text{-direction} \\
x_3 &= w_1 && && \text{top floor displacement in the } z\text{-direction} \\
x_4 &= u_2 && && \text{second from top floor displacement in the } x\text{-direction} \\
x_5 &= v_2 && && \text{second from top floor displacement in the } y\text{-direction} \\
x_6 &= w_2 && && \text{second from top floor displacement in the } z\text{-direction} \\
&\vdots \\
x_{n-2} &= u_n && && \text{bottom floor displacement in the } x\text{-direction} \\
x_{n-1} &= v_n && && \text{bottom floor displacement in the } y\text{-direction} \\
x_n &= w_n && && \text{bottom floor displacement in the } z\text{-direction} \\
\\
x_{n+1} &= \dot{u}_1 &&= \dot{x}_1 && \text{top floor velocity in the } x\text{-direction} \\
x_{n+2} &= \dot{v}_1 &&= \dot{x}_2 && \text{top floor velocity in the } y\text{-direction} \\
x_{n+3} &= \dot{w}_1 &&= \dot{x}_3 && \text{top floor velocity in the } z\text{-direction} \\
x_{n+4} &= \dot{u}_2 &&= \dot{x}_4 && \text{second from top floor velocity in the } x\text{-direction} \\
x_{n+5} &= \dot{v}_2 &&= \dot{x}_5 && \text{second from top floor velocity in the } y\text{-direction} \\
x_{n+6} &= \dot{w}_2 &&= \dot{x}_6 && \text{second from top floor velocity in the } z\text{-direction} \\
&\vdots \\
x_{2n-2} &= \dot{u}_n &&= \dot{x}_{n-2} && \text{bottom floor velocity in the } x\text{-direction} \\
x_{2n-1} &= \dot{v}_n &&= \dot{x}_{n-1} && \text{bottom floor velocity in the } y\text{-direction} \\
x_{2n} &= \dot{w}_n &&= \dot{x}_n && \text{bottom floor velocity in the } z\text{-direction}
\end{aligned}
$$

There are, therefore, $\tilde{n} = 2n$ states, where n is the number of DOFs.

Eq. 3.31 can then be written in the state-space form, as in Eqs. 3.26a and 3.26, where the state matrix is

$$\mathbf{A}_c = \begin{bmatrix} \mathbf{0}_{n\times n} & \mathbf{I}_{n\times n} \\ -\hat{\mathbf{M}}^{-1}\mathbf{K} & -\hat{\mathbf{M}}^{-1}\mathbf{C} \end{bmatrix}_{2n\times 2n} \tag{3.32}$$

where $\mathbf{I}_{n\times n}$ is a $n\times n$ identity matrix.

The input matrix corresponding to the control forces is

$$\mathbf{B}_c = \begin{bmatrix} \mathbf{0}_{n\times s} \\ -\hat{\mathbf{M}}^{-1}\mathbf{\Gamma}_{n\times s} \end{bmatrix}_{2n\times s} \tag{3.33}$$

The matrix $\mathbf{\Gamma}_{n\times s}$ is a $n\times s$ matrix that contains ones at the DOF where the control forces act and zeros elsewhere, where s is the number of control forces. For the PTMD system located at the top of the structure,

$$\mathbf{\Gamma}_{n\times 3} = \begin{bmatrix} 1 & 0 & 0 \\ 0 & 1 & 0 \\ 0 & 0 & 1 \\ \multicolumn{3}{c}{\mathbf{0}_{(n-3)\times 3}} \end{bmatrix}_{n\times 3} \tag{3.34}$$

The input matrix corresponding to the external forces is

$$\mathbf{E}_c = \begin{bmatrix} \mathbf{0_{n\times q}} \\ -\hat{\mathbf{M}}^{-1}\mathbf{\Pi}_{n\times q} \end{bmatrix}_{2n\times q} \tag{3.35}$$

The matrix $\mathbf{\Pi}_{n\times q}$ is a $n\times q$ matrix that contains ones at the DOFs where the external forces act and zeros elsewhere, where q is the number of external forces. If an external forces were applied to every DOF, the $\mathbf{\Pi}_{n\times q}$ matrix becomes the identity matrix and q=n. The selection of the output matrix, $\mathbf{C}_c$, and the direct feedthrough matrices, $\mathbf{D}_c$ and $\mathbf{F}_c$, are dependent on the desired outputs of the system. For the case where all the states are measured, $\mathbf{C}_c$=$\mathbf{I}$, and $\mathbf{D}_c$ and $\mathbf{F}_c$ are empty matrices.

The system of equations for a PTMD coupled with the dynamics of a flexible structure are modelled using a state-space realization so they can be conveniently implemented into the MATLAB® and the real-time Simulink® environment. From Eqs. 3.32 to 3.35, only the main structure properties are contained within the state matrices, with the exception of the auxiliary mass, which is appended to the main mass of the structure in Eq. 3.28. In essence, the effect of the PTMD is simulated as though it introduces a feedback force into the main structure. The remainder of the auxiliary parameters are included in the

input vector, $\mathbf{u}(t)$, corresponding to the control force produced by the PTMD (Eq. 3.29). The system is modelled by assembling a Simulink® [40] block diagram and numerically integrating the equations of motion.

The primary shortcoming of the approach described above is that when the auxiliary system is at rest, $\theta(t) = 0$, Eq. 3.19 becomes singular. This also occurs at each zero crossing of the auxiliary mass. It is straightforward to overcome these shortcoming in the simulation of the numerical model by disabling the default behaviour of Simulink® to determine the zero crossings. In the event that $\theta(t)$ falls inside a user-defined threshold near zero, a small perturbation is introduced to prevent Eq. 3.19 from becoming singular. Alternatively, the position of the auxiliary mass can be described in Cartesian coordinates; this formulation is presented in Appendix A. The resulting equations of motion are less concise, but do not become singular for the case of $\theta(t) = 0$.

3.5 Formulation for non-linear auxiliary damping

For the case where the auxiliary damper is non-linear, the governing equations are modified where the effect of the auxiliary damping is considered as a non-conservative force, rather than part of the Raleigh dissipation function. Consider velocity proportional auxiliary damping, the degree to which is denoted by $\bar{n}$. For example for linear viscous damping, $\bar{n} = 1$. For velocity-squared proportional damping, $\bar{n} = 2$. The auxiliary damping force in each horizontal direction is given as

$$F_{d,x} = c_x v_{p,x} \left| v_{p,x} \right|^{\bar{n}-1} \tag{3.36a}$$

$$F_{d,y} = c_y v_{p,y} \left| v_{p,y} \right|^{\bar{n}-1} \tag{3.36b}$$

where the damping coefficients are c_x in the x-direction and c_y in the y-direction; $v_{p,x}$ and $v_{p,y}$ are the velocity of the connection point of the damper to the auxiliary mass relative to the main mass, in the x- and y-directions, respectively. The velocity term outside the absolute value operator determines the direction of the damping force, which is always in the same direction as the relative velocity of the mass. The damper and spring are

connected to the pendulum length at a distance h_x and h_y from the suspension point, in the x- and y-directions, respectively, and are assumed to remain horizontal. The auxiliary and main system kinetic and potential energies remain unchanged. Lagrange's equation, for the case of no Raleigh dissipation function, is given by

$$\frac{d}{dt}\frac{\partial \mathcal{T}}{\partial \dot{q}_r} - \frac{\partial \mathcal{T}}{\partial q_r} + \frac{\partial \mathcal{V}}{\partial q_r} = Q_r \tag{3.37}$$

In order to determine the generalized forces acting on the system, it is necessary to first calculate the work done by non-conservative forces.

$$\begin{aligned}
\delta \mathcal{W}_{nc} &= P_u \delta u + P_v \delta v + P_w \delta w + \mathbf{P_r} \delta \mathbf{\Delta}_r \\
&\quad - c_x v_{p,x} \left| v_{p,x} \right|^{\bar{n}-1} \delta \left(h_x \sin\theta \cos\varphi \right) - c_y v_{p,y} \left| v_{p,y} \right|^{\bar{n}-1} \delta \left(h_y \sin\theta \sin\varphi \right) - \mathbf{C}\dot{\mathbf{\Delta}} \delta \mathbf{\Delta} \\
&= P_u \delta u + P_v \delta v + P_w \delta w + \mathbf{P_r} \delta \mathbf{\Delta}_r \\
&\quad - c_x v_{p,x} \left| v_{p,x} \right|^{\bar{n}-1} \left(h_x \cos\theta \cos\varphi \delta\theta - h_x \sin\theta \sin\varphi \delta\varphi \right) \\
&\quad - c_y v_{p,y} \left| v_{p,y} \right|^{\bar{n}-1} \left(h_y \cos\theta \sin\varphi \delta\theta + h_y \sin\theta \cos\varphi \delta\varphi \right) - \mathbf{C}\dot{\mathbf{\Delta}} \delta \mathbf{\Delta}
\end{aligned} \tag{3.38}$$

where $\mathbf{C}$ is the damping matrix given by

$$\mathbf{C} = \begin{bmatrix} c_{uu} & c_{uv} & c_{uw} & \mathbf{C_{ur}} \\ c_{vu} & c_{vv} & c_{vw} & \mathbf{C_{vr}} \\ c_{wu} & c_{wv} & c_{ww} & \mathbf{C_{wr}} \\ \mathbf{C_{ru}} & \mathbf{C_{rv}} & \mathbf{C_{rw}} & \mathbf{C_{rr}} \end{bmatrix} \tag{3.39}$$

Therefore, the generalized forces are

$$Q_1 = P_u - c_{uu}\dot{u} - c_{uv}\dot{v} - c_{uw}\dot{w} - \mathbf{C}_{ur}\dot{\mathbf{\Delta}}_r \tag{3.40a}$$

$$Q_2 = P_v - c_{vu}\dot{u} - c_{vv}\dot{v} - c_{vw}\dot{w} - \mathbf{C}_{vr}\dot{\mathbf{\Delta}}_r \tag{3.40b}$$

$$Q_3 = P_w - c_{wu}\dot{u} - c_{wv}\dot{v} - c_{ww}\dot{w} - \mathbf{C}_{wr}\dot{\mathbf{\Delta}}_r \tag{3.40c}$$

$$Q_4 = -c_x v_{p,x} \left|v_{p,x}\right|^{\bar{n}-1} h_x \cos\theta \cos\varphi - c_y v_{p,y} \left|v_{p,y}\right|^{\bar{n}-1} h_y \cos\theta \sin\varphi \tag{3.40d}$$

$$Q_5 = c_x v_{p,x} \left|v_{p,x}\right|^{\bar{n}-1} h_x \sin\theta \sin\varphi - c_y v_{p,y} \left|v_{p,y}\right|^{\bar{n}-1} h_y \sin\theta \cos\varphi \tag{3.40e}$$

$$\mathbf{Q_r} = \mathbf{P}_r - \mathbf{C}_{ru}\dot{u} - \mathbf{C}_{rv}\dot{v} - \mathbf{C}_{rw}\dot{w} - \mathbf{C}_{rr}\dot{\mathbf{\Delta}}_r \tag{3.40f}$$

where the relative velocities of the damper, $v_{p,x}$ and $v_{p,y}$, are given in Eq. A.4.

3.5.1 Velocity-squared proportional auxiliary damping

For the case of velocity-squared proportional auxiliary damping $\bar{n} = 2$, the generalized forces corresponding to $\theta(t)$ and $\varphi(t)$ become

$$\begin{aligned} Q_4 = &-c_x h_x^3 \left(\cos^2\theta\cos^2\varphi\dot{\theta} - \sin\theta\cos\theta\sin\varphi\cos\varphi\dot{\varphi}\right)\left|\cos\theta\cos\varphi\dot{\theta} - \sin\theta\sin\varphi\dot{\varphi}\right| \\ &- c_y h_y^3 \left(\cos^2\theta\sin^2\varphi\dot{\theta} + \sin\theta\cos\theta\sin\varphi\cos\varphi\dot{\varphi}\right)\left|\cos\theta\sin\varphi\dot{\theta} + \sin\theta\cos\varphi\dot{\varphi}\right| \end{aligned} \tag{3.41a}$$

$$Q_5 = -c_x h_x^3 \left(-\sin\theta\cos\theta\sin\varphi\cos\varphi\dot{\theta} + \sin^2\theta\sin^2\varphi\dot{\varphi}\right)\left|\cos\theta\cos\varphi\dot{\theta} - \sin\theta\sin\varphi\dot{\theta}\right| \tag{3.41b}$$

$$- c_y h_y^3 \left(\sin\theta\cos\theta\sin\varphi\cos\varphi\dot{\theta} + \sin^2\theta\cos^2\varphi\dot{\varphi}\right)\left|\cos\theta\sin\varphi\dot{\theta} + \sin\theta\cos\varphi\dot{\varphi}\right| \tag{3.41c}$$

Substituting Eqs. 3.8, 3.17, 3.40, and 3.41 into Eq. 3.23 produces the differential equations of motion for the MDOF main structure coupled with the PTMD dynamics. The equations of motion corresponding to the translational degrees of freedom of the main MDOF structure remain unchanged (Eq. 3.24). The equation of motion corresponding to

the planar ($\theta(t)$-DOF) motion of the pendulum is

$$\begin{aligned}
&L_a\ddot{\theta} - L_a \sin\theta\cos\theta\dot{\varphi}^2 + \cos\theta\cos\varphi\ddot{u} + \cos\theta\sin\varphi\ddot{v} + \sin\theta\ddot{w} + g\sin\theta \\
&\quad + \frac{k_x h_x^2}{m_a L_a}\sin\theta\cos\theta\cos^2\varphi + \frac{k_y h_y^2}{m_a L_a}\sin\theta\cos\theta\sin^2\varphi \\
&\quad + \frac{c_x h_x^3}{m_a L_a}\left(\cos^2\theta\cos^2\varphi\dot{\theta} - \cos\theta\cos\varphi\sin\theta\sin\varphi\dot{\varphi}\right)\left|\cos\theta\cos\varphi\dot{\theta} - \sin\theta\sin\varphi\dot{\varphi}\right| \\
&\quad + \frac{c_y h_y^3}{m_a L_a}\left(\cos^2\theta\sin^2\varphi\dot{\theta} + \cos\theta\cos\varphi\sin\theta\sin\varphi\dot{\varphi}\right)\left|\cos\theta\sin\varphi\dot{\theta} + \sin\theta\cos\varphi\dot{\varphi}\right| = 0
\end{aligned} \tag{3.42}$$

The equation of motion corresponding to spherical ($\varphi(t)$-DOF) motion of the pendulum is

$$\begin{aligned}
&L_a\sin\theta\ddot{\varphi} + 2L_a\cos\theta\dot{\theta}\dot{\varphi} - \sin\varphi\ddot{u} + \cos\varphi\ddot{v} - \frac{k_x h_x^2 - k_y h_y^2}{m_a L_a}(\sin\theta\sin\varphi\cos\varphi) \\
&\quad + \frac{c_x h_x^2}{m_a L_a}\left(-\cos\theta\cos\varphi\sin\varphi\dot{\theta} + \sin\theta\sin^2\varphi\dot{\varphi}\right)\left|\cos\theta\cos\varphi\dot{\theta} - \sin\theta\sin\varphi\dot{\theta}\right| \\
&\quad + \frac{c_y h_y^2}{m_a L_a}\left(\cos\theta\cos\varphi\sin\varphi\dot{\theta} + \sin\theta\cos^2\varphi\dot{\varphi}\right)\left|\cos\theta\sin\varphi\dot{\theta} + \sin\theta\cos\varphi\dot{\varphi}\right| = 0
\end{aligned} \tag{3.43}$$

Eqs. 3.24 and 3.42 through 3.43 are the integrated finite element representation of a MDOF flexible structure with coupled dynamics of a PTMD for forced vibration with non-linear velocity-squared proportional auxiliary damping. For the case where damping is velocity proportional ($\bar{n} = 1$), the equations of motion simplify to those presented in Eqs. 3.24, 3.18, and 3.19.

3.5.2 Equivalent linear viscous damping

As a simplification, an equivalent linear damping coefficient is found using the equivalent power consumption approach proposed by Pekcan *et al* [73] for the case of velocity-squared proportional damping.

For velocity-dependant systems, power is an appropriate measure to seek equivalent linear damping properties. The method equates the power, or rate of energy dissipation, of the two damping systems over one cycle of sinusoidal loading. The average power consumption over one cycle for the non-linear damper ($\bar{P}_\alpha$) is equated to the linear damper ($\bar{P}_{eq}$) by

$$\bar{P}_\alpha = \bar{P}_{eq} \tag{3.44}$$

Eq. 3.44 seeks to equate the areas under the force-velocity curves, where

$$\bar{P}_\alpha = \frac{1}{1+\alpha} c_\alpha \dot{u}_0^{\alpha+1} \tag{3.45}$$

c_α is the non-linear damper coefficient in N s^2/m^2 (lbf s^2/in^2) and $\dot{u}_0$ is the maximum damper velocity in m/s (in/s). Also,

$$\bar{P}_{eq} = \frac{1}{2} c_{eq} \dot{u}_0^2 \tag{3.46}$$

where c_{eq} is the linear damper coefficient in N m/s. Note that Eq. 3.46 is the same as Eq. 3.45 with $\alpha = 1$. Solving the above equations for c_{eq} gives

$$c_{eq} = \frac{2}{1+\alpha} c_\alpha \dot{x}_0^{\alpha-1} \tag{3.47}$$

This equivalent linear damping coefficient can be used within the system of equations for linear auxiliary damping (c_x and c_y) in Sec. 3.3.

3.6 Wind-induced excitation from boundary layer wind tunnel studies

Several types of excitations have been considered in the analysis of tuned mass dampers (TMDs) using numerical models, for example, harmonic inputs [75, 74], earthquake time histories [75, 58], or broadband, filtered, or band-limited white noise [3, 28]. It has been

demonstrated that the performance of TMDs is generally overestimated when using the aforementioned conventional approaches rather than realistic wind loads measured from a wind tunnel study [104]. There is limited literature predicting the responses of structures equipped with TMDs using synthetic wind time histories [105, 77], or directly measuring the response of TMD-equipped structures through wind tunnel studies [88, 104]. The aforementioned approach, where scale models of the structure and the TMD are constructed and tested in a wind tunnel, suffers from inherent scale issues, particularly a limited ability to accurately model the auxiliary damping. The strength of using wind tunnel studies is the ability to accurately quantify the response characteristics for all wind directions and perform a statistical analysis using several return period wind events. While Eqs. 3.24, 3.18, and 3.19 can easily be handle various deterministic and specified excitations to systems, due to the nature of the application at hand, the aforementioned equations need to be capable of accepting experimental inputs (from wind tunnel studies) into the computational framework.

The high frequency base balance (HFBB) method is commonly adopted for predicting the response of structures to wind excitations using wind tunnel experiments. It was first developed in the early 1980s [91] and has been routinely applied for predicting wind-induced forces on tall structures. The structure's geometry is modelled using a lightweight, rigid scale model. This is mounted on a highly sensitive force balance device, which is capable of measuring the base overturning moments in each lateral direction as well as the torque. The base moments are measured within a wind tunnel while a design wind event is being simulated. The premise of the method is that the base overturning and torsional moments measured on a lightweight rigid scale model in a wind tunnel can be used to estimate the generalized forces exerted on the structure [91, 49]. Using classic modal analysis, the generalized force for the j^{th} mode of vibration is

$$w_j = \sum_{i}^{n} \left(w_{xi}\phi_{jx,i} + w_{yi}\phi_{jy,i} + w_{\theta i}\phi_{j\theta,i} \right) \tag{3.48}$$

where $i = 1, 2, \ldots, n$ denotes the rigid floor diaphragm at level i, w_{xi}, w_{yi}, and $w_{\theta i}$ are the generalize force components for the i^{th} rigid diaphragm in the x-, y-, and θ-directions,

respectively, and, and $\phi_{jx,i}$, $\phi_{jy,i}$, and $\phi_{j\theta,i}$ are the corresponding mode shape coefficients ($i = 1$ denotes the top of the structure). For linear lateral and constant torsional mode shapes, this becomes

$$w_j(t) = \phi_{jx,1}\frac{M_{yy}(t)}{h_n} - \phi_{jy,1}\frac{M_{xx}(t)}{h_n} + \phi_{j\theta,1}M_z z(t) \tag{3.49}$$

Once the generalized wind forces are estimated from the measurements, the following expression is used to calculate the standard deviation of the modal response (for the j^{th} mode) [92]:

$$\sigma_j = \frac{1}{K_j}\left[\int_0^\infty |H_j(\omega)|^2 S_{wj}(\omega)\ d\omega\right]^{\frac{1}{2}} \tag{3.50}$$

where

$$|H_j(\omega)|^2 = \frac{1}{\left[1 - \left(\frac{\omega}{\omega_{n,j}}\right)^2\right]^2 + \left(\frac{2\omega\zeta_j}{\omega_{n,j}}\right)^2} \tag{3.51}$$

is the mechanical admittance function, ζ_j is the modal damping, K_j is the generalized stiffness and $S_{wj}(\omega)$ is the power spectral density of the generalized wind forces.

The accuracy of the HFBB method is primarily based on the level of contribution to the overall response of the higher order modes. The underlying assumption is that the generalized forces are proportional to the measured base moments for structures with uncoupled mode shapes that are approximately linear. The response of the structure to the wind excitation is then determined by solving the generalized form of the equations of motion. The main advantage of the HFBB method is that, under the simplifying assumptions of mode shape linearity and broadband stationary excitation, the response of the structure can be solved in closed form using random vibration theory. For nonlinear and coupled mode shapes, correction factors can be applied [34, 108, 110, 8, 57, 92]. However, applying the modes which uncouple the main system to the PTMD controlled system does not allow the overall system of equations to be solved in the frequency domain. Hence, the solution to the case of the structure equipped with a PTMD can be pursued in the time domain, as explained next.

The equations of motion for the flexible structure coupled with a planar-spherical PTMD (Eqs. 3.24, 3.18, and 3.19) are cast in the generalized form to include rotation about the vertical axis and translation in each horizontal direction. It is assumed that the mode shapes of the primary structure are not affected by the addition of the PTMD, and that the mode shapes for the primary translational modes remain linear. The modal responses for the main structure are transformed back into the physical domain at each time step and the control force is calculated, in order to account for the coupling between the pendulum and the main structure in the physical domain. The control force is transformed into modal coordinates and applied to the structure together with the generalized force measured using the HFBB. The equations of motion in the modal domain for the j^{th} mode are

$$M_j \ddot{y}_j(t) + C_j \dot{y}_j(t) + K_j y_j(t) = u_j(t) + w_j(t) \tag{3.52}$$

where

$$M_j = \phi_j^T \left\{ \mathbf{M} + \begin{bmatrix} m_a & 0 & 0 & \mathbf{0} \\ 0 & m_a & 0 & \mathbf{0} \\ 0 & 0 & 0 & \mathbf{0} \\ \mathbf{0} & \mathbf{0} & \mathbf{0} & \mathbf{0} \end{bmatrix} \right\} \phi_j \tag{3.53}$$

Note that the first three degrees of freedom of the mass matrix correspond to the translation in the x- and y-direction and rotation about the z-direction of the rigid diaphragm mass to which the PTMD is fixed. Similarly, the generalized damping, C_j is given by $C_j = \phi_j^T \mathbf{C} \phi_j$, where $\mathbf{C}$ is the proportional damping matrix of the main system, and $K_j = \phi_j^T \mathbf{K} \phi_j$, where $\mathbf{K}$ is the stiffness matrix of the main structure. The mass moment of inertia of the pendulum about its own axis is neglected.

The generalized wind force, $w_j(t)$, is measured directly from the HFBB model.

$$w_j(t) = X_{jx}\phi_{j1}\frac{M_{yy}(t)}{h_n} - X_{jy}\phi_{j2}\frac{M_{xx}(t)}{h_n} + X_{jzz}\phi_{j3}M_{zz}(t) \tag{3.54}$$

where M_{xx}, M_{yy}, and M_{zz} are the base moments about the x-, y-, and z-axis, respectively, and h_n is the height of the structure. The coefficients ϕ_{j1}, ϕ_{j2}, and ϕ_{j3} are the x-, y-, and θ_z-components of the mode shape coefficients at the top of the building for the j^{th} mode.

The commonly used mode shape correction factors of $X_{jx} = X_{jy} = 1$ and $X_{jzz} = 0.7$ [92] are introduced to account for non-ideal mode shapes.

The modal domain control force, $u_j(t)$ exerted on the structure by the PTMD is transformed into the modal domain using

$$u_j(t) = \left\{ \begin{array}{c} \phi_{1j} \\ \phi_{2j} \end{array} \right\}^T m_a L_a \left\{ \begin{array}{l} -\cos\varphi\ddot{\theta} + \theta\cos\varphi\dot{\theta}^2 + 2\sin\varphi\dot{\theta}\dot{\varphi} + \theta\sin\varphi\ddot{\varphi} + \theta\cos\varphi\dot{\varphi}^2 \\ -\sin\varphi\ddot{\theta} + \theta\sin\varphi\dot{\theta}^2 - 2\cos\varphi\dot{\theta}\dot{\varphi} - \theta\cos\varphi\ddot{\varphi} + \theta\sin\varphi\dot{\varphi}^2 \end{array} \right\} \tag{3.55}$$

$\theta(t)$ and $\varphi(t)$ and their first and second time derivatives are found by solving the corresponding equations of motion with $\ddot{w} = 0$; $\ddot{u}$ and $\ddot{v}$ are found by transforming the modal responses back into physical coordinates at each time step by the following transformation:

$$\ddot{u} = \sum_{j=1}^{N} \phi_{j1}\ddot{y} \tag{3.56a}$$

$$\ddot{v} = \sum_{j=1}^{N} \phi_{j2}\ddot{y} \tag{3.56b}$$

These transformations are necessary since the calculation of the control forces, according to Eq. 3.55, depend on the physical coordinates. At each time step, the following operations are carried out. First, the main structure dynamic analysis is carried out in the modal domain, since the generalized force is directly measurable from the HFBB model. Second, the directional coupling of the PTMD is captured in physical domain, by first transforming the acceleration responses for the suspension point into the physical coordinates ($\ddot{u}(t)$ and $\ddot{v}(t)$) at each time step. Third, the control force exerted by the PTMD on the main structure is transformed back into modal coordinates. In doing so, the HFBB method can be adapted to solve the nonlinear PTMD equations in the time domain.

Having provided the necessary background information on the equations of motion and the HFBB method, the estimation of optimal PTMD parameters is pursued next.

Chapter 4

Parametric studies of a PTMD

The primary focus of many studies on the subject of tuned mass dampers (TMDs) has been to estimate the optimal design parameters [18, 41, 89, 1, 75, 58, 3, 28]. The majority of studies have considered translational-type TMDs, with relatively little attention given to pendulum tuned mass dampers (PTMDs) [26, 78, 79]. This is despite many PTMD applications in full-scale structures today.

Previous studies of PTMDs have considered linearized planar pendulum models coupled with structural models in the modal domain to find the optimal auxiliary stiffness and damping, and to determine the structural responses [26]. Such models are adequate, for example, in analyzing the response of flexible structures where the dominant response is believed to be primarily in one direction. When the responses in both along-wind and across-wind directions are of concern, then it is important to realistically model the effect of the PTMD by including its three-dimensional behaviour.

The main objectives of this chapter within the context of the proposed work on condition assessment are two-fold:

(i) Develop numerical estimates for the optimal design parameters that will be subsequently used in the condition assessment step.

(ii) Compare the design estimates obtained with existing values in the literature.

Both these objectives will be met using extensive numerical simulations. The nonlinear nature of the governing equations does not lend itself to closed-form equations. It will be shown that the optimal design parameters depend on the modal characteristics of the bare structure, and hence in order to perform condition assessment, it will be necessary to estimate the bare modal properties, in addition to other measures such as equivalent damping (Chapter 6).

This chapter is organized in two main sections. First, various means to assess the performance of TMDs are reviewed and the effects of frequency and damping detuning are demonstrated. Additionally, the effect of increasing the auxiliary to main mass ratio of the damping device is also investigated. Second, a parametric study of the numerical model of a PTMD developed in Chapter 3 is performed, where the biaxial motion of the mass is considered in order to establish the optimal damper parameters. These results are compared with the simplified planar models presented in the literature. Design equations are developed using curve fitting techniques to predict optimal damper parameter when the bare structure's modal properties are known. These can then be compared to as-measured PTMD parameters in the condition assessment stage.

4.1 Parametric studies

The optimal design parameters consists of the optimal mass ratio, μ, frequency ratio, $f_{r,opt}$, and auxiliary damping ratio, $\zeta_{a,opt}$. The mass ratio, μ, is a ratio of the auxiliary mass, m_a, to the modal mass, $M_{r,j}$, for the mode to be controlled (typically, the fundamental mode of vibration). The frequency ratio is the ratio of the frequency of the PTMD to the natural frequency of the main system and is directly related to the pendulum length, L. The damping ratio, the ratio of the auxiliary damping coefficient to the critical auxiliary damping, is directly related to the auxiliary damping coefficients, c_x and c_y.

4.1.1 Assessing the performance of PTMDs

There are two primary approaches for quantifying TMD performance. The first is a concept known as effective damping or equivalent damping. The term refers to a single-degree-of-freedom (SDOF) system with damping parameter, ζ_e with the same performance of the combined main and auxiliary system. This is accomplished by equating the root mean squared (RMS) displacement response of the combined main-TMD structure with that of a SDOF oscillator with the same natural frequency, and solving for the damping in the SDOF system. Equations which relate the effective damping introduced by the TMD are available for the case of main mass-excited structures [66] and base excited structures [26], for both conventional translational TMDs and PTMDs [26]. Maximizing the effective damping introduced by the TMD has been used as a cost function for selecting optimal damper parameters by various researchers [55, 88, 94].

The approach for calculating the effective damping introduced by a TMD is quite simple and is easily theoretically demonstrated. However, it requires knowledge of the RMS displacement response of the primary system, which is not directly available from acceleration response measurements and must be inferred. This issue is of particular importance when the performance of an in-service TMD must be demonstrated to verify that a prescribed level of effective damping has been achieved. This issue is explored more closely in Chapter 6.

The second and more common means of quantifying performance of TMDs is to measure their ability to reduce the responses of the main structure. Generally, the RMS displacement or acceleration responses for the combined system are determined and compared with the uncontrolled structural responses. The result is normalized with respect to the uncontrolled structure, and the reduction is reported. In the conventional design of TMDs, the displacement response has largely been considered.

From a designer's perspective, the desire is to reduce the peak or RMS acceleration response at the top floors to within acceptable levels for various return period events [104]. Therefore, in assessing the performance of TMDs and determining optimal parameters, the acceleration response should be used. Xu and Kwok found that normalized performance

improvement, expressed as a percent reduction in the response, was comparable regardless of whether displacement or acceleration responses were considered, but that the optimal damper parameter varied depending on the selection of the cost function [104].

The present work is proposed in the context of improving occupant comfort in tall structures; therefore, the ensuing study will measure performance based on the TMD's ability to reduce the acceleration response of the structure and optimal damper parameters will be found using the acceleration response cost function. It must also be stated that, particularly for longer return period events, the reduction in the displacement response of the structure must be investigated, as excessive displacement may result in damage to the structure's finishes.

4.1.2 Effect of detuning

Detuning of a TMD is said to occur if there is a substantial difference between the as-built and theoretical optimal values of the auxiliary parameters. Causes of detuning include structural deterioration, inadvertent changes to the structure, design forecasting, or varying mass due to occupancy. To demonstrate the effect of detuning, a single main mass system is used, free to translate in each direction, coupled with a three-dimensional PTMD.

The effect of inaccurately predicting the current or future structural condition, causing the absorber to move outside the frequency range, is investigated. The optimal PTMD parameters were determined from from a numerical search approach, where the main system acceleration response was minimized. From Eq. 2.12, the optimal length is inversely proportional to the natural frequency, ω_a, and subsequently directly proportional to the main mass and inversely proportional to the stiffness. In predicting the structural condition, the designer's tendency is to employ a conservative design approach, overestimating the mass and underestimating the stiffness. For example, if the mass were overestimated by 10%, and the stiffness underestimated by 10%, then the resulting calculated optimal pendulum length, L, would be 22% greater than the actual optimal pendulum length.

To demonstrate the effect of frequency detuning, the auxiliary damping was set to its optimal value, and the pendulum length was varied. Pendulum length was selected to be

optimal based on the design equations presented in Eq. 2.19 after introducing the errors in the mass and stiffness design forecasts. The system was excited by a series of harmonic excitations. The peak acceleration response at each frequency was plotted in Fig. 4.1 for the various cases. A 1% mass ratio is considered.

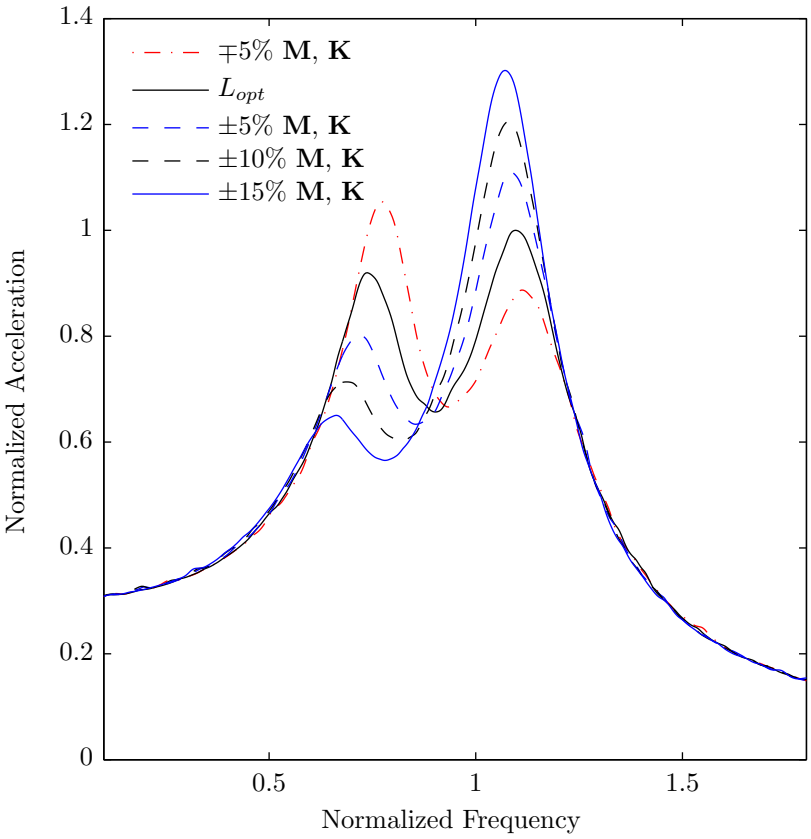

Figure 4.1: Effect of frequency detuning resulting from design forecasting for optimal auxiliary damping

Even small variations in the design forecast of the structure's mass and stiffness can result in TMD performance issues; for this particular example, peak acceleration response increases of 30% are reported for the case of harmonic excitations. A similar analysis was undertaken to investigate the effect of damping detuning for the case of optimal pendulum

length selection, with auxiliary damping coefficients ranging from $0.5c_{opt}$ to $2c_{opt}$. The selection of damping is inherently more robust and less susceptible to the effects of detuning. The results are presented in Fig. 4.2 and are normalized with respect to the optimal case.

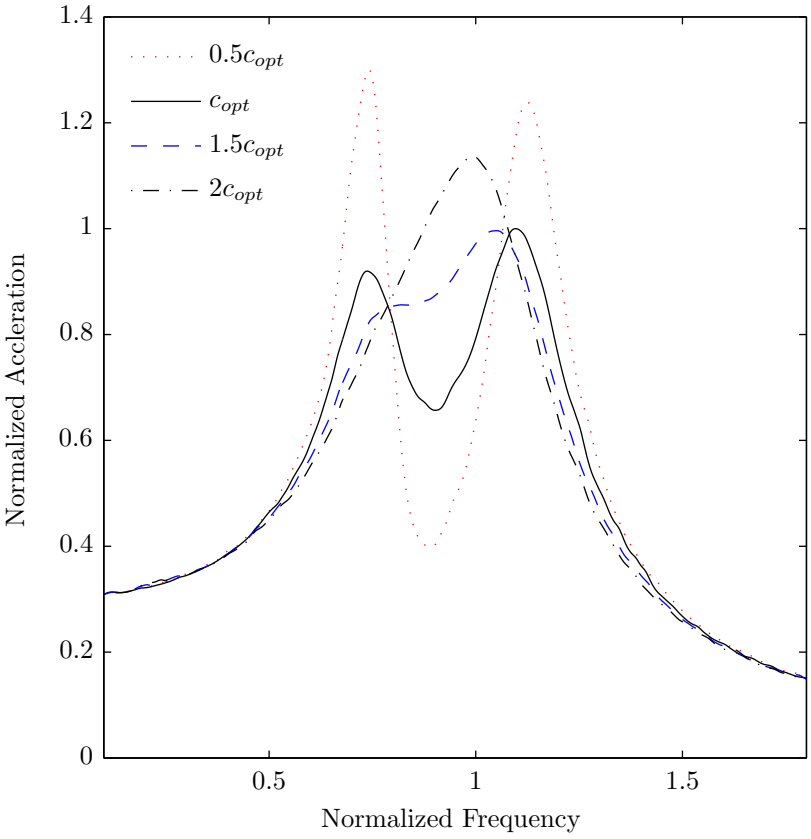

Figure 4.2: Effect of damping detuning for optimal pendulum length

The performance degradation for suboptimal damping coefficients is more pronounced than for super-optimal damping coefficients. Therefore, in selecting optimal auxiliary damping, the design should ensure it is at least optimal [83]. Other reasons for selecting damping coefficients above optimal are to reduce the motion of the TMD, where space constraints are a concern, or to guarantee more uniform performance to varying excitations at the expense of a reduction in optimal performance.

4.1.3 Effect of mass ratio

For practical applications, it is important to understand under what conditions the effect of detuning will become important. In this study, this issue is specifically addressed from the standpoint of detuning versus the auxiliary to main mass ratio of the PTMD. To evaluate the effect of the mass ratio on the optimal auxiliary parameters $f_{r,opt}$ and $\zeta_{a,opt}$, a mass, free to translate in each direction, coupled with a planar-spherical PTMD is considered. Main mass damping is fixed at 2% for illustration purposes, and mass ratios of $\mu = 0.01$, 0.02, 0.03, 0.05, 0.07, and 0.09 are considered. The system is excited in both horizontal directions by Gaussian white noise. The auxiliary damping coefficient and pendulum length are varied, and the RMS of the acceleration response in the horizontal plane is used as the performance indicator. The results are averaged over many realizations of the input. Fig. 4.4 shows the variation in the optimal auxiliary damping coefficient at various mass ratios for a fixed pendulum length, and Fig. 4.3 shows the change in optimal pendulum length at various mass ratios for a fixed level of auxiliary damping. Both axes are normalized with respect to the optimal values for the $\mu = 1\%$ mass.

Several observations can be made regarding the optimal parameters as the mass ratio is increased. First, the optimal pendulum length decreases slightly with increasing mass ratio. Second, the sensitivity to frequency detuning reduces as the mass ratio increases, indicated by the flattening of the curves in Figs. 4.3 and 4.4. This implies that selection of optimal damper parameters for higher mass ratios is less critical, and reasonable performance can be expected even when the auxiliary parameters are away from their optimal values. The optimal pendulum length curves (Figure 4.3) become flatter in both directions with increasing mass ratio, implying similar performance is expected for a PTMD that has a pendulum length away from the optimal length, regardless of whether it is shorter or longer than optimal.

The optimal auxiliary damping coefficient is also less susceptible to detuning as the mass ratio increases, but only for damping greater than the optimal level, as seen in Fig. 4.4. Therefore, in selecting the level of auxiliary damping for higher mass ratios, it is critical that the damping coefficient is at least optimal. The optimal damping coefficients increase

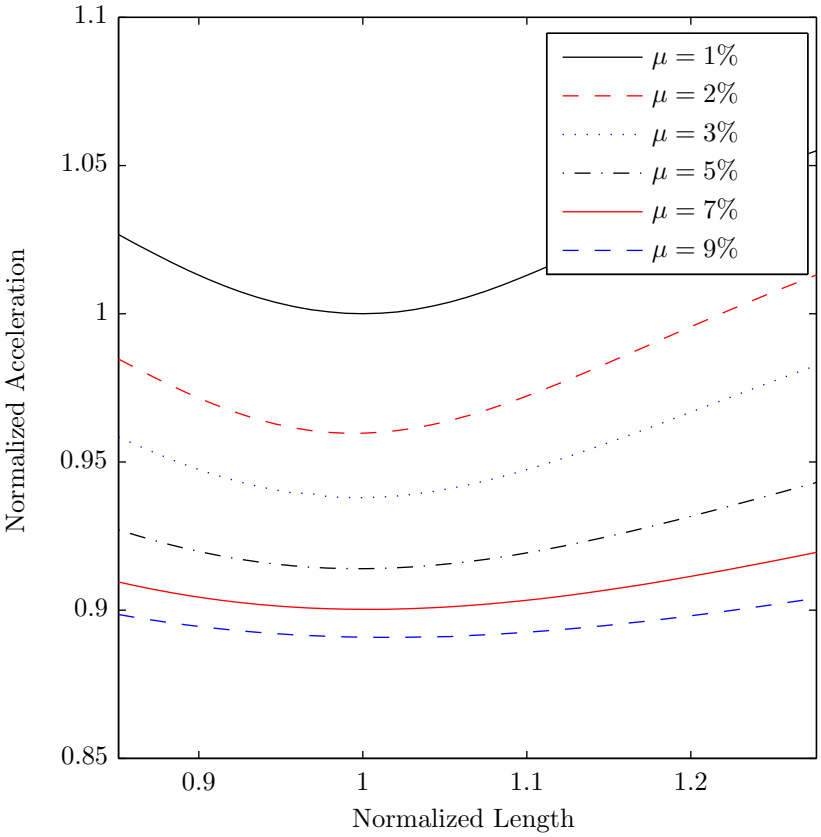

Figure 4.3: Sensitivity of frequency parameter (pendulum length L) to auxiliary to main mass ratio, μ, for optimal auxiliary damping.

with mass ratio, indicating that the structure must be designed to withstand a larger control force. Frequently the selection of the damping coefficient is to reduce the stroke of the TMD, and subsequently the space requirements. As Fig. 4.4 indicates, this comes at the cost of a substantial performance sacrifice for lower mass ratios. Therefore, the designer may want to consider the impact of a larger or more dense mass, above-optimal damping, and larger mass ratios when the amount of space available for an auxiliary damping device is the primary design concern.

There are a few important considerations when selecting the auxiliary to main mass

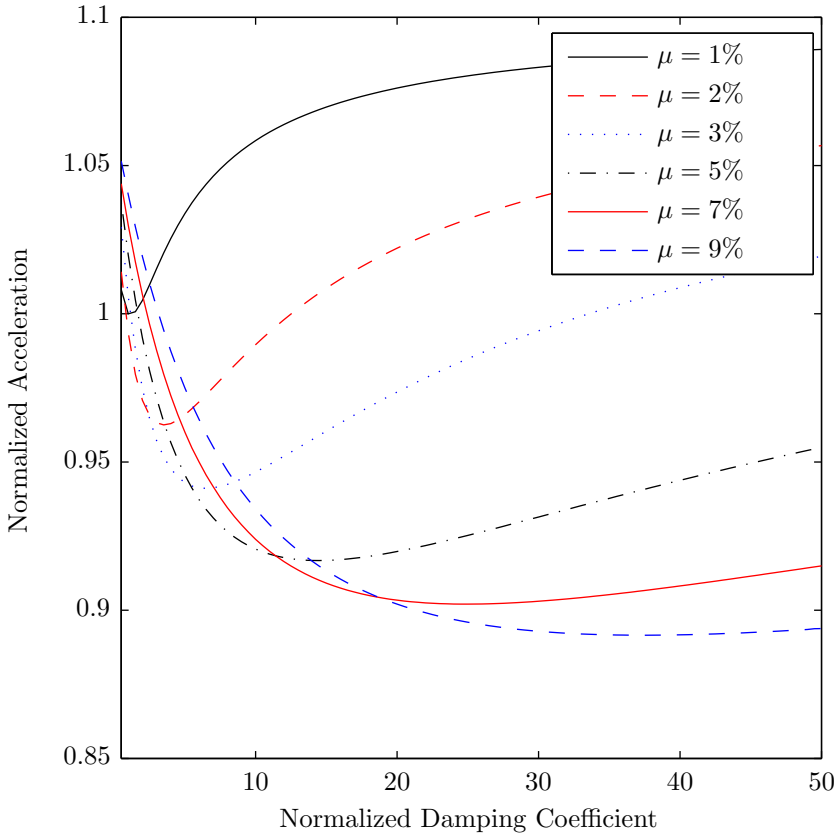

Figure 4.4: Sensitivity of auxiliary damping parameter (c_a) to auxiliary to main mass ratio, μ, for optimal pendulum length.

ratio. It is desirable to reduce the auxiliary to main mass ratio as this reduces the overall weight of the materials and the size of the dampers; however, as has been demonstrated, higher mass ratios offer better performance. Even though it is well known that the performance of a TMD increases with increasing mass ratio, often the mass ratio is determined by other design considerations and project constraints. Hence, the ensuing study assumes the designer has the ability to select an auxiliary mass based on such constraints and focuses on determining the optimal auxiliary damping and pendulum length for a range of mass ratios.

Mass ratios greater than $1\% - 2\%$ are difficult to practically attain for the application of tall buildings, so the issues associated with detuning remain a concern. A recent trend is emerging where researchers are considering the effects of using segmented upper stories or sliding roof systems as mass damping systems, where much higher mass ratios can be achieved economically and without the typical space limitations [16, 9, 10, 90, 111, 21].

4.2 PTMD design equations

Values for the optimal frequency ratio and auxiliary system damping ratio under random main mass excitation are calculated using two main approaches. The first seeks to minimize the RMS displacement response of the primary system using closed-form solutions that are documented in the literature [26]. The approach relies on the presence of "fixed-point" frequencies, where the transmissibility of vibration is independent of the auxiliary damping; for structures that exhibit main mass damping, these frequencies no longer exist. Therefore, closed-form solutions are only possible for the special case of an undamped primary structure [26, 75, 3]. However, close agreement with numerical results for low to moderate main mass damping in structures has been demonstrated by approximating the fixed-point frequencies [28].

The second approach, which is necessary for structures with a damped primary system, involves a numerical search. The optimal values for the parameters are determined using simulations of the coupled response of the primary and auxiliary systems. Results have been demonstrated by several researchers for conventional translational TMDs [41, 97, 89, 3] and PTMDs [26]. Even in numerical approaches, many researchers have used linearized equations. Hence, the issues in accurately predicting the responses still remain.

4.2.1 Closed-form solution

Consider a multi-degree-of-freedom (MDOF) system with a PTMD (Figure 3.1b). The equations of motion given in Eqs. 3.25a and 3.25b are simplified for a mixed 2-degree-of-

freedom (DOF) system, one translational (primary) in the modal domain and one rotational (auxiliary).

$$M_{r,j}\ddot{y}_j(t) + C_{r,j}\dot{y}_j(t) + K_{r,j}y_j(t) + m_a\ddot{y}_j(t) + m_aL\ddot{\theta}(t) = F_{r,j}(t) \tag{4.1}$$

and

$$m_aL^2\ddot{\theta}(t) + c_ah^2\dot{\theta}(t) + \left(m_agL + k_ah^2\right)\theta(t) + m_aL\ddot{y}_j(t) = 0 \tag{4.2}$$

where $M_{r,j}$, $C_{r,j}$, $K_{r,j}$, and $F_{r,j}(t)$ are the modal mass, damping, stiffness, and force of the primary system for the j^{th} mode, which is to be controlled. Here the primary system is modelled as a SDOF system with a translational modal coordinate $y(t)$. The auxiliary system has a rotational DOF $\theta(t)$, auxiliary mass, m_a, pendulum length L, and distance between the suspension point and the spring/damper attachment point, h. The auxiliary stiffness is comprised of the inherent stiffness of the pendulum, m_agL, and the auxiliary spring with stiffness k_a; c_a is the damping of the auxiliary damper.

The damping ratio, ζ_a, for a PTMD is defined as

$$\zeta_a = \frac{c_ah^2}{2m_aL_a^2\omega_a} \tag{4.3}$$

where the circular natural frequency of the auxiliary system, ω_a, is given by

$$\omega_a = \sqrt{\frac{m_agL_a + k_ash^2}{m_aL^2}} \tag{4.4}$$

which simplifies to $\omega_a = \sqrt{g/L_a}$ for the case where there is no auxiliary spring. Optimum tuning parameters for PTMDs have been presented in the literature that minimize the RMS displacement response of the primary system, for the case of the undamped primary system [26]. The optimal frequency ratio for force excited main mass with a PTMD, where

the mass is assumed to be lumped at the free end of the pendulum length, is

$$f_{opt} = \frac{\omega_{2_{opt}}}{\omega_1} = \frac{\sqrt{1+\mu\left(1-\frac{3}{2r_a}\right)}}{1+\mu} \tag{4.5}$$

The optimal auxiliary damping ratio is

$$\zeta_{a,opt} = \sqrt{\frac{\mu+\mu^2\left(1-\frac{1}{4r_a}\right)}{4r_a+2\mu\left(4r_a-1\right)+2\mu^2\left(2r_a-1\right)}} \tag{4.6}$$

where

$$r_a = \frac{I_a}{m_a L^2} \tag{4.7}$$

and I_a is the moment of inertia of the mass about the suspension point. For a point mass, $I_a = m_a L^2$ ($r_a = 1$), and the optimal auxiliary parameters simplify to

$$f_{r,opt} = \frac{\omega_{a_{opt}}}{\omega_n} = \frac{\sqrt{1+\frac{\mu}{2}}}{1+\mu} \tag{4.8}$$

where $\omega_{n,j} = \sqrt{K_{r,j}/M_{r,j}}$ is the undamped circular natural frequency of the primary system, The optimal auxiliary damping ratio is

$$\zeta_{a,opt} = \sqrt{\frac{\mu+\frac{3\mu^2}{4}}{4+6\mu+2\mu^2}} \tag{4.9}$$

4.2.2 Planar PTMD with main mass damping

Since main mass damping is considered and the designer is generally interested in reducing the acceleration response of the structure, a numerical search approach is employed to determine the optimal damper parameters. Various numerical simulations were performed and averaged for main mass damping ratios of $\zeta_p = 1\%$ to 5% and auxiliary to main mass ratios varying from $\mu = 0.01$ to 0.15. The equations of motion were implemented in Simulink [40] using state-space representation and the numerical integration was performed

using Runge-Kutta method. The RMS acceleration response (rather than displacement) of the main mass was used as the performance index, since the PTMD is usually designed to reduce this response to within acceptable serviceability criteria limits [104]. Using standard curve fitting techniques, the following relationships were found for the optimal frequency and auxiliary damping ratios:

$$f_{r,opt} = -0.64\mu - 0.23\zeta_p + 0.99 \tag{4.10a}$$

$$\zeta_{a,opt} = -4.89\mu^2 + 1.89\mu + 0.018 \tag{4.10b}$$

The proposed design equations for the planar PTMD are plotted in Figs. 4.5 and 4.6 for 1%, 3%, and 5% main mass damping together with the closed-form solutions for no main mass damping (Eqs. 4.8 and 4.9).

4.2.3 Planar-spherical PTMD with main mass damping

In order to determine the optimal damper parameters from the combined planar-spherical PTMD model, a numerical search method is employed using a 5-DOF model with x-, y-, and z-translational degrees of freedom as well as θ and φ. Several simulation trials are performed using a broadband white noise main mass excitation, and a cost function is evaluated each time based on the RMS acceleration response in both horizontal directions. The optimal frequency and damping ratios are determined for various main structure damping ratios and auxiliary to main mass ratios. Damping ratios from 1% to 5% critical in the primary structure were considered. Auxiliary to main mass ratios ranged from 0.005 to 0.125. To simplify the analysis, the auxiliary damping in the x- and y-directions are assumed to be equal ($c_x = c_y$). Also, the damper attachment point coincides with the pendulum length ($h_x = h_y = L$). Finally, no additional auxiliary stiffness was introduced in the form of auxiliary springs ($k_x = k_y = 0$). The optimal frequency ratio found using the numerical search method is shown in Fig. 4.7 together with the closed-form solution for no main mass damping (Eqs. 4.8).

The optimal frequency ratio results demonstrate less sensitivity to mass ratio than

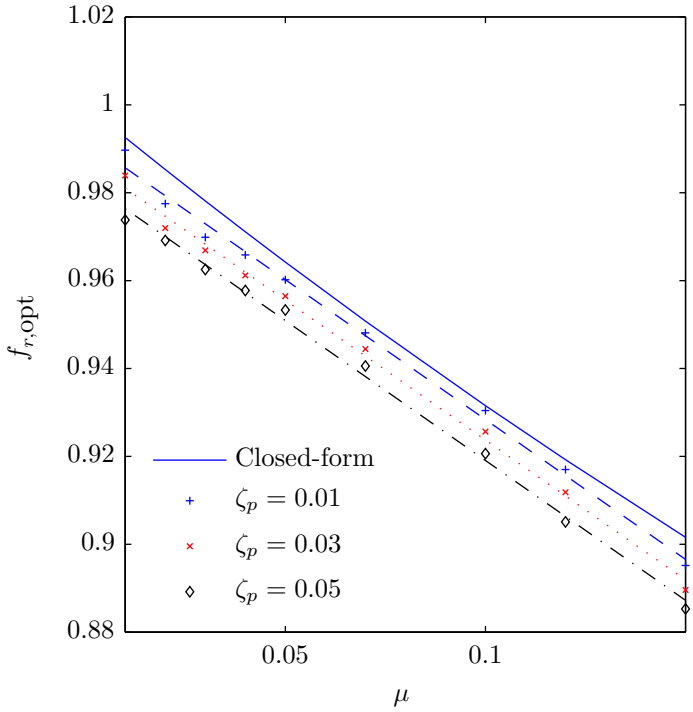

Figure 4.5: Optimal frequency ratio for a planar PTMD found using a numerical search algorithm for $\zeta = 1\%$, 3%, and 5%.

what is predicted by the closed-form solutions and the numerical search of the planar PTMD model. Furthermore, varying the main mass damping has the effect of changing the sensitivity of the frequency ratio to the mass ratio. For the main mass damping ratios considered, the sensitivity of the results indicate that the primary system damping and auxiliary to main mass ratio do not play a significant role in the selection of the optimal frequency ratio. For large mass ratio, a disparity in the optimal frequency ratio presents itself. However, it has already been demonstrated that the increasing mass ratio reduces the sensitivity to errors in the auxiliary damper parameter selection. Therefore, it is not expected that selecting the optimal damper parameters based on the closed-form solutions will have a significant impact on the performance of the TMD, even for higher mass ratios.

The optimal damping ratio found using the numerical search method is shown in Fig.

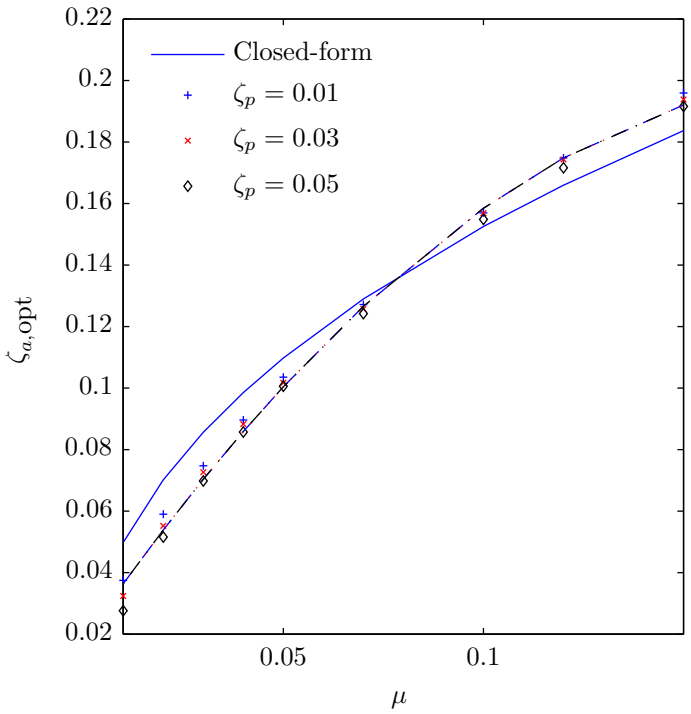

Figure 4.6: Optimal auxiliary damping ratio for a planar PTMD found using a numerical search algorithm for $\zeta = 1\%$, 3%, and 5%.

4.8 together with the closed-form solution for no main mass damping (Eq. 4.9). The numerical search of the planar-spherical system resulted in slightly greater damping ratios than the closed-form optimal auxiliary damping equations. For mass ratios of less than approximately 3%, optimal auxiliary damping ratios decreased with increasing main mass damping ratios, and increased with increasing mass ratios for mass ratio greater than approximately 3%. As the mass ratios moves into the upper range of the values considered, the disparity between the closed-form optimal auxiliary damping and the planar-spherical prediction grows, with the latter producing greater optimal auxiliary damping.

Using standard curve fitting techniques, the following relationships were found for the

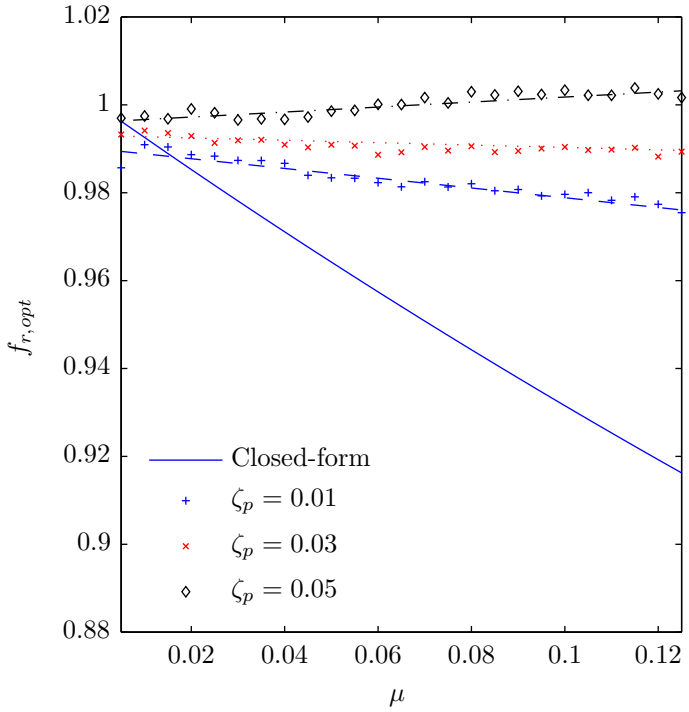

Figure 4.7: Optimal frequency ratio for a planar-spherical PTMD found using a numerical search algorithm for $\zeta = 1\%$, 3%, and 5%.

optimal frequency and auxiliary damping ratios:

$$f_{r,opt} = (4.2\zeta_p - 0.15)\,\mu + 0.15\zeta_p + 0.99 \tag{4.11a}$$

$$\zeta_{a,opt} = (-45\zeta_p - 2.4)\,\mu^2 + (9.7\zeta_p + 1.5)\,\mu - 0.22\zeta_p + 0.05 \tag{4.11b}$$

Once the frequency and damping ratios are calculated, they can be converted into the appropriate physical parameters. When no auxiliary springs are included ($k_x = k_y = 0$), the optimal pendulum length is related to the frequency ratio by the following relationship:

$$L_{opt} = \frac{g}{f_{r,opt}^2 \omega_{n,j}^2} \tag{4.12}$$

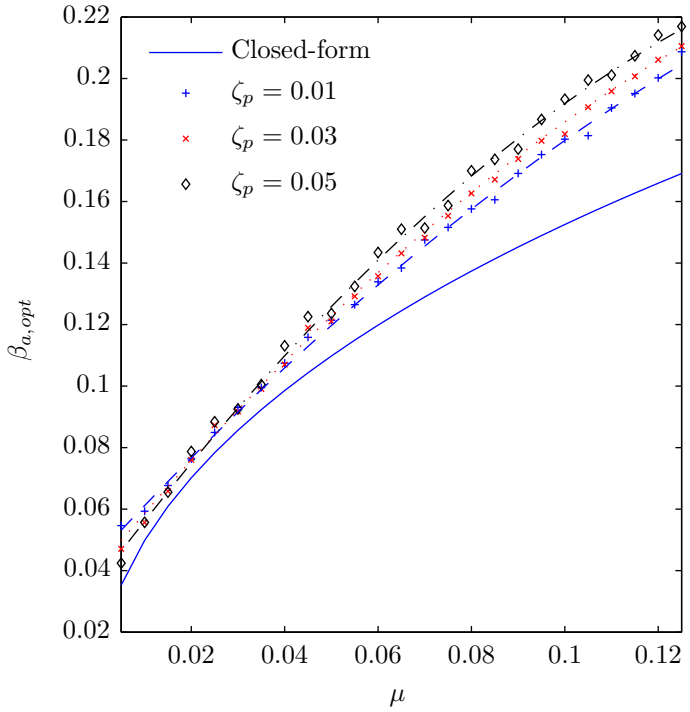

Figure 4.8: Optimal auxiliary damping ratio for a planar-spherical PTMD found using a numerical search algorithm for $\zeta = 1\%$, 3%, and 5%.

The optimal auxiliary damping is related to the damping ratio by the following relationship:

$$c_{a,opt} = 2\zeta_{a,opt} m_a f_{r,opt} \omega_{n,j} \tag{4.13}$$

The different approaches differed in their prediction of the optimal damper parameter, particularly at higher mass ratios. However, it is not expected that the variation in the optimal parameter predicted by each approach will have a significant impact in the overall performance of the structure. For low mass ratios, the optimal frequency and damping ratios are similar. For higher ratios, it is expected that the reduced sensitivity to detuning will overcome the error in the incorrect optimal parameter estimates. This will be investigated further in Chapter 7.

In order to predict the optimal auxiliary parameters, the underlying structure's natural frequencies, and to a lesser extent, damping ratios and mode shape vectors need to be determined. For the purpose of condition assessment, these bare structure parameters must be identified from response data of the combined main-auxiliary system. Therefore, determining the underlying modal properties from TMD attenuated acceleration response measurements is considered next.

Chapter 5

Extended Kalman filter as a parameter estimation tool

The fundamental question that needs to be answered for the condition assessment of tuned mass dampers (TMDs) is how well the design estimates for the optimal TMD parameters (in Eqs. 4.11a and 4.11b) represent the actual as-built condition. In other words, this is a check to assess and quantify detuning. The answer to this question lies in the estimation of the mass ratio (μ), the natural frequency ($\omega_{n,j}$), and modal damping (ζ_j) for the controlled mode. Assuming that the mass of the structure is known with a good degree of confidence, then the design parameters can be obtained by estimating the corresponding mode shape (mode to which the TMD is tuned to), natural frequency, and modal damping ratio. In some applications, several TMDs can be tuned to multiple modes, or a single adaptive TMD can be tuned to several modes depending on the dominant mode that is being excited (for example, in pedestrian bridges). In all these cases, the fundamental task is one of estimating the bare modal characteristics based on measurements. Due to practical limitations in imparting controlled force excitations, the process of estimating these parameters has to rely on ambient vibration measurements only.

Only a handful of studies have considered this issue in the literature [30, 99, 59]. While some of them utilize heuristic or experience-based approaches using approximations (only

for the frequency and damping) [99], others employ nonparametric data-driven modal identification approaches [30, 59], where the modal characteristics for the combined system are identified. To the author's knowledge, no previous studies have sought to directly identify the underlying structure's modal properties from the attenuated response measurements. The aforementioned methods do not provide a convenient means to deploy these estimation algorithms for online estimation to be used in control devices. Practitioners have overcome this difficulty by restraining the TMD motion and performing condition assessment [78]. While restraining the TMD and undertaking modal identification may suffice for condition assessment, this course of action is not suitable for online control. Furthermore, the process of restraining the TMD is both labour intensive and time consuming.

In this chapter, a methodology to identify the modal properties of the bare structure using ambient vibration measurements obtained from the structure while the TMD is in operation, is proposed. The main advantages of this method are that the estimation process can be implemented online using measurement data only and can be used equally effectively for both condition assessment and online control. Additionally, the proposed approach makes no assumption about the present performance of the TMD; that is, whether the TMD's parameters are near or far from their optimal values.

5.1 Kalman filter as an estimation tool

The concept of state estimation is extended for the purpose of parametric identification within the present work. State estimation is performed by modelling a process in order to provide an estimate of an internal (generally unobserved) state given measurements of the output of the actual system. The Kalman filter is first introduced, as it is classically used for state estimation problems. In its most limited form, state estimation is performed using a mathematical model of a known physical system, relating the known inputs, measured outputs, and unknown internal states to be determined.

5.1.1 Kalman filter for state estimation

The Kalman filter, first published by R. E. Kalman [45], addresses the problem of estimating the state vector $\mathbf{x}_k$ based on knowledge of the linear discrete-time process given by

$$\mathbf{x}_k = \mathbf{A}_{k-1}\mathbf{x}_{k-1} + \mathbf{G}_{k-1}\mathbf{u}_{k-1} + \mathbf{w}_{k-1} \tag{5.1}$$

with noisy measurement $\mathbf{z}_k$ given by

$$\mathbf{z}_k = \mathbf{C}_k\mathbf{x}_k + \mathbf{v}_k \tag{5.2}$$

where $\mathbf{A}_k$, $\mathbf{G}_k$, and $\mathbf{C}_k$ are the discrete time system equations, which may vary with each time step. The vectors $\mathbf{x}_k$ and $\mathbf{u}_k$ are the state and input vector at the k^{th} time step. The process or disturbance noise $\mathbf{w}_k$ and measurement noise $\mathbf{v}_k$ are assumed to be zero mean, white, uncorrelated, and have known covariances $\mathbf{Q}_k$ and $\mathbf{R}_k$, respectively. That is,

$$\mathbf{w}_k \sim (0, \mathbf{Q}_k) \tag{5.3a}$$
$$\mathbf{v}_k \sim (0, \mathbf{R}_k) \tag{5.3b}$$
$$E\left[\mathbf{w}_k\mathbf{w}_j^T\right] = \mathbf{Q}_k\delta k, j \tag{5.3c}$$
$$E\left[\mathbf{v}_k\mathbf{v}_j^T\right] = \mathbf{R}_k\delta k, j \tag{5.3d}$$
$$E\left[\mathbf{w}_k\mathbf{v}_j^T\right] = \mathbf{0} \tag{5.3e}$$

where $\delta_{k,j}$ is the Kronecker delta function; $\delta_{k,j} = 1$ for $k = j$ and $\delta_{k,j} = 0$ for $k \neq j$. Define two estimates of the quantity $\mathbf{x}_k$. The first is known as the *a posteriori* estimate $\hat{\mathbf{x}}_{k|k}$, which is the estimate of $\mathbf{x}_k$ when all the measurements up to and including k are available. If all the measurements before (but not including time k) are available, then the *a priori* estimate $\hat{\mathbf{x}}_{k|k-1}$ can be formed.

$$\hat{\mathbf{x}}_{k|k-1} = E\left[\mathbf{x}_k|\mathbf{z}_1, \mathbf{z}_2, \ldots, \mathbf{z}_{k-1}\right] \tag{5.4}$$
$$\hat{\mathbf{x}}_{k|k} = E\left[\mathbf{x}_k|\mathbf{z}_1, \mathbf{z}_2, \ldots, \mathbf{z}_{k-1}, \mathbf{z}_k\right] \tag{5.5}$$

Define the *a priori* and *a posteriori* estimate errors, $\epsilon_{k|k-1}$ and $\epsilon_{k|k}$, respectively, as

$$\epsilon_{k|k-1} = \mathbf{x}_k - \hat{\mathbf{x}}_{k|k-1} \tag{5.6}$$

$$\epsilon_{k|k} = \mathbf{x}_k - \hat{\mathbf{x}}_{k|k} \tag{5.7}$$

It follows that the covariance of the estimation errors, $\mathbf{P}_{k|k-1}$ and $\mathbf{P}_{k|k}$, are given by

$$\mathbf{P}_{k|k-1} = E\left[\epsilon_{k|k-1}\epsilon_{k|k-1}^T\right] = E\left[\left(\mathbf{x}_k - \hat{\mathbf{x}}_{k|k-1}\right)\left(\mathbf{x}_k - \hat{\mathbf{x}}_{k|k-1}\right)^T\right] \tag{5.8}$$

$$\mathbf{P}_{k|k} = E\left[\epsilon_{k|k}\epsilon_{k|k}^T\right] = E\left[\left(\mathbf{x}_k - \hat{\mathbf{x}}_{k|k}\right)\left(\mathbf{x}_k - \hat{\mathbf{x}}_{k|k}\right)^T\right] \tag{5.9}$$

The *a priori* state estimated propagates with time by

$$\hat{\mathbf{x}}_{k|k-1} = \mathbf{A}_{k-1}\hat{\mathbf{x}}_{k-1|k-1} + \mathbf{G}_{k-1}\mathbf{u}_{k-1} \tag{5.10}$$

which is known as the *time update* equation. To determine how the covariance of the state estimate propagates with time, compute the *a priori* state estimation error using the transition equation 5.1 together with the estimate $\hat{\mathbf{x}}_{k|k-1}$ (Eq. 5.10).

$$\begin{aligned}\epsilon_{k|k-1} &= \mathbf{x}_k - \hat{\mathbf{x}}_{k|k-1} \\ &= \mathbf{A}_{k-1}\mathbf{x}_{k-1} + \mathbf{G}_{k-1}\mathbf{u}_{k-1} + \mathbf{w}_{k-1} - \mathbf{A}_{k-1}\hat{\mathbf{x}}_{k-1|k-1} - \mathbf{G}_{k-1}\mathbf{u}_{k-1} \\ &= \mathbf{A}_{k-1}\epsilon_{k-1|k-1} + \mathbf{w}_{k-1}\end{aligned} \tag{5.11}$$

The expectation given in Eq. 5.8 is

$$\mathbf{P}_{k|k-1} = \mathbf{A}_{k-1}\mathbf{P}_{k-1|k-1}\mathbf{A}_{k-1}^T + \mathbf{Q}_{k-1} \tag{5.12}$$

In developing the Kalman filter, the following equation is used to relate the *a posteriori* state estimate as a linear combination of the *a priori* state estimate and a weighted residual, which is the difference between the actual measurement $\mathbf{z}_k$ and the measurement predicted

by the *a priori* state estimate, $\mathbf{C}_k\hat{\mathbf{x}}_{\mathbf{k|k-1}}$.

$$\hat{\mathbf{x}}_{k|k} = \hat{\mathbf{x}}_{k|k-1} + \mathbf{K}_k\left(\mathbf{z}_k - \mathbf{C}_k\hat{\mathbf{x}}_{k|k-1}\right) \tag{5.13}$$

The weighting or gain matrix $\mathbf{K}_k$ is chosen to minimize the *a posteriori* error covariance in Eq. 5.9. This is performed by substituting Eq. 5.13 into Eq. 5.9 and performing the expectation. Taking the partial derivative of the trace of $\mathbf{P}_{k|k}$ with respect to $\mathbf{K}_k$, setting it equal to zero, and then solving for the gain gives

$$\mathbf{K}_k = \mathbf{P}_{k|k-1}\mathbf{C}_k^T\left(\mathbf{C}_k\mathbf{P}_{k|k-1}\mathbf{C}_k^T + \mathbf{R}_k\right)^{-1} \tag{5.14}$$

The *a posteriori* state estimate error covariance is then found by substituting this result together with the measurement update given in Eq. 5.13 into Eq. 5.9 and performing the expectation.

$$\begin{aligned}\mathbf{P}_{k|k} &= \left(\mathbf{I} - \mathbf{K}_k\mathbf{C}_k\right)\mathbf{P}_{k|k-1}\left(\mathbf{I} - \mathbf{K}_k\mathbf{C}_k\right)^T + \mathbf{K}_k\mathbf{R}_k\mathbf{K}_k^T \\ &= \left(\mathbf{I} - \mathbf{K}_k\mathbf{C}_k\right)\mathbf{P}_{k|k-1}\end{aligned} \tag{5.15}$$

where the *a posteriori* state estimate error in Eq. 5.9 is found using the measurement update equation (Eq. 5.13).

$$\begin{aligned}\epsilon_{k|k} &= \mathbf{x}_k - \hat{\mathbf{x}}_{k|k} \\ &= \mathbf{x}_k - \hat{\mathbf{x}}_{k|k-1} - \mathbf{K}_k\left(\mathbf{z}_k - \mathbf{C}_k\hat{\mathbf{x}}_{k|k-1}\right) \\ &= \epsilon_{k|k-1} - \mathbf{K}_k\left(\mathbf{C}_k\epsilon_{k|k-1} + \mathbf{v}_k\right)\end{aligned} \tag{5.16}$$

The Kalman filter algorithm is summarized below [100, 85].

1. The dynamic system is given by the following process and measurement equations:

$$\mathbf{x}_k = \mathbf{A}_{k-1}\mathbf{x}_{k-1} + \mathbf{G}_{k-1}\mathbf{u}_{k-1} + \mathbf{w}_{k-1} \tag{5.17a}$$
$$\mathbf{z}_k = \mathbf{C}_k\mathbf{x}_k + \mathbf{v}_k \tag{5.17b}$$
$$\mathbf{w}_k \sim (0, \mathbf{Q}_k) \tag{5.17c}$$
$$\mathbf{v}_k \sim (0, \mathbf{R}_k) \tag{5.17d}$$
$$E\left[\mathbf{w}_k\mathbf{w}_j^T\right] = \mathbf{Q}_k\delta_{k,j} \tag{5.17e}$$
$$E\left[\mathbf{v}_k\mathbf{v}_j^T\right] = \mathbf{R}_k\delta_{k,j} \tag{5.17f}$$
$$E\left[\mathbf{w}_k\mathbf{v}_j^T\right] = \mathbf{0} \tag{5.17g}$$

2. The filter is initialized as follows:

$$\hat{\mathbf{x}}_{0|0} = E\left[\mathbf{x}_0\right] \tag{5.18}$$
$$\mathbf{P}_{0|0} = E\left[\left(\mathbf{x}_0 - \hat{\mathbf{x}}_{0|0}\right)\left(\mathbf{x}_0 - \hat{\mathbf{x}}_{0|0}\right)^T\right] \tag{5.19}$$

3. At each time step, $k = 1, 2, \ldots, N$, the following filter equations are computed:

$$\mathbf{P}_{k|k-1} = \mathbf{A}_{k-1}\mathbf{P}_{k-1|k-1}\mathbf{A}_{k-1}^T + \mathbf{Q}_{k-1} \tag{5.20}$$
$$\mathbf{K}_k = \mathbf{P}_{k|k-1}\mathbf{C}_k^T\left(\mathbf{C}_k\mathbf{P}_{k|k-1}\mathbf{C}_k^T + \mathbf{R}_k\right)^{-1} \tag{5.21}$$
$$\hat{\mathbf{x}}_{k|k-1} = \mathbf{A}_{k-1}\hat{\mathbf{x}}_{k-1|k-1} + \mathbf{G}_{k-1}\mathbf{u}_{k-1} \tag{5.22}$$
$$\hat{\mathbf{x}}_{k|k} = \hat{\mathbf{x}}_{k|k-1} + \mathbf{K}_k\left(\mathbf{z}_k - \mathbf{C}_k\hat{\mathbf{x}}_{k|k-1}\right) \tag{5.23}$$
$$\mathbf{P}_{k|k} = \left(\mathbf{I} - \mathbf{K}_k\mathbf{C}_k\right)\mathbf{P}_{k|k-1} \tag{5.24}$$

The key point to note here is that Eq. 5.21 does not depend on either the measurements or the states. Therefore, the Kalman gain can be computed and stored prior to the start of the estimation task, which is greater advantage for online implementation.

If there is direct feedthrough of the known input $\mathbf{u}_k$, true for the case where the acceleration response is measured from a main mass excited structure, the measurement equation

becomes

$$\mathbf{z}_k = \mathbf{C}_k \mathbf{x}_k + \mathbf{D}_k \mathbf{u}_k + \mathbf{v}_k \tag{5.25}$$

where $\mathbf{D}_k$ is a direct feedthrough matrix corresponding to the known deterministic external excitation or input, $\mathbf{u}_k$. For the direct feedthrough case, *a posteriori* state estimation error is given by

$$\begin{aligned}
\epsilon_{k|k} &= \mathbf{x}_k - \hat{\mathbf{x}}_{k|k} \\
&= \mathbf{x}_k - \hat{\mathbf{x}}_{k|k-1} - \mathbf{K}_k \left(\mathbf{z}_k - \mathbf{C}_k \hat{\mathbf{x}}_{k|k-1} - \mathbf{D}_k \mathbf{u}_k \right) \\
&= \mathbf{x}_k - \hat{\mathbf{x}}_{k|k-1} - \mathbf{K}_k \left(\mathbf{C}_k \mathbf{x}_k + \mathbf{D}_k \mathbf{u}_k + \mathbf{v}_k - \mathbf{C}_k \hat{\mathbf{x}}_{k|k-1} - \mathbf{D}_k \mathbf{u}_k \right) \\
&= \epsilon_{k|k-1} - \mathbf{K}_k \left(\mathbf{C}_k \epsilon_{k|k-1} + \mathbf{v}_k \right)
\end{aligned} \tag{5.26}$$

which is the same result as Eq. 5.16; therefore, the Kalman filter equations are unchanged, with the exception of the measurement prediction within the measurement update equation. Eq. 5.13 becomes

$$\hat{\mathbf{x}}_{k|k} = \hat{\mathbf{x}}_{k|k-1} + \mathbf{K}_k \left(\mathbf{z}_k - \mathbf{C}_k \hat{\mathbf{x}}_{k|k-1} - \mathbf{D}_k \mathbf{u}_k \right) \tag{5.27}$$

5.1.2 Extended Kalman filter for combined state and parameter estimation

For state estimation in the traditional Kalman approach, it is generally assumed that the model parameters are known. When the model parameters are unknown, the conventional approach is to treat the unknown parameters as states, with constant transitions, and append them to the state vector [85, 2]. The resulting system of equations can conceptually be treated as being amenable to traditional state estimation, but for the extended state vector. However, the system becomes nonlinear, even though the underlying physical system can still be linear. This is due to the presence of states (appended parameters) in the system matrix $\mathbf{A}_k$ and measurement matrix $\mathbf{C}_k$, that, when multiplied by the state vector, produce a product of states within the transition and measurement equations. Hence, the Kalman filter cannot be applied directly to this case.

The extended Kalman filter (EKF) is essentially an extension of the Kalman filter for nonlinear systems. Stated simply, the EKF is a Kalman filter that linearizes about the current mean and covariance. This is accomplished by finding the partial derivative of the nonlinear transition and measurement equations with respect to the state and input vectors (Jacobian matrices of partial derivatives), and evaluating them at the current estimate of the states. With the estimation error covariance matrices described using linearized system and measurement matrices, the same basic operation of the Kalman filter proceeds.

The EKF is used to estimate the states of the process which is governed by the following non-linear difference equation, for the case of deterministic input $\mathbf{u}_k$ and additive process noise $\mathbf{w}_k$ [100]:

$$\mathbf{x}_k = f\left(\mathbf{x}_{k-1}, \mathbf{u}_{k-1}\right) + \mathbf{w}_{k-1} \tag{5.28}$$

with noisy measurement

$$\mathbf{z}_k = h\left(\mathbf{x}_k, \mathbf{u}_k\right) + \mathbf{v}_k \tag{5.29}$$

where $\mathbf{w}_k$ and $\mathbf{v}_k$ are the additive disturbance and measurement noises, respectively, which are both assumed to be zero mean Gaussian noise with covariance $\mathbf{Q}_k$ and $\mathbf{R}_k$.

The *a priori* state estimate, $\hat{\mathbf{x}}_{k|k-1}$, is determined using the transition equation.

$$\mathbf{x}_{k|k-1} = f\left(\mathbf{x}_{k-1}, \mathbf{u}_{k-1}\right) \tag{5.30}$$

Similarly, the estimate of the output is found using the nonlinear measurement equation and the *a priori* state estimate, $\hat{\mathbf{x}}_{k|k-1}$.

$$\hat{\mathbf{z}}_k = h\left(\hat{\mathbf{x}}_{k|k-1}, \mathbf{u}_k\right) \tag{5.31}$$

The state estimate error covariance is projected forward by

$$\mathbf{P}_{k|k-1} = \bar{\mathbf{A}}_{k-1}\mathbf{P}_{k-1|k-1}\bar{\mathbf{A}}_{k-1}^T + \mathbf{Q}_{k-1} \tag{5.32}$$

where $\bar{\mathbf{A}}_{k-1}$ is the Jacobian matrix of partial derivatives of $f\left(\mathbf{x}_{k-1}, \mathbf{u}_{k-1}\right)$ with respect to

$\mathbf{x}$, evaluated at the previous *a posteriori* state estimate, $\hat{\mathbf{x}}_{k-1|k-1}$.

$$\bar{\mathbf{A}}_{k-1} = \left.\frac{\partial f}{\partial \mathbf{x}}\right|_{\hat{\mathbf{x}}_{k-1|k-1}} \tag{5.33}$$

The Kalman gain, $\mathbf{K}_k$, is given by

$$\mathbf{K}_k = \mathbf{P}_{k|k-1}\bar{\mathbf{C}}_k^T \left(\bar{\mathbf{C}}_k \mathbf{P}_{k|k-1}\bar{\mathbf{C}}_k^T + \mathbf{R}_k\right)^{-1} \tag{5.34}$$

where $\bar{\mathbf{C}}_k$ is the Jacobian matrix of partial derivatives of $h\left(\mathbf{x}_k, \mathbf{u}_k\right)$ with respect to $\mathbf{x}_k$, evaluated at the current *a priori* state estimate, $\hat{\mathbf{x}}_{k|k-1}$.

$$\bar{\mathbf{C}}_k = \left.\frac{\partial h}{\partial \mathbf{x}}\right|_{\hat{\mathbf{x}}_{k|k-1}} \tag{5.35}$$

The measurement update equation for the state estimate is

$$\begin{aligned} \hat{\mathbf{x}}_{k|k} &= \hat{\mathbf{x}}_{k|k-1} + \mathbf{K}_k\left(\mathbf{z} - \hat{\mathbf{z}}_k\right) \\ &= \hat{\mathbf{x}}_{k|k-1} + \mathbf{K}_k\left[\mathbf{z} - h\left(\hat{\mathbf{x}}_{k|k-1}, \mathbf{u}_k\right)\right] \end{aligned} \tag{5.36}$$

The updated state estimate error covariance matrix, $\mathbf{P}_{k|k}$, is

$$\mathbf{P}_{k|k} = \left(\mathbf{I} - \mathbf{K}_k\bar{\mathbf{C}}_k\right)\mathbf{P}_{k|k-1} \tag{5.37}$$

The EKF for nonlinear estimation is no longer an optimal state estimator. Also, the introduction of the linearization of the transition and measurement equations for the purpose of projecting the state estimation error covariances tends to underestimate the error covariance, and may lead to filter divergence [85]. However, the EKF has been successfully implemented in numerous nonlinear state estimation problems, including combined state and parameter estimation for structural systems [36, 63, 53, 27, 84, 95, 109, 102].

The EKF algorithm is summarized as follows:

1. The dynamic system is given by the following process and measurement equations:

$$\mathbf{x}_k = f\left(\mathbf{x}_{k-1}, \mathbf{u}_{k-1}\right) + \mathbf{w}_{k-1} \tag{5.38a}$$
$$\mathbf{z}_k = h\left(\mathbf{x}_k, \mathbf{u}_k\right) + \mathbf{v}_k \tag{5.38b}$$
$$\mathbf{w}_k \sim (0, \mathbf{Q}_k) \tag{5.38c}$$
$$\mathbf{v}_k \sim (0, \mathbf{R}_k) \tag{5.38d}$$
$$E\left[\mathbf{w}_k \mathbf{w}_j^T\right] = \mathbf{Q}_k \delta_{k,j} \tag{5.38e}$$
$$E\left[\mathbf{v}_k \mathbf{v}_j^T\right] = \mathbf{R}_k \delta_{k,j} \tag{5.38f}$$
$$E\left[\mathbf{w}_k \mathbf{v}_j^T\right] = \mathbf{0} \tag{5.38g}$$

2. The filter is initialized as follows:

$$\hat{\mathbf{x}}_{0|0} = E\left[\mathbf{x}_0\right] \tag{5.39}$$
$$\mathbf{P}_{0|0} = E\left[\left(\mathbf{x}_0 - \hat{\mathbf{x}}_{0|0}\right)\left(\mathbf{x}_0 - \hat{\mathbf{x}}_{0|0}\right)^T\right] \tag{5.40}$$

3. At each time step, $k = 1, 2, \ldots, N$, the following filter equations are computed:

$$\mathbf{P}_{k|k-1} = \bar{\mathbf{A}}_{k-1} \mathbf{P}_{k-1|k-1} \bar{\mathbf{A}}_{k-1}^T + \mathbf{Q}_{k-1} \tag{5.41}$$
$$\mathbf{K}_k = \mathbf{P}_{k|k-1} \bar{\mathbf{C}}_k^T \left(\bar{\mathbf{C}}_k \mathbf{P}_{k|k-1} \bar{\mathbf{C}}_k^T + \mathbf{R}_k\right)^{-1} \tag{5.42}$$
$$\mathbf{x}_{k|k-1} = f\left(\mathbf{x}_{k-1}, \mathbf{u}_{k-1}\right) \tag{5.43}$$
$$\hat{\mathbf{x}}_{k|k} = \hat{\mathbf{x}}_{k|k-1} + \mathbf{K}_k \left[\mathbf{z} - h\left(\hat{\mathbf{x}}_{k|k-1}, \mathbf{u}_k\right)\right] \tag{5.44}$$
$$\mathbf{P}_{k|k} = \left(\mathbf{I} - \mathbf{K}_k \bar{\mathbf{C}}_k\right) \mathbf{P}_{k|k-1} \tag{5.45}$$

where

$$\bar{\mathbf{A}}_{k-1} = \left.\frac{\partial f}{\partial \mathbf{x}}\right|_{\hat{\mathbf{x}}_{k-1|k-1}} \tag{5.46}$$
$$\bar{\mathbf{C}}_k = \left.\frac{\partial h}{\partial \mathbf{x}}\right|_{\hat{\mathbf{x}}_{k|k-1}} \tag{5.47}$$

5.1.3 Discretization

For software implementation, the continuous time linear differential equations must be converted to discrete time difference equations. The zero-order hold method assumes that the input to the system is fixed between time steps. The resulting discretized system equations are [17]

$$\mathbf{A}_d = e^{\mathbf{A}_c T} \tag{5.48}$$

$$\mathbf{G}_d = \left(\int_{\tau=0}^{T} e^{\mathbf{A}_c \tau} \, d\tau \right) \mathbf{G}_c \tag{5.49}$$

$$\mathbf{C}_d = \mathbf{C}_c \tag{5.50}$$

$$\mathbf{D}_d = \mathbf{D}_c \tag{5.51}$$

where T is the uniform sample time. It is difficult to track variables through the matrix exponential and integrals; therefore, the following approximate discretization approach is used. Using the relationship $t = kT$, where t is the continuous time, and k is the integer time index, the continuous system can be converted to a discrete-time system using the definition of the derivative.

$$\dot{x}(t) = \lim_{T \to 0} \frac{x(t+T) - x(t)}{T} \tag{5.52}$$

The limit can be ignored since a discrete system is being considered, where the interval between samples is positive and non-negligible. Therefore,

$$\begin{aligned} \dot{\mathbf{x}}(t+T) &= \mathbf{x}(t) + \mathbf{A}_c \mathbf{x}(t) T + \mathbf{G}_c \mathbf{u}(t) T \\ &= (\mathbf{I} + \mathbf{A}_c T)\, \mathbf{x}(t) + \mathbf{G}_c T \mathbf{u}(t) \end{aligned} \tag{5.53}$$

The equivalent discrete time state matrices are

$$\mathbf{A}_d = \mathbf{I} + \mathbf{A}_c T \tag{5.54}$$

$$\mathbf{G}_d = \mathbf{G}_c T \tag{5.55}$$

$$\mathbf{C}_d = \mathbf{C}_c \tag{5.56}$$

$$\mathbf{D}_d = \mathbf{D}_c \tag{5.57}$$

where the subscript d denotes the discrete time system matrices; subsequently this subscript is replaced with the time step indices, k and $k-1$. A sufficiently small sample time must be selected for this approximation to be valid. The state space equations in discrete time form are

$$\mathbf{x}_k = \mathbf{A}_{k-1}\mathbf{x}_{k-1} + \mathbf{G}_{k-1}\mathbf{u}_{k-1} \tag{5.58}$$

$$\mathbf{z}_k = \mathbf{C}_d\mathbf{x}_k + \mathbf{D}_d\mathbf{u}_k \tag{5.59}$$

where the subscript denotes the time step. It was found that a relatively fast sampling rate was required to provide adequate results for the parameter estimation by extended Kalman filtering; this finding has been corroborated by other researchers [27] when compared to other system identification approaches.

5.2 Direct feedthrough of unknown external disturbance

The EKF has been used for structural engineering applications such as damage detection [62, 107, 106], system identification [36, 63, 53, 27, 84, 95, 109, 102], and input estimation [39]. Most of these previous studies have not considered the case of feedthrough of the process noise in the measurement equation. This issue arises when (i) the system is excited by a main mass forcing function, such as a wind excitation, and (ii) acceleration response measurements are used. Previous parameter estimation work has often considered

base excited structures using known earthquake time histories [102], or have assumed the availability of displacement or velocity (direct state) measurements [109, 95, 61, 36]. The concept of feedthrough process noise has been considered for the purpose of input estimation [39, 38, 64]; however, these studies only considered that one aspect and parameter estimation was not attempted.

5.2.1 Kalman filter for feedthrough disturbance noise

The traditional form of the Kalman filter described in Sec. 5.1.1 is not suitable for the state estimation where the system is excited by unknown main mass forcing such as a wind excitation, and acceleration response measurements are used. For a known external disturbance, feedthrough of the input (for the case of acceleration response measurements) can be overcome by adapting the Kalman filter residual calculation to include the direct feedthrough of the input, $\mathbf{u}_k$. This procedure has been presented briefly by Einicke and White [19]. The ensuing discussion lists all the intermediate steps in the derivation.

The linear, discrete-time process equation is given by

$$\mathbf{x}_k = \mathbf{A}_{k-1}\mathbf{x}_{k-1} + \mathbf{E}_{k-1}\mathbf{d}_{k-1} + \mathbf{w}_{k-1} \tag{5.60}$$

where $\mathbf{E}_k$ is the discrete time input matrix corresponding to the unknown external disturbance $\mathbf{d}_k$ with covariance $\mathbf{S}_k$, and $\mathbf{w}_k$ is the process noise with covariance $\mathbf{Q}_k$, which accounts for any additional disturbance noise and model uncertainty. The measurement equation is given by

$$\mathbf{z}_k = \mathbf{C}_k\mathbf{x}_k + \mathbf{F}_k\mathbf{d}_k + \mathbf{v}_k \tag{5.61}$$

where $\mathbf{F}_k$ is the discrete time direct feedthrough matrix corresponding to $\mathbf{d}_k$ and $\mathbf{v}_k$ is the additive measurement noise with covariance $\mathbf{R}_k$. The presence of the unknown disturbance noise in Eq. 5.61 requires an alternate formulation of the discrete time Kalman filter.

Using the concept of correlated process and measurement noise [2, 85, 19], the Kalman filter is adapted for the case of direct feedthrough of the disturbance noise. It is assumed

that the unknown external excitation $\mathbf{d}_k$, the process noise $\mathbf{w}_k$, and the additive measurement noise $\mathbf{v}_k$ are all zero mean, white, uncorrelated, and have known covariances $\mathbf{S}_k$, $\mathbf{Q}_k$, and $\mathbf{R}_k$, respectively. By considering the noise terms in the transition and measurement equations as effective additive noise terms, given by

$$\mathbf{w}'_k = \mathbf{E}_k\mathbf{d}_k + \mathbf{w}_k \tag{5.62}$$

$$\mathbf{v}'_k = \mathbf{F}_k\mathbf{d}_k + \mathbf{v}_k \tag{5.63}$$

it becomes clear that the effective process noise in the transition equation and the effective measurement noise in the measurement equation are correlated, with cross covariance $\mathbf{E}_k\mathbf{S}_k\mathbf{F}_k^T\delta_{k,j}$, where $\delta_{k,j}$ is the Kronecker delta function. A two-step Kalman filter is designed where the correlation between the process and measurement equation is removed in the time-update step; this allows the subsequent formulation of the Kalman filter equations to proceed as usual.

Begin by defining the following *a priori* and *a posteriori* estimation errors:

$$\epsilon_{k|k-1} = \mathbf{x}_k - \hat{\mathbf{x}}_{k|k-1} \tag{5.64}$$

$$\epsilon_{k|k} = \mathbf{x}_k - \hat{\mathbf{x}}_{k|k} \tag{5.65}$$

where

$$\hat{\mathbf{x}}_{k|k-1} = \mathbf{A}_{k-1}\hat{\mathbf{x}}_{k-1|k-1} + \mathbf{J}_{k-1}\left(\mathbf{z}_{k-1} - \mathbf{C}_{k-1}\hat{\mathbf{x}}_{k-1|k-1}\right) \tag{5.66}$$

$$\hat{\mathbf{x}}_{k|k} = \hat{\mathbf{x}}_{k|k-1} + \mathbf{K}_k\left(\mathbf{z}_k - \mathbf{C}_k\hat{\mathbf{x}}_{k|k-1}\right) \tag{5.67}$$

The gain $\mathbf{J}_k$ is the one-step predictor gain selected to eliminate the correlation between the process and measurement equations. The gain $\mathbf{K}_k$ is the Kalman gain to be determined,

rather than that defined in Eq. 5.14. Eq. 5.64 can be expanded as

$$\begin{aligned}
\epsilon_{k|k-1} &= \mathbf{x}_k - \hat{\mathbf{x}}_{k|k-1} \\
&= \mathbf{A}_{k-1}\mathbf{x}_{k-1} + \mathbf{E}_{k-1}\mathbf{d}_{k-1} + \mathbf{w}_{k-1} - \mathbf{A}_{k-1}\hat{\mathbf{x}}_{k-1|k-1} \\
&\quad - \mathbf{J}_{k-1}\left(\mathbf{z}_{k-1} - \mathbf{C}_{k-1}\hat{\mathbf{x}}_{k-1|k-1}\right) \\
&= \mathbf{A}_{k-1}\mathbf{x}_{k-1} + \mathbf{E}_{k-1}\mathbf{d}_{k-1} + \mathbf{w}_{k-1} - \mathbf{A}_{k-1}\hat{\mathbf{x}}_{k-1|k-1} \\
&\quad - \mathbf{J}_{k-1}\mathbf{C}_{k-1}\mathbf{x}_{k-1} - \mathbf{J}_{k-1}\mathbf{F}_{k-1}\mathbf{d}_{k-1} - \mathbf{J}\mathbf{v}_{k-1} + \mathbf{J}_{k-1}\mathbf{C}_{k-1}\hat{\mathbf{x}}_{k-1|k-1} \\
&= \left(\mathbf{A}_{k-1} - \mathbf{J}_{k-1}\mathbf{C}_{k-1}\right)\left(\mathbf{x}_k - \hat{\mathbf{x}}_{k-1|k-1}\right) \\
&\quad + \left(\mathbf{E}_{k-1} - \mathbf{J}_{k-1}\mathbf{F}_{k-1}\right)\mathbf{d}_{k-1} + \mathbf{w}_{k-1} - \mathbf{J}_{k-1}\mathbf{v}_{k-1} \\
&= \left(\mathbf{A}_{k-1} - \mathbf{J}_{k-1}\mathbf{C}_{k-1}\right)\epsilon_{k|k-1} + \left(\mathbf{E}_{k-1} - \mathbf{J}_{k-1}\mathbf{F}_{k-1}\right)\mathbf{d}_{k-1} \\
&\quad + \mathbf{w}_{k-1} - \mathbf{J}_{k-1}\mathbf{v}_{k-1}
\end{aligned} \tag{5.68}$$

The *a priori* estimation error covariance is given by

$$\begin{aligned}
\mathbf{P}_{k|k-1} &= E\left[\epsilon_{k|k-1}\epsilon_{k|k-1}^T\right] \\
&= E\left\{\left[\left(\mathbf{A}_{k-1} - \mathbf{J}_{k-1}\mathbf{C}_{k-1}\right)\epsilon_{k|k-1} + \left(\mathbf{E}_{k-1} - \mathbf{J}_{k-1}\mathbf{F}_{k-1}\right)\mathbf{d}_{k-1} + \mathbf{w}_{k-1} - \mathbf{J}_{k-1}\mathbf{v}_{k-1}\right]\right. \\
&\qquad \left.\left[\left(\mathbf{A}_{k-1} - \mathbf{J}_{k-1}\mathbf{C}_{k-1}\right)\epsilon_{k|k-1} + \left(\mathbf{E}_{k-1} - \mathbf{J}_{k-1}\mathbf{F}_{k-1}\right)\mathbf{d}_{k-1} + \mathbf{w}_{k-1} - \mathbf{J}_{k-1}\mathbf{v}_{k-1}\right]^T\right\} \\
&= \left(\mathbf{A}_{k-1} - \mathbf{J}_{k-1}\mathbf{C}_{k-1}\right)\mathbf{P}_{k-1|k-1}\left(\mathbf{A}_{k-1} - \mathbf{J}_{k-1}\mathbf{C}_{k-1}\right)^T \\
&\quad + \left(\mathbf{E}_{k-1} - \mathbf{J}_{k-1}\mathbf{F}_{k-1}\right)\mathbf{S}_{k-1}\left(\mathbf{E}_{k-1} - \mathbf{J}_{k-1}\mathbf{F}_{k-1}\right)^T \\
&\quad + \mathbf{Q}_{k-1} + \mathbf{J}_{k-1}\mathbf{R}_{k-1}\mathbf{J}_{k-1}^T
\end{aligned} \tag{5.69}$$

Presently, it has been assumed that

$$E\left\{\left[\left(\mathbf{E}_{k-1} - \mathbf{J}_{k-1}\mathbf{F}_{k-1}\right)\mathbf{d}_{k-1} + \mathbf{w}_{k-1} - \mathbf{J}_{k-1}\mathbf{v}_{k-1}\right]\epsilon_{k-1|k-1}^T\right\} = 0 \tag{5.70}$$

in Eq. 5.69, which will be shown later to be true.

The matrix $\mathbf{J}_k$ is a one-step predictor gain matrix selected to eliminate the correlation between the process and measurement noises. Add the "zero term" $\mathbf{J}_k\left(\mathbf{z}_k - \mathbf{C}_k\mathbf{x}_k - \mathbf{F}_k\mathbf{d}_k - \mathbf{v}_k\right)$

to the right-hand side of Eq. 5.60.

$$\begin{aligned}\mathbf{x}_k &= \mathbf{A}_{k-1}\mathbf{x}_{k-1} + \mathbf{E}_{k-1}\mathbf{d}_{k-1} + \mathbf{w}_{k-1} + \mathbf{J}_k\left(\mathbf{z}_k - \mathbf{C}_k\mathbf{x}_k - \mathbf{F}_k\mathbf{d}_k - \mathbf{v}_k\right) \\ &= \left(\mathbf{A}_{k-1} - \mathbf{J}_{k-1}\mathbf{C}_{k-1}\right)\mathbf{x}_{k-1} + \left(\mathbf{E}_{k-1} - \mathbf{J}_{k-1}\mathbf{F}_{k-1}\right)\mathbf{d}_{k-1} \\ &\quad + \mathbf{w}_{k-1} - \mathbf{J}_{k-1}\mathbf{v}_{k-1} + \mathbf{J}_{k-1}\mathbf{z}_{k-1} \\ &= \mathbf{A}'_{k-1}\mathbf{x}_{k-1} + \mathbf{J}_{k-1}\mathbf{z}_{k-1} + \mathbf{w}'_{k-1}\end{aligned} \tag{5.71}$$

where

$$\mathbf{A}'_k = \mathbf{A}_k - \mathbf{J}_k\mathbf{C}_k \tag{5.72}$$

$$\mathbf{w}'_k = \left(\mathbf{E}_k - \mathbf{J}_k\mathbf{F}_k\right)\mathbf{d}_k + \mathbf{w}_k - \mathbf{J}_k\mathbf{v}_k \tag{5.73}$$

Evaluating the expectation

$$\begin{aligned}E\left[\mathbf{w}'_k\left(\mathbf{F}_k\mathbf{d}_k + \mathbf{v}_k\right)^T\right] &= E\left[\left(\mathbf{E}_k\mathbf{d}_k - \mathbf{J}_k\mathbf{F}_k\mathbf{d}_k + \mathbf{w}_k - \mathbf{J}_k\mathbf{v}_k\right)\left(\mathbf{F}_k\mathbf{d}_k + \mathbf{v}_k\right)^T\right] \\ &= \mathbf{E}_k\mathbf{S}_k\mathbf{F}_k^T - \mathbf{J}_k\mathbf{F}_k\mathbf{S}_k\mathbf{F}_k^T - \mathbf{J}_k\mathbf{R}_k \\ &= \mathbf{E}_k\mathbf{S}_k\mathbf{F}_k^T - \mathbf{J}_k\left(\mathbf{F}_k\mathbf{S}_k\mathbf{F}_k^T + \mathbf{R}_k\right)\end{aligned} \tag{5.74}$$

which equals zero when

$$\mathbf{J}_k = \mathbf{E}_k\mathbf{S}_k\mathbf{F}_k^T\left(\mathbf{F}_k\mathbf{S}_k\mathbf{F}_k^T + \mathbf{R}_k\right)^{-1} \tag{5.75}$$

Eq. 5.69 can be simplified using this result.

$$\begin{aligned}
\mathbf{P}_{k|k-1} &= \left(\mathbf{A}_{k-1} - \mathbf{J}_{k-1}\mathbf{C}_{k-1}\right)\mathbf{P}_{k-1|k-1}\left(\mathbf{A}_{k-1} - \mathbf{J}_{k-1}\mathbf{C}_{k-1}\right)^T \\
&\quad + \mathbf{E}_{k-1}\mathbf{S}_{k-1}\mathbf{E}_{k-1}^T - \mathbf{J}_{k-1}\mathbf{F}_{k-1}\mathbf{S}_{k-1}\mathbf{E}_{k-1}^T - \mathbf{E}_{k-1}\mathbf{S}_{k-1}\mathbf{F}_{k-1}^T\mathbf{J}_{k-1}^T \\
&\quad + \mathbf{J}_{k-1}\mathbf{F}_{k-1}\mathbf{S}_{k-1}\mathbf{F}_{k-1}^T\mathbf{J}_{k-1}^T + \mathbf{Q}_{k-1} + \mathbf{J}_{k-1}\mathbf{R}_{k-1}\mathbf{J}_{k-1}^T \\
&= \left(\mathbf{A}_{k-1} - \mathbf{J}_{k-1}\mathbf{C}_{k-1}\right)\mathbf{P}_{k-1|k-1}\left(\mathbf{A}_{k-1} - \mathbf{J}_{k-1}\mathbf{C}_{k-1}\right)^T \\
&\quad + \mathbf{E}_{k-1}\mathbf{S}_{k-1}\mathbf{E}_{k-1}^T - \mathbf{J}_{k-1}\mathbf{F}_{k-1}\mathbf{S}_{k-1}\mathbf{E}_{k-1}^T - \mathbf{E}_{k-1}\mathbf{S}_{k-1}\mathbf{F}_{k-1}^T\mathbf{J}_{k-1}^T \\
&\quad + \mathbf{J}_{k-1}\left(\mathbf{F}_{k-1}\mathbf{S}_{k-1}\mathbf{F}_{k-1}^T + \mathbf{R}_{k-1}\right)\mathbf{J}_{k-1}^T + \mathbf{Q}_{k-1} \\
&= \left(\mathbf{A}_{k-1} - \mathbf{J}_{k-1}\mathbf{C}_{k-1}\right)\mathbf{P}_{k-1|k-1}\left(\mathbf{A}_{k-1} - \mathbf{J}_{k-1}\mathbf{C}_{k-1}\right)^T \\
&\quad + \mathbf{E}_{k-1}\mathbf{S}_{k-1}\mathbf{E}_{k-1}^T - \mathbf{J}_{k-1}\mathbf{F}_{k-1}\mathbf{S}_{k-1}\mathbf{E}_{k-1}^T + \mathbf{Q}_{k-1}
\end{aligned} \tag{5.76}$$

Eq. 5.65 can be expanded as

$$\begin{aligned}
\epsilon_{k|k} &= \mathbf{x}_k - \left[\hat{\mathbf{x}}_{k|k-1} + \mathbf{K}_k\left(\mathbf{z}_k - \mathbf{C}_k\hat{\mathbf{x}}_{k|k-1}\right)\right] \\
&= \epsilon_{k|k-1} - \mathbf{K}_k\left(\mathbf{C}_k\mathbf{x}_k + \mathbf{F}_k\mathbf{d}_k + \mathbf{v}_k - \mathbf{C}_k\hat{\mathbf{x}}_{k|k-1}\right) \\
&= \left(\mathbf{I} - \mathbf{K}_k\mathbf{C}_k\right)\epsilon_{k|k-1} - \mathbf{K}_k\mathbf{F}_k\mathbf{d}_k - \mathbf{K}_k\mathbf{v}_k
\end{aligned} \tag{5.77}$$

The *a posteriori* estimation error covariance is

$$\begin{aligned}
\mathbf{P}_{k|k} &= E\left[\epsilon_{k|k}\epsilon_{k|k}^T\right] \\
&= E\left\{\left[\left(\mathbf{I} - \mathbf{K}_k\mathbf{C}_k\right)\epsilon_{k|k-1} - \mathbf{K}_k\mathbf{F}_k\mathbf{d}_k - \mathbf{K}_k\mathbf{v}_k\right]\right. \\
&\qquad \left.\left[\left(\mathbf{I} - \mathbf{K}_k\mathbf{C}_k\right)\epsilon_{k|k-1} - \mathbf{K}_k\mathbf{F}_k\mathbf{d}_k - \mathbf{K}_k\mathbf{v}_k\right]^T\right\} \\
&= \left(\mathbf{I} - \mathbf{K}_k\mathbf{C}_k\right)\mathbf{P}_{k|k-1}\left(\mathbf{I} - \mathbf{K}_k\mathbf{C}_k\right)^T + \mathbf{K}_k\mathbf{F}_k\mathbf{S}_k\mathbf{F}_k^T\mathbf{K}_k^T + \mathbf{K}_k\mathbf{R}_k\mathbf{K}_k^T
\end{aligned} \tag{5.78}$$

In order to determine the gain $\mathbf{K}_k$, find the gain that minimizes the trace of the *a posteriori* state estimate error. This is accomplished by finding the gain in order to make

the following partial derivative equal to zero:

$$\begin{aligned}\frac{\partial \operatorname{Tr}\left(\mathbf{P}_{k|k}\right)}{\partial \mathbf{K}_k} &= -2\left(\mathbf{I}-\mathbf{K}_k\mathbf{C}_k\right)\mathbf{P}_{k|k-1}\mathbf{C}_k^T + 2\mathbf{K}_k\mathbf{F}_k\mathbf{S}_k\mathbf{F}_k^T + 2\mathbf{K}_k\mathbf{R}_k \\ &= -2\mathbf{P}_{k|k-1}\mathbf{C}_k^T + 2\mathbf{K}_k\mathbf{C}_k\mathbf{P}_{k|k-1}\mathbf{C}_k^T + 2\mathbf{K}_k\mathbf{F}_k\mathbf{S}_k\mathbf{F}_k^T + 2\mathbf{K}_k\mathbf{R}_k \\ &= 2\left[\mathbf{K}_k\left(\mathbf{C}_k\mathbf{P}_{k|k-1}\mathbf{C}_k^T + \mathbf{F}_k\mathbf{S}_k\mathbf{F}_k^T + \mathbf{R}_k\right) - \mathbf{P}_{k|k-1}\mathbf{C}_k^T\right]\end{aligned} \tag{5.79}$$

The gain which makes this partial derivative equal to zero is

$$\mathbf{K}_k = \mathbf{P}_{k|k-1}\mathbf{C}_k^T\left(\mathbf{C}_k\mathbf{P}_{k|k-1}\mathbf{C}_k^T + \mathbf{F}_k\mathbf{S}_k\mathbf{F}_k^T + \mathbf{R}_k\right)^{-1} \tag{5.80}$$

The *a posteriori* estimation error covariance can be further simplified.

$$\begin{aligned}\mathbf{P}_{k|k} &= \mathbf{P}_{k|k-1} - \mathbf{K}_k\mathbf{C}_k\mathbf{P}_{k|k-1} - \mathbf{P}_{k|k-1}\mathbf{C}_k^T\mathbf{K}_k^T + \mathbf{K}_k\mathbf{C}_k\mathbf{P}_{k|k-1}\mathbf{C}_k^T\mathbf{K}_k^T \\ &\quad \mathbf{K}_k\mathbf{F}_k\mathbf{S}_k\mathbf{F}_k^T\mathbf{K}_k^T + \mathbf{K}_k\mathbf{R}_k\mathbf{K}_k^T \\ &= \mathbf{P}_{k|k-1} - \mathbf{K}_k\mathbf{C}_k\mathbf{P}_{k|k-1} - \mathbf{P}_{k|k-1}\mathbf{C}_k^T\mathbf{K}_k^T \\ &\quad + \mathbf{K}_k\left(\mathbf{C}_k\mathbf{P}_{k|k-1}\mathbf{C}_k^T + \mathbf{F}_k\mathbf{S}_k\mathbf{F}_k^T + \mathbf{R}_k\right)\mathbf{K}_k^T \\ &= \mathbf{P}_{k|k-1} - \mathbf{K}_k\mathbf{C}_k\mathbf{P}_{k|k-1} - \mathbf{P}_{k|k-1}\mathbf{C}_k^T\mathbf{K}_k^T \\ &\quad + \mathbf{P}_{k|k-1}\mathbf{C}_k^T\mathbf{K}_k^T \\ &= \left(\mathbf{I}-\mathbf{K}_k\mathbf{C}_k\right)\mathbf{P}_{k|k-1}\end{aligned} \tag{5.81}$$

Consider the expectation in Eq. 5.70.

$$
\begin{aligned}
E\left[\mathbf{w}_k'\epsilon_{k-1|k-1}^T\right] &= E\left\{\left[\left(\mathbf{E}_{k-1}-\mathbf{J}_{k-1}\mathbf{F}_{k-1}\right)\mathbf{d}_{k-1}+\mathbf{w}_{k-1}-\mathbf{J}_{k-1}\mathbf{v}_{k-1}\right]\right. \\
&\qquad \left.\epsilon_{k-1|k-1}^T\right\} \\
&= E\left\{\left[\left(\mathbf{E}_{k-1}-\mathbf{J}_{k-1}\mathbf{F}_{k-1}\right)\mathbf{d}_{k-1}+\mathbf{w}_{k-1}-\mathbf{J}_{k-1}\mathbf{v}_{k-1}\right]\right. \\
&\qquad \left.\left[\left(\mathbf{I}-\mathbf{K}_k\mathbf{C}_k\right)\epsilon_{k|k-1}-\mathbf{K}_k\mathbf{F}_k\mathbf{d}_k-\mathbf{K}_k\mathbf{v}_k\right]\right\} \\
&= -\left(\mathbf{E}_{k-1}-\mathbf{J}_{k-1}\mathbf{F}_{k-1}\right)\mathbf{S}_{k-1}\mathbf{F}_{k-1}^T\mathbf{K}_{k-1}^T+\mathbf{J}_{k-1}\mathbf{R}_{k-1}\mathbf{K}_{k-1}^T \\
&= -\mathbf{E}_{k-1}\mathbf{S}_{k-1}\mathbf{F}_{k-1}^T\mathbf{K}_{k-1}^T \\
&\qquad +\mathbf{J}_{k-1}\left(\mathbf{F}_{k-1}\mathbf{S}_{k-1}\mathbf{F}_{k-1}^T+\mathbf{R}_{k-1}\right)\mathbf{K}_{k-1}^T \\
&= -\mathbf{E}_{k-1}\mathbf{S}_{k-1}\mathbf{F}_{k-1}^T\mathbf{K}_{k-1}^T+\mathbf{E}_{k-1}\mathbf{S}_{k-1}\mathbf{F}_{k-1}^T\mathbf{K}_{k-1}^T \\
&= 0
\end{aligned}
\tag{5.82}
$$

This result validates the assumption made earlier. An updated measurement estimate is given by [19]

$$
\hat{\mathbf{z}}_k = \mathbf{C}_k\hat{\mathbf{x}}_{k|k}+\mathbf{F}_k\mathbf{S}_k\mathbf{F}_k^T\left(\mathbf{F}_k\mathbf{S}_k\mathbf{F}_k^T+\mathbf{R}_k\right)^{-1}\left(\mathbf{z}_k-\mathbf{C}_k\hat{\mathbf{x}}_{k|k}\right) \tag{5.83}
$$

The general discrete time Kalman filter where measurements contain direct feedthrough of an unknown external disturbance, which is treated as process noise, is summarized below.

1. The dynamic system is given by the following process and measurement equations:

$$\mathbf{x}_k = \mathbf{A}_{k-1}\mathbf{x}_{k-1} + \mathbf{E}_{k-1}\mathbf{d}_{k-1} + \mathbf{w}_{k-1} \tag{5.84a}$$
$$\mathbf{z}_k = \mathbf{C}_k\mathbf{x}_k + \mathbf{F}_k\mathbf{d}_k + \mathbf{v}_k \tag{5.84b}$$
$$\mathbf{w}_k \sim (0, \mathbf{Q}_k) \tag{5.84c}$$
$$\mathbf{d}_k \sim (0, \mathbf{S}_k) \tag{5.84d}$$
$$\mathbf{v}_k \sim (0, \mathbf{R}_k) \tag{5.84e}$$
$$E\left[\mathbf{w}_k\mathbf{w}_j^T\right] = \mathbf{Q}_k\delta_{k,j} \tag{5.84f}$$
$$E\left[\mathbf{d}_k\mathbf{d}_j^T\right] = \mathbf{S}_k\delta_{k,j} \tag{5.84g}$$
$$E\left[\mathbf{v}_k\mathbf{v}_j^T\right] = \mathbf{R}_k\delta_{k,j} \tag{5.84h}$$
$$E\left[\mathbf{w}_k\mathbf{d}_j^T\right] = E\left[\mathbf{d}_k\mathbf{w}_j^T\right] = \mathbf{0} \tag{5.84i}$$
$$E\left[\mathbf{w}_k\mathbf{v}_j^T\right] = E\left[\mathbf{v}_k\mathbf{w}_j^T\right] = \mathbf{0} \tag{5.84j}$$
$$E\left[\mathbf{d}_k\mathbf{v}_j^T\right] = E\left[\mathbf{v}_k\mathbf{d}_j^T\right] = \mathbf{0} \tag{5.84k}$$

2. The initialization of the filter is as follows:

$$\hat{\mathbf{x}}_{0|0} = E\left[\mathbf{x}_0\right] \tag{5.85}$$
$$\mathbf{P}_{0|0} = E\left[\left(\mathbf{x}_0 - \hat{\mathbf{x}}_{0|0}\right)\left(\mathbf{x}_0 - \hat{\mathbf{x}}_{0|0}\right)^T\right] \tag{5.86}$$

3. For each time step, $k = 1, 2, \ldots, N$, the filter equations are

$$\mathbf{J}_k = \mathbf{E}_k \mathbf{S}_k \mathbf{F}_k^T \left(\mathbf{F}_k \mathbf{S}_k \mathbf{F}_k^T + \mathbf{R}_k \right)^{-1} \tag{5.87}$$

$$\hat{\mathbf{x}}_{k|k-1} = \mathbf{A}_{k-1} \hat{\mathbf{x}}_{k-1|k-1} + \mathbf{J}_{k-1} \left(\mathbf{z}_{k-1} - \mathbf{C}_{k-1} \hat{\mathbf{x}}_{k-1|k-1} \right) \tag{5.88}$$

$$\begin{aligned} \mathbf{P}_{k|k-1} = & \left(\mathbf{A}_{k-1} - \mathbf{J}_{k-1} \mathbf{C}_{k-1} \right) \mathbf{P}_{k-1|k-1} \left(\mathbf{A}_{k-1} - \mathbf{J}_{k-1} \mathbf{C}_{k-1} \right)^T \\ & + \mathbf{E}_{k-1} \mathbf{S}_{k-1} \mathbf{E}_{k-1}^T - \mathbf{J}_{k-1} \mathbf{F}_{k-1} \mathbf{S}_{k-1} \mathbf{E}_{k-1}^T + \mathbf{Q}_{k-1} \end{aligned} \tag{5.89}$$

$$\mathbf{K}_k = \mathbf{P}_{k|k-1} \mathbf{C}_k^T \left(\mathbf{C}_k \mathbf{P}_{k|k-1} \mathbf{C}_k^T + \mathbf{F}_k \mathbf{S}_k \mathbf{F}_k^T + \mathbf{R}_k \right)^{-1} \tag{5.90}$$

$$\hat{\mathbf{x}}_{k|k} = \hat{\mathbf{x}}_{k|k-1} + \mathbf{K}_k \left(\mathbf{z}_k - \mathbf{C}_k \hat{\mathbf{x}}_{k|k-1} \right) \tag{5.91}$$

$$\mathbf{P}_{k|k} = \left(\mathbf{I} - \mathbf{K}_k \mathbf{C}_k \right) \mathbf{P}_{k|k-1} \tag{5.92}$$

$$\hat{\mathbf{z}}_k = \mathbf{C}_k \hat{\mathbf{x}}_{k|k} + \mathbf{F}_k \mathbf{S}_k \mathbf{F}_k^T \left(\mathbf{F}_k \mathbf{S}_k \mathbf{F}_k^T + \mathbf{R}_k \right)^{-1} \left(\mathbf{y}_k - \mathbf{C}_k \hat{\mathbf{x}}_{k|k} \right) \tag{5.93}$$

5.2.2 EKF for feedthrough disturbance noise

The combined state and parameter estimation filter is inherently nonlinear; therefore, the algorithm presented for pure state estimation in Sec. 5.2.1 is extended similarly to the EKF. For the case of unknown feedthrough stochastic disturbance noise, $\mathbf{d}_k$, the transition of the states is governed by the following non-linear difference equation:

$$\mathbf{x}_k = f\left(\mathbf{x}_{k-1}, \mathbf{d}_{k-1} \right) + \mathbf{w}_{k-1} \tag{5.94}$$

with noisy measurements given by

$$\mathbf{z}_k = h\left(\mathbf{x}_k, \mathbf{d}_k \right) + \mathbf{v}_k \tag{5.95}$$

The predicted state or *a priori* state estimate, from the *a posteriori* state estimate for the $k - 1^{\text{th}}$ time step, can be found by

$$\hat{\mathbf{x}}_{k|k-1} = f\left(\hat{\mathbf{x}}_{k-1|k-1}, \mathbf{0} \right) + \mathbf{J}_{k-1} \left[\mathbf{y}_{k-1} - h\left(\hat{\mathbf{x}}_{k-1|k-1}, \mathbf{0} \right) \right] \tag{5.96}$$

where the one-step predictor gain matrix is

$$\mathbf{J}_k = \bar{\mathbf{E}}_k \mathbf{S}_k \bar{\mathbf{F}}_k^T \left(\bar{\mathbf{F}}_k \mathbf{S}_k \bar{\mathbf{F}}_k^T + \mathbf{R}_k \right)^{-1} \tag{5.97}$$

The predicted estimate covariance is given by

$$\begin{aligned} \mathbf{P}_{k|k-1} = & \left(\bar{\mathbf{A}}_{k-1} - \mathbf{J}_{k-1} \bar{\mathbf{C}}_{k-1} \right) \mathbf{P}_{k-1|k-1} \left(\bar{\mathbf{A}}_{k-1} - \mathbf{J}_{k-1} \bar{\mathbf{C}}_{k-1} \right)^T \\ & + \bar{\mathbf{E}}_{k-1} \mathbf{S}_{k-1} \bar{\mathbf{E}}_{k-1}^T + \mathbf{Q}_{k-1} - \mathbf{J}_{k-1} \bar{\mathbf{F}}_{k-1} \mathbf{S}_{k-1} \bar{\mathbf{E}}_{k-1}^T \end{aligned} \tag{5.98}$$

where $\bar{\mathbf{A}}_{k-1}$ is the Jacobian matrix of partial derivatives of $f(\mathbf{x}, \mathbf{0})$ with respect to $\mathbf{x}$ evaluated at the previous *a posterior* state estimate, $\mathbf{x}_{k-1|k-1}$; that is

$$\bar{\mathbf{A}}_{k-1} = \left. \frac{\partial f(\mathbf{x}, \mathbf{0})}{\partial \mathbf{x}} \right|_{\hat{\mathbf{x}}_{k-1|k-1}} \tag{5.99}$$

and $\bar{\mathbf{E}}_{k-1}$ is the Jacobian matrix of partial derivatives of $f(\mathbf{x}, \mathbf{d})$ with respect to $\mathbf{d}$ evaluated at the previous *a posterior* state estimate; that is

$$\bar{\mathbf{E}}_{k-1} = \left. \frac{\partial f(\mathbf{x}, \mathbf{d})}{\partial \mathbf{d}} \right|_{\hat{\mathbf{x}}_{k-1|k-1}} \tag{5.100}$$

Similarly, $\bar{\mathbf{C}}_{k-1}$ is the Jacobian matrix of partial derivatives of $h(\mathbf{x}, \mathbf{0})$ with respect to $\mathbf{x}$ evaluated at the previous *a priori* state estimate, $\mathbf{x}_{k-1|k-2}$; that is

$$\bar{\mathbf{C}}_{k-1} = \left. \frac{\partial h(\mathbf{x}, \mathbf{0})}{\partial \mathbf{x}} \right|_{\hat{\mathbf{x}}_{k-1|k-2}} \tag{5.101}$$

and $\bar{\mathbf{F}}_{k-1}$ is the Jacobian matrix of partial derivatives of $h(\mathbf{x}, \mathbf{d})$ with respect to $\mathbf{d}$ evaluated at the previous *a priori* state estimate; that is

$$\bar{\mathbf{F}}_{k-1} = \left. \frac{\partial h(\mathbf{x}, \mathbf{d})}{\partial \mathbf{d}} \right|_{\hat{\mathbf{x}}_{k-1|k-2}} \tag{5.102}$$

The measurement residual or innovation, ν_k, is

$$\nu_k = \mathbf{z}_k - h\left(\hat{\mathbf{x}}_{k|k-1}, \mathbf{0}\right) \tag{5.103}$$

The residual covariance is

$$\tilde{\mathbf{R}}_k = \bar{\mathbf{C}}_k \mathbf{P}_{k|k-1} \bar{\mathbf{C}}_k^T + \bar{\mathbf{F}}_k \mathbf{S}_k \bar{\mathbf{F}}_k^T + \mathbf{R}_k \tag{5.104}$$

where $\bar{\mathbf{C}}_k$ is the Jacobian matrix of partial derivatives of $h\left(\mathbf{x}, \mathbf{0}\right)$ with respect to $\mathbf{x}$ evaluated at the current *a priori* state estimate, $\hat{\mathbf{x}}_{k|k-1}$; that is

$$\bar{\mathbf{C}}_k = \left.\frac{\partial h\left(\mathbf{x}, \mathbf{0}\right)}{\partial \mathbf{x}}\right|_{\hat{\mathbf{x}}_{k|k-1}} \tag{5.105}$$

and $\bar{\mathbf{F}}_k$ is the Jacobian matrix of partial derivatives of $h\left(\mathbf{x}, \mathbf{d}\right)$ with respect to $\mathbf{d}$ evaluated at the current *a priori* state estimate; that is

$$\bar{\mathbf{F}}_k = \left.\frac{\partial h\left(\mathbf{x}, \mathbf{d}\right)}{\partial \mathbf{d}}\right|_{\hat{\mathbf{x}}_{k|k-1}} \tag{5.106}$$

The Kalman gain is then

$$\begin{aligned} \mathbf{K}_k &= \mathbf{P}_{k|k-1} \bar{\mathbf{C}}_k^T \tilde{\mathbf{R}}_k^{-1} \\ &= \mathbf{P}_{k|k-1} \bar{\mathbf{C}}_k^T \left(\bar{\mathbf{C}}_k \mathbf{P}_{k|k-1} \bar{\mathbf{C}}_k^T + \bar{\mathbf{F}}_k \mathbf{S}_k \bar{\mathbf{F}}_k^T + \mathbf{R}_k\right)^{-1} \end{aligned} \tag{5.107}$$

The updated state estimate with measurement $\mathbf{z}_k$ is

$$\begin{aligned} \hat{\mathbf{x}}_{k|k} &= \hat{\mathbf{x}}_{k|k-1} + \mathbf{K}_k \nu_k \\ &= \hat{\mathbf{x}}_{k|k-1} + \mathbf{K}_k \left[\mathbf{z}_k - h\left(\hat{\mathbf{x}}_{k|k-1}, \mathbf{0}\right)\right] \end{aligned} \tag{5.108}$$

and the updated error covariance is

$$\mathbf{P}_{k|k} = \left(\mathbf{I} - \mathbf{K}_k \bar{\mathbf{C}}_k\right) \mathbf{P}_{k|k-1} \tag{5.109}$$

The updated measurement is given by

$$\hat{\mathbf{z}}_k = h\left(\hat{\mathbf{x}}_{k|k}\right) + \bar{\mathbf{F}}_k \mathbf{S}_k \bar{\mathbf{F}}_k^T \left(\bar{\mathbf{F}}_k \mathbf{S}_k \bar{\mathbf{F}}_k^T + \mathbf{R}_k\right)^{-1} \left[\mathbf{y}_k - h\left(\hat{\mathbf{x}}_{k|k}, \mathbf{0}\right)\right] \tag{5.110}$$

The EKF algorithm is summarized below for the case where the measurement contains process noise.

1. The dynamic system is given by the following process and measurement equations:

$$\mathbf{x}_k = f\left(\mathbf{x}_{k-1}, \mathbf{d}_{k-1}\right) + \mathbf{w}_{k-1} \tag{5.111a}$$
$$\mathbf{z}_k = h\left(\mathbf{x}_k, \mathbf{d}_k\right) + \mathbf{v}_k \tag{5.111b}$$
$$\mathbf{w}_k \sim (0, \mathbf{Q}_k) \tag{5.111c}$$
$$\mathbf{d}_k \sim (0, \mathbf{S}_k) \tag{5.111d}$$
$$\mathbf{v}_k \sim (0, \mathbf{R}_k) \tag{5.111e}$$
$$E\left[\mathbf{w}_k \mathbf{w}_j^T\right] = \mathbf{Q}_k \delta k, j \tag{5.111f}$$
$$E\left[\mathbf{d}_k \mathbf{d}_j^T\right] = \mathbf{S}_k \delta k, j \tag{5.111g}$$
$$E\left[\mathbf{v}_k \mathbf{v}_j^T\right] = \mathbf{R}_k \delta k, j \tag{5.111h}$$
$$E\left[\mathbf{w}_k \mathbf{d}_j^T\right] = E\left[\mathbf{d}_k \mathbf{w}_j^T\right] = \mathbf{0} \tag{5.111i}$$
$$E\left[\mathbf{w}_k \mathbf{v}_j^T\right] = E\left[\mathbf{v}_k \mathbf{w}_j^T\right] = \mathbf{0} \tag{5.111j}$$
$$E\left[\mathbf{d}_k \mathbf{v}_j^T\right] = E\left[\mathbf{v}_k \mathbf{d}_j^T\right] = \mathbf{0} \tag{5.111k}$$

2. The initialization of the filter is as follows:

$$\hat{\mathbf{x}}_{0|0} = E\left[\mathbf{x}_0\right] \tag{5.112}$$
$$\mathbf{P}_{0|0} = E\left[\left(\mathbf{x}_0 - \hat{\mathbf{x}}_{0|0}\right)\left(\mathbf{x}_0 - \hat{\mathbf{x}}_{0|0}\right)^T\right] \tag{5.113}$$

3. For each time step, $k = 1, 2, \ldots, N$, the time update filter equations are

$$\mathbf{J}_k = \bar{\mathbf{E}}_k \mathbf{S}_k \bar{\mathbf{F}}_k^T \left(\bar{\mathbf{F}}_k \mathbf{S}_k \bar{\mathbf{F}}_k^T + \mathbf{R}_k \right)^{-1} \tag{5.114}$$

$$\hat{\mathbf{x}}_{k|k-1} = f\left(\hat{\mathbf{x}}_{k-1|k-1}, \mathbf{0} \right) + \mathbf{J}_{k-1} \left[\mathbf{z}_{k-1} - h\left(\hat{\mathbf{x}}_{k-1|k-1}, \mathbf{0} \right) \right] \tag{5.115}$$

$$\begin{aligned} \mathbf{P}_{k|k-1} = & \left(\bar{\mathbf{A}}_{k-1} - \mathbf{J}_{k-1} \bar{\mathbf{C}}_{k-1} \right) \mathbf{P}_{k-1|k-1} \left(\bar{\mathbf{A}}_{k-1} - \mathbf{J}_{k-1} \bar{\mathbf{C}}_{k-1} \right)^T \\ & + \bar{\mathbf{E}}_{k-1} \mathbf{S}_{k-1} \bar{\mathbf{E}}_{k-1}^T + \mathbf{Q}_{k-1} - \mathbf{J}_{k-1} \bar{\mathbf{F}}_{k-1} \mathbf{S}_{k-1} \bar{\mathbf{E}}_{k-1}^T \end{aligned} \tag{5.116}$$

where

$$\bar{\mathbf{A}}_{k-1} = \left. \frac{\partial f\left(\mathbf{x}, \mathbf{0} \right)}{\partial \mathbf{x}} \right|_{\hat{\mathbf{x}}_{k-1|k-1}} \tag{5.117}$$

$$\bar{\mathbf{E}}_{k-1} = \left. \frac{\partial f\left(\mathbf{x}, \mathbf{d} \right)}{\partial \mathbf{d}} \right|_{\hat{\mathbf{x}}_{k-1|k-1}} \tag{5.118}$$

$$\bar{\mathbf{C}}_{k-1} = \left. \frac{\partial h\left(\mathbf{x}, \mathbf{0} \right)}{\partial \mathbf{x}} \right|_{\hat{\mathbf{x}}_{k-1|k-2}} \tag{5.119}$$

$$\bar{\mathbf{F}}_{k-1} = \left. \frac{\partial h\left(\mathbf{x}, \mathbf{d} \right)}{\partial \mathbf{d}} \right|_{\hat{\mathbf{x}}_{k-1|k-2}} \tag{5.120}$$

The measurement update equations are

$$\mathbf{K}_k = \mathbf{P}_{k|k-1} \bar{\mathbf{C}}_k^T \left(\bar{\mathbf{C}}_k \mathbf{P}_{k|k-1} \bar{\mathbf{C}}_k^T + \bar{\mathbf{F}}_k \mathbf{S}_k \bar{\mathbf{F}}_k^T + \mathbf{R}_k \right)^{-1} \tag{5.121}$$

$$\hat{\mathbf{x}}_{k|k} = \hat{\mathbf{x}}_{k|k-1} + \mathbf{K}_k \left[\mathbf{z}_k - h\left(\hat{\mathbf{x}}_{k|k-1}, \mathbf{0} \right) \right] \tag{5.122}$$

$$\mathbf{P}_{k|k} = \left(\mathbf{I} - \mathbf{K}_k \mathbf{C}_k \right) \mathbf{P}_{k|k-1} \tag{5.123}$$

where

$$\bar{\mathbf{C}}_k = \left. \frac{\partial h\left(\mathbf{x}, \mathbf{0} \right)}{\partial \mathbf{x}} \right|_{\hat{\mathbf{x}}_{k|k-1}} \tag{5.124}$$

$$\bar{\mathbf{F}}_k = \left. \frac{\partial h\left(\mathbf{x}, \mathbf{d} \right)}{\partial \mathbf{d}} \right|_{\hat{\mathbf{x}}_{k|k-1}} \tag{5.125}$$

An updated measurement estimate is given by

$$\hat{\mathbf{z}}_k = h\left(\hat{\mathbf{x}}_{k|k}\right) + \bar{\mathbf{F}}_k \mathbf{S}_k \bar{\mathbf{F}}_k^T \left(\bar{\mathbf{F}}_k \mathbf{S}_k \bar{\mathbf{F}}_k^T + \mathbf{R}_k\right)^{-1} \left[\mathbf{z}_k - h\left(\hat{\mathbf{x}}_{k|k}, \mathbf{0}\right)\right] \tag{5.126}$$

The previous adaptation addresses the issue of the presence of the unknown process noise in the measurement equation. It remains to find a means of estimating the covariance of this process noise, as well as the covariance of the additive measurement noise. This is considered next.

5.3 Unknown noise statistics

Optimum Kalman filtering requires exact knowledge of the process noise covariances matrices $\mathbf{Q}_k$, unknown feedthrough input noise covariance $\mathbf{S}_k$, and the measurement noise covariance $\mathbf{R}_k$. However, these noise statistics are generally unknown for ambient measurement cases involving wind excitation, and have to be estimated from measurements. For the application of state estimation for the flexible structure coupled with a pendulum tuned mass damper (PTMD), the process noises capture the effect of the unknown wind excitation as well as modelling uncertainties and the measurements are corrupted with noise; therefore, both noise statistics are unknown. The problem of Kalman filtering with unknown noise covariances is more commonly referred to adaptive filtering.

Previous studies involving parameter estimation of structural systems [36, 63, 53, 27, 84, 62, 95, 109, 107, 106, 102] have not addressed situations where *a priori* knowledge of the process and noise covariances are not available. *A prior* knowledge of both the disturbance and measurement noise covariances are difficult to obtain at the start of the experiment. In the present work, these statistics are estimated first, prior to the parameter estimation step, using the initial estimate of the model.

Mehra identified the following four main approaches to adaptive filtering [67]; Bayesian estimation, maximum likelihood estimation, covariance-matching techniques, and correlation methods, which are considered more closely in the present work. The basic premise

of the autocorrelation methods is as follows. A set of equations are derived relating the system parameters to observed autocorrelation functions, either the autocorrelation of the output $\mathbf{z}_k$ or the innovation term, $\nu_k = \mathbf{z}_k - \mathbf{C}_k\hat{\mathbf{x}}_{k|k-1}$. Using output correlation is generally considered more restrictive [6]; therefore, residual correlation is considered further.

5.3.1 Evaluating filter performance

It is well established that the optimum Kalman filter residual sequence is a white stochastic process with a known covariance, $\mathbf{C}_k\mathbf{P}_{k|k-1}\mathbf{C}_k^T + \mathbf{R}_k$ [85] when the noise covariance matrices are known. The same will be demonstrated for the case when a feedthrough process noise, $\mathbf{d}_k$, is introduced, as in Sec. 5.2.1.

Recall the linear discrete transition and measurement equations for the state estimation problem described earlier.

$$\mathbf{x}_k = \mathbf{A}_{k-1}\mathbf{x}_{k-1} + \mathbf{E}_{k-1}\mathbf{d}_{k-1} + \mathbf{w}_{k-1} \tag{5.127}$$

$$\mathbf{z}_k = \mathbf{C}_{k-1}\mathbf{x}_k + \mathbf{F}_{k-1}\mathbf{d}_k + \mathbf{v}_k \tag{5.128}$$

The innovation sequence is

$$\begin{aligned} \nu_k &= \mathbf{z}_k - \mathbf{C}_k\hat{\mathbf{x}}_{k|k-1} \\ &= \mathbf{C}_k\mathbf{x}_k + \mathbf{F}_k\mathbf{d}_k + \mathbf{v}_k - \mathbf{C}_k\hat{\mathbf{x}}_{k|k-1} \\ &= \mathbf{C}_k\epsilon_{k|k-1} + \mathbf{F}_k\mathbf{d}_k + \mathbf{v}_k \end{aligned} \tag{5.129}$$

where

$$\epsilon_{k|k-1} = \mathbf{x}_k - \hat{\mathbf{x}}_{k|k-1} \tag{5.130}$$

For an optimal filter, the innovation sequence is zero mean Gaussian white noise (zero autocorrelation for non-zero lag). However, for a suboptimal filter, the autocorrelation of the innovation sequence does not satisfy this property. Therefore, one must determine an expression for the autocorrelation of the innovation sequence for suboptimal gain. For

$k > j$, the covariance of the residuals is given by

$$\begin{aligned} E\left[\nu_k \nu_j^T\right] &= E\left[\left(\mathbf{C}_k \epsilon_{k|k-1} + \mathbf{F}_k \mathbf{d}_k + \mathbf{v}_k\right)\left(\mathbf{C}_j \epsilon_{j|j-1} + \mathbf{F}_j \mathbf{d}_j + \mathbf{v}_j\right)^T\right] \\ &= \mathbf{C}_k E\left[\epsilon_{k|k-1}\epsilon_{j|j-1}^T\right]\mathbf{C}_j^T + \mathbf{C}_k E\left[\epsilon_{k|k-1}\mathbf{d}_j^T\right]\mathbf{F}_j^T + \mathbf{C}_k E\left[\epsilon_{k|k-1}\mathbf{v}_j^T\right] \\ &\quad \mathbf{F}_k E\left[\mathbf{d}_k \epsilon_{j|j-1}^T\right]\mathbf{C}_j^T + \mathbf{F}_k E\left[\mathbf{d}_k \mathbf{d}_j^T\right]\mathbf{F}_j^T + \mathbf{F}_k E\left[\mathbf{d}_k \mathbf{v}_j^T\right] \\ &\quad E\left[\mathbf{v}_k \epsilon_{j|j-1}^T\right]\mathbf{C}_j^T + E\left[\mathbf{v}_k \mathbf{d}_j^T\right]\mathbf{F}_j^T + E\left[\mathbf{v}_k \mathbf{v}_j^T\right] \\ &= \mathbf{C}_k E\left[\epsilon_{k|k-1}\epsilon_{j|j-1}^T\right]\mathbf{C}_j^T + \mathbf{C}_k E\left[\epsilon_{k|k-1}\mathbf{d}_j^T\right]\mathbf{F}_j^T + \mathbf{C}_k E\left[\epsilon_{k|k-1}\mathbf{v}_j^T\right] \end{aligned} \tag{5.131}$$

For $k = j$, the covariance of the residuals is given by

$$\begin{aligned} E\left[\nu_j \nu_j^T\right] &= \mathbf{C}_j \mathbf{P}_{j|j-1}\mathbf{C}_j^T + \mathbf{F}_j \mathbf{S}_j \mathbf{F}_j^T + \mathbf{R}_j \\ &= \mathbf{\Gamma}_0 \end{aligned} \tag{5.132}$$

A recursive relationship for the *a priori* state estimate error can be developed as follows:

$$\begin{aligned} \epsilon_{k+1|k} &= \mathbf{x}_{k+1} - \hat{\mathbf{x}}_{k+1|k} \\ &= \mathbf{A}_k \mathbf{x}_k + \mathbf{E}_k \mathbf{d}_k + \mathbf{w}_k - \mathbf{A}_k \hat{\mathbf{x}}_{k|k} - \mathbf{J}_k\left(\mathbf{x}_k - \mathbf{C}_k \hat{\mathbf{x}}_{k|k}\right) \\ &= \mathbf{A}_k \mathbf{x}_k + \mathbf{E}_k \mathbf{d}_k + \mathbf{w}_k - \mathbf{A}_k \hat{\mathbf{x}}_{k|k} - \mathbf{A}_k \mathbf{K}_k \mathbf{C}_k \mathbf{x}_k \\ &\quad - \mathbf{A}_k \mathbf{F}_k \mathbf{d}_k - \mathbf{A}_k \mathbf{K}_k \mathbf{v}_k + \mathbf{A}_k \mathbf{K}_k \mathbf{C}_k \hat{\mathbf{x}}_{k|k-1} \\ &\quad + \mathbf{J}_k \mathbf{C}_k \hat{\mathbf{x}}_{k|k-1} + \mathbf{J}_k \mathbf{C}_k \mathbf{K}_k \mathbf{C}_k \mathbf{x}_k + \mathbf{J}_k \mathbf{C}_k \mathbf{K}_k \mathbf{F}_k \mathbf{d}_k \\ &\quad + \mathbf{J}_k \mathbf{C}_k \mathbf{K}_k \mathbf{v}_k - \mathbf{J}_k \mathbf{C}_k \mathbf{K}_k \mathbf{C}_k \hat{\mathbf{x}}_{k|k-1} - \mathbf{J}_k \mathbf{C}_k \mathbf{x}_k \\ &\quad - \mathbf{J}_k \mathbf{F}_k \mathbf{d}_k - \mathbf{J}_k \mathbf{v}_k \\ &= \left(\mathbf{A}_k - \mathbf{A}_k \mathbf{K}_k \mathbf{C}_k + \mathbf{J}_k \mathbf{C}_k \mathbf{K}_k \mathbf{C}_k - \mathbf{J}_k \mathbf{C}_k\right)\epsilon_{k|k-1} \\ &\quad + \left(\mathbf{E}_k + \mathbf{A}_k \mathbf{K}_k \mathbf{F}_k + \mathbf{J}_k \mathbf{C}_k \mathbf{K}_k \mathbf{F}_k - \mathbf{J}_k \mathbf{F}_k\right)\mathbf{d}_k + \mathbf{w}_k \\ &\quad - \left(\mathbf{A}_k \mathbf{K}_k - \mathbf{J}_k \mathbf{C}_k \mathbf{K}_k + \mathbf{J}_k\right)\mathbf{v}_k \\ &= \tilde{\phi}_k' \epsilon_{k|k-1} + \mathbf{v}_k' \end{aligned} \tag{5.133}$$

where

$$\tilde{\phi}'_k = \mathbf{A}_k - \mathbf{A}_k\mathbf{K}_k\mathbf{C}_k + \mathbf{J}_k\mathbf{C}_k\mathbf{K}_k\mathbf{C}_k - \mathbf{J}_k\mathbf{C}_k \tag{5.134}$$

$$\mathbf{v}'_k = \left(\mathbf{E}_k + \mathbf{A}_k\mathbf{K}_k\mathbf{F}_k + \mathbf{J}_k\mathbf{C}_k\mathbf{K}_k\mathbf{F}_k - \mathbf{J}_k\mathbf{F}_k\right)\mathbf{d}_k + \mathbf{w}_k \tag{5.135}$$

$$- \left(\mathbf{A}_k\mathbf{K}_k - \mathbf{J}_k\mathbf{C}_k\mathbf{K}_k + \mathbf{J}_k\right)\mathbf{v}_k \tag{5.136}$$

$$\tag{5.137}$$

Note that the gain $\mathbf{K}_k$ is not the Kalman gain, since the covariance of the residuals for a suboptimal filter are to be determined. Proceed by defining

$$\tilde{\phi}'_{k,j} = \begin{cases} \tilde{\phi}'_{k-1}\tilde{\phi}'_{k-2}\cdots\tilde{\phi}'_j & k > j \\ \mathbf{I} & k = j \end{cases} \tag{5.138}$$

Then $\epsilon_{k|k-1}$ can be written as

$$\epsilon_{k|k-1} = \tilde{\phi}'_{k,j}\epsilon_{j|j-1} + \sum_{i=j}^{k-1}\tilde{\phi}'_{k,i+1}\mathbf{v}'_i \tag{5.139}$$

Evaluating the expectations in Eq. 5.131 gives

$$\begin{aligned} E\left[\epsilon_{k|k-1}\epsilon_{j|j-1}^T\right] &= \tilde{\phi}'_{k,j}E\left[\epsilon_{j|j-1}\epsilon_{j|j-1}^T\right] \\ &= \tilde{\phi}'_{k,j+1}\tilde{\phi}'_j\mathbf{P}_{j|j-1} \end{aligned} \tag{5.140}$$

$$\begin{aligned} E\left[\epsilon_{k|k-1}\mathbf{d}_j^T\right] &= \tilde{\phi}'_{k,j+1}\left(\mathbf{E}_j + \mathbf{A}_j\mathbf{K}_j\mathbf{F}_j + \mathbf{J}_j\mathbf{C}_j\mathbf{K}_j\mathbf{F}_j - \mathbf{J}_j\mathbf{F}_j\right)E\left[\mathbf{d}_j\mathbf{d}_j^T\right] \\ &= \tilde{\phi}'_{k,j+1}\left(\mathbf{E}_j + \mathbf{A}_j\mathbf{K}_j\mathbf{F}_j + \mathbf{J}_j\mathbf{C}_j\mathbf{K}_j\mathbf{F}_j - \mathbf{J}_j\mathbf{F}_j\right)\mathbf{S}_j \end{aligned} \tag{5.141}$$

$$\begin{aligned} E\left[\epsilon_{k|k-1}\mathbf{v}_j^T\right] &= -\tilde{\phi}'_{k,j+1}\left(\mathbf{A}_k\mathbf{K}_k - \mathbf{J}_k\mathbf{C}_k\mathbf{K}_k + \mathbf{J}_k\right)E\left[\mathbf{v}_j\mathbf{v}_j^T\right] \\ &= -\tilde{\phi}'_{k,j+1}\left(\mathbf{A}_k\mathbf{K}_k - \mathbf{J}_k\mathbf{C}_k\mathbf{K}_k + \mathbf{J}_k\right)\mathbf{R}_j \end{aligned} \tag{5.142}$$

By taking advantage the result $\tilde{\phi}'_j = \mathbf{A}_j - \mathbf{A}_j\mathbf{K}_j\mathbf{C}_j + \mathbf{J}_j\mathbf{C}_j\mathbf{K}_j\mathbf{C}_j - \mathbf{J}_j\mathbf{C}_j$ Eq. 5.131 becomes

(for $k > j$)

$$\begin{aligned} E\left[\nu_k \nu_j^T\right] &= \mathbf{C}_k \tilde{\phi}'_{k,j+1} \tilde{\phi}'_j \mathbf{P}_{j|j-1} \mathbf{C}_j^T \\ &\quad + \mathbf{C}_k \tilde{\phi}'_{k,j+1} \left(\mathbf{E}_j + \mathbf{A}_j \mathbf{K}_j \mathbf{F}_j + \mathbf{J}_j \mathbf{C}_j \mathbf{K}_j \mathbf{F}_j - \mathbf{J}_j \mathbf{F}_j\right) \mathbf{S}_j \mathbf{F}_j^T \\ &\quad - \mathbf{C}_k \tilde{\phi}'_{k,j+1} \left(\mathbf{A}_k \mathbf{K}_k - \mathbf{J}_k \mathbf{C}_k \mathbf{K}_k + \mathbf{J}_k\right) \mathbf{R}_j \\ &= \mathbf{C}_k \tilde{\phi}'_{k,j+1} \left[\mathbf{A}_j \mathbf{P}_{j|j-1} \mathbf{C}_j^T + \mathbf{E}_j \mathbf{S}_j \mathbf{F}_j^T \right. \\ &\quad \left. - \left(\mathbf{A}_j \mathbf{K}_j - \mathbf{J}_j \mathbf{C}_j \mathbf{K}_j + \mathbf{J}_j\right) \left(\mathbf{C}_j \mathbf{P}_{j|j-1} \mathbf{C}_j^T + \mathbf{F}_j \mathbf{S}_j \mathbf{F}_j^T + \mathbf{R}_j\right)\right] \end{aligned} \tag{5.143}$$

Substituting in the result for the one-step predictor gain matrix in Eq. 5.75 gives

$$\begin{aligned} E\left[\nu_k \nu_j^T\right] &= \mathbf{C}_k \tilde{\phi}'_{k,j+1} \left[\mathbf{A}_j \mathbf{P}_{j|j-1} \mathbf{C}_j^T + \mathbf{E}_j \mathbf{S}_j \mathbf{F}_j^T \right. \\ &\quad - \left(\mathbf{A}_j \mathbf{K}_j - \mathbf{J}_j \mathbf{C}_j \mathbf{K}_j\right) \left(\mathbf{C}_j \mathbf{P}_{j|j-1} \mathbf{C}_j^T + \mathbf{F}_j \mathbf{S}_j \mathbf{F}_j^T + \mathbf{R}_j\right) \\ &\quad \left. - \mathbf{J}_j \mathbf{C}_j \mathbf{P}_{j|j-1} \mathbf{C}_j^T - \mathbf{J}_j \left(\mathbf{F}_j \mathbf{S}_j \mathbf{F}_j^T + \mathbf{R}_j\right)\right] \\ &= \mathbf{C}_k \tilde{\phi}'_{k,j+1} \left(\mathbf{A}_j - \mathbf{J}_j \mathbf{C}_j\right) \\ &\quad \left[\mathbf{P}_{j|j-1} \mathbf{C}_j^T - \mathbf{K}_j \left(\mathbf{C}_j \mathbf{P}_{j|j-1} \mathbf{C}_j^T + \mathbf{F}_j \mathbf{S}_j \mathbf{F}_j^T + \mathbf{R}_j\right)\right] \\ &= \mathbf{C}_k \tilde{\phi}'_{k,j+1} \left(\mathbf{A}_j - \mathbf{J}_j \mathbf{C}_j\right) \left(\mathbf{P}_{j|j-1} \mathbf{C}_j^T - \mathbf{K}_j \mathbf{\Gamma}_0\right) \end{aligned} \tag{5.144}$$

Note that substitution of the optimal Kalman gain given in Eq. 5.80 makes $E\left[\nu_k \nu_j^T\right]$ vanish for all $k \neq j$. The performance of the filter can be evaluated based on this knowledge. The residual sequence of the filter can be measured and its statistics computed, namely the mean and covariance. These are compared with the known mean and covariance for the optimal filter. Incorrect selection of the noise covariance matrices can cause the residual sequence statistics to deviate from the theoretical values. This feature is exploited for the purpose of noise estimation by correlation methods.

5.3.2 Noise estimation by correlation methods

The basic approach used here is one that was initially proposed by Bélanger [4]. However, the author did not consider the direct feedthrough term, $\mathbf{d}_k$, in the measurement equation. Hence, the relevant expressions are rederived. A set of equations are derived relating the

system matrices, filter gain, and noise covariance matrices to observed autocorrelation of the innovation term, $\nu_k = \mathbf{z}_k - \mathbf{C}_k\hat{\mathbf{x}}_{k|k-1}$. By setting the covariance matrices as a linear combination of a set of parameters, it was shown that the correlation function of the filter's residuals is also a linear function of the same set of parameters [4]. By measuring the actual correlation of the residual sequence, a weighted least-squares fit can then be used to estimate these parameters, and subsequently, the noise covariance matrices. In the ensuing discussion, it will be shown that such a linear relationship also exists in the presence of the direct feedthrough term, and hence the method can be used for the case at hand.

Note that a one-step Kalman filter is first developed for the case of feedthrough process noise, where the time and measurement update steps are performed simultaneously, and there is no longer a need for the one-step predictor gain matrix, $\mathbf{J}_k$. Given the following linear system:

$$\mathbf{x}_k = \mathbf{A}_{k-1}\mathbf{x}_{k-1} + \mathbf{E}_{k-1}\mathbf{d}_{k-1} + \mathbf{w}_{k-1} \tag{5.145}$$

$$\mathbf{z}_k = \mathbf{C}_k\mathbf{x}_k + \mathbf{F}_k\mathbf{d}_k + \mathbf{v}_k \tag{5.146}$$

$$\mathbf{w}_k \sim (0, \mathbf{Q}_k) \tag{5.147}$$

$$\mathbf{d}_k \sim (0, \mathbf{S}_k) \tag{5.148}$$

$$\mathbf{v}_k \sim (0, \mathbf{R}_k) \tag{5.149}$$

$$E\left[\mathbf{w}_k\mathbf{w}_j^T\right] = \mathbf{Q}_k\delta k, j \tag{5.150}$$

$$E\left[\mathbf{d}_k\mathbf{d}_j^T\right] = \mathbf{S}_k\delta k, j \tag{5.151}$$

$$E\left[\mathbf{v}_k\mathbf{v}_j^T\right] = \mathbf{R}_k\delta k, j \tag{5.152}$$

$$E\left[\mathbf{w}_k\mathbf{d}_j^T\right] = E\left[\mathbf{d}_k\mathbf{w}_j^T\right] = \mathbf{0} \tag{5.153}$$

$$E\left[\mathbf{w}_k\mathbf{v}_j^T\right] = E\left[\mathbf{v}_k\mathbf{w}_j^T\right] = \mathbf{0} \tag{5.154}$$

$$E\left[\mathbf{d}_k\mathbf{v}_j^T\right] = E\left[\mathbf{v}_k\mathbf{d}_j^T\right] = \mathbf{0} \tag{5.155}$$

it is assumed that the noise covariance matrices $\mathbf{Q}_k$, $\mathbf{S}_k$, and $\mathbf{R}_k$ are linear functions of $\hat{N}$

components of a vector α. That it

$$\mathbf{Q}_k = \sum_{l=1}^{\hat{N}} \alpha_l \mathbf{Q}_l \tag{5.156}$$

$$\mathbf{S}_k = \sum_{l=1}^{\hat{N}} \alpha_l \mathbf{S}_l \tag{5.157}$$

$$\mathbf{R}_k = \sum_{l=1}^{\hat{N}} \alpha_l \mathbf{R}_l \tag{5.158}$$

with $\mathbf{Q}_l$, $\mathbf{S}_l$, and $\mathbf{R}_l$ are known constant matrices, each containing one element of the assumed initial noise covariance matrices.

Assume a one-step filter of the form [85]

$$\hat{\mathbf{x}}_{k|k-1} = \mathbf{A}_{k-1}\hat{\mathbf{x}}_{k-1|k-2} + \mathbf{K}_{k-1}\nu_{k-1} \tag{5.159}$$

where the residual is given by

$$\nu_k = \mathbf{z}_k - \mathbf{C}_k\hat{\mathbf{x}}_{k|k-1} \tag{5.160}$$

The *a priori* state estimate error is

$$\begin{aligned}
\epsilon_{k|k-1} &= \mathbf{x}_k - \hat{\mathbf{x}} \\
&= \mathbf{x}_k - \mathbf{A}_{k-1}\hat{\mathbf{x}}_{k-1|k-2} - \mathbf{K}_{k-1}\mathbf{z}_{k-1} + \mathbf{K}_{k-1}\mathbf{C}_{k-1}\hat{\mathbf{x}}_{k|k-1} \\
&= \mathbf{x}_k - \left(\mathbf{A}_{k-1} - \mathbf{K}_{k-1}\mathbf{C}_{k-1}\right)\hat{\mathbf{x}}_{k-1|k-2} - \mathbf{K}_{k-1}\mathbf{z}_{k-1} \\
&= \mathbf{A}_{k-1}\mathbf{x}_{k-1} - \left(\mathbf{A}_{k-1} - \mathbf{K}_{k-1}\mathbf{C}_{k-1}\right)\hat{\mathbf{x}}_{k-1|k-2} + \mathbf{E}_{k-1}\mathbf{d}_{k-1} + \mathbf{w}_{k-1} \\
&\quad - \mathbf{K}_{k-1}\left(\mathbf{C}_{k-1}\mathbf{x}_{k-1} + \mathbf{F}_{k-1}\mathbf{d}_{k-1} - \mathbf{K}_{k-1}\mathbf{v}_{k-1}\right) \\
&= \left(\mathbf{A}_{k-1} - \mathbf{K}_{k-1}\mathbf{C}_{k-1}\right)\left(\mathbf{x}_{k-1} - \hat{\mathbf{x}}_{k-1|k-2}\right) \\
&\quad + \left(\mathbf{E}_{k-1} - \mathbf{K}_{k-1}\mathbf{F}_{k-1}\right)\mathbf{d}_{k-1} + \mathbf{w}_{k-1} - \mathbf{K}_{k-1}\mathbf{v}_{k-1} \\
&= \left(\mathbf{A}_{k-1} - \mathbf{K}_{k-1}\mathbf{C}_{k-1}\right)\epsilon_{k-1|k-2} + \left(\mathbf{E}_{k-1} - \mathbf{K}_{k-1}\mathbf{F}_{k-1}\right)\mathbf{d}_{k-1} \\
&\quad + \mathbf{w}_{k-1} - \mathbf{K}_{k-1}\mathbf{v}_{k-1}
\end{aligned} \tag{5.161}$$

The error covariance is given by

$$\begin{aligned}
\mathbf{P}_{k|k-1} &= E\left[\epsilon_{k|k-1}\epsilon_{k|k-1}^T\right] \\
&= E\left\{\left[\left(\mathbf{A}_{k-1}-\mathbf{K}_{k-1}\mathbf{C}_{k-1}\right)\epsilon_{k-1|k-2}+\left(\mathbf{E}_{k-1}-\mathbf{K}_{k-1}\mathbf{F}_{k-1}\right)\mathbf{d}_{k-1}\right.\right. \\
&\quad \left.+\mathbf{w}_{k-1}-\mathbf{K}_{k-1}\mathbf{v}_{k-1}\right]\left[\left(\mathbf{A}_{k-1}-\mathbf{K}_{k-1}\mathbf{C}_{k-1}\right)\epsilon_{k-1|k-2}\right. \\
&\quad \left.\left.+\left(\mathbf{E}_{k-1}-\mathbf{K}_{k-1}\mathbf{F}_{k-1}\right)\mathbf{d}_{k-1}+\mathbf{w}_{k-1}-\mathbf{K}_{k-1}\mathbf{v}_{k-1}\right]^T\right\} \\
&= \left(\mathbf{A}_{k-1}-\mathbf{K}_{k-1}\mathbf{C}_{k-1}\right)\mathbf{P}_{k-1|k-2}\left(\mathbf{A}_{k-1}-\mathbf{K}_{k-1}\mathbf{C}_{k-1}\right)^T \\
&\quad +\left(\mathbf{E}_{k-1}-\mathbf{K}_{k-1}\mathbf{F}_{k-1}\right)\mathbf{S}_{k-1}\left(\mathbf{E}_{k-1}-\mathbf{K}_{k-1}\mathbf{F}_{k-1}\right)^T \\
&\quad +\mathbf{Q}_{k-1}+\mathbf{K}_{k-1}\mathbf{R}_{k-1}\mathbf{K}_{k-1}^T
\end{aligned} \tag{5.162}$$

Note that

$$E\left\{\epsilon_{k-1|k-2}\left[\left(\mathbf{E}_{k-1}-\mathbf{K}_{k-1}\mathbf{F}_{k-1}\right)\mathbf{d}_{k-1}+\mathbf{w}_{k-1}-\mathbf{K}_{k-1}\mathbf{v}_{k-1}\right]^T\right\}=\mathbf{0} \tag{5.163}$$

since the error at the previous time step is uncorrelated with the present unknown stochastic input, process noise, and measurement noise.

The optimal gain is one that minimizes $\mathrm{Tr}\left(\mathbf{P}_{k|k-1}\right)$.

$$\begin{aligned}
\frac{\partial\,\mathrm{Tr}\left(\mathbf{P}_{k|k-1}\right)}{\partial\mathbf{K}_{k-1}} &= -2\left(\mathbf{A}_{k-1}-\mathbf{K}_{k-1}\mathbf{C}_{k-1}\right)\mathbf{P}_{k-1|k-2}\mathbf{C}_{k-1}^T \\
&\quad -2\left(\mathbf{E}_{k-1}-\mathbf{K}_{k-1}\mathbf{F}_{k-1}\right)\mathbf{S}_{k-1}\mathbf{F}_{k-1}^T+2\mathbf{K}_{k-1}\mathbf{R}_{k-1} \\
&= 2\mathbf{K}_{k-1}\left(\mathbf{C}\mathbf{P}_{k-1|k-2}\mathbf{C}_{k-1}^T+\mathbf{F}_{k-1}\mathbf{S}_{k-1}\mathbf{F}_{k-1}^T+\mathbf{R}_{k-1}\right) \\
&\quad -2\mathbf{A}_{k-1}\mathbf{P}_{k-1|k-2}\mathbf{C}_{k-1}^T-2\mathbf{E}_{k-1}\mathbf{S}_{k-1}\mathbf{F}_{k-1}^T \\
&= 0
\end{aligned} \tag{5.164}$$

Therefore,

$$\mathbf{K}_k=\left(\mathbf{A}_k\mathbf{P}_{k|k-1}\mathbf{C}_k^T+\mathbf{E}_k\mathbf{S}_k\mathbf{F}_k^T\right)\left(\mathbf{C}_k\mathbf{P}_{k|k-1}\mathbf{C}_k^T+\mathbf{F}_k\mathbf{S}_k\mathbf{F}_k^T+\mathbf{R}_k\right)^{-1} \tag{5.165}$$

The state error covariance can be rewritten as

$$\begin{aligned}\mathbf{P}_{k|k-1} = &\left(\mathbf{A}_{k-1} - \mathbf{K}_{k-1}\mathbf{C}_{k-1}\right)\mathbf{P}_{k-1|k-2}\mathbf{A}_{k-1}^{T} \\ &+ \left(\mathbf{E}_{k-1} - \mathbf{K}_{k-1}\mathbf{F}_{k-1}\right)\mathbf{S}_{k-1}\mathbf{E}_{k-1}^{T} + \mathbf{Q}_{k-1}\end{aligned} \tag{5.166}$$

Using

$$\epsilon_{k|k-1} = \mathbf{x}_k - \hat{\mathbf{x}}_{k|k-1} \tag{5.167}$$

the innovation sequence can be rewritten as

$$\begin{aligned}\nu_k &= \mathbf{z}_k - \mathbf{C}_k\hat{\mathbf{x}}_{k|k-1} \\ &= \mathbf{C}_k\mathbf{x}_k + \mathbf{F}_k\mathbf{d}_k + \mathbf{v}_k - \mathbf{C}_k\hat{\mathbf{x}}_{k|k-1} \\ &= \mathbf{C}_k\epsilon_{k|k-1} + \mathbf{F}_k\mathbf{d}_k + \mathbf{v}_k\end{aligned} \tag{5.168}$$

The covariance of the innovation is given by (for $k > j$)

$$\begin{aligned}E\left[\nu_k\nu_j^T\right] &= E\left[\left(\mathbf{C}_k\epsilon_{k|k-1} + \mathbf{F}_k\mathbf{d}_k + \mathbf{v}_k\right)\left(\mathbf{C}_j\epsilon_{j|j-1} + \mathbf{F}_j\mathbf{d}_j + \mathbf{v}_j\right)^T\right] \\ &= \mathbf{C}_k E\left[\epsilon_{k|k-1}\epsilon_{j|j-1}^T\right]\mathbf{C}_j^T + \mathbf{C}_k E\left[\epsilon_{k|k-1}\mathbf{d}_j^T\right]\mathbf{F}_j^T + \mathbf{C}_k E\left[\epsilon_{k|k-1}\mathbf{v}_j^T\right] \\ &\quad \mathbf{F}_k E\left[\mathbf{d}_k\epsilon_{j|j-1}^T\right]\mathbf{C}_j^T + \mathbf{F}_k E\left[\mathbf{d}_k\mathbf{d}_j^T\right]\mathbf{F}_j^T + \mathbf{F}_k E\left[\mathbf{d}_k\mathbf{v}_j^T\right] \\ &\quad E\left[\mathbf{v}_k\epsilon_{j|j-1}^T\right]\mathbf{C}_j^T + E\left[\mathbf{v}_k\mathbf{d}_j^T\right]\mathbf{F}_j^T + E\left[\mathbf{v}_k\mathbf{v}_j^T\right] \\ &= \mathbf{C}_k E\left[\epsilon_{k|k-1}\epsilon_{j|j-1}^T\right]\mathbf{C}_j^T + \mathbf{C}_k E\left[\epsilon_{k|k-1}\mathbf{d}_j^T\right]\mathbf{F}_j^T + \mathbf{C}_k E\left[\epsilon_{k|k-1}\mathbf{v}_j^T\right]\end{aligned} \tag{5.169}$$

For $k = j$, the covariance of the residuals is given by

$$E\left[\nu_k\nu_k^T\right] = \mathbf{C}_k\mathbf{P}_{k|k-1}\mathbf{C}_k^T + \mathbf{F}_k\mathbf{S}_k\mathbf{F}_k^T + \mathbf{R}_k \tag{5.170}$$

The recursive form of the state estimate error in Eq. 5.161 can be rewritten as

$$\epsilon_{k|k-1} = \phi'_{k-1}\epsilon_{k-1|k-2} + \mathbf{v}'_{k-1} \tag{5.171}$$

where

$$\phi'_k = \mathbf{A}_k - \mathbf{K}_k\mathbf{C}_k \tag{5.172}$$

$$\mathbf{v}'_k = (\mathbf{E}_k - \mathbf{K}_k\mathbf{F}_k)\,\mathbf{d}_k + \mathbf{w}_k - \mathbf{K}_k\mathbf{v}_k \tag{5.173}$$

Define

$$\tilde{\phi}'_{k,j} = \begin{cases} \phi'_{k-1}\phi'_{k-2}\cdots\phi'_j & k > j \\ \mathbf{I} & k = j \end{cases} \tag{5.174}$$

Then

$$\epsilon_{k|k-1} = \tilde{\phi}'_{k,j}\epsilon_{j|j-1} + \sum_{i=j}^{k-1} \tilde{\phi}'_{k,i+1}\mathbf{v}'_i \tag{5.175}$$

or

$$\epsilon_{k|k-1} = \tilde{\phi}'_{k,0}\epsilon_0 + \sum_{i=0}^{k-1} \tilde{\phi}'_{k,i+1}\mathbf{v}'_i \tag{5.176}$$

Now, there exists real numbers $a, b > 0$ such that [46]

$$\left|\left|\tilde{\phi}'_{k,0}\right|\right| \leq ae^{-bk} \tag{5.177}$$

Therefore, by waiting for some time to pass before beginning to process the measurements, the term $\tilde{\phi}'_{k,0}\epsilon_0$ can be dropped. It follows that

$$\epsilon_{k|k-1} = \sum_{i=0}^{k-1} \tilde{\phi}'_{k,i+1}\mathbf{v}'_i \tag{5.178}$$

Evaluating the expectations in Eq. 5.169 gives

$$
\begin{aligned}
E\left[\epsilon_{k|k-1}\epsilon_{j|j-1}^{T}\right] &= E\left[\left(\sum_{i=0}^{k-1}\tilde{\phi}'_{k,i+1}\mathbf{v}'_i\right)\left(\sum_{i=0}^{j-1}\tilde{\phi}'_{j,i+1}\mathbf{v}'_i\right)^{T}\right] \\
&= E\left\{\left[\sum_{i=0}^{k-1}\tilde{\phi}'_{k,i+1}\left(\left(\mathbf{E}_i-\mathbf{K}_i k\mathbf{F}_i\right)\mathbf{d}_i+\mathbf{w}_i-\mathbf{K}_i\mathbf{v}_i\right)\right]\right. \\
&\qquad \left.\left[\sum_{i=0}^{j-1}\tilde{\phi}'_{j,i+1}\left(\left(\mathbf{E}_i-\mathbf{K}_i\mathbf{F}_i\right)\mathbf{d}_i+\mathbf{w}_i-\mathbf{K}_i\mathbf{v}_i\right)\right]^{T}\right\} \\
&= \sum_{i=0}^{j-1}\left\{\tilde{\phi}_{k,i+1}\left[\left(\mathbf{E}_i-\mathbf{K}_i\mathbf{F}_i\right)\mathbf{S}_i\left(\mathbf{E}_i-\mathbf{K}_i\mathbf{F}_i\right)^{T}+\mathbf{Q}_i\right.\right. \\
&\qquad \left.\left.+\mathbf{K}_i\mathbf{R}_i\mathbf{K}_i^{T}\right]\tilde{\phi}'^{T}_{j,i+1}\right\}
\end{aligned}
\tag{5.179}
$$

$$
\begin{aligned}
E\left[\epsilon_{k|k-1}\mathbf{d}_j^{T}\right] &= E\left[\left(\sum_{i=0}^{k-1}\tilde{\phi}'_{k,i+1}\mathbf{v}'_i\right)\mathbf{d}_j^{T}\right] \\
&= E\left\{\left[\sum_{i=0}^{k-1}\tilde{\phi}'_{k,i+1}\left(\left(\mathbf{E}_i-\mathbf{K}_i k\mathbf{F}_i\right)\mathbf{d}_i+\mathbf{w}_i-\mathbf{K}_i\mathbf{v}_i\right)\right]\mathbf{d}_j^{T}\right\} \\
&= \tilde{\phi}'_{k,j+1}\left(\mathbf{E}_j-\mathbf{K}_j\mathbf{F}_j\right)\mathbf{S}_j
\end{aligned}
\tag{5.180}
$$

$$
\begin{aligned}
E\left[\epsilon_{k|k-1}\mathbf{v}_j^{T}\right] &= E\left[\left(\sum_{i=0}^{k-1}\tilde{\phi}'_{k,i+1}\mathbf{v}'_i\right)\mathbf{v}_j^{T}\right] \\
&= E\left\{\left[\sum_{i=0}^{k-1}\tilde{\phi}'_{k,i+1}\left(\left(\mathbf{E}_i-\mathbf{K}_i k\mathbf{F}_i\right)\mathbf{d}_i+\mathbf{w}_i-\mathbf{K}_i\mathbf{v}_i\right)\right]\mathbf{v}_j^{T}\right\} \\
&= -\tilde{\phi}'_{k,j+1}\mathbf{K}_j\mathbf{R}_j
\end{aligned}
\tag{5.181}
$$

The correlation of the residual sequence is then

$$\begin{aligned} E\left[\nu_k \nu_j^T\right] = \mathbf{C}_k \Bigg\{ \sum_{i=0}^{j-1} \tilde{\phi}_{k,i+1} \Big[(\mathbf{E}_i - \mathbf{K}_i \mathbf{F}_i) \, \mathbf{S}_i \, (\mathbf{E}_i - \mathbf{K}_i \mathbf{F}_i)^T + \mathbf{Q}_i \\ + \mathbf{K}_i \mathbf{R}_i \mathbf{K}_i^T \Big] \tilde{\phi}'^T_{j,i+1} \Bigg\} \mathbf{C}_j^T + \mathbf{C}_k \tilde{\phi}'_{k,j+1} \, (\mathbf{E}_j - \mathbf{K}_j \mathbf{F}_j) \, \mathbf{S}_j \mathbf{F}_j^T \\ - \mathbf{C}_k \tilde{\phi}'_{k,j+1} \mathbf{K}_j \mathbf{R}_j \end{aligned} \tag{5.182}$$

for $k > j$.

Assuming that the noise covariance matrices as given by the linear relationship in Eqs. 5.156 through 5.158, the correlation of the residual sequence can be written as

$$E\left[\nu_k \nu_j^T\right] = \sum_{l=1}^{\hat{N}} \mathbf{\Psi}_{l,k,j} \alpha_l \tag{5.183}$$

where

$$\begin{aligned} \mathbf{\Psi}_{l,k,j} = \mathbf{C}_k \Bigg\{ \sum_{i=0}^{j-1} \tilde{\phi}'_{k,i+1} \Big[(\mathbf{E}_i - \mathbf{K}_i \mathbf{F}_i) \, \mathbf{S}_l \, (\mathbf{E}_i - \mathbf{K}_i \mathbf{F}_i)^T + \mathbf{Q}_l \\ + \mathbf{K}_i \mathbf{R}_l \mathbf{K}_i^T \Big] \tilde{\phi}'^T_{j,i+1} \Bigg\} \mathbf{C}_j^T + \mathbf{C}_k \tilde{\phi}'_{k,j+1} \, (\mathbf{E}_j - \mathbf{K}_j \mathbf{F}_j) \, \mathbf{S}_{l,j} \mathbf{F}_j^T \\ - \mathbf{C}_k \tilde{\phi}'_{k,j+1} \mathbf{K}_j \mathbf{R}_{l,j} \end{aligned} \tag{5.184}$$

In order to reduce the computational effort required to calculate 5.184, a recursive algorithm can be developed. Define

$$\mathbf{\Gamma}_{l,k} = \sum_{i=0}^{k-1} \tilde{\phi}'_{k,i+1} \left[(\mathbf{E}_i - \mathbf{K}_i \mathbf{F}_i) \, \mathbf{S}_l \, (\mathbf{E}_i - \mathbf{K}_i \mathbf{F}_i)^T + \mathbf{Q}_l + \mathbf{K}_i \mathbf{R}_l \mathbf{K}_k^T \right] \tilde{\phi}'^T_{k,i+1} \tag{5.185}$$

This can be written in an incremental form,

$$\mathbf{\Gamma}_{l,k+1} = \phi'_k \mathbf{\Gamma}_{l,k} \phi'^T_k + (\mathbf{E}_k - \mathbf{K}_k \mathbf{F}_k) \, \mathbf{S}_l \, (\mathbf{E}_k - \mathbf{K}_k \mathbf{F}_k)^T + \mathbf{Q}_l + \mathbf{K}_k \mathbf{R}_l \mathbf{K}_k^T \tag{5.186}$$

Note in passing that the state estimation error covariance is also linear in the parameter α, by comparing Eq. 5.186 and Eq. 5.166.

$$\mathbf{P}_{k|k-1} = \sum_{l=1}^{\hat{N}} \alpha_l \mathbf{\Gamma}_{l,k} \tag{5.187}$$

Since

$$\begin{aligned} \tilde{\phi}'_{k,i+1} &= \tilde{\phi}'_{k,j} \tilde{\phi}'_{j,i+1} \\ &= \phi'_{k-1}\phi'_{k-2} \cdots \phi'_j \phi'_{j-1}\phi'_{j-2} \cdots \phi'_{i+1} \end{aligned} \tag{5.188}$$

Then Eq. 5.184 becomes

$$\begin{aligned} \mathbf{\Psi}_{l,k,j} = \mathbf{C}_k \tilde{\phi}'_{k,j} \mathbf{\Gamma}_{l,j} \mathbf{C}_j^T + \mathbf{C}_k \tilde{\phi}'_{k,j+1} \left(\mathbf{E}_j - \mathbf{K}_j \mathbf{F}_j\right) \mathbf{S}_l \mathbf{F}_j^T \\ - \mathbf{C}_k \tilde{\phi}'_{k,j+1} \mathbf{K}_j \mathbf{R}_l \end{aligned} \tag{5.189}$$

where

$$\tilde{\phi}'_{k,j} \mathbf{\Gamma}_{l,j} = \sum_{i=0}^{j-1} \tilde{\phi}'_{k,i+1} \left[\left(\mathbf{E}_i - \mathbf{K}_i \mathbf{F}_i\right) \mathbf{S}_l \left(\mathbf{E}_i - \mathbf{K}_i \mathbf{F}_i\right)^T + \mathbf{Q}_l + \mathbf{K}_i \mathbf{R}_l \mathbf{K}_i^T \right] \tilde{\phi}'^T_{j,i+1} \tag{5.190}$$

and

$$\mathbf{\Gamma}_{l,j} = \sum_{i=0}^{j-1} \tilde{\phi}'_{j,i+1} \left[\left(\mathbf{E}_i - \mathbf{K}_i \mathbf{F}_i\right) \mathbf{S}_l \left(\mathbf{E}_i - \mathbf{K}_i \mathbf{F}_i\right)^T + \mathbf{Q}_l + \mathbf{K}_i \mathbf{R}_l \mathbf{K}_i^T \right] \tilde{\phi}'^T_{j,i+1} \tag{5.191}$$

Further simplification is accomplished by defining the following:

$$\mathbf{\Pi}_{l,k,k} = \mathbf{\Gamma}_{l,k} \mathbf{C}_k^T \tag{5.192}$$

$$\mathbf{\Pi}_{l,k,j} = \tilde{\phi}'_{k,j} \mathbf{\Gamma}_{l,j} \mathbf{C}_j^T + \tilde{\phi}'_{k,j+1} \left[\left(\mathbf{E}_j - \mathbf{K}_j \mathbf{F}_j\right) \mathbf{S}_l \mathbf{F}_j^T - \mathbf{K}_j \mathbf{R}_l \right] \qquad k > j \tag{5.193}$$

Then, the subsequent recursive relationship can be developed:

$$\begin{aligned}\boldsymbol{\Pi}_{l,k,k-1} &= \tilde{\phi}'_{k,k-1}\boldsymbol{\Gamma}_{l,k-1}\mathbf{C}_{k-1}^T + \tilde{\phi}'_{k,k}\left[\left(\mathbf{E}_{k-1} - \mathbf{K}_{k-1}\mathbf{F}_{k-1}\right)\mathbf{S}_l\mathbf{F}_{k-1}^T - \mathbf{K}_{k-1}\mathbf{R}_l\right] \\ &= \tilde{\phi}'_{k,k-1}\boldsymbol{\Gamma}_{l,k-1}\mathbf{C}_{k-1}^T + \left(\mathbf{E}_{k-1} - \mathbf{K}_{k-1}\mathbf{F}_{k-1}\right)\mathbf{S}_l\mathbf{F}_{k-1}^T - \mathbf{K}_{k-1}\mathbf{R}_l \\ &= \phi'_{k-1}\boldsymbol{\Pi}_{l,k-1,k-1} + \left(\mathbf{E}_{k-1} - \mathbf{K}_{k-1}\mathbf{F}_{k-1}\right)\mathbf{S}_{l,k-1}\mathbf{F}_{k-1}^T - \mathbf{K}_{k-1}\mathbf{R}_{l,k-1}\end{aligned} \tag{5.194}$$

$$\begin{aligned}\boldsymbol{\Pi}_{l,k,k-2} &= \tilde{\phi}'_{k,k-2}\boldsymbol{\Gamma}_{l,k-2}\mathbf{C}_{k-2}^T + \tilde{\phi}'_{k,k-1}\left[\left(\mathbf{E}_{k-2} - \mathbf{K}_{k-2}\mathbf{F}_{k-2}\right)\mathbf{S}_l\mathbf{F}_{k-2}^T - \mathbf{K}_{k-2}\mathbf{R}_l\right] \\ &= \phi'_{k-1}\phi'_{k-2}\boldsymbol{\Pi}_{l,k-2,k-2} + \phi'_{k-1}\left[\left(\mathbf{E}_{k-2} - \mathbf{K}_{k-2}\mathbf{F}_{k-2}\right)\mathbf{S}_l\mathbf{F}_{k-2}^T - \mathbf{K}_{k-2}\mathbf{R}_l\right] \\ &= \phi'_{k-1}\boldsymbol{\Pi}_{l,k-1,k-2}\end{aligned} \tag{5.195}$$

$$\begin{aligned}\boldsymbol{\Pi}_{l,k,k-3} &= \tilde{\phi}'_{k,k-3}\boldsymbol{\Gamma}_{l,k-3}\mathbf{C}_{k-3}^T + \tilde{\phi}'_{k,k-2}\left[\left(\mathbf{E}_{k-3} - \mathbf{K}_{k-3}\mathbf{F}_{k-3}\right)\mathbf{S}_l\mathbf{F}_{k-3}^T - \mathbf{K}_{k-3}\mathbf{R}_l\right] \\ &= \phi'_{k-1}\phi'_{k-2}\phi'_{k-3}\boldsymbol{\Pi}_{l,k-3,k-3} + \phi'_{k-1}\phi'_{k-2}\left[\left(\mathbf{E}_{k-3} - \mathbf{K}_{k-3}\mathbf{F}_{k-3}\right)\mathbf{S}_l\mathbf{F}_{k-3}^T - \mathbf{K}_{k-3}\mathbf{R}_l\right] \\ &= \phi'_{k-1}\boldsymbol{\Pi}_{l,k-1,k-3}\end{aligned} \tag{5.196}$$

$$\vdots$$

$$\boldsymbol{\Pi}_{l,k,j} = \phi'_{k-1}\boldsymbol{\Pi}_{l,k-1,j} \tag{5.197}$$

Also, note that

$$\boldsymbol{\Pi}_{l,k,j} = 0 \tag{5.198}$$

when $j < 0$.

Therefore, Eq. 5.189 becomes

$$\boldsymbol{\Psi}_{l,k,j} = \mathbf{C}_k\boldsymbol{\Pi}_{l,k,j} \tag{5.199}$$

For the case where $k = j$, the covariance of the residual calculation given in Eq. 5.170

can be written as

$$\begin{aligned} E\left[\nu_k \nu_k^T\right] &= \sum_{l=1}^{\hat{N}} \left(\mathbf{C}_k \mathbf{\Gamma}_{l,k} \mathbf{C}_k^T + \mathbf{F}_k \mathbf{S}_l \mathbf{F}_k^T + \mathbf{R}_l\right) \alpha_l \\ &= \sum_{l=1}^{\hat{N}} \mathbf{\Psi}_{l,k,k} \alpha_l \end{aligned} \tag{5.200}$$

where $\mathbf{\Psi}_{l,k,k}$ is given by

$$\begin{aligned} \mathbf{\Psi}_{l,k,k} &= \mathbf{C}_k \mathbf{\Gamma}_{l,k} \mathbf{C}_k^T + \mathbf{F}_k \mathbf{S}_l \mathbf{F}_k^T + \mathbf{R}_l \\ &= \mathbf{C}_k \mathbf{\Pi}_{l,k,k} + \mathbf{F}_k \mathbf{S}_l \mathbf{F}_k^T + \mathbf{R}_l \end{aligned} \tag{5.201}$$

It has been shown that the correlation of the residual sequence, given in Eqs. 5.183 and 5.200, is linear in α_l. This makes the problem amenable to a least-squares formulation.

5.3.3 Recast problem for least-squares solution

In order to implement a conventional least-squares solution, it is necessary to vectorize the correlation of the residual sequence and the matrices $\mathbf{\Psi}_{l,k,j}$, thereby converting the matrix into a column vector. Introducing the vec function, where the columns of a matrix are stacked to produce a column vector.

$$\text{vec}\mathbf{A} = \text{vec}\begin{bmatrix} \mathbf{a}_1 & \mathbf{a}_2 & \dots & \mathbf{a}_n \end{bmatrix} = \begin{bmatrix} \mathbf{a}_1 \\ \mathbf{a}_2 \\ \vdots \\ \mathbf{a}_n \end{bmatrix} \tag{5.202}$$

Defining a vector containing the product of the residual sequence with its own transpose as

$$\sigma_{k,j} = \text{vec}\left[\nu_k \nu_j^T\right] \qquad k \geq j \tag{5.203}$$

which can be directly observed from the filter residual sequence. Additionally, let

$$\beta_{k,j} = \begin{bmatrix} \text{vec}\boldsymbol{\Psi}_{1,k,j} & \text{vec}\boldsymbol{\Psi}_{2,k,j} & \dots & \text{vec}\boldsymbol{\Psi}_{\hat{N},k,j} \end{bmatrix} \tag{5.204}$$

for $k \geq j$. It follows that

$$\sigma_{k,j} = \beta_{k,j}\alpha + \eta_{k,j} \tag{5.205}$$

where $\eta_{k,j}$ is a zero-mean noise term. Beginning at time step k, a number of observations would be as follows:

$$\begin{aligned}
\sigma_{k-l_n,k-l_n} &= \beta_{k-l_n,k-l_n}\alpha + \eta_{k-l_n,k-l_n} \\
\sigma_{k-l_n,k-l_n-1} &= \beta_{k-l_n,k-l_n-1}\alpha + \eta_{k-l_n,k-l_n-1} \\
&\vdots \\
\sigma_{k-l_n,j-l_n} &= \beta_{k-l_n,j-l_n}\alpha + \eta_{k-l_n,j-l_n} \\
&\vdots \\
\sigma_{k-1,k-1} &= \beta_{k-1,k-1}\alpha + \eta_{k-1,k-1} \\
\sigma_{k-1,k-2} &= \beta_{k+1,k}\alpha + \eta_{k+1,k} \\
&\vdots \\
\sigma_{k-1,j-1} &= \beta_{k-1,j-1}\alpha + \eta_{k-1,j-1} \\
\sigma_{k,k} &= \beta_{k,k}\alpha + \eta_{k,k} \\
\sigma_{k,k-1} &= \beta_{k,k-1}\alpha + \eta_{k,k-1} \\
&\vdots \\
\sigma_{k,j} &= \beta_{k,j}\alpha + \eta_{k,j}
\end{aligned} \tag{5.206}$$

The variable l_n denotes the number of time steps that are stored, or $k - l_n$ is the time step in the past at which the recursive least-squares estimation began. Note that $\sigma_{k,k}$ is a $p^2 \times 1$ vector, $\beta_{k,k}$ is a $p^2 \times \hat{N}$ matrix, α is a $\hat{N} \times 1$ vector, and η is a $p^2 \times 1$ vector, where p is the number of measurements for the original filter. A new counter variable, t, is introduced to

increment between each row of Eq. 5.206. With this new definition, Eq. 5.204 becomes

$$\sigma_t = \beta_t \alpha + \eta_t \tag{5.207}$$

The problem is now cast in a such a way that the vector α can be solved using a least-squares approach.

5.3.4 Recursive least squares algorithm

For online implementation, it is convenient to recast Eq. 5.207 in a recursive least-squares form as follows [76]:

$$\hat{\alpha}_t = \hat{\alpha}_{t-1} + \mathbf{K}_t \left(\sigma_t - \beta_t \hat{\alpha}_{t-1}\right) \tag{5.208}$$

$$\mathbf{K}_t = \mathbf{\Theta}_{t-1}\beta_t \left(\mathbf{W}_t + \beta_t \mathbf{\Theta}_{t-1}\beta_t^T\right) \tag{5.209}$$

$$\mathbf{\Theta}_t = \mathbf{\Theta}_{t-1} - \mathbf{K}_t \beta_t \mathbf{\Theta}_{t-1} \tag{5.210}$$

where $\mathbf{K}_t$ is the $\hat{N} \times 1$ gain vector, $\mathbf{\Theta}_t$ is the $\hat{N} \times \hat{N}$ covariance matrix of the estimate given by $E\left[\left(\hat{\alpha} - \alpha\right)\left(\hat{\alpha} - \alpha\right)^T\right]$, and $\mathbf{W}_t$ is the variance of the noise, η_t.

The initial α_0 is arbitrarily chosen, and the corresponding state estimate covariance $\mathbf{\Theta}_t$ is selected to be large to assign a low confidence in the initial state estimate. It remains to select the matrix $\mathbf{W}_t$. The variance of the noise η_t is $E\left[\eta_t \eta_t^T\right]$. From Eq. 5.207, it follows that

$$\eta_t \eta_t^T = \left\{\sigma_t - E\left[\sigma_t\right]\right\}\left\{\sigma_t - E\left[\sigma_t\right]\right\}^T \tag{5.211}$$

If the residual sequence is a sequence of independent random values, then the sequence is white. This is known to be true for the case where the main Kalman filter process noise, unknown stochastic disturbance, and measurement noise are Gaussian white and the estimator is optimal. Also, the elements of σ are $\nu_{\alpha,k}\nu_{\beta,j}$, where $\alpha = 1, 2, \ldots, p$ and $\beta = 1, 2, \ldots, p$ denote to which output the residual observation corresponds. Assuming the innovations process is white, the following pairwise product rule for the expected value of

a product of Gaussian variables can be applied:

$$\begin{aligned} E\left[\eta\eta^T\right] &= E\left\{\left[\nu_{\alpha,k}\nu_{\beta,j} - E\left[\nu_{\alpha,k}\nu_{\beta,j}\right]\right]\left[\nu_{\alpha,k}\nu_{\beta,j} - E\left[\nu_{\alpha,k}\nu_{\beta,j}\right]\right]\right\} \\ &= E\left[\nu_{\alpha,k}\nu_{\alpha,k}\right] E\left[\nu_{\beta,j}\nu_{\beta,j}\right] + E\left[\nu_{\alpha,k}\nu_{\beta,k}\right] E\left[\nu_{\beta,k}\nu_{\alpha,k}\right] \delta_{k,j} \end{aligned} \tag{5.212}$$

where $\delta_{k,j}$ is the Kronecker delta function. If the initial estimate of α_0 were exact, then the noise covariances $\mathbf{S}_k$, $\mathbf{Q}_k$, and $\mathbf{R}_k$ would be precisely known, and the Kalman gain for the original filter$\mathbf{K}_k$, would be optimal. The residual sequence of the filter would be white for the case of Gaussian process and measurement noises. In order to apply Eq. 5.212, it is necessary to assume that the initial estimate of the α_0 is exact; the following equation is used to evaluate the expectations in Eq. 5.212:

$$E\left[\nu\nu^T\right] = \sum_{l=1}^{\hat{N}} \left(\alpha_0\right)_i \mathbf{\Psi}_{l,k,k} \tag{5.213}$$

Simulation results indicate that the above approach produces a reasonable estimate of the noise covariance matrices, notwithstanding the incorrect assumption that the initial estimate of the parameter α_0 is exact. The procedure introduced above allows the least squares estimation of the parameter vector α, which can be used in Eqs. 5.156 through 5.158 to give estimates of the noise covariance matrices.

5.4 Simple investigative example

A simple 2-degree-of-freedom (DOF) system, presented by Wu and Smyth [102], is considered here. The results for a base excited structure represented in the physical domain are presented first to benchmark the method. Subsequently, several extensions are considered. First, the system's modal characteristics are identified from acceleration response measurements to a known base excitation. Second, a known main mass excitation is considered and parameter estimation is performed using ambient vibration measurements; the initial states are no longer known precisely since it is not known to begin from rest. Third, the case of an unknown excitation with known noise covariances is considered. Finally, the

case of unknown excitation and unknown noise covariances is presented.

5.4.1 Base-excited 2DOF example

Wu and Smyth [102] presented the following simple 2-DOF linear system subjected to Chi-Chi earthquake base excitation:

$$m_1\ddot{u}_1(t) + c_1\dot{u}_1(t) + c_2\left[\dot{u}_1(t) - \dot{u}_2(t)\right] + k_1\dot{u}_1(t) + k_2\left[u_1(t) - u_2(t)\right] = -m_1\ddot{u}_g(t) \quad (5.214a)$$

$$m_2\ddot{u}_2(t) + c_2\left[\dot{u}_2(t) - \dot{u}_1(t)\right] + k_2\left[u_2(t) - u_1(t)\right] = -m_2\ddot{u}_g(t) \quad (5.214b)$$

which can be written in matrix form as

$$\mathbf{M}\ddot{\mathbf{u}}(t) + \mathbf{C}\dot{\mathbf{u}}(t) + \mathbf{K}\mathbf{u}(t) = -\mathbf{M}\boldsymbol{\Gamma}\ddot{u}_g(t) \quad (5.215)$$

where $\boldsymbol{\Gamma} = \begin{bmatrix} 1 & 1 \end{bmatrix}^T$ is the influence vector and the mass ($\mathbf{M}$), damping ($\mathbf{C}$), and stiffness ($\mathbf{K}$) matrices are

$$\mathbf{M} = \begin{bmatrix} m_1 & 0 \\ 0 & m_2 \end{bmatrix} \quad \mathbf{C} = \begin{bmatrix} c_1 + c_2 & -c_2 \\ -c_2 & c_2 \end{bmatrix} \quad \mathbf{K} = \begin{bmatrix} k_1 + k_2 & -k_2 \\ -k_2 & k_2 \end{bmatrix} \quad (5.216)$$

The displacement and velocity response and both DOFs are selected as the states of the system; that is, $\mathbf{x}(t) = \begin{bmatrix} u_1(t) & u_2(t) & \dot{u}_1(t) & \dot{u}_2(t) \end{bmatrix}^T$. The continuous time state transition matrices are

$$\mathbf{A}_c = \begin{bmatrix} \mathbf{0} & \mathbf{I} \\ -\mathbf{M}^{-1}\mathbf{K} & -\mathbf{M}^{-1}\mathbf{C} \end{bmatrix} \quad (5.217)$$

$$\mathbf{G}_c = -\begin{bmatrix} \mathbf{0} \\ \boldsymbol{\Gamma} \end{bmatrix} \quad (5.218)$$

where $\mathbf{G}_c$ is the continuous time $\tilde{n} \times r$ input matrix corresponding to the known input, $\mathbf{u}(t)$, where $u(t) = \ddot{u}_g(t)$ $(r = 1)$. The total acceleration at each DOF is measured. Therefore,

$$\mathbf{z}(t) = \left\{ \begin{array}{c} z_1(t) \\ z_2(t) \end{array} \right\} = \left\{ \begin{array}{c} \ddot{u}_1(t) + \ddot{u}_g(t) \\ \ddot{u}_2(t) + \ddot{u}_g(t) \end{array} \right\} \tag{5.219}$$

The measurement matrices are

$$\mathbf{C}_c = \left[\begin{array}{cc} -\mathbf{M}^{-1}\mathbf{K} & -\mathbf{M}^{-1}\mathbf{C} \end{array} \right] \tag{5.220}$$

$$\mathbf{D}_c = \mathbf{0} \tag{5.221}$$

Note that with the measurement of the total acceleration for a base-excited system, the feedthrough matrix $\mathbf{D}_c$ is empty. The state transition matrices are discretized, according to Sec. 5.1.3, converting the continuous time state matrices into their discrete time counterparts. For the present example, the stiffnesses k_1 and k_2 as well as the damping coefficient c_1 and c_2 are unknown parameters to be identified. They are appended to the state vector, which becomes

$$\mathbf{x}_k = \left[\begin{array}{cccccccc} u_1 & u_2 & \dot{u}_1 & \dot{u}_2 & k_1 & k_2 & c_1 & c_2 \end{array} \right]^T \tag{5.222}$$

A constant transition within the state matrix is assumed for the appended parameters; that is $x_i(t) = 0$ (continuous time) or $x_i[k] = x_i[k-1]$ (discrete time). The nonlinear

state transition equations are

$$x_1[k+1] = x_1[k] + x_3[k]T + w_1[k] \tag{5.223a}$$

$$x_2[k+1] = x_2[k] + x_4[k]T + w_2[k] \tag{5.223b}$$

$$\begin{aligned} x_3[k+1] = &-\frac{x_5[k]+x_6[k]}{m_1}Tx_1[k] + \frac{x_6[k]}{m_2}Tx_2[k] \\ &+ \left(1 - \frac{x_7[k]+x_8[k]}{m_1}T\right)x_3[k] + \frac{x_8[k]}{m_2}Tx_4[k] - Tu[k] + w_3[k] \end{aligned} \tag{5.223c}$$

$$\begin{aligned} x_4[k+1] = &\frac{x_6[k]}{m_2}Tx_1[k] - \frac{x_6[k]}{m_2}Tx_2[k] \\ &+ \frac{x_8[k]}{m_2}Tx_3[k] + \left(1 - \frac{x_8[k]}{m_2}T\right)x_4[k] - Tu[k] + w_4[k] \end{aligned} \tag{5.223d}$$

$$x_5[k+1] = x_5[k] + w_5[k] \tag{5.223e}$$

$$x_6[k+1] = x_6[k] + w_6[k] \tag{5.223f}$$

$$x_7[k+1] = x_7[k] + w_7[k] \tag{5.223g}$$

$$x_8[k+1] = x_8[k] + w_8[k] \tag{5.223h}$$

where T is the sample time. The nonlinear measurement equations are

$$z_1[k] = -\frac{x_5[k]+x_6[k]}{m_1}x_1[k] + \frac{x_6[k]}{m_2}x_2[k] - \frac{x_7[k]+x_8[k]}{m_1}x_3[k] + \frac{x_8[k]}{m_2}x_4[k] + v_1[k] \tag{5.224a}$$

$$z_2[k] = \frac{x_6[k]}{m_2}x_1[k] - \frac{x_6[k]}{m_2}x_2[k] + \frac{x_8[k]}{m_2}x_3[k] - \frac{x_8[k]}{m_2}x_4[k] + v_2[k] \tag{5.224b}$$

The Jacobian matrices of partial deviates of the transition ($\bar{\mathbf{A}}_{k-1}$) and measurement ($\bar{\mathbf{C}}_k$) equations, with respect to $\mathbf{x}$, are given in Table 5.1. Note that the $[k]$ notation is dropped for convenience.

The acceleration response for the Chi-Chi earthquake excitation is recorded with a sampling frequency of 400 Hz, for $m_1 = m_2 = 1$ kg, $c_1 = 0.6$ N s/m, $c_2 = 0.5$ N s/m, $k_1 = 12$ N/m, and $k_2 = 10$ N/m. Additive white measurement noise $\mathbf{v}_k$ is introduced at signal-to-noise ratios (SNRs) of 20, 10, and 5. Structural system identification is performed

Table 5.1: Jacobian matrices of partial derivatives of the transition and measurement equations with respect to $\mathbf{x}$ for the 2-DOF shear-beam base excited system

$$\bar{\mathbf{A}}_k = \begin{bmatrix} 1 & 0 & T & 0 & 0 & 0 & 0 & 0 \\ 0 & 1 & 0 & T & 0 & 0 & 0 & 0 \\ -\frac{x_5+x_6}{m_1}T & \frac{x_6}{m_2}T & 1-\frac{x_7+x_8}{m_1}T & \frac{x_8}{m_2}T & -\frac{1}{m_1}Tx_1 & \frac{1}{m_1}T(x_2-x_1) & -\frac{1}{m_1}Tx_3 & \frac{1}{m_1}T(x_4-x_3) \\ \frac{x_6}{m_2}T & -\frac{x_6}{m_2}T & \frac{x_8}{m_2}T & 1-\frac{x_8}{m_2}T & 0 & \frac{1}{m_2}T(x_1-x_2) & 0 & \frac{1}{m_2}T(x_3-x_4) \\ 0 & 0 & 0 & 0 & 1 & 0 & 0 & 0 \\ 0 & 0 & 0 & 0 & 0 & 1 & 0 & 0 \\ 0 & 0 & 0 & 0 & 0 & 0 & 1 & 0 \\ 0 & 0 & 0 & 0 & 0 & 0 & 0 & 1 \end{bmatrix}$$

$$\bar{\mathbf{C}}_k = \begin{bmatrix} -\frac{x_5+x_6}{m_1} & \frac{x_6}{m_2} & -\frac{x_7+x_8}{m_1} & \frac{x_8}{m_2} & -\frac{1}{m_1}x_1 & \frac{1}{m_1}(x_2-x_1) & -\frac{1}{m_1}x_3 & \frac{1}{m_1}(x_4-x_3) \\ \frac{x_6}{m_2} & -\frac{x_6}{m_2} & \frac{x_8}{m_2}T & -\frac{x_8}{m_2} & 0 & \frac{1}{m_2}(x_1-x_2) & 0 & \frac{1}{m_2}(x_3-x_4) \end{bmatrix}$$

using the EKF algorithm described in Sec. 5.1.2, using initial estimates of the damping coefficients and stiffnesses $\hat{c}_{1,0} = \hat{c}_{2,0} = 0.2$ N s/m and $\hat{k}_1 = \hat{k}_2 = 2$ N/m. The initial states (displacements and velocities) were chosen to be zero. The initial state estimate error covariance was zero for the states (since the system is known to begin from rest) and $\mathbf{P}_0 = 5$ for the stiffness parameter estimates and $\mathbf{P}_0 = 0.5$ for the damping estimates in order to establish a level of confidence in the initial parameter estimates. The process noise covariance is $\mathbf{Q}_k = \mathbf{0}$ and the measurement noise covariance matrix, $\mathbf{R}_k$ is based on the known noise covariance of additive measurement noise. The masses are fixed to the actual values for the duration of the filter. The final identified values after 60 s for one realization of the filter for each level of measurement noise are presented in Table 5.2, compared with the results presented by Wu and Smyth [102]. The analysis results for the four parameter estimates are plotted in Fig. 5.2 for each level of measurement noise.

Table 5.2: Identification results using EKF for a 2-DOF linear base excited system

		Identified Parameter			
		c_1	c_2	k_1	k_2
		N s/m	N s/m	N/m	N/m
	Actual	0.6	0.6	12	10
	Initial	0.2	0.2	2	2
SNR	Error (%)	66.7	66.7	83.3	80.0
20	Estimate	0.619	0.527	11.979	9.9997
	Error (%)	3.18	5.38	0.171	0.003
	Estimate [102]	0.587	0.525	12.012	9.902
	Error (%)	2.25	5.02	0.102	0.978
10	Estimate	0.624	0.529	11.996	9.9638
	Error (%)	3.97	5.75	0.030	0.362
	Estimate [102]	0.581	0.542	12.028	9.895
	Error (%)	3.13	8.46	0.229	1.05
5	Estimate	0.626	0.529	12.034	9.9422
	Error (%)	4.32	5.86	0.282	0.578
	Estimate [102]	0.572	0.556	11.996	9.959
	Error (%)	4.70	11.2	0.032	0.413

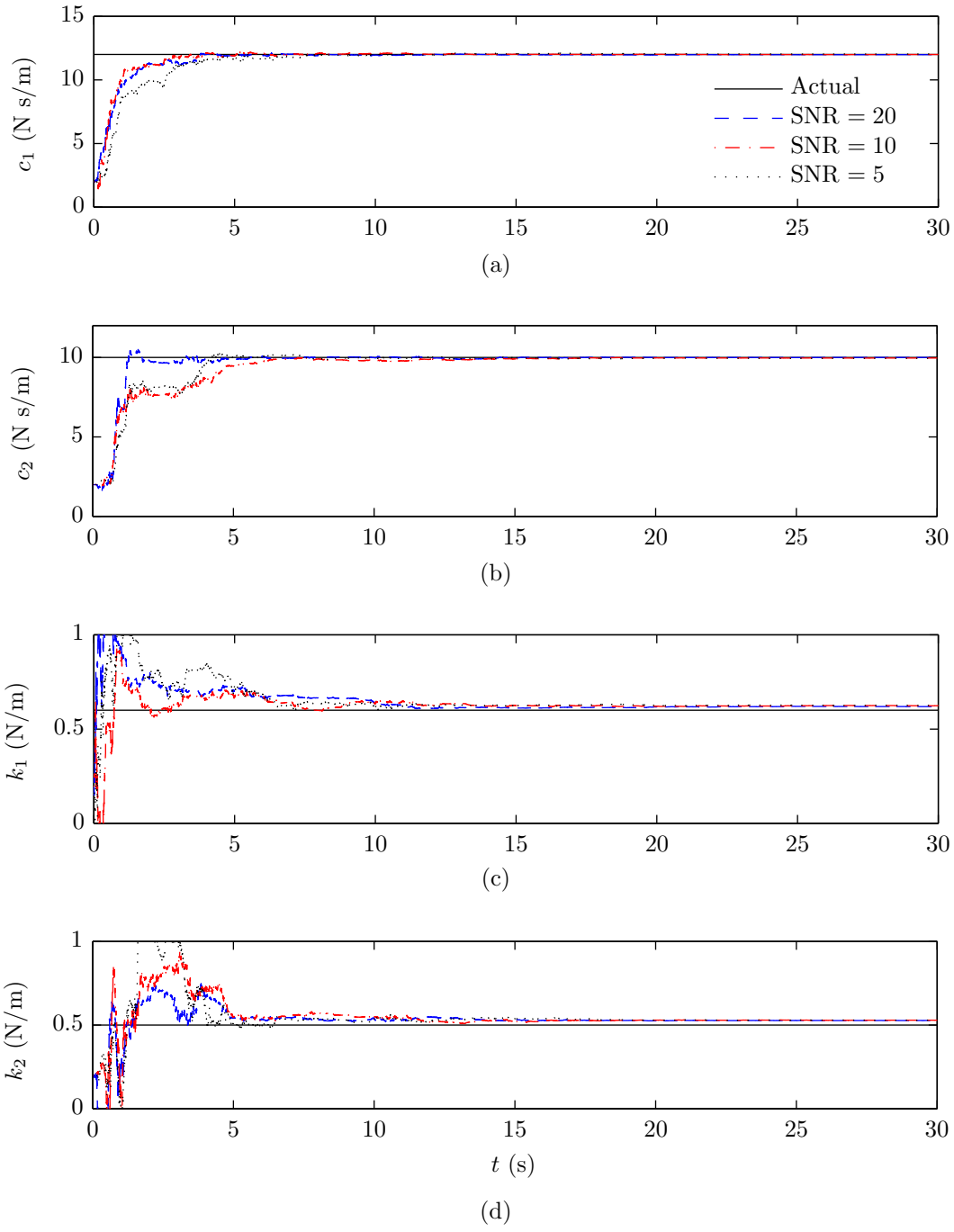

Figure 5.1: Parameter estimates for (a) c_1, (b) c_2, (c) k_1, and (d) k_2, for SNRs of 20, 10, and 5 using EKF combined state and parameter identification of a base-excited 2DOF linear structure.

There is close correspondence between these results and those presented by Wu and Smyth [102]. Generally, there is a slight decline in identification performance with decreasing SNR. The identification of the stiffness is considerably better than the damping estimates, though the damping estimates are still acceptable. Reasonable performance of the filter for the combined state and parameter estimation problem described is expected. The underlying system is linear, and the problem is amenable to classic EKF theory; that is, a known input excitation and no feedthrough of the input in the measurement equation. The primary challenge in the approach is the lack of availability of direct state measurements, in that no displacements or velocities are directly measured. This may lead to a drift in the identified parameters due to accelerometer bias caused by integrating the noise contaminated accelerations [60, 86].

5.4.2 EKF for modal identification of structures

The present work is interested in identifying the modal parameters of the structure, namely the natural frequencies, damping ratios, and mode shape vectors. The example 2-DOF structure presented prescribed as a shear-beam model; using a modal identification approach allows is to be applied more generally for the purpose of structural system identification. The base-excited system is discussed first, followed by the situation where the structure is excited by a known main mass excitation, such as wind.

The equation of motion for a general multi-degree-of-freedom (MDOF) system was given in Eq. 5.215. The following transformation converts the physical response coordinates into the modal domain:

$$\mathbf{y}(t) = \mathbf{\Phi}\mathbf{u}(t) \tag{5.225}$$

where $\mathbf{\Phi}$ is the modal matrix and $\mathbf{y}(t)$ is the modal displacement response. Similar relationships exist for the modal velocity, $\dot{\mathbf{y}}(t)$, and modal acceleration, $\ddot{\mathbf{y}}(t)$. Substituting these relationships in Eq. 5.215 and premultiply by $\mathbf{\Phi}^T$, the equations are recast in modal

coordinates. For the case of proportional damping,

$$\begin{aligned} \mathbf{\Phi}^T\mathbf{M}\mathbf{\Phi}\ddot{\mathbf{u}}(t) + \mathbf{\Phi}^T\mathbf{C}\mathbf{\Phi}\dot{\mathbf{u}}(t) + \mathbf{\Phi}^T\mathbf{K}\mathbf{\Phi}\mathbf{u}(t) &= -\mathbf{\Phi}^T\mathbf{\Gamma}\ddot{u}_g(t) \\ \ddot{\mathbf{y}}(t) + \hat{\mathbf{C}}\dot{\mathbf{y}}(t) + \mathbf{\Lambda}\mathbf{y}(t) &= -\mathbf{M}_r^{-1}\mathbf{\Phi}^T\mathbf{\Gamma}\ddot{u}_g(t) \end{aligned} \tag{5.226}$$

where $\mathbf{M}_r$ is the modal mass matrix. $\hat{\mathbf{C}}$ is the classical modal damping matrix, given by

$$\hat{\mathbf{C}} = \begin{bmatrix} 2\zeta_1\omega_{n,1} & 0 & \dots & 0 \\ 0 & 2\zeta_2\omega_{n,2} & \dots & 0 \\ \vdots & \vdots & \ddots & \vdots \\ 0 & 0 & \dots & 2\zeta_n\omega_{n,n} \end{bmatrix} \tag{5.227}$$

where ζ_j and $\omega_{n,j}$ are the the modal damping ratios and circular natural frequencies, respectively, for the j^{th} mode. $\mathbf{\Lambda}$ is the spectral matrix, defined as

$$\mathbf{\Lambda} = \begin{bmatrix} \omega_{n,1}^2 & 0 & \dots & 0 \\ 0 & \omega_{n,2}^2 & \dots & 0 \\ \vdots & \vdots & \ddots & \vdots \\ 0 & 0 & \dots & \omega_{n,n}^2 \end{bmatrix} \tag{5.228}$$

Selecting as states of the system for the 2-DOF example, $\mathbf{x}(t) = \begin{bmatrix} y_1(t) & y_2(t) & \dot{y}_1(t) & \dot{y}_2(t) \end{bmatrix}^T$, and input $u(t) = \ddot{u}_g(t)$, the state transition matrices are

$$\mathbf{A}_c = \begin{bmatrix} \mathbf{0} & \mathbf{I} \\ -\mathbf{\Lambda} & -\hat{\mathbf{C}} \end{bmatrix} \tag{5.229}$$

$$\mathbf{G}_c = -\begin{bmatrix} \mathbf{0} \\ \mathbf{M}_r^{-1}\mathbf{\Phi}^T\mathbf{M}\mathbf{\Gamma} \end{bmatrix} \tag{5.230}$$

For the case where the overall acceleration of each DOF is measured,

$$\mathbf{z}(t) = \begin{Bmatrix} z_1(t) \\ z_2(t) \end{Bmatrix} = \begin{Bmatrix} \phi_{11}\ddot{y}_1(t) + \phi_{12}\ddot{y}_2(t) \\ \phi_{21}\ddot{y}_1(t) + \phi_{22}\ddot{y}_2(t) \end{Bmatrix} \tag{5.231}$$

where ϕ_{ij} is the mode shape coefficient at the i^{th} DOF for the j^{th} mode of vibration. The measurement matrices are

$$\mathbf{C}_c = \begin{bmatrix} -\mathbf{\Phi\Lambda} & -\mathbf{\Phi}\hat{\mathbf{C}} \end{bmatrix} \tag{5.232}$$

$$\mathbf{D}_c = \mathbf{0} \tag{5.233}$$

The system matrices are converted into their discrete-time counterpars. The natural frequencies, modal damping ratios, and mode shape vectors are selected as the parameters to be identified. The mode shape vectors are normalized with respect to the first DOF. The mass is assumed to be known. The appended state vector becomes

$$\mathbf{x}_k = \begin{bmatrix} u_1 & u_2 & \dot{u}_1 & \dot{u}_2 & \omega_{n,1} & \omega_{n,2} & \zeta_1 & \zeta_2 & \phi_{21} & \phi_{22} \end{bmatrix}^T \tag{5.234}$$

Therefore, the modal identification seeks to identify additional unknown parameters, since the system model is no longer prescribed to be a shear-beam model, as in the previous example.

The state transition equations are

$$x_1[k+1] = x_1[k] + x_3[k]T + w_1[k] \tag{5.235a}$$

$$x_2[k+1] = x_2[k] + x_4[k]T + w_2[k] \tag{5.235b}$$

$$x_3[k+1] = -x_5[k]^2 T x_1[k] + \left(1 - 2x_7[k]x_5[k]T\right) x_3[k] + \frac{\phi_{12} - x_{10}[k]}{\phi_{11}x_{10}[k] - \phi_{12}x_9[k]} Tu + w_3[k] \tag{5.235c}$$

$$x_4[k+1] = -x_6[k]^2 T x_1[k] + \left(1 - 2x_8[k]x_6[k]T\right) x_4[k] + \frac{\phi_{11} - x_9[k]}{\phi_{11}x_{10}[k] - \phi_{12}x_9[k]} Tu + w_4[k] \tag{5.235d}$$

$$x_5[k+1] = x_5[k] + w_4[k] \tag{5.235e}$$

$$\vdots$$

$$x_{10}[k+1] = x_{10}[k] + w_{10}[k] \tag{5.235f}$$

where T is the sample time. The measurement equations are

$$\begin{aligned} z_1[k] = &-\phi_{11}x_5[k]^2x_1[k] - \phi_{12}x_6[k]^2x_2[k] \\ &- 2\phi_{11}x_7[k]x_5[k]x_3[k] - 2\phi_{12}x_8[k]x_6[k]x_4[k] + v_1[k] \end{aligned} \tag{5.236a}$$

$$\begin{aligned} z_2[k] = &-x_9[k]x_5[k]^2x_1[k] - x_{10}[k]x_6[k]^2x_2[k] \\ &- 2x_9[k]x_7[k]x_5[k]x_3[k] - 2x_{10}[k]x_8[k]x_6[k]x_4[k] + v_2[k] \end{aligned} \tag{5.236b}$$

The Jacobian matrices of partial derivatives of $f(\mathbf{x}, u)$ and $h(\mathbf{x}, u)$ with respect to $\mathbf{x}$ are given in Table 5.3.

5.4.3 EKF modal identification using ambient vibration measurements

Attention is now turned to considering the case of main mass excitation, or identification of the structural parameters using ambient vibration measurements. There are two primary distinctions from the previous example. First, the system is no longer likely to begin from an at-rest position ($u = \dot{u} = 0$); therefore, there is less confidence in the initial state estimates (displacements and velocities). Secondly, when only acceleration responses are measured, the main mass excitation is present in the measurement equation as a direct feedthrough; for the case of known input, this is easily accommodated by the EKF.

Consider the equation of motion for a main mass excited system.

$$\mathbf{M}\ddot{\mathbf{u}}(t) + \mathbf{C}\dot{\mathbf{u}}(t) + \mathbf{K}\mathbf{u}(t) = \mathbf{P}(t) \tag{5.237}$$

where $\mathbf{P}(t)$ is an arbitrary main mass time-varying force applied to each DOF. Using the modal transformation in Eq. 5.225 and premultiplying by $\mathbf{\Phi}^T$, the equation of motion becomes

$$\begin{aligned} \mathbf{\Phi}^T\mathbf{M}\mathbf{\Phi}\ddot{\mathbf{u}}(t) + \mathbf{\Phi}^T\mathbf{C}\mathbf{\Phi}\dot{\mathbf{u}}(t) + \mathbf{\Phi}^T\mathbf{K}\mathbf{\Phi}\mathbf{u}(t) &= \mathbf{\Phi}^T\mathbf{P}(t) \\ \ddot{\mathbf{y}}(t) + \hat{\mathbf{C}}\dot{\mathbf{y}}(t) + \mathbf{\Lambda}\mathbf{y}(t) &= \mathbf{M}_r^{-1}\mathbf{\Phi}^T\mathbf{P}(t) \end{aligned} \tag{5.238}$$

Table 5.3: Jacobian matrices of partial derivatives of the transition and measurement equations with respect to $\mathbf{x}$ for the 2-DOF base excited system described in modal coordinates

$$\bar{\mathbf{A}}_k = \begin{bmatrix} 1 & 0 & T & 0 & 0 & 0 \\ 0 & 1 & 0 & T & 0 & 0 \\ -{x_5}^2 T & 0 & 1-2x_7x_5T & 0 & -2\left(x_5x_1+x_7x_3\right)T & 0 \\ 0 & -{x_6}^2 & 0 & 1-2x_8x_6T & 0 & -2\left(x_6x_2+x_8x_4\right)T \\ 0 & 0 & 0 & 0 & 1 & 0 \\ 0 & 0 & 0 & 0 & 0 & 1 \\ 0 & 0 & 0 & 0 & 0 & 0 \\ 0 & 0 & 0 & 0 & 0 & 0 \\ 0 & 0 & 0 & 0 & 0 & 0 \\ 0 & 0 & 0 & 0 & 0 & 0 \end{bmatrix}$$

$$\begin{bmatrix} 0 & 0 & 0 & 0 \\ 0 & 0 & 0 & 0 \\ -2x_5Tx_3 & 0 & \dfrac{\phi_{12}\left(\phi_{12}-x_{10}\right)}{\left(\phi_{11}x_{10}-\phi_{12}x_9\right)^2}Tu & -\dfrac{\phi_{12}\left(\phi_{11}-x_9\right)}{\left(\phi_{11}x_{10}-\phi_{12}x_9\right)^2}Tu \\ 0 & -2x_6Tx_4 & -\dfrac{\phi_{11}\left(\phi_{12}-x_{10}\right)}{\left(\phi_{11}x_{10}-\phi_{12}x_9\right)^2}Tu & \dfrac{\phi_{11}\left(\phi_{11}-x_9\right)}{\left(\phi_{11}x_{10}-\phi_{12}x_9\right)^2}Tu \\ 0 & 0 & 0 & 0 \\ 0 & 0 & 0 & 0 \\ 1 & 0 & 0 & 0 \\ 0 & 1 & 0 & 0 \\ 0 & 0 & 1 & 0 \\ 0 & 0 & 0 & 1 \end{bmatrix}$$

$$\bar{\mathbf{C}}_k = \begin{bmatrix} -\phi_{11}{x_5}^2 & -\phi_{12}{x_6}^2 & -2\phi_{11}x_7x_5 & -2\phi_{12}x_8x_6 & -2\phi_{11}\left(x_5x_1+x_7x_3\right) & -2\phi_{12}\left(x_6x_2+x_8x_4\right) \\ -x_9{x_5}^2 & -x_{10}{x_6}^2 & -2x_9x_7x_5 & -2x_{10}x_8x_6 & -2x_9\left(x_5x_1+x_7x_3\right) & -2x_{10}\left(x_6x_2+x_8x_4\right) \\ -2\phi_{11}x_5x_3 & -2\phi_{12}x_6x_4 & 0 & 0 & & \\ -2x_9x_5x_3 & -2x_{10}x_6x_4 & -{x_5}^2x_1-2x_7x_5x_3 & -{x_6}^2x_2-2x_8x_6x_4 & & \end{bmatrix}$$

Selecting the same states and measurements of the system for the 2-DOF example, and the input vector as $\mathbf{u}(t) = \mathbf{P}(t)$, the system matrix $\mathbf{A}_c$ and measurement matrix $\mathbf{C}_c$ are unchanged; the input matrix $\mathbf{G}_c$ and direct feedthrough matrix $\mathbf{D}_c$ are

$$\mathbf{G}_c = \begin{bmatrix} \mathbf{0} \\ \mathbf{M}_r^{-1}\mathbf{\Phi}^T \end{bmatrix} \tag{5.239}$$

$$\mathbf{D}_c = \mathbf{\Phi}\mathbf{M}_r^{-1}\mathbf{\Phi}^T \tag{5.240}$$

For the special case where the number of measurements is equal to the number of modes of vibration considered ($\mathbf{\Phi}$ is square), the direct feedthrough matrix becomes $\mathbf{D}_c = \mathbf{M}^{-1}$. Once again, selecting the appended state vector as in Eq. 5.234, the state transition equations are

$$x_1[k+1] = x_1[k] + x_3[k]T + w_1[k] \tag{5.241a}$$

$$x_2[k+1] = x_2[k] + x_4[k]T + w_2[k] \tag{5.241b}$$

$$\begin{aligned} x_3[k+1] = {} & -x_5[k]^2 T x_1[k] + (1 - 2x_7[k]x_5[k]T)\, x_3[k] \\ & + \frac{x_{10}[k]}{m_1\phi_{11}x_{10}[k] - m_1\phi_{12}x_9[k]} T u_1[k] - \frac{\phi_{12}}{m_2\phi_{11}x_{10}[k] - m_2\phi_{12}x_9[k]} T u_2[k] + w_3[k] \end{aligned} \tag{5.241c}$$

$$\begin{aligned} x_4[k+1] = {} & -x_6[k]^2 T x_1[k] + (1 - 2x_8[k]x_6[k]T)\, x_4[k] \\ & - \frac{x_9[k]}{m_1\phi_{11}x_{10}[k] - m_1\phi_{12}x_9[k]} T u_1 + \frac{\phi_{11}}{m_2\phi_{11}x_{10}[k] - m_2\phi_{12}x_9[k]} T u_2 + w_4[k] \end{aligned} \tag{5.241d}$$

$$x_5[k+1] = x_5[k] + w_9[k] \tag{5.241e}$$

$$\vdots$$

$$x_{10}[k+1] = x_{10}[k] + w_{10}[k] \tag{5.241f}$$

The measurement equations are

$$\begin{aligned} z_1[k] = &-\phi_{11}x_5[k]^2x_1[k] - \phi_{12}x_6[k]^2x_2[k] \\ &- 2\phi_{11}x_7[k]x_5[k]x_3[k] - 2\phi_{12}x_8[k]x_6[k]x_4[k] + \frac{1}{m_1}u_1[k] + v_1[k] \end{aligned} \tag{5.242a}$$

$$\begin{aligned} z_2[k] = &-x_9[k]x_5[k]^2x_1[k] - x_{10}[k]x_6[k]^2x_2[k] \\ &- 2x_9[k]x_7[k]x_5[k]x_3[k] - 2x_{10}[k]x_8[k]x_6[k]x_4[k] + \frac{1}{m_2}u_2[k] + v_2[k] \end{aligned} \tag{5.242b}$$

The Jacobian matrices of partial derivatives of $f(\mathbf{x}, \mathbf{u})$ and $h(\mathbf{x}, \mathbf{u})$ with respect to $\mathbf{x}$ are given in Table 5.6.

The results for base-excitation and main mass-excitation are considered for modal parameter identification using the 2-DOF system presented in Sec. 5.4.1. The actual system and the initial estimates in the physical domain are converted to modal coordinates by the following transformations:

$$\mathbf{M}_r = \mathbf{\Phi}^T\mathbf{M}\mathbf{\Phi} \tag{5.243}$$

$$\hat{\mathbf{C}} = \mathbf{M}_r^{-1}\mathbf{\Phi}^T\mathbf{C}\mathbf{\Phi} \tag{5.244}$$

$$\mathbf{\Lambda} = \mathbf{M}_r^{-1}\mathbf{\Phi}^T\mathbf{K}\mathbf{\Phi} \tag{5.245}$$

since the shear-beam model is a form of proportional damping. The actual parameter values and the initial estimates are presented in Table 5.5. EKF modal identification is performed for the case where the structure is excited by the Chi-Chi earthquake ground motion time history, as well as a Gaussian white noise main mass-excitation process. The mass of the systems are assumed known. For the base-excited system, the original state estimates (displacements and velocities) are zero with zero initial state estimation error covariance ($\mathbf{P}_0 = \mathbf{0}$) since the system is known to begin from rest. For the main mass excited structure, the initial state estimates are also set equal to zero, but a lower level of confidence in the initial estimates was assigned by setting $\mathbf{P}_0 = \texttt{diag}\begin{bmatrix} 5\times10^{-4} & 1\times10^{-4} & 5\times10^{-3} & 1\times10^{-3} \end{bmatrix}$. A period of time passes before data is collected for the main mass excited structure to ensure the system does not begin from rest. For both systems, the initial error covariance

Table 5.4: Jacobian matrices of partial derivatives of the transition and measurement equations with respect to $\mathbf{x}$ for the 2DOF main mass excited system described in modal coordinates

$$\bar{\mathbf{A}}_k = \begin{bmatrix}
1 & 0 & T & 0 & 0 & 0 \\
0 & 1 & 0 & T & 0 & 0 \\
-{x_5}^2 T & 0 & 1 - 2x_7 x_5 T & 0 & -2\left(x_5 x_1 + x_7 x_3\right) T & 0 \\
0 & -{x_6}^2 & 0 & 1 - 2x_8 x_6 T & 0 & -2\left(x_6 x_2 + x_8 x_4\right) T \\
0 & 0 & 0 & 0 & 1 & 0 \\
0 & 0 & 0 & 0 & 0 & 1 \\
0 & 0 & 0 & 0 & 0 & 0 \\
0 & 0 & 0 & 0 & 0 & 0 \\
0 & 0 & 0 & 0 & 0 & 0 \\
0 & 0 & 0 & 0 & 0 & 0
\end{bmatrix}$$

$$\begin{bmatrix}
0 & 0 & 0 & 0 \\
0 & 0 & 0 & 0 \\
-2x_5 T x_3 & 0 & -\dfrac{\phi_{12}\left(m_1\phi_{12}u_2 - m_2 x_{10} u_1\right)}{m_1 m_2 \left(\phi_{11}x_{10} - \phi_{12}x_9\right)^2} T & \dfrac{\phi_{12}\left(m_1\phi_{11}u_2 - m_2 x_9 u_1\right)}{m_1 m_2 \left(\phi_{11}x_{10} - \phi_{12}x_9\right)^2} T \\
0 & -2x_6 T x_4 & \dfrac{\phi_{11}\left(m_1\phi_{12}u_2 - m_2 x_{10} u_1\right)}{m_1 m_2 \left(\phi_{11}x_{10} - \phi_{12}x_9\right)^2} T & -\dfrac{\phi_{11}\left(m_1\phi_{11}u_2 - m_2 x_9 u_1\right)}{m_1 m_2 \left(\phi_{11}x_{10} - \phi_{12}x_9\right)^2} T \\
0 & 0 & 0 & 0 \\
0 & 0 & 0 & 0 \\
1 & 0 & 0 & 0 \\
0 & 1 & 0 & 0 \\
0 & 0 & 1 & 0 \\
0 & 0 & 0 & 1
\end{bmatrix}$$

$$\bar{\mathbf{C}}_k = \begin{bmatrix}
-\phi_{11}{x_5}^2 & -\phi_{12}{x_6}^2 & -2\phi_{11}x_7 x_5 & -2\phi_{12}x_8 x_6 & -2\phi_{11}\left(x_5 x_1 + x_7 x_3\right) & -2\phi_{12}\left(x_6 x_2 + x_8 x_4\right) \\
-x_9{x_5}^2 & -x_{10}{x_6}^2 & -2x_9 x_7 x_5 & -2x_{10}x_8 x_6 & -2x_9\left(x_5 x_1 + x_7 x_3\right) & -2x_{10}\left(x_6 x_2 + x_8 x_4\right) \\
 & & -2\phi_{11}x_5 x_3 & -2\phi_{12}x_6 x_4 & 0 & 0 \\
 & & -2x_9 x_5 x_3 & -2x_{10}x_6 x_4 & -{x_5}^2 x_1 - 2x_7 x_5 x_3 & -{x_6}^2 x_2 - 2x_8 x_6 x_4
\end{bmatrix}$$

is $\mathbf{P}_0 = \texttt{diag}\begin{bmatrix} 2.5 & 5 \end{bmatrix}$ corresponding to the circular natural frequency parameter and $\mathbf{P}_0 = \texttt{diag}\begin{bmatrix} 2.5 \times 10^{-2} & 5 \times 10^{-2} \end{bmatrix}$ for damping ratio and $\mathbf{P}_0 = 1 \times 10^{-2}$ for the mode shape coefficient estimates. The process noise covariance is $\mathbf{Q}_k = \mathbf{0}$ and the measurement noise covariance matrix, $\mathbf{R}_k$ is based on the noise level of additive measurement noise. The results are compared for both cases in Table 5.5 for SNRs of 20, 10, and 5. The introduction of the additive measurement noise for the main mass excited system was based on the acceleration response of the structure with the feedthrough input removed, in order to provide a useful comparison to the base-excited system. The convergence of each parameter estimate is shown in Figs. 5.2 (base-excited) and 5.3 (main mass excited). There is little difference in the final parameter estimates and convergence of the identified parameters when comparing the main mass excited 2-DOF system and the base-excited system. The at-rest initial conditions assumption is no longer valid; this is the primary reason for the increase in the complexity of the identification.

Table 5.5: Modal identification results using EKF for a 2DOF linear base-excited and main mass excited system

		Identified Parameter					
		$\omega_{n,1}$	$\omega_{n,2}$	ζ_1	ζ_2	ϕ_{21}	ϕ_{22}
		rad/s	rad/s				
	Actual	2.08	5.26	0.0521	0.132	1.77	-0.57
	Initial	0.874	2.29	0.0437	0.114	1.62	-0.62
SNR	Error (%)	58.0	56.5	16.1	13.0	8.39	9.16
Base-excited by Chi-Chi earthquake time history							
20	Estimate	2.08	5.25	0.0547	0.137	1.76	-0.567
	Error (%)	0.026	0.188	5.07	4.33	0.227	0.106
10	Estimate	2.08	5.25	0.0544	0.138	1.76	-0.565
	Error (%)	0.050	0.160	4.44	5.02	0.166	0.241
5	Estimate	2.08	5.25	0.0546	0.137	1.77	-0.569
	Error (%)	0.004	0.155	4.82	4.48	0.028	0.563
White noise main mass excited							
20	Estimate	2.08	5.25	0.0542	0.138	1.75	-0.563
	Error (%)	0.064	0.163	4.16	4.83	0.801	0.496
10	Estimate	2.08	5.25	0.0551	0.138	1.77	-0.568
	Error (%)	0.153	0.115	5.83	4.77	0.004	0.364
5	Estimate	2.08	5.25	0.0542	0.137	1.75	-0.564
	Error (%)	0.206	0.103	4.05	4.41	1.13	0.377

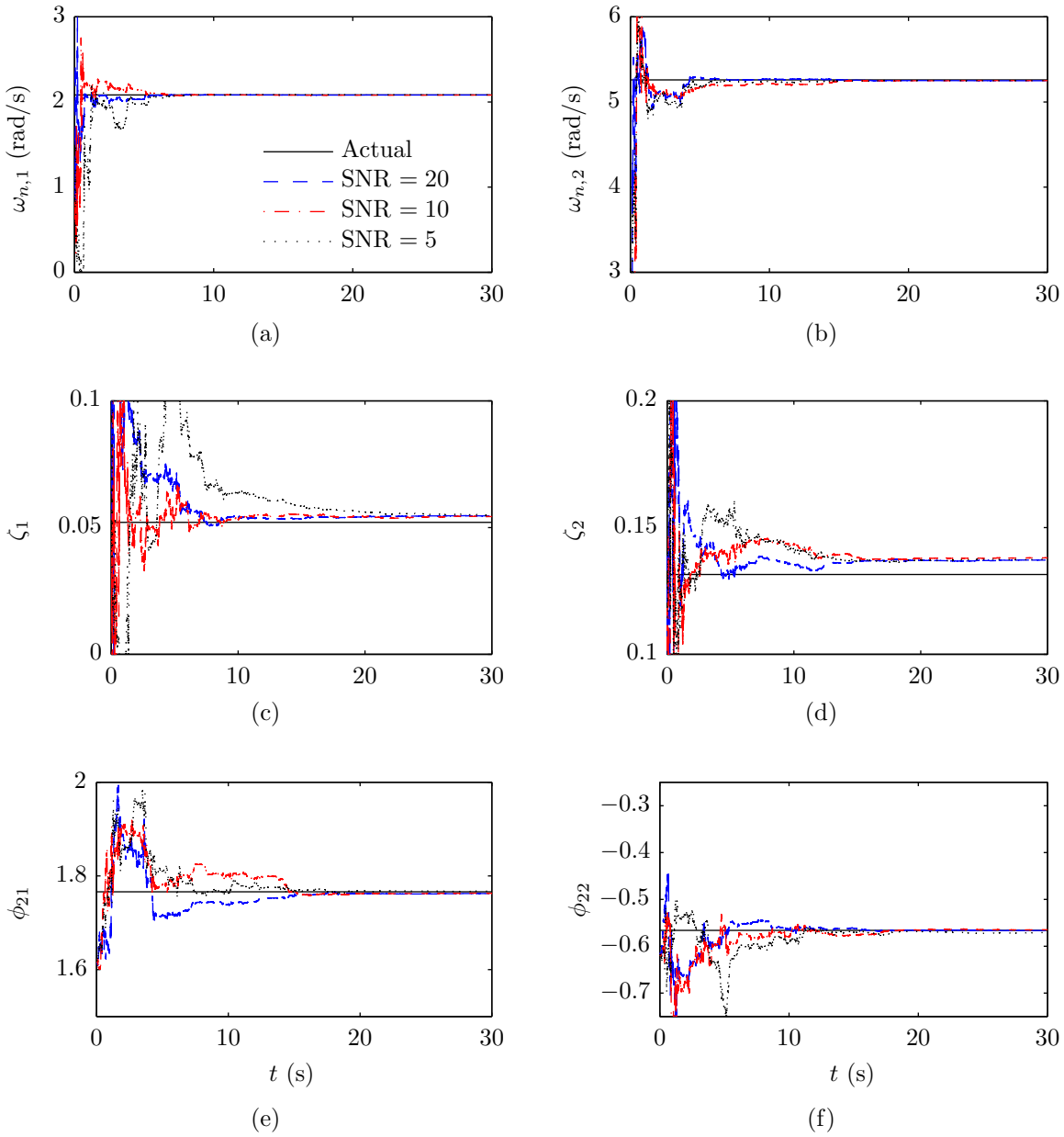

Figure 5.2: Modal parameter estimates for (a) $\omega_{n,1}$ and (b) $\omega_{n,2}$, (c) ζ_1 and (d) ζ_2, and (e) ϕ_{21} and (f) ϕ_{22} for SNRs of 20, 10, and 5 using EKF combined state and modal parameter identification of a base-excited 2DOF linear structure.

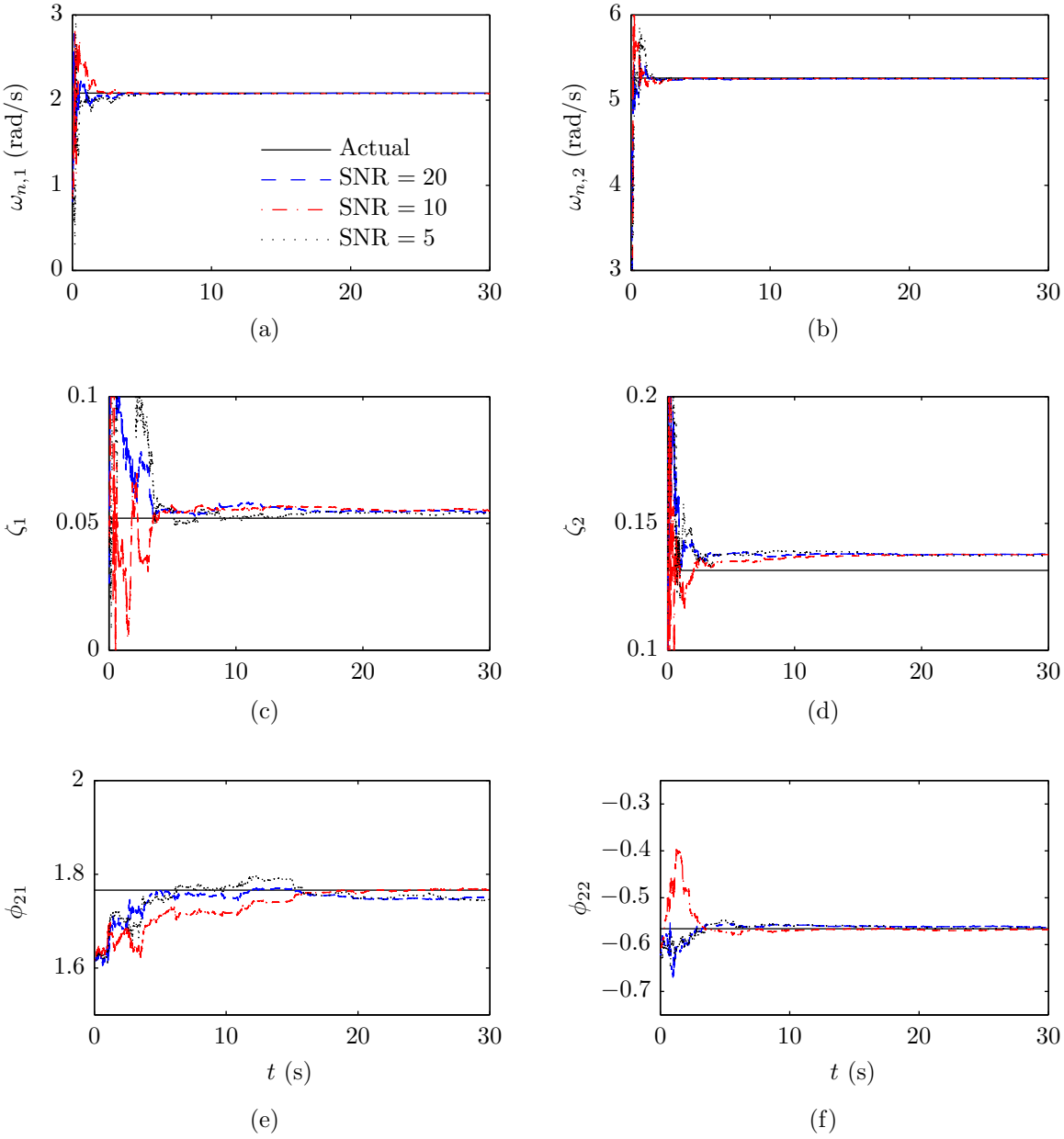

Figure 5.3: Modal parameter estimates for (a) $\omega_{n,1}$ and (b) $\omega_{n,2}$, (c) ζ_1 and (d) ζ_2, and (e) ϕ_{21} and (f) ϕ_{22} for SNRs of 20, 10, and 5 using EKF combined state and modal parameter identification of a main mass excited 2DOF linear structure.

5.4.4 Main mass excited 2-DOF example with unknown excitation

Combined state and parameter estimation for an unknown main mass excitation is demonstrated by means of the 2-DOF example presented earlier. The nonlinear transition equations are

$$x_1[k+1] = x_1[k] + x_3[k]T + w_1[k] \tag{5.246a}$$

$$x_2[k+1] = x_2[k] + x_4[k]T + w_2[k] \tag{5.246b}$$

$$\begin{aligned} x_3[k+1] = &-x_5[k]^2 T x_1[k] + (1 - 2x_7[k]x_5[k]T)\, x_3[k] \\ &+ \frac{x_{10}[k]}{m_1\phi_{11}x_{10}[k] - m_1\phi_{12}x_9[k]} T d_1 - \frac{\phi_{12}}{m_2\phi_{11}x_{10}[k] - m_2\phi_{12}x_9[k]} T d_2 + w_3[k] \end{aligned} \tag{5.246c}$$

$$\begin{aligned} x_4[k+1] = &-x_6[k]^2 T x_1[k] + (1 - 2x_8[k]x_6[k]T)\, x_4[k] \\ &- \frac{x_9[k]}{m_1\phi_{11}x_{10}[k] - m_1\phi_{12}x_9[k]} T d_1 + \frac{\phi_{11}}{m_2\phi_{11}x_{10}[k] - m_2\phi_{12}x_9[k]} T d_2 + w_4[k] \end{aligned} \tag{5.246d}$$

$$x_5[k+1] = x_5[k] + w_9[k] \tag{5.246e}$$

$$\vdots$$

$$x_{10}[k+1] = x_{10}[k] + w_{10}[k] \tag{5.246f}$$

The nonlinear measurement equations are

$$\begin{aligned} z_1[k] = &-\phi_{11}x_5[k]^2 x_1[k] - \phi_{12}x_6[k]^2 x_2[k] \\ &- 2\phi_{11}x_7[k]x_5[k]x_3[k] - 2\phi_{12}x_8[k]x_6[k]x_4[k] + \frac{1}{m_1} d_1[k] + v_1[k] \end{aligned} \tag{5.247a}$$

$$\begin{aligned} z_2[k] = &-x_9[k]x_5[k]^2 x_1[k] - x_{10}[k]x_6[k]^2 x_2[k] \\ &- 2x_9[k]x_7[k]x_5[k]x_3[k] - 2x_{10}[k]x_8[k]x_6[k]x_4[k] + \frac{1}{m_2} d_2[k] + v_2[k] \end{aligned} \tag{5.247b}$$

The Jacobian matrices of partial derivatives of $f(\mathbf{x}, \mathbf{0})$ and $h(\mathbf{x}, \mathbf{0})$ with respect to $\mathbf{x}$ as well as $f(\mathbf{x}, \mathbf{d})$ and $h(\mathbf{x}, \mathbf{d})$ with respect to $\mathbf{d}$ are given in Table 5.6.

The results of the filter with SNRs of 20, 10, and 5 are presented in Fig. 5.4 for data lengths of 120 s. The figure shows the mean convergence for 100 realizations of the filter at each SNR. The final estimates, coefficient of variation ($\hat{c}_v$), and percent error are given in Table 5.7. The initial state estimate error covariance is

$$\mathbf{P}_0 = \mathtt{diag}\left[\begin{array}{cccccc} 0.5 & 2 & 1 \times 10^{-3} & 1 \times 10^{-3} & 5 \times 10^{-2} & 5 \times 10^{-2} \end{array}\right] \tag{5.248}$$

corresponding to the appended parameter vector. The measurement noise covariance, $\mathbf{R}_k$ is based on the known level of measurement noise introduced; the additive process noise is $\mathbf{Q}_k = \mathbf{0}$. An additional level of error was introduced for the initial modal damping coefficient estimates, as compared to the examples presented earlier.

Table 5.6: Jacobian matrices of partial derivatives of the transition and measurement equations with respect to $\mathbf{x}$ and $\mathbf{d}$ for the 2DOF main mass excited system described in modal coordinates with unknown input excitation

$$\bar{\mathbf{A}}_k = \begin{bmatrix} 1 & 0 & T & 0 & 0 & 0 & 0 & 0 & 0 & 0 \\ 0 & 1 & 0 & T & 0 & 0 & 0 & 0 & 0 & 0 \\ -{x_5}^2 T & 0 & 1-2x_7x_5T & 0 & -2\left(x_5x_1+x_7x_3\right)T & 0 & -2x_5Tx_3 & 0 & 0 & 0 \\ 0 & -{x_6}^2 & 0 & 1-2x_8x_6T & 0 & -2\left(x_6x_2+x_8x_4\right)T & 0 & -2x_6Tx_4 & 0 & 0 \\ 0 & 0 & 0 & 0 & 1 & 0 & 0 & 0 & 0 & 0 \\ 0 & 0 & 0 & 0 & 0 & 1 & 0 & 0 & 0 & 0 \\ 0 & 0 & 0 & 0 & 0 & 0 & 1 & 0 & 0 & 0 \\ 0 & 0 & 0 & 0 & 0 & 0 & 0 & 1 & 0 & 0 \\ 0 & 0 & 0 & 0 & 0 & 0 & 0 & 0 & 1 & 0 \\ 0 & 0 & 0 & 0 & 0 & 0 & 0 & 0 & 0 & 1 \end{bmatrix}$$

$$\bar{\mathbf{C}}_k = \begin{bmatrix} -\phi_{11}{x_5}^2 & -\phi_{12}{x_6}^2 & -2\phi_{11}x_7x_5 & -2\phi_{12}x_8x_6 & -2\phi_{11}\left(x_5x_1+x_7x_3\right) & -2\phi_{12}\left(x_6x_2+x_8x_4\right) \\ -x_9{x_5}^2 & -x_{10}{x_6}^2 & -2x_9x_7x_5 & -2x_{10}x_8x_6 & -2x_9\left(x_5x_1+x_7x_3\right) & -2x_{10}\left(x_6x_2+x_8x_4\right) \\ & & -2\phi_{11}x_5x_3 & -2\phi_{12}x_6x_4 & 0 & 0 \\ & & -2x_9x_5x_3 & -2x_{10}x_6x_4 & -{x_5}^2x_1-2x_7x_5x_3 & -{x_6}^2x_2-2x_8x_6x_4 \end{bmatrix}$$

$$\bar{\mathbf{E}}_k = \begin{bmatrix} 0 & 0 \\ 0 & 0 \\ \dfrac{x_{10}}{m_1\left(\phi_{11}x_{10}-\phi_{12}x_9\right)}T & -\dfrac{\phi_{12}}{m_2\left(\phi_{11}x_{10}-\phi_{12}x_9\right)}T \\ -\dfrac{x_9}{m_1\left(\phi_{11}x_{10}-\phi_{12}x_9\right)}T & \dfrac{\phi_{11}}{m_2\left(\phi_{11}x_{10}-\phi_{12}x_9\right)}T \\ 0 & 0 \\ 0 & 0 \\ 0 & 0 \\ 0 & 0 \\ 0 & 0 \\ 0 & 0 \\ 0 & 0 \end{bmatrix} \qquad \bar{\mathbf{F}}_k = \begin{bmatrix} \dfrac{1}{m_1} & 0 \\ 0 & \dfrac{1}{m_2} \end{bmatrix}$$

Table 5.7: Modal identification results using EKF for a 2DOF linear system with unknown main mass excitation

		Identified Parameter					
		$\omega_{n,1}$	$\omega_{n,2}$	ζ_1	ζ_2	ϕ_{21}	ϕ_{22}
		rad/s	rad/s				
	Actual	2.08	5.26	0.0521	0.132	1.77	-0.57
	Initial	0.874	2.29	0.02	0.09	1.62	-0.62
SNR	Error (%)	58.0	56.5	61.6	31.6	8.39	9.16
20	Estimate	2.08	5.2	0.054	0.133	1.73	-0.601
	Error (%)	0.0401	1.04	3.77	1.13	1.77	6.09
	$\hat{c}_v$ (%)	1.47	1.70	20.0	9.04	3.70	-18.3
10	Estimate	2.08	5.21	0.0542	0.133	1.74	-0.595
	Error (%)	0.0742	0.947	4.07	1.19	1.24	5.04
	$\hat{c}_v$ (%)	1.55	1.87	20.7	8.8	3.32	-19.6
5	Estimate	2.08	5.21	0.0549	0.133	1.75	-0.604
	Error (%)	0.0371	0.899	5.35	1.21	0.782	6.74
	$\hat{c}_v$ (%)	1.44	1.78	20.4	9.10	2.80	-19.3

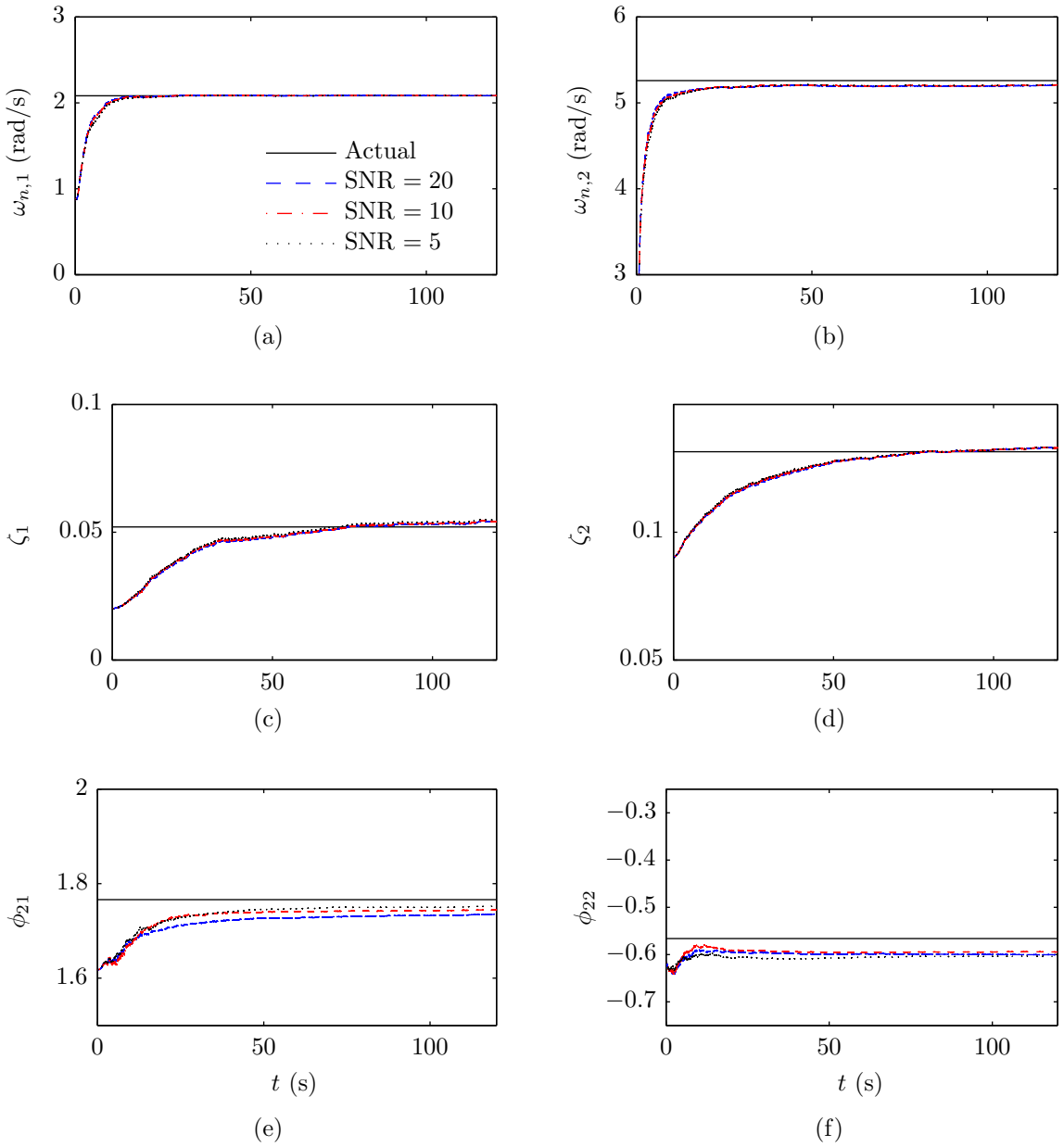

Figure 5.4: Modal parameter estimates for (a) $\omega_{n,1}$ and (b) $\omega_{n,2}$, (c) ζ_1 and (d) ζ_2, and (e) ϕ_{21} and (f) ϕ_{22} for SNRs of 20, 10, and 5 using EKF combined state and modal parameter identification of a 2DOF linear structure with unknown main mass excitation.

The uncertainty introduced to the system by the unknown external disturbance has generally degraded the performance of the parameter estimation. Performance of the modal damping ratios (Figs. 5.4c and 5.4d) is respectable, but a considerably longer data set is required before convergence near the actual values. This is due to the stochastic noise process driving the system dynamics and competing with the damping ratio parameter estimate as a means of attenuating or amplifying the responses. While the mode shape vectors converge more quickly, there is more error in the final estimate. Of primary importance is the circular natural frequencies, (Figs. 5.4a and 5.4b), which are still precisely identified, though convergence is delayed with respect to the known inputs case.

5.4.5 Main mass excited 2-DOF example with unknown excitation and unknown noise covariances

The noise covariance estimation is considered using the same example. The noise covariance estimation algorithm assumes prefect knowledge of the model of the system; therefore, two cases are considered. The first case uses the actual model to estimate the noise covariances. The second uses the initial estimate of the model for estimating the noise covariances, which is a more realistic scenario. The two cases are considered to demonstrate the effectiveness of the algorithm and to show that error in the model has a nominal impact on the parameter estimation step.

The term, $\mathbf{d}_k$, models the wind excitation imposed on the main structure. The quality of noise estimation depends on the relative contributions of the unknown feedthrough disturbance, process, and measurement noises. Since the contribution of the process noise $\mathbf{w}_k$ to the transition of the state vector and of the measurements noise $\mathbf{w}_k$ to the measurement is small relative to the level of unknown feedthrough disturbance $\mathbf{d}_k$, the estimation of $\mathbf{d}_k$ is expected to be reasonably good, which as will be shown is the case.

By separating $\mathbf{d}_k$ and $\mathbf{w}_k$, the relative contribution of external disturbance from other sources driving the system dynamics (such as model uncertainty) are distinguished. Unlike $\mathbf{Q}_k$, $\mathbf{S}_k$ has a large impact on the result, and $\mathbf{Q}_k$ is used to prescribe the level of confidence

Table 5.8: Noise covariance parameter α estimates using the actual model and initial model parameter estimate for a main mass excited 2-DOF system

Index		Actual model			Initial estimate		
	Actual	Estimate	Error	$\hat{c}_v$	Estimate	Error	$\hat{c}_v$
			%	%		%	%
$\mathbf{S}_k$							
1	0.22	0.22	0.102	0.845	0.22	0.074	0.846
2	0.15	0.15	0.188	0.542	0.15	0.216	0.544
$\mathbf{R}_k$							
3	2.58	2.03	21.1	39.7	3.27	26.8	24.7
4	2.58	2.12	17.8	22.2	2.94	14.2	16.0

on the measurements versus the model. This simplifies the problem to the identification of $\mathbf{S}_k$ and $\mathbf{R}_k$, and $\mathbf{Q}_k$ can be at the user's discretion.

Table 5.8 gives the initial estimate of the noise covariances matrices, and the final mean estimates for the known and initial estimate model cases, together with the percent error and coefficient of variation. The performance of the known model case is very good, with small performance degradation for the unknown model case. However, the results are quite satisfactory considering the initial estimate of the noise covariance matrices are arbitrary the initial model estimate is considerably in error. It will be shown that this does not significantly impact the parameter estimation step. For both cases, there is a more accurate estimate of the process noise covariance when compared to the measurement noise covariance estimate. The covariance estimate parameter, α is normalized with respect to its actual value and plotted in Fig. 5.5.

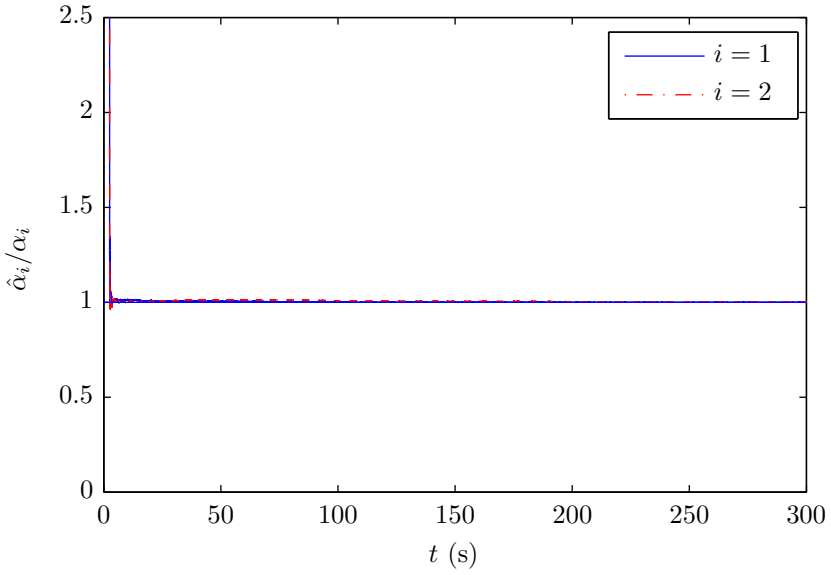

(a)

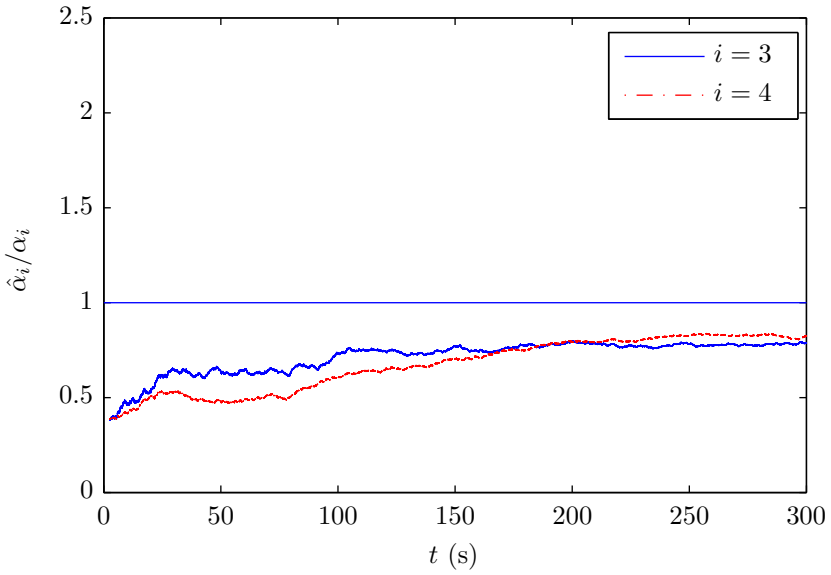

(b)

Figure 5.5: Normalized (a) feedthrough disturbance noise covariance $\hat{\mathbf{S}}$ and (b) measurement noise covariance $\hat{\mathbf{R}}$ parameter estimates averaged over 100 filter realizations.

Table 5.9: Modal identification results using EKF for a 2DOF linear system with unknown main mass excitation and unknown process and measurement noise covariances

	Identified Parameter					
	$\omega_{n,1}$	$\omega_{n,2}$	ζ_1	ζ_2	ϕ_{21}	ϕ_{22}
	rad/s	rad/s				
Actual	2.08	5.26	0.02	0.05	1.77	-0.57
Initial	1.75	4.57	0.05	0.09	1.61	-0.62
Error (%)	16.0	13.0	150	80.0	8.39	9.16
Known $\mathbf{S}_k$ and $\mathbf{R}_k$						
Estimate	2.08	5.25	0.025	0.057	1.76	-0.57
Error (%)	0.025	0.19	26.3	14.3	0.104	1.78
$\hat{c}_v$ (%)	0.582	0.619	23.7	9.94	0.736	-6.26
Unknown $\mathbf{S}_k$ and $\mathbf{R}_k$						
Estimate	2.08	5.25	0.025	0.057	1.77	-0.59
Error (%)	0.0034	0.23	25.7	13.3	0.147	3.89
$\hat{c}_v$ (%)	0.583	0.591	23.5	9.82	0.727	-4.95

The parameter identification step is performed next. The results are compared with the known noise covariance case (similar to that presented in Sec. 5.4.4). The final mean parameter estimates after 100 realizations of the filter, together with the percent error and coefficient of variation are summarized in Table 5.9. The performance of the parameter estimation using the estimated noise covariances is comparable to the case where the noise covariances are known *a priori*.

The concept of parameter estimation by EKF is extended for the purposes of modal identification of a structure equipped with a PTMD next. The main conceptual difference is that the underlying structure's modal characteristics are identified from PTMD-attenuated response measurements. The underlying structure's modal properties are necessary to determine the optimal damper parameters, and compare those values with the measured in-service parameters in order to perform the condition assessment.

Chapter 6

Numerical study on online parameter estimation for PTMD equipped structures

A key aspect to ensure good performance of tuned mass dampers (TMDs) is to tune the auxiliary parameters to their optimal values. When the bare structural modal characteristics are known, design formulae for selecting the optimal parameters are available and have been presented in Chapter 4, including the case where the coupling effect of biaxial motion of a pendulum tuned mass damper (PTMD) is considered. This has been the subject of a vast amount of research in the area of TMDs [58, 26, 33, 59, 83, 75, 1, 97, 96, 20]. However, little attention has been focused on identifying the underlying structure's modal properties; extracting these modal properties is crucial, as the optimal auxiliary parameters are functions of the bare structure's modal characteristics.

A few researches have sought to identify the modal characteristics of a coupled main and auxiliary system with a TMD [30, 59]. A well-tuned TMD produces two closely-spaced modes with a relatively high level of damping, introducing a level of difficulty into the identification process. Even after identifying these natural frequencies, extracting the underlying structure's modal characteristics remains a challenge. Hazra *et al* presented a

heuristic approach, where the natural frequency of the main structure is approximated as the arithmetic mean of the bimodal frequencies introduced by the TMD [30]. Similarly, Ricciardelli *et al* used an experienced-based approach and subsequently updated this in an iterative framework for the adjustment of a semi-active tuned mass damper (STMD), though no explicit identification of the underlying structural modes is performed [77]. A shortcoming of these approaches is that they rely on a TMD that is tuned near the mode to be controlled, producing the bimodal frequency response, and the availability of a relatively smooth response spectra.

In this work, the problem of modal identification is cast within the framework of parameter estimation using extended Kalman filter (EKF). EKF is used because it allows for relatively straightforward online implementation and addresses the inherent nonlinearity in the system of equations for the combined state and parameter estimation. The approach adopted is as follows. First, the equations of motion for the structure and PTMD are transformed to the modal domain. Second, the main system is described using unknown modal properties, namely the circular natural frequencies, mode shape vectors, and modal damping ratios. The PTMD is treated as known, since its properties can generally be measured precisely. Third, the unknown model parameters are appended to the state vector, and state estimation proceeds. Appending the unknown model parameters to the state vector results in a non-linear system; therefore, it is necessary to linearize the system and measurement matrices (for the purpose of estimate covariance propagation) and perform the estimation. Only acceleration measurements are assumed to be available in this study.

The following rationale is presented demonstrating why this approach is advantageous:

- For the purpose of selecting optimal auxiliary damper parameters, the main structure's natural frequency is of primary interest. It has been demonstrated that the performance of EKF identification of the bare structure's natural frequencies is extremely precise, even for the case of unknown input excitation.

- It has been shown previously that the EKF identification algorithm adequately identifies the modal damping ratios; however, there is a greater level of uncertainty in the final converged values. As was shown in Chapter 4, and confirmed by various

researchers [79, 3, 26, 75], the optimal auxiliary frequency and damping ratios are not particularly sensitive to the main mass damping ratio, so this shortcoming is not expected to dramatically affect the selection of optimal damper parameters. Additionally, the selection of the auxiliary damping coefficient is often governed by other design constraints, such as reducing the stroke of the TMD [77].

- It is proposed that the auxiliary damper parameters are measured and included as part of the model governing the dynamics of the filter (part of the system matrix, $\mathbf{A}_k$). Therefore, the identification approach is expected to be independent of the level of detuning present in the auxiliary system. Attention is not focused on identifying the auxiliary damper parameters (namely, c_a, k_a, m_a, L and h) as these can be readily measured or based on manufacturer's specifications, which are closely controlled during the construction of the TMD.

- Since the proposed identification is being performed in the modal domain, it doesn't artificially impose constraints on the model, aside from the proportional damping assumption (that is, $\mathbf{\Phi}^T\mathbf{C}\mathbf{\Phi}$ is a diagonal matrix), a necessary condition in order to decouple the modes of vibration when transforming from physical to modal coordinates.

- The EKF combined state and parameter identification can readily be applied on-line, for the purpose of real-time adjustment of the damper parameters, with limited user intervention.

The equations of motion for a planar PTMD coupled with a uniaxial multi-degree-of-freedom (MDOF) main structure are presented. The system is cast into a form amenable to the EKF combined state and parameter estimation. A simple numerical example is presented for the case of unknown inputs, but with known measurement, stochastic disturbance, and process noise covariances. The issue of unknown noise covariances is then addressed, followed by a numerical example demonstrating noise covariance, state, and parameter estimation for bare structural system identification.

6.1 Equations of motion for a MDOF structure equipped with a planar PTMD

Consider a MDOF with a planar PTMD attached to the top floor, as shown in Figure 6.1. The main structure consists of $n$degree-of-freedom (DOF); therefore, the total system has n+1 degrees-of-freedom when the auxiliary rotational mass is included. Assume the structure is of the shear-beam type with classical (proportional) damping. The equations of motion are

$$\begin{bmatrix} m_1 & 0 & \dots & 0 \\ 0 & m_2 & \dots & 0 \\ \vdots & \vdots & \ddots & \vdots \\ 0 & 0 & \dots & m_n \end{bmatrix} \begin{Bmatrix} \ddot{u}_1 \\ \ddot{u}_2 \\ \vdots \\ \ddot{u}_n \end{Bmatrix} + \begin{bmatrix} c_{11} & c_{12} & \dots & c_{1n} \\ c_{21} & c_{22} & \dots & c_{2n} \\ \vdots & \vdots & \ddots & \vdots \\ c_{n1} & c_{n2} & \dots & c_{nn} \end{bmatrix} \begin{Bmatrix} \dot{u}_1 \\ \dot{u}_2 \\ \vdots \\ \dot{u}_n \end{Bmatrix} + \begin{bmatrix} k_1 & -k_1 & \dots & 0 \\ -k_1 & k_1+k_2 & \dots & 0 \\ \vdots & \vdots & \ddots & \vdots \\ 0 & 0 & \dots & k_{n-1}+k_n \end{bmatrix} \begin{Bmatrix} u_1 \\ u_2 \\ \vdots \\ u_n \end{Bmatrix} = \begin{Bmatrix} P_1(t) \\ P_2(t) \\ \vdots \\ P_3(t) \end{Bmatrix} - \begin{Bmatrix} m_a\left(L\ddot{\theta}+\ddot{u}_1\right) \\ 0 \\ \vdots \\ 0 \end{Bmatrix} \tag{6.1a}$$

$$m_a L^2\ddot{\theta} + c_a h^2\dot{\theta} + \left(m_a g L + k_a h^2\right)\theta = -m_a L\ddot{u}_1 \tag{6.1b}$$

Eqs. 6.1a can be rewritten as

$$\mathbf{M}\ddot{\mathbf{u}} + \mathbf{C}\dot{\mathbf{u}} + \mathbf{K}\mathbf{u} = \mathbf{P}(t) - \mathbf{\Gamma} m_a\left(L\ddot{\theta}+\ddot{u}_1\right) \tag{6.2}$$

where the influence vector $\mathbf{\Gamma}$ is given by $\mathbf{\Gamma} = \begin{bmatrix} 1 & 0 & \dots & 0 \end{bmatrix}^T$. Note that the ensuing development of the equations of motion assumes the PTMD is suspended from the top floor; a similar system of equations can be developed for the case where a PTMD is coupled with a different DOF by revising the selection of the influence vector. Using the mode shape

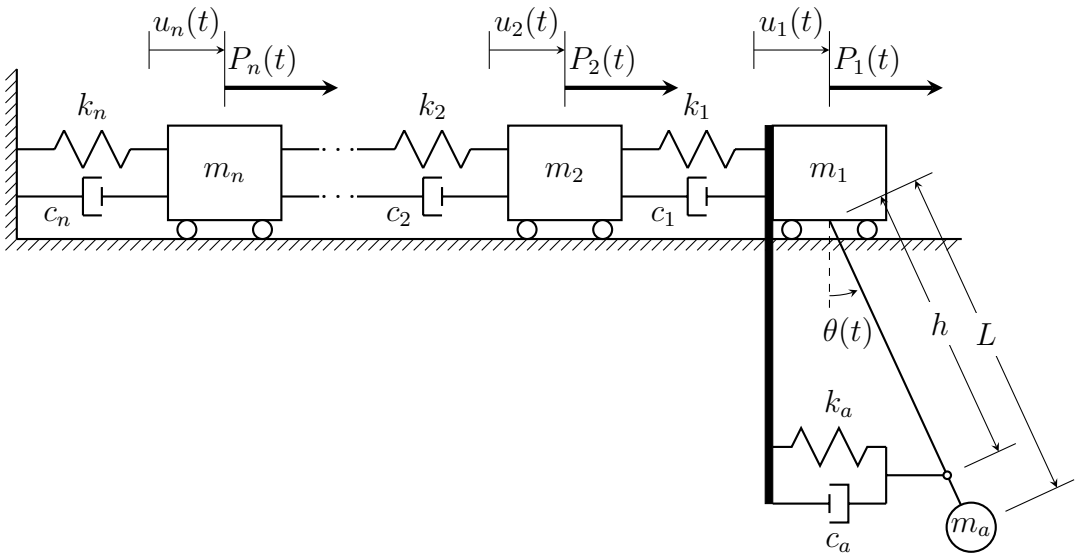

Figure 6.1: MDOF main structure with point mass planar PTMD

matrix, $\mathbf{\Phi}$, given by

$$\mathbf{\Phi} = \begin{bmatrix} \phi_1 & \phi_2 & \dots & \phi_n \end{bmatrix} = \begin{bmatrix} \phi_{11} & \phi_{12} & \dots & \phi_{1n} \\ \phi_{21} & \phi_{22} & \dots & \phi_{2n} \\ \vdots & \vdots & \ddots & \vdots \\ \phi_{n1} & \phi_{n2} & \dots & \phi_{nn} \end{bmatrix} \tag{6.3}$$

the main structure can be transformed into the modal domain by letting $\ddot{\mathbf{u}} = \mathbf{\Phi}\ddot{\mathbf{y}}$, $\dot{\mathbf{u}} = \mathbf{\Phi}\dot{\mathbf{y}}$, and $\mathbf{u} = \mathbf{\Phi}\mathbf{y}$ in Eq. 6.2, and premultiplying by $\mathbf{\Phi}^T$. Eq. 6.2 becomes

$$\mathbf{\Phi}^T\mathbf{M}\mathbf{\Phi}\ddot{\mathbf{y}} + \mathbf{\Phi}^T\mathbf{C}\mathbf{\Phi}\dot{\mathbf{y}} + \mathbf{\Phi}^T\mathbf{K}\mathbf{\Phi}\mathbf{y} = \mathbf{\Phi}^T\left[\mathbf{P}(t) - \mathbf{\Gamma}m_a\left(L\ddot{\theta} + \ddot{u}_1\right)\right] \tag{6.4}$$

This transformation assumes that the auxiliary system has no effect on the mode shapes of the main structure, which is a reasonable assumption for relatively light auxiliary mass systems [26]. For mass normalized modes and proportional damping, the uncoupled equations

of motion in the modal domain can be written as

$$\ddot{y}_1 + 2\zeta_1\omega_{n,1}\dot{y}_1 + \omega_{n,1}^2 y_1 = \phi_1^T \left[\mathbf{P}(t) - \mathbf{\Gamma} m_a \left(L\ddot{\theta} + \ddot{u}_1\right)\right] \tag{6.5}$$

$$\ddot{y}_2 + 2\zeta_2\omega_{n,2}\dot{y}_2 + \omega_{n,2}^2 y_2 = \phi_2^T \left[\mathbf{P}(t) - \mathbf{\Gamma} m_a \left(L\ddot{\theta} + \ddot{u}_1\right)\right] \tag{6.6}$$

$$\vdots$$

$$\ddot{y}_n + 2\zeta_n\omega_{n,n}\dot{y}_n + \omega_{n,n}^2 y_n = \phi_n^T \left[\mathbf{P}(t) - \mathbf{\Gamma} m_a \left(L\ddot{\theta} + \ddot{u}_1\right)\right] \tag{6.7}$$

Substitute Eq. 6.1b into Eqs. 6.6 through 6.7 to eliminate $\ddot{u}_1$. Eqs. 6.6 through 6.7 become

$$\ddot{y}_j = -\omega_{n,j}^2 y_j - 2\zeta_j\omega_{n,j}\dot{y}_j + \phi_{1j}\frac{m_a g L + k_a h^2}{L}\theta + \phi_{1j}\frac{c_a h^2}{L}\dot{\theta} + \phi_j^T \mathbf{P}(t); \qquad j = 1, 2, \ldots, n \tag{6.8}$$

This can be written more concisely in matrix form as

$$\ddot{\mathbf{y}}(t) = -\hat{\mathbf{C}}\dot{\mathbf{y}}(t) - \mathbf{\Lambda}\mathbf{y}(t) + \mathbf{M}_r^{-1}\mathbf{\Phi}^T\mathbf{\Gamma}\left[\frac{c_a h^2}{L}\dot{\theta}(t) + \frac{m_a g L + k_a h^2}{L}\theta(t)\right] + \mathbf{M}_r^{-1}\mathbf{\Phi}^T\mathbf{P}(t) \tag{6.9}$$

where $\hat{\mathbf{C}}$ (Eq. 5.227) is the classical modal damping matrix, $\mathbf{\Lambda}$ (Eq. 5.228) is the spectral matrix, and $\mathbf{M}_r$ is the modal mass. Substituting $\ddot{u}_1 = \phi_{11}\ddot{y}_1 + \phi_{12}\ddot{y}_2 + \ldots + \phi_{1n}\ddot{y}_n$ into Eq. 6.1b and rearranging to solve for $\ddot{\theta}$ produces

$$\begin{aligned}\ddot{\theta}(t) = {} & \frac{1}{L}\mathbf{\Gamma}^T\mathbf{\Phi}\left[\hat{\mathbf{C}}\dot{\mathbf{y}}(t) + \mathbf{\Lambda}\mathbf{y}(t)\right] - \frac{1}{L}\mathbf{\Gamma}^T\mathbf{\Phi}\mathbf{M}_r^{-1}\mathbf{\Phi}^T\mathbf{P}(t) \\ & - \left(1 + m_a\mathbf{\Gamma}^T\mathbf{\Phi}\mathbf{M}_r^{-1}\mathbf{\Phi}^T\right)\left[\frac{c_a h^2}{m_a L^2}\dot{\theta}(t) + \frac{m_a g L + k_a h^2}{m_a L^2}\theta(t)\right]\end{aligned} \tag{6.10}$$

The modal displacements and velocities as well as the auxiliary mass rotation and angular velocity are selected as the states of the system. Therefore,

$$\mathbf{x}(t) = \left[\begin{array}{ccccccccc} y_1(t) & y_2(t) & \ldots y_n(t) & \theta(t) & \dot{y}_1(t) & \dot{y}_2(t) & \ldots & \dot{y}_n(t) & \dot{\theta}(t) \end{array}\right]^T \tag{6.11}$$

The continuous time state transition equation is given by

$$\dot{\mathbf{x}}(t) = \mathbf{A}_c\mathbf{x}(t) + \mathbf{E}_c\mathbf{d}(t) + \mathbf{w}(t) \tag{6.12}$$

where $\mathbf{A}_c$ is the system matrix and $\mathbf{E}_c$ is the input matrix. The state transition and measurement matrices are given in Table 6.1.

For the case of wind excitation, the input force is not easily measured and is generally considered unknown. To accommodate this, the external excitation, $\mathbf{d}(t)$, is treated as an unknown stochastic input (previously denoted by $\mathbf{P}(t)$). The additive process noise is denoted by $\mathbf{w}(t)$. For structural monitoring applications, it is most convenient to measure the acceleration responses. Specifically, the acceleration responses of the main DOF $\ddot{u}_1(t)$, $\ddot{u}_2(t)$, ..., $\ddot{u}_n(t)$ are measured, as well as the horizontal acceleration of the auxiliary mass. Since the states of the main system correspond to the modal responses, they need to be combined using the modal matrix to determine the physical responses and the output vector $\mathbf{z}(t)$.

$$\begin{aligned}
\mathbf{z}(t) &= \begin{Bmatrix} z_1(t) \\ z_2(t) \\ \vdots \\ z_{\bar{n}}(t) \\ z_{\bar{n}+1}(t) \end{Bmatrix} = \begin{Bmatrix} \ddot{u}_1(t) \\ \ddot{u}_2(t) \\ \vdots \\ \ddot{u}_{\bar{n}}(t) \\ L\ddot{\theta}(t) + \ddot{u}_1(t) \end{Bmatrix} \\
&= \begin{Bmatrix} \phi_{11}\ddot{y}_1(t) + \phi_{12}\ddot{y}_2(t) + \ldots + \phi_{1\hat{n}}\ddot{y}_{\hat{n}}(t) \\ \phi_{21}\ddot{y}_1(t) + \phi_{22}\ddot{y}_2(t) + \ldots + \phi_{2\hat{n}}\ddot{y}_{\hat{n}}(t) \\ \vdots \\ \phi_{\bar{n}1}\ddot{y}_1(t) + \phi_{\bar{n}2}\ddot{y}_2(t) + \ldots + \phi_{\bar{n}\hat{n}}\ddot{y}_{\hat{n}}(t) \\ L\ddot{\theta}(t) + \phi_{11}\ddot{y}_1(t) + \phi_{12}\ddot{y}_2(t) + \ldots + \phi_{1\hat{n}}\ddot{y}_{\hat{n}}(t) \end{Bmatrix}
\end{aligned} \tag{6.13}$$

The continuous time measurement equation is given by

$$\mathbf{z}(t) = \mathbf{C}_c\mathbf{x}(t) + \mathbf{F}_c\mathbf{d}(t) + \mathbf{v}(t) \tag{6.14}$$

where $\mathbf{C}_c$ is the measurement matrix and $\mathbf{F}_c$ is the direct feed-through matrix. The additive measurement noise is denoted by $\mathbf{v}(t)$. The corresponding output and direct feed-through matrices are given in Table 6.1.

6.1.1 Combined state and parameter estimation example with known noise covariances

An idealized shear-frame 5-DOF structure is considered for a numerical example to demonstrate the performance of the algorithm described for combined state and parameter estimation (of the underlying structure's modal properties). The characteristic properties of the structure, namely the mass, damping, and stiffness matrices as well as the natural frequencies and modal damping ratios are provided in Table 6.2. The damping ratios for the first two modes were selected to be 1% and 5%, respectively; the modal damping ratios for the remaining modes were selected assuming Raleigh (stiffness and mass) proportional damping. The parameters to be identified are the natural frequencies, modal damping ratios, and mode shapes. A normalization procedure for the mode shapes is selected, wherein the mode shape coefficients corresponding to the DOF to which the PTMD is connected are set to unity; the remaining coefficients are parameters to be identified.

The auxiliary system parameters are measured by field investigation, or set based on engineering design drawings and manufacturers specifications. For example, the pendulum length L and the spring or damper attachment point, h can be field measured in the as-constructed state. It's generally impractical to measure the auxiliary mass, m_a, but unlike the main structure mass, this measurement is precisely quantified in the design stage and closely controlled during the construction and installation. The auxiliary damping, c_a, and stiffness, k_a, are generally specified by the product manufacturer and based on measured data. The auxiliary system parameters are assumed to be known perfectly throughout the filtering process. For the present example, the selection of the auxiliary damper parameters are based on Eqs. 4.8 and 4.9, based on a mass ratio of $\mu = 0.005$ ($m_a = 70.2$ kg). The pendulum length is coincident with the attachment point for the auxiliary damping, and equal to $L = h = 1.22$ m. The auxiliary damping coefficient is $c_a = 14.0$ N s/m and there

Table 6.1: Continuous time state matrices for uniaxial MDOF system with planar PTMD

$$\mathbf{A}_c = \begin{bmatrix} \mathbf{0} & & \mathbf{I} & \\ -\mathbf{\Lambda} & \mathbf{M}_r^{-1}\mathbf{\Phi}^T\mathbf{\Gamma}\dfrac{m_a g L + k_a h^2}{L} & -\hat{\mathbf{C}} & \mathbf{M}_r^{-1}\mathbf{\Phi}^T\mathbf{\Gamma}\dfrac{c_a h^2}{L} \\ \frac{1}{L}\mathbf{\Gamma}^T\mathbf{\Phi}\mathbf{\Lambda} & -\left(1 + m_a\mathbf{\Gamma}^T\mathbf{\Phi}\mathbf{M}_r^{-1}\mathbf{\Phi}^T\mathbf{\Gamma}\right)\dfrac{m_a g L + k_a h^2}{m_a L^2} & \dfrac{1}{L}\mathbf{\Gamma}^T\mathbf{\Phi}\hat{\mathbf{C}} & -\left(1 + m_a\mathbf{\Gamma}^T\mathbf{\Phi}\mathbf{M}_r^{-1}\mathbf{\Phi}^T\mathbf{\Gamma}\right)\dfrac{c_a h^2}{m_a L^2} \end{bmatrix}$$

$$\mathbf{E}_c = \begin{bmatrix} \mathbf{0} \\ \mathbf{M}_r^{-1}\mathbf{\Phi}^T \\ -\frac{1}{L}\mathbf{\Gamma}^T\mathbf{\Phi}\mathbf{M}_r^{-1}\mathbf{\Phi}^T \end{bmatrix}$$

$$\mathbf{C}_c = \begin{bmatrix} -\mathbf{\Phi}\mathbf{\Lambda} & \mathbf{\Phi}\mathbf{M}_r^{-1}\mathbf{\Phi}^T\mathbf{\Gamma}\dfrac{m_a g L + k_a h^2}{L} & -\mathbf{\Phi}\hat{\mathbf{C}} & \mathbf{\Phi}\mathbf{M}_r^{-1}\mathbf{\Phi}^T\mathbf{\Gamma}\dfrac{c_a h^2}{L} \\ \mathbf{0} & -\dfrac{1}{m_a}\dfrac{m_a g L + k_a h^2}{L} & \mathbf{0} & -\dfrac{1}{m_a}\dfrac{c_a h^2}{L} \end{bmatrix}$$

$$\mathbf{F}_c = \begin{bmatrix} \mathbf{\Phi}\mathbf{M}_r^{-1}\mathbf{\Phi}^T \\ \mathbf{0} \end{bmatrix}$$

is no auxiliary spring ($k_a = 0$).

Aside from the introduction of the auxiliary system, the subsequent example differs from those presented previously in that a mass matrix with some error with respect to the actual model is used in the identification process. Therefore, a reasonable initial estimate of the system mass is beneficial. To explore the effect of greater error in the mass estimate, three cases are considered. Each element of the shear-beam model for the initial estimate model is selected from a normal distribution with standard deviation of 5% of the actual stiffness and a mean 15% below the actual stiffness, as finite element models generally underestimate the stiffness of a tall structure by only modelling the primary structural members and neglecting the additional stiffness introduced by features such as the cladding and interior finishes. Three different cases of mass matrix are selected; each element of the mass matrix is selected from a normal distribution with standard deviation of 1% of the actual value about a mean of 5%, 10%, and 15% above the actual mass. Selecting about a mean above the actual mass is because a conservative designer will generally overestimate the mass when performing a static analysis. The resulting percent errors in circular natural frequencies vary between $8.9\% - 15.4\%$ (Table 6.3). The initial damping ratio estimates were chosen from a normal distribution with standard deviation of 0.0125 about an arbitrarily selected mean value of 0.05. The mode shape vectors are not sensitive to the initial errors as introduced above in the stiffness and mass matrix. In order to demonstrate the effectiveness of the EKF algorithm, an additional perturbation is introduced to the mode shape coefficients, selected randomly from a normal distribution with a standard deviation of 15% of the initial estimate about the initial estimate; the mode shapes are subsequently normalized such that the coefficient at the DOF to which to PTMD is connected is unity.

Table 6.2: Properties of a 5DOF PTMD-equipped structure

$$\mathbf{M} = \begin{bmatrix} 5 & 0 & 0 & 0 & 0 \\ 0 & 5 & 0 & 0 & 0 \\ 0 & 0 & 5 & 0 & 0 \\ 0 & 0 & 0 & 5 & 0 \\ 0 & 0 & 0 & 0 & 5 \end{bmatrix} \times 10^3 \text{ kg}$$

$$\mathbf{K} = \begin{bmatrix} 0.5 & -0.5 & 0 & 0 & 0 \\ -0.5 & 1 & -0.5 & 0 & 0 \\ 0 & -0.5 & 1 & -0.5 & 0 \\ 0 & 0 & -0.5 & 1 & -0.5 \\ 0 & 0 & 0 & -0.5 & 1 \end{bmatrix} \times 10^6 \text{ N/m}$$

$$\zeta = \begin{bmatrix} 0.0200 & 0.0500 & 0.122 & 0.156 & 0.178 \end{bmatrix}$$
$$f_n = \begin{bmatrix} 0.453 & 1.32 & 2.08 & 2.68 & 3.05 \end{bmatrix} \text{ Hz}$$

The structure was excited with a externally applied force at each DOF. The variance of the applied force was

$$\mathbf{S}_k = \texttt{diag}\begin{bmatrix} 3.11 & 5.99 & 5.70 & 5.30 & 4.61 \end{bmatrix} \times 10^5 \tag{6.15}$$

The acceleration response at each DOF was measured as well as the horizontal acceleration of the PTMD. Additive measurement noise was introduced at each measurement based on a signal-to-noise ratio (SNR) of 20 with respect to the auxiliary response. A total of 100 realizations of the filter were performed with a length of 300 s. The sampling frequency is 400 Hz. The initial state estimates (displacements and velocities) were assumed to be zero (at rest conditions), though 150 s of data was discarded from the beginning of the simulations to ensure the system did not begin from rest and transient effects had decayed. The initial parameter estimates were based on the corresponding finite element models. The initial state estimate error covariance was selected based on reasonable modal responses variances from the initial model estimates subjected to a similar external input.

The selection of the state estimation error covariance corresponding to the parameters (appended states) was based on 10% variance for the circular natural frequencies, 2.5% for the modal damping ratios, and 1% for the mode shape coefficients.

For the present application, the additive process noise $\mathbf{w}_k$ is treated as a tuneable parameter used to assign confidence in the model. If the process noise is assumed larger than actual, than the effect on the state estimation is to put greater emphasis on the measurements, and reduce the confidence in the model [85]. If the filter has too little process noise, it may become susceptible to modelling errors. On the other hand, too much process noise would prevent the filter from estimating the state accurately. For the problem at hand, it is generally obvious when too much process noise is used, as the state estimates become noisy. This is especially true for the case of constant states when the parameters are appended to the state vector. A small level of process noise covariance, $\mathbf{Q}_k$, is introduced at the displacement and velocity state positions, equal to 1×10^{-6} times the initial state estimate error covariance. The primary purpose of this is to prevent the state estimates from drifting due to accelerometer bias, resulting from the integration of noisy acceleration measurements to determine velocities and displacements.

The results of the final converged values, percent error, and coefficient of variation ($\hat{c}_v$) are given in Tables 6.3 (circular natural frequency) and 6.4 (damping ratios). The parameter estimates averaged over the 100 realizations are shown in Figs. 6.2 (circular natural frequency) and 6.3 (damping ratios). The final mode shape vectors are normalized with respect to their maximum displacements and plotted in Fig. 6.4 for the case where the mass matrix has a mean error of 5%.

Table 6.3: Comparison of natural frequency identification results for 5DOF system equipped with a PTMD for various levels of error in the main mass matrix

Error in $\mathbf{M}$		Identified Parameter				
		$f_{n,1}$	$f_{n,2}$	$f_{n,3}$	$f_{n,4}$	$f_{n,5}$
%		Hz	Hz	Hz	Hz	Hz
	Actual	0.453	1.32	2.08	2.68	3.05
5	Initial	0.409	1.21	1.87	2.41	2.77
	Error (%)	9.70	8.87	10.2	9.88	9.40
	Estimate	0.453	1.32	2.08	2.68	3.06
	Error (%)	0.0782	0.0336	0.177	0.246	0.0515
	$\hat{c}_v$ (%)	0.661	0.52	0.734	0.669	0.639
10	Initial	0.396	1.17	1.86	2.34	2.69
	Error (%)	12.5	11.2	10.9	12.8	11.9
	Estimate	0.453	1.32	2.09	2.68	3.06
	Error (%)	0.0896	0.111	0.0491	0.133	0.188
	$\hat{c}_v$ (%)	0.669	0.521	0.730	0.677	0.644
15	Initial	0.387	1.12	1.77	2.29	2.58
	Error (%)	14.7	15.0	14.9	14.5	15.4
	Estimate	0.453	1.32	2.09	2.7	3.05
	Error (%)	0.109	0.146	0.163	0.818	0.0196
	$\hat{c}_v$ (%)	0.673	0.520	0.738	0.678	0.625

Table 6.4: Comparison of modal damping ratio identification results for 5DOF system equipped with a PTMD for various levels of error in the main mass matrix

Error in $\mathbf{M}$		Identified Parameter				
		ζ_1	ζ_2	ζ_3	ζ_4	ζ_5
%						
	Actual	0.02	0.05	0.122	0.156	0.178
5	Initial	0.0483	0.0572	0.0406	0.0311	0.0516
	Error (%)	141	14.3	66.6	80.1	71.0
	Estimate	0.0276	0.0592	0.136	0.174	0.200
	Error (%)	37.8	18.3	11.5	11.5	12.4
	$\hat{c}_v$ (%)	23.5	7.43	4.40	3.15	3.03
10	Initial	0.0452	0.0474	0.0678	0.0479	0.065
	Error (%)	126	5.11	44.3	69.3	63.5
	Estimate	0.0278	0.0587	0.136	0.177	0.202
	Error (%)	39.2	17.4	12.2	13.5	13.6
	$\hat{c}_v$ (%)	22.9	7.47	4.48	3.23	3.08
15	Initial	0.0485	0.0198	0.0453	0.0367	0.0502
	Error (%)	143	60.4	62.8	76.5	71.8
	Estimate	0.0281	0.0574	0.137	0.177	0.202
	Error (%)	40.3	14.8	12.2	13.4	13.5
	$\hat{c}_v$ (%)	22.6	7.37	4.48	3.27	3.05

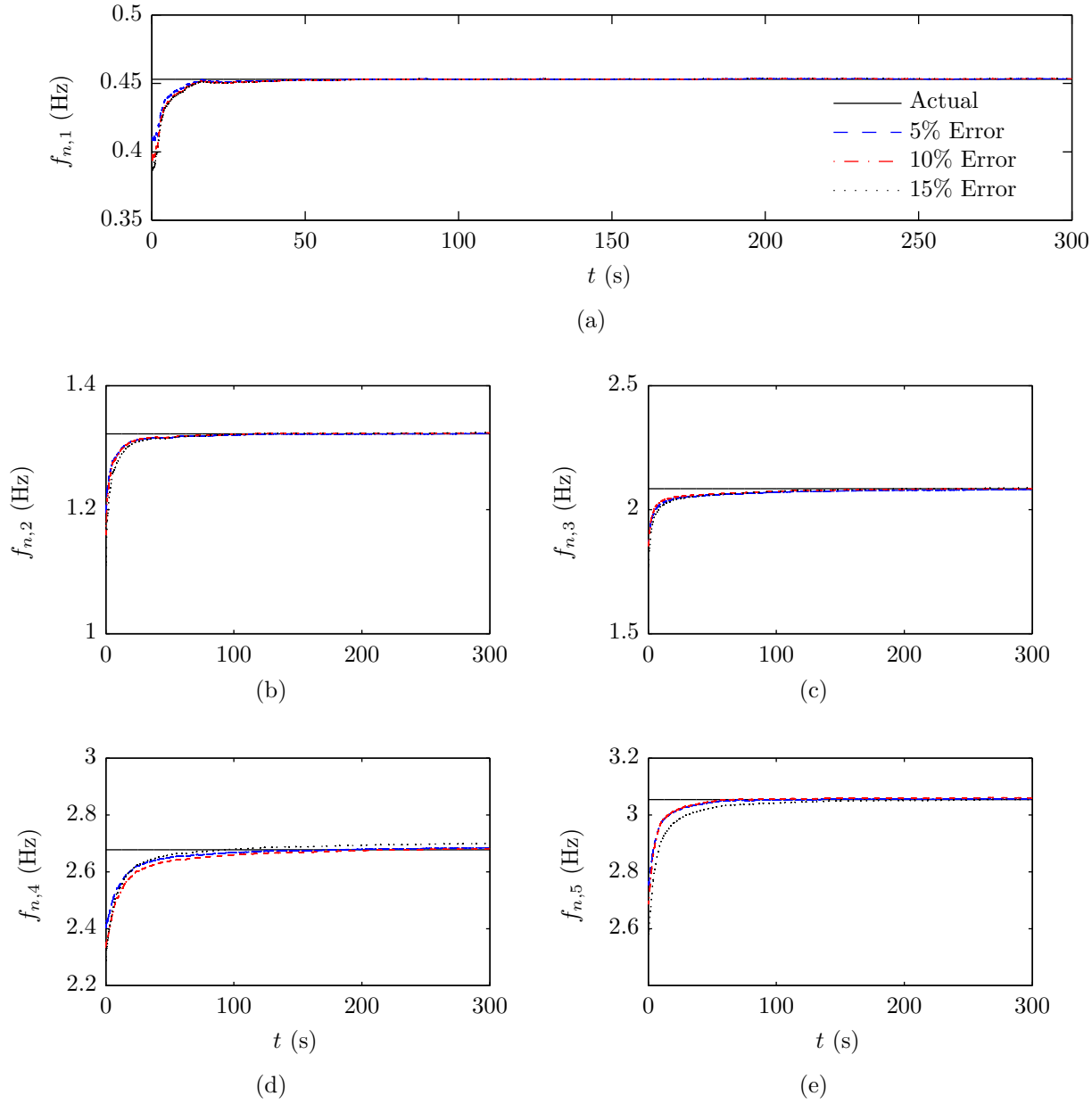

Figure 6.2: Parameter estimates for (a) $\omega_{n,1}$, (b) $\omega_{n,2}$, (c) $\omega_{n,3}$, (d) $\omega_{n,4}$, and (e) $\omega_{n,5}$ with initial errors in the mass matrix, $\mathbf{M}$ of 5%, 10%, and 15%.

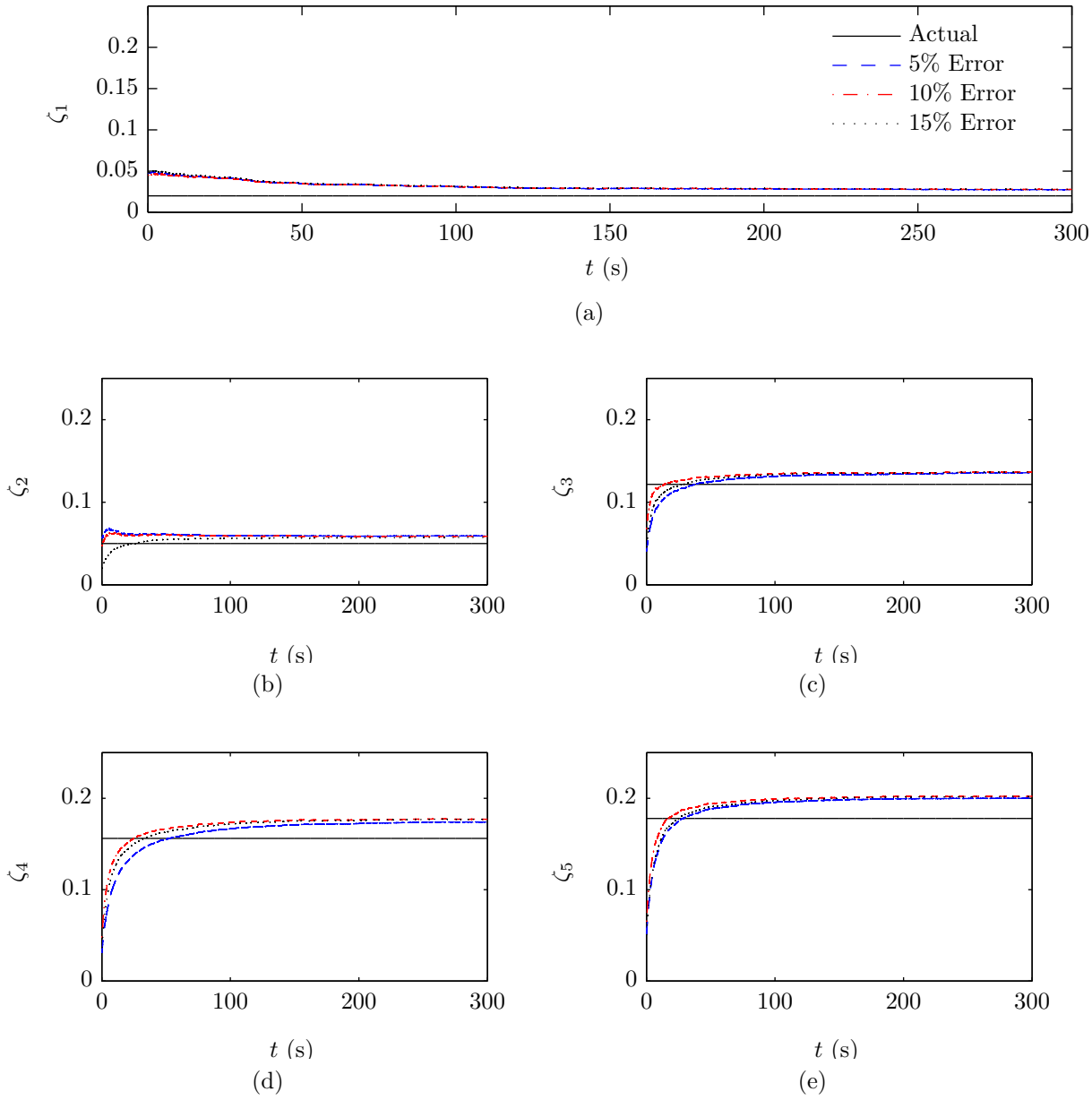

Figure 6.3: Parameter estimates for (a) ζ_1, (b) ζ_2, (c) ζ_3, (d) ζ_4, and (e) ζ_5 with initial errors in the mass matrix, $\mathbf{M}$ of 5%, 10%, and 15%.

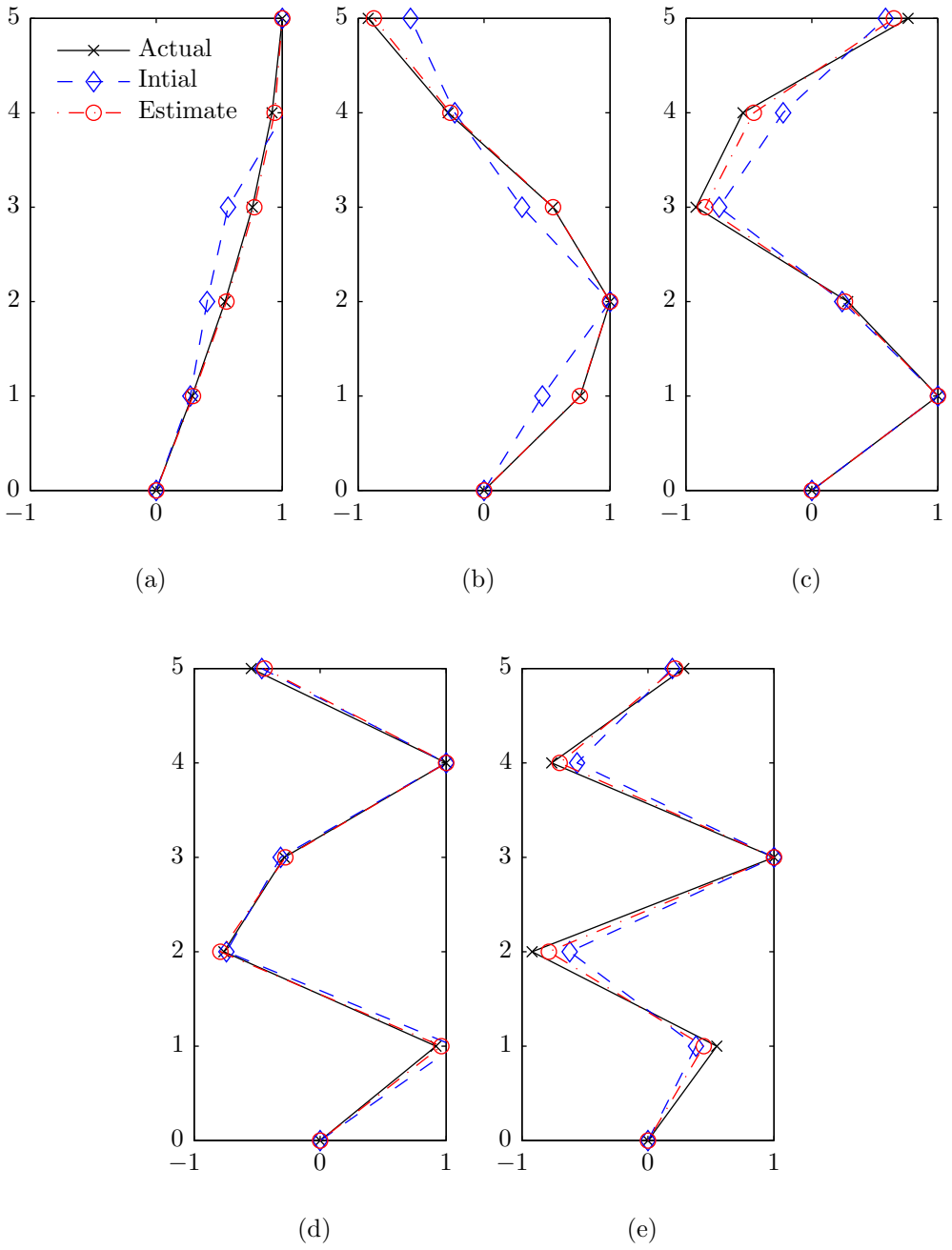

Figure 6.4: Final mode shape vector estimates for (a) 1st, (b) 2nd, (c) 3rd, (d) 4th, and (e) 5th mode for a 5% error in the initial mass matrix

There is no trend for decreased performance in the final converged natural frequency estimates for greater levels of error in the main mass. The estimation of the bare structure natural frequencies is extremely precise, despite initial estimates being incorrect by up to 15.4%. While there is generally considerable improvement in the estimate of the damping ratios (over the initial arbitrary estimates), the errors in the final converged estimates varies from 11.5% to 18.3% for the higher order modes, and up to 40.3% for the first mode of vibration. The results are similar to those presented for the 2-DOF example presented earlier in Sec. 6.3, where the lower levels of modal damping are more difficult to accurately estimate. It is noted that the absolute error in each of the estimates is similar; the level of error is therefore overemphasized when the relative error is considered. There is also an additional performance degradation with greater error in the main mass estimate. The mode shape vector identification for the main mass system with 5% errors are given in Fig. 6.4 and demonstrate good estimation results, particularly for the lower modes. The results for the 5% case are representative of the other cases considered.

6.1.2 Example of noise covariance estimation for a 5DOF PTMD-equipped structure

It is important to note that the noise covariance estimation step is performed prior and separately from the combined state and parameter filter. Accurate knowledge of the system model is likely not available; therefore, several cases are considered for this example. For the first case, the actual model is used to demonstrate the effectiveness of the noise covariance estimation algorithm presented in Secs. 5.3.2 through 5.3.4. For the second case, a model based on the initial finite element representation, where the stiffness elements are underestimated by a mean of 15% with a standard deviation of $\pm 5\%$ of the actual values; the mass is overestimated by a mean of 5% with a standard deviation of $\pm 1\%$ of the actual values. The auxiliary system parameters are known and optimally tuned to the actual structure (provided in Sec. 6.1.1). A third case is considered, to understand the effect that a detuned PTMD has on the noise covariance estimation step. In this situation, the auxiliary parameters are chosen such that they would be optimally tuned to the initial

estimate of the main structure; however, since this auxiliary system is connected to the actual structure, it is effectively detuned (by 12.5% frequency ratio) with respect to the actual structure. This condition seeks to emulate the scenario where the designer has forecasted the bare structural properties and designed the PTMD accordingly. The pendulum length is $L = h = 1.50$ m and auxiliary damping coefficient is $c_a = 12.4$ N s/m. There is no auxiliary spring ($k_a = 0$) and the auxiliary mass is as in the tuned case. As in the example presented in Sec. 5.4.5, only the feedthrough process noise covariances $\mathbf{S}_k$ and measurement noise covariance $\mathbf{R}_k$ are estimated; the additive process noise covariance $\mathbf{Q}_k$ is a tunable parameter selected by the designer to assign a level of confidence in the model.

The actual unknown stochastic input process noise covariance, $\mathbf{S}_k$, is given in Eqs. 6.15. The additive measurement noise was assigned to each measurement (acceleration response) based on a SNR of 20 at the auxiliary DOF. The initial unknown disturbance and measurement noise covariance estimates are $\mathbf{S} = \texttt{diag}\begin{bmatrix} 1 & 1 & 1 & 1 & 1 \end{bmatrix} \times 10^7$ and $\mathbf{R} = \texttt{diag}\begin{bmatrix} 3 & 3 & 3 & 3 & 3 \end{bmatrix} \times 10^{-3}$, respectively. Each are assembled into matrices $\mathbf{S}_l$ and $\mathbf{R}_l$, where $l = 1, 2, \ldots, \hat{N}$. When multiplied by the true value of α,

$$\alpha = \begin{bmatrix} 0.0311 & 0.0599 & 0.0570 & 0.0530 & 0.0461 & 0.391 & 0.391 & 0.389 & 0.389 & 0.390 & 0.391 \end{bmatrix}$$

as in Eqs. 5.157 and 5.158, the actual state covariance matrices are returned. The model parameters are set to the actual parameters or the initial estimates, depending on which case is being considered. The components of α are initially set to unity. The parameter vector α is then estimated according to the algorithm described in Eqs. 5.183 through 5.213. The normalized estimates for the values of mean $\hat{\alpha}$ (normalized with respect to true values), for the case where the model is set to the actual parameters, are shown in Fig. 6.5. Fig. 6.5a corresponds to the estimation of $\mathbf{S}_k$ while Fig. 6.5b corresponds to $\mathbf{R}_k$. Details on the actual parameter values, initial estimates, mean values of the final estimates, and the coefficients of variation ($\hat{c}_v$) are detailed in Table 6.5.

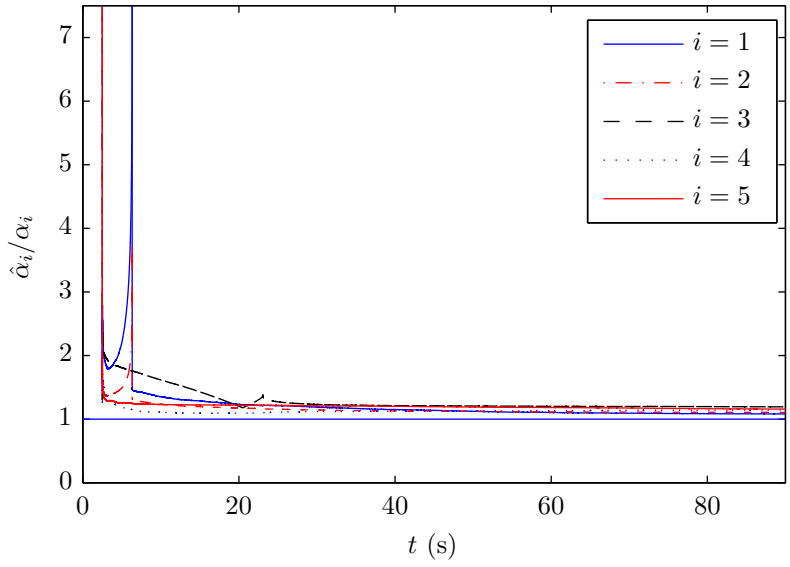

(a)

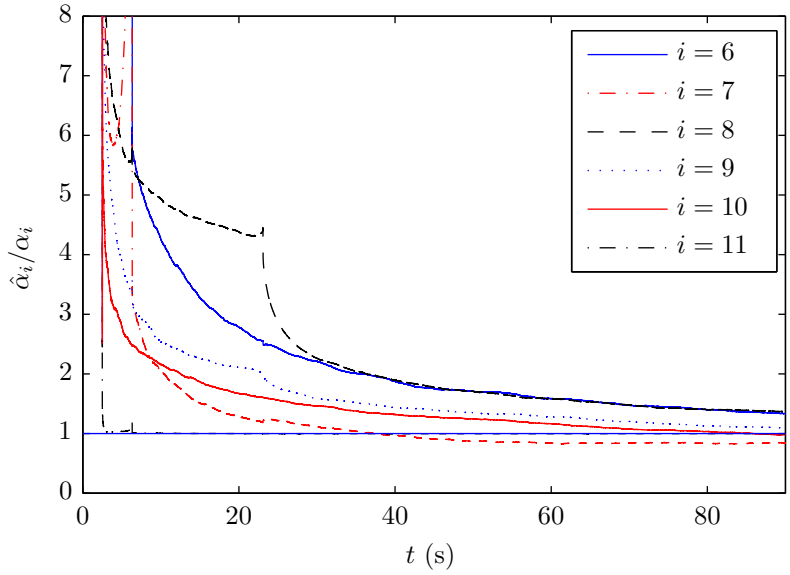

(b)

Figure 6.5: Normalized (a) feedthrough disturbance noise covariance $\hat{\mathbf{S}}$ and (b) measurement noise covariance $\hat{\mathbf{R}}$ parameter estimates averaged over 100 filter realizations.

Table 6.5: Noise covariance parameter α estimates using the actual model parameters, initial model parameter estimate with tuned PTMD, and initial model parameter estimate with detuned PTMD

Index		Actual model		Initial estimate of model			
				Tuned		Detuned	
	Actual	Estimate	Error	Estimate	Error	Estimate	Error
			%		%		%
$\mathbf{S}_k$							
1	0.0311	0.0312	0.506	0.0335	7.81	0.0337	8.31
2	0.0599	0.0600	0.0677	0.0664	10.8	0.0662	10.5
3	0.0570	0.0571	0.0701	0.0657	15.1	0.0657	15.3
4	0.0530	0.0527	0.506	0.0580	9.46	0.0585	10.4
5	0.0461	0.0462	0.325	0.0528	14.6	0.0526	14.3
$\mathbf{R}_k$							
6	0.391	0.391	0.0174	0.470	20.3	0.454	17.5
7	0.391	0.384	1.58	0.310	20.6	0.297	22.7
8	0.389	0.392	0.998	0.343	11.8	0.332	14.3
9	0.389	0.383	1.44	0.321	17.5	0.310	20.1
10	0.390	0.376	3.52	0.361	7.25	0.359	6.95
11	0.391	0.391	0.0398	0.391	0.0214	0.387	0.547

The noise covariance estimation for the case of known model parameters is precise. Initial estimates of the noise covariance were arbitrary and considerably in error, and convergence close to the actual noise covariances was realized. The residual correlation approach used here is deemed a suitable approach for the problem at hand. For practical applications, however, the model parameters will not be known precisely. Therefore, two examples were considered using the initial parameter estimates, which were assumed known for the purpose of noise covariance estimation. The improvement over the initial noise covariance estimate is dramatic, with errors in the final converged values of up to 15.3% and 22.7% for the process noise, $\mathbf{S}_k$, and measurement noise, $\mathbf{R}_k$, respectively. It will be demonstrated that this level of error has no noticeable effect on the final parameter

estimates in the following section.

6.2 Combined state, parameter, and noise covariance estimation for a PTMD equipped structure

The noise covariance estimates obtained from the previous step are then used in the combined state and parameter estimation. The initial state vector was selected as $\hat{\mathbf{x}}_0 = \begin{bmatrix} \mathbf{0} & \hat{\omega}_{n,j,0} & \hat{\zeta}_{j,0} & \hat{\phi}_{ij,0} \end{bmatrix}^T$, where $\hat{\omega}_{n,j}$, $\hat{\zeta}_j$, and $\hat{\phi}_{ij}$ are vectors that contain the initial estimates of the appended parameter, and are based on a modal analysis using the crude finite element model. Two cases are considered, as described in the Sec. 6.1.2. The first is for the case where the auxiliary system is properly tuned to the actual structure. The second is where the auxiliary system is tuned to the initial estimate of the unknown model; therefore, detuned with respect to the actual model.

The initial state covariance $\mathbf{P}_0$ for the actual state estimates is established based on knowledge of the state variance from the noise estimation procedure. The initial state estimation error covariance for the appended parameters is established using a 10% variance in the initial estimate for the natural frequencies, 2.5% variance for the damping ratio estimates, and 1% for the normalized mode shape vector estimates. The selection of the process noise covariance $\mathbf{Q}_k$ is to compensate for any modelling errors and to improve the constant state (appended parameter) estimates; a small amount of process noise covariance equal to 1×10^{-6} times the initial state estimation error covariance was introduced at each of the displacement and velocity states, primarily to compensate for accelerometer bias. The combined state and parameter estimate was performed using 100 data sets, each 300 s long. The system was excited for 150 s before recording data in order to ensure transient effects had decayed and the data sets were not based on at rest initial conditions.

Table 6.6: Natural frequency identification results for 5-DOF system equipped with a PTMD for unknown external excitation and unknown noise statistics

	Identified Parameter				
	$f_{n,1}$	$f_{n,2}$	$f_{n,3}$	$f_{n,4}$	$f_{n,5}$
	Hz	Hz	Hz	Hz	Hz
Actual	0.453	1.32	2.08	2.68	3.05
Initial	0.409	1.21	1.87	2.41	2.77
Error (%)	9.7	8.87	10.2	9.88	9.4
Tuned					
Estimate	0.453	1.32	2.08	2.68	3.05
Error (%)	0.028	0.0403	0.371	0.00919	0.164
$\hat{c}_v$ (%)	0.668	0.496	0.584	0.696	0.643
Detuned					
Estimate	0.453	1.32	2.08	2.67	3.05
Error (%)	0.0291	0.00206	0.307	0.14	0.272
$\hat{c}_v$ (%)	0.442	0.364	0.711	0.6	0.793

Table 6.6 provides the actual structure's natural frequencies, $f_{n,j}$ (Hz), together with the mean of the final estimated value, $\hat{f}_{n,j}$ and coefficient of variation ($\hat{c}_v$). The percent error is reported with respect to the actual values for the final converged and initial parameter estimates. The final estimate for the natural frequencies for all cases converged close to the actual values. The results demonstrate that without any knowledge of the input excitation, including the statistics, the combined state-noise covariance estimation followed by the state-parameter estimation provides an accurate and reliable estimate of the natural frequencies. The convergence of the natural frequency estimates is fast, as illustrated in Fig. 6.6. The tuned and detuned auxiliary system cases's performance is comparable; for the purpose of frequency identification, the performance is relatively insensitive to the level of tuning of the auxiliary damping device.

Table 6.7: Modal damping ratio identification results for 5-DOF system equipped with a PTMD for unknown external excitation and unknown noise statistics

	Identified Parameter				
	ζ_1	ζ_2	ζ_3	ζ_4	ζ_5
Actual	0.02	0.05	0.122	0.156	0.178
Initial	0.0483	0.0572	0.0406	0.0311	0.0516
Error (%)	141	14.3	66.6	80.1	71
Tuned					
Estimate	0.0287	0.0592	0.135	0.173	0.199
Error (%)	43.4	18.4	10.9	10.8	11.9
$\hat{c}_v$ (%)	22.9	7.1	3.96	2.75	3.09
Detuned					
Estimate	0.0242	0.0591	0.135	0.172	0.199
Error (%)	21.1	18.1	10.9	10.5	11.7
$\hat{c}_v$ (%)	22.4	8.1	4.2	2.74	3.13

Damping ratio identification results are provided in Table 6.7, and generally demonstrate reasonable performance over the initial estimate of the modal damping ratio. For the mode to which the PTMD is tuned, the error is more pronounced. The cause of this error is two-fold. First, treating the unknown excitation as a stochastic process noise allows the filter itself to be able to compensate for the attenuation introduced by the damping ratios. Second, it can be observed that the absolute error in the estimates is generally consistent, always slightly overestimating the damping ratio. Numerical errors introduced as a result of the approximate discretization approach (Sec. 5.1.3) contribute to this effect. Using a faster sampling rate improves the estimate, but there is a significant trade-off related to the computational effort required. From the detuned case, the damping ratio estimate for the first mode is vastly improved when compared to the tuned case. The introduction of the auxiliary damping device makes modal damping identification markedly more challenging. Fig. 6.7 plots the convergence of the damping estimates for both the tuned and detuned auxiliary systems. The results demonstrate that a considerable length of data must be

processed by the filter before convergence occurs.

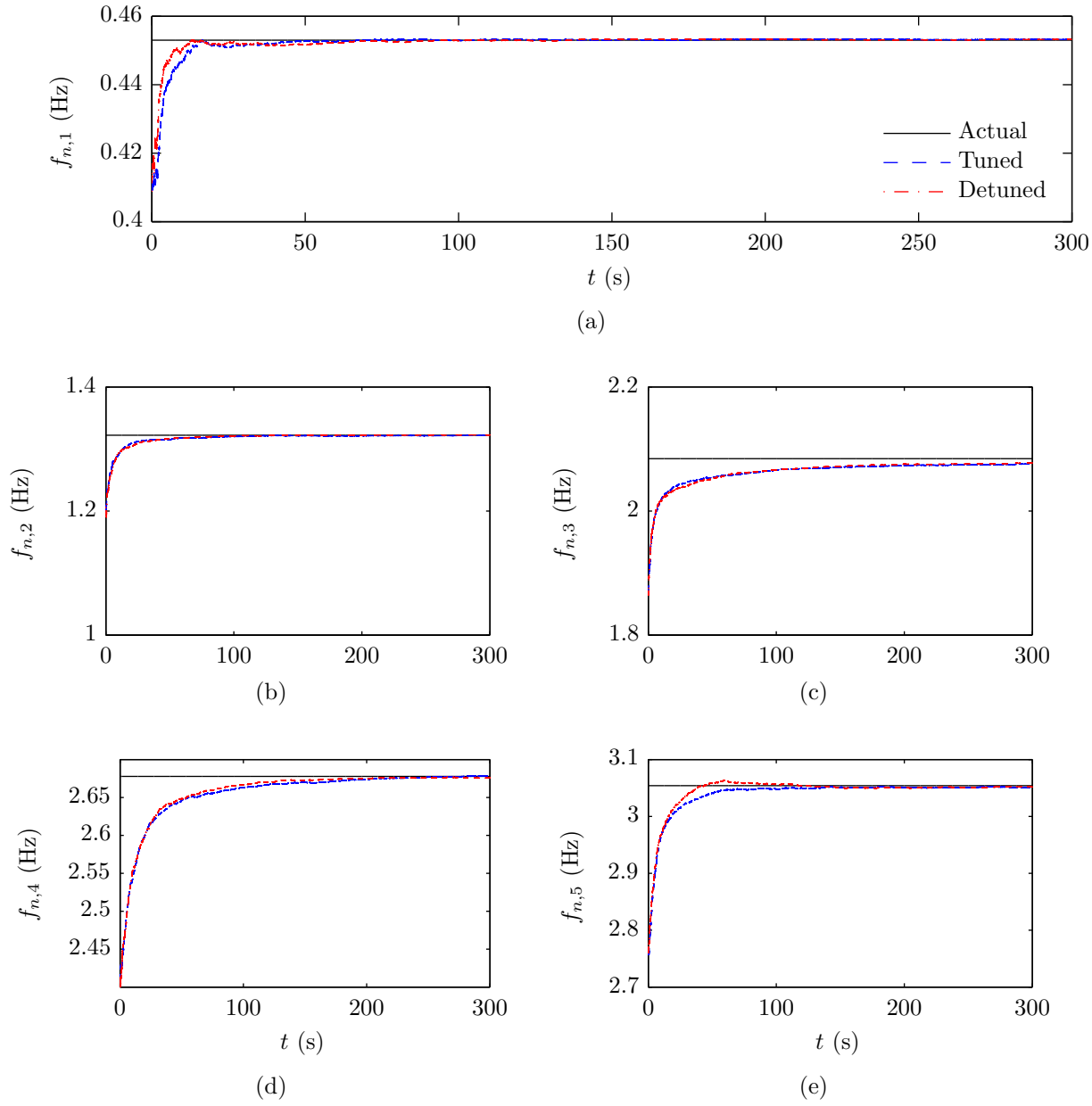

Figure 6.6: Parameter estimates for (a) $\omega_{n,1}$, (b) $\omega_{n,2}$, (c) $\omega_{n,3}$, (d) $\omega_{n,4}$, and (e) $\omega_{n,5}$ for a tuned and detuned auxiliary mass where the process and measurement noise covariances are unknown.

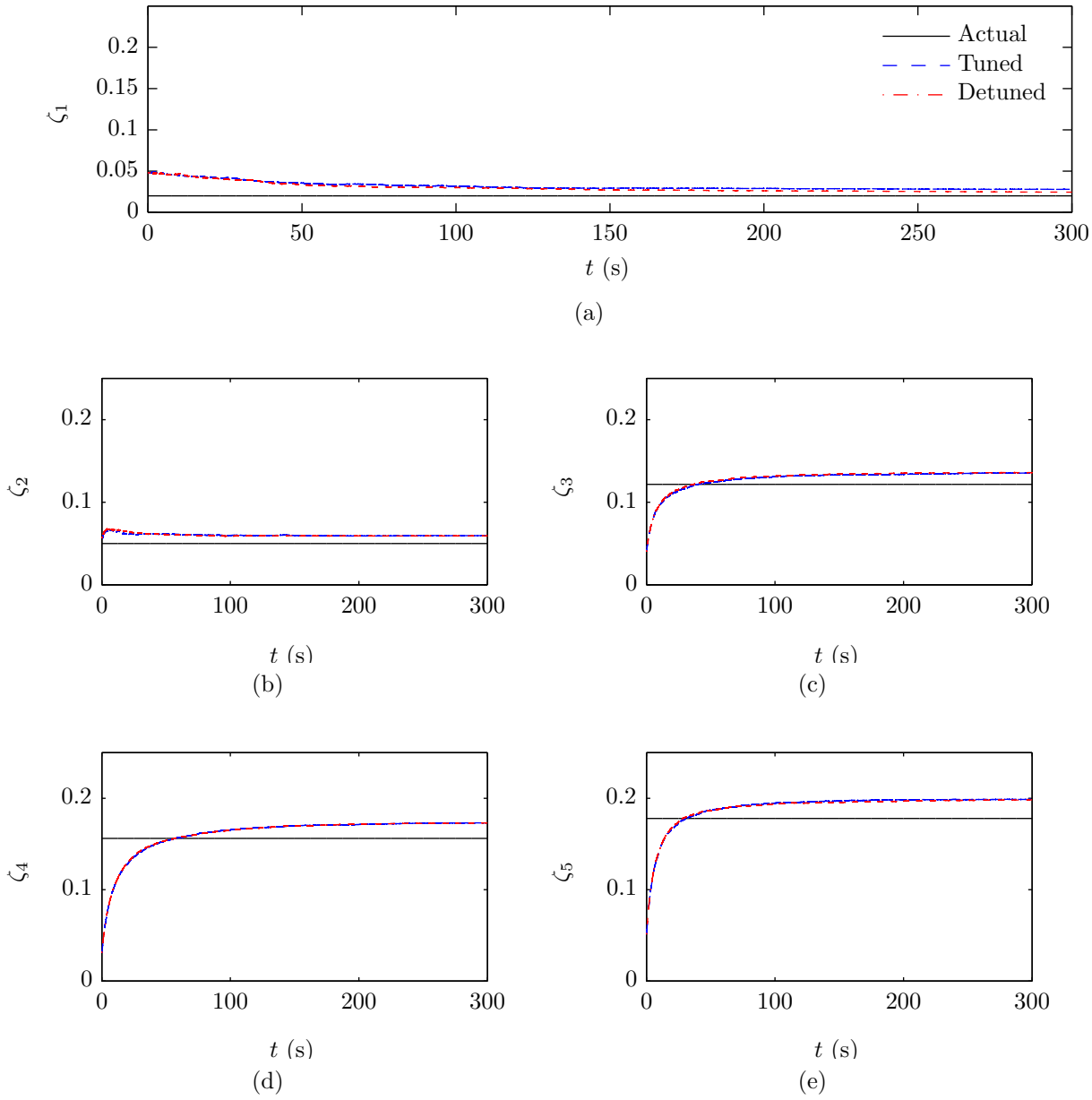

Figure 6.7: Parameter estimates for (a) ζ_1, (b) ζ_2, (c) ζ_3, (d) ζ_4, and (e) ζ_5 for a tuned and detuned auxiliary mass where the process and measurement noise covariances are unknown.

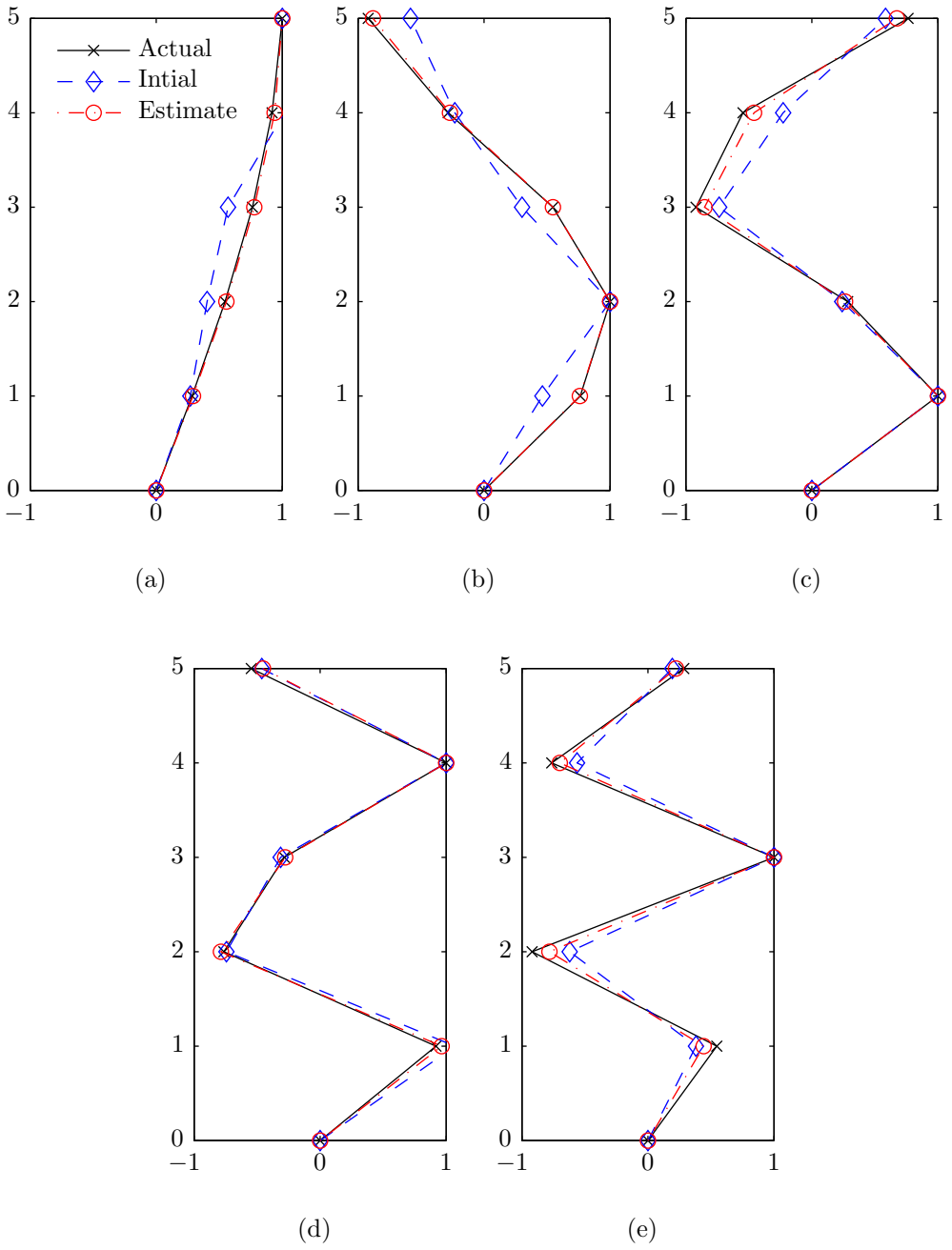

Figure 6.8: Final mode shape vector estimates for (a) 1st, (b) 2nd, (c) 3rd, (d) 4th, and (e) 5th mode for a tuned auxiliary mass where the process and measurement noise covariances are unknown.

For the purpose of tuning TMDs, researches have noted that the main mass damping ratio has little effect on the optimal parameters [75, 26, 3, 79]; therefore, accurate identification of the modal damping ratios is not as crucial as frequency identification for the purpose of retuning TMDs. Also, the optimal auxiliary to main mass damping ratio that minimizes the root mean squared (RMS) response of the main structure or maximizes the effective damping introduced generally results in substantial motion of the auxiliary mass, particularly for small mass ratios. Space constraints within the structure may require limiting the motion, or stroke, of the TMD; therefore, a damping ratio greater than optimal may be selected at a sacrifice of TMD efficiency [77, 55, 101].

The initial estimates of the mode shape vectors, assembled using the estimated mass and stiffness matrix, are not sensitive to the error introduced and are not substantially different from the actual mode shapes. To demonstrate the effectiveness of the identification method presented, an additional random perturbation is introduced to each element of the mode shape vectors. These values were then normalized with respect to the DOF to which to PTMD is coupled, and used as the initial estimates in the state-noise covariances-parameter estimation filter. A mean and coefficient of variation of the mode shape coefficient estimates for 100 filter realizations are summarized in Table 6.8. The mode shape vectors are also plotted in Fig. 6.8 together with the initial estimate, normalized with respect to the maximum displacement coordinate, for the tuned auxiliary mass condition.

The results demonstrate good performance in the identification of the mode shape vectors, particularly in the lower-order modes, which are of greater interest as they contribute to the majority of the structural response. Most importantly, there is excellent identification of the mode shape vector for the mode to which the PTMD is tuned.

There is no noticeable decline in performance of the combined state and parameter estimation using the estimated noise covariance matrices, despite errors of up to 15.3% and 22.7% in the process noise covariance, $\mathbf{S}_k$, and measurement noise covariance, $\mathbf{R}_k$, respectively. This validates the noise covariance estimation approach.

The approach presented in this section overcomes several issues not previously explored in time domain parametric identification. First, an unknown main mass excitation

Table 6.8: Mode shape identification results for 5-DOF system equipped with a PTMD for unknown external excitation and unknown noise statistics

Mode	Normalized shape coefficient for j^{th} mode											
	Actual	Estimate		Actual	Estimate		Actual	Estimate		Actual	Estimate	
	ϕ_{2j}	$\hat{\phi}_{2j}$	$\hat{c}_v$	ϕ_{3j}	$\hat{\phi}_{3j}$	$\hat{c}_v$	ϕ_{4j}	$\hat{\phi}_{4j}$	$\hat{c}_v$	ϕ_{5j}	$\hat{\phi}_{5j}$	$\hat{c}_v$
			%			%			%			%
Tuned												
1	0.919	0.939	0.86	0.764	0.779	1.0	0.546	0.557	1.1	0.285	0.292	1.9
2	0.310	0.306	3.4	-0.594	-0.620	3.5	-1.09	-1.13	3.0	-0.831	-0.861	3.4
3	-0.715	-0.679	5.1	-1.20	-1.26	4.5	0.373	0.388	10	1.31	1.48	5.4
4	-1.83	-2.18	4.2	0.521	0.610	7.7	1.40	1.74	4.7	-1.68	-2.13	5.4
5	-2.68	-3.16	4.6	3.51	4.49	3.8	-3.23	-3.49	3.8	1.92	1.97	4.3
Detuned												
1	0.919	0.925	0.53	0.764	0.768	0.68	0.546	0.55	0.99	0.285	0.288	1.7
2	0.310	0.308	3.6	-0.594	-0.623	3.6	-1.09	-1.14	2.6	-0.831	-0.867	2.8
3	-0.715	-0.688	5.8	-1.20	-1.27	4.2	0.373	0.396	8.2	1.31	1.49	5.2
4	-1.83	-2.18	5.0	0.521	0.599	11	1.4	1.73	5.6	-1.68	-2.11	4.7
5	-2.68	-3.14	3.5	3.51	4.49	4.0	-3.23	-3.54	3.4	1.92	1.99	6.1

was considered; this was treated as a unknown stochastic process noise. Second, since only acceleration responses were assumed to be available, the traditional form of the EKF had to be adapted for the case of feedthrough of the unknown disturbance noise. Third, in addition to the process noise being unknown, it's statistics, namely, the covariance matrix $\mathbf{S}_k$, as well as the covariance of the additive measurement noise, $\mathbf{R}_k$, were also treated as unknown. A process noise estimation step was invoked to determine these noise covariances. A recursive least squares estimator was used to estimate the noise covariance parameters that produced a residual sequence with a measured correlation that fit its theoretical value. These estimated noise statistics are used to drive the combined state and parameter estimation filter. The development of the method was systematically benchmarked against an existing EKF identification example presented in the literature. A numerical example was presented, where precise estimation of the natural frequencies was demonstrated, which is of primary concern for the purpose of tuning TMDs. Estimation of the modal damping ratios was deemed adequate, though poorer performance was documented for modal damping ratio estimation of the controlled mode. Effective or equivalent damping introduced by a TMD is another parameter of interest in assessing the performance of in-service TMDs; estimating this quantity using the EKF is considered next.

6.3 Estimating effective viscous damping in TMD-equipped structures

The concept of "effective damping" or "equivalent damping", first proposed by Vickery [94] and McNamara [66], is commonly referenced when quantifying TMD performance. The term refers to equating the performance of the combined main and auxiliary system to that of a single-degree-of-freedom (SDOF) system with modal damping parameter, ζ_e, and operating at the same natural frequency for the controlled mode of vibration. Equations which relate the effective damping introduced by the TMD are available for the case of main mass excited [66] and base excited structures [26], for both conventional translational TMDs and PTMDs [26]. Maximizing the effective damping introduced by the TMD has

been used as a cost function for selecting optimal damper parameters by various researchers [55, 48, 88, 94].

Despite its simplicity, effective damping has experienced relatively little use in describing the performance of TMDs in actual applications. This is because its theoretical calculation is based on the RMS displacement response of the TMD-equipped structure, which is seldom measured; instead, acceleration response measurements are taken from which displacements need to be inferred. Accelerometer bias results from direct integration of the noisy acceleration responses, and assumptions of at-rest initial and final displacements is generally not appropriate from wind excitation. This issue is of particular significance when the performance of an in-service TMD must be demonstrated to verify that a prescribed level of effective damping has been achieved.

It is proposed to apply the same identification approach presented earlier, namely EKF modal identification, for the purpose of estimating effective damping. This is accomplished by fitting the measurement data to a SDOF model of the structure described in the modal domain with known frequency characteristics and unknown damping. The damping parameter is appended to the state vector and estimated as the effective damping introduced by the TMD. A simple example is demonstrated first. Subsequently, the method is extended for the case of unknown underlying structure modal properties by running two simultaneous filters. The first estimates the underlying modal characteristics (as described in Chapter 5) and the second uses the current estimate of the natural frequency for the controlled mode to estimate the effective damping. These results are demonstrated using a numerical example and compared to the theoretical calculation, which is derived next.

6.3.1 Theoretical calculation of effective damping introduced by a PTMD

In order to determine a closed form expression for the effective damping, ζ_e, the equations of motion for a SDOF main structure equipped with a PTMD, described in Eqs. 2.10 and

2.11, must be first transformed into the modal domain.

$$M_{r,j}\ddot{y}_j(t) + C_{r,j}\dot{y}_j(t) + K_{r,j}y_j(t) + m_a\ddot{\theta}L = F_{r,j}(t) \tag{6.16a}$$

$$m_aL^2\ddot{\theta}(t) + c_ah^2\dot{\theta}(t) + \left(m_agL + k_ah^2\right)\theta(t) + m_aL\ddot{y}_j(t) = 0 \tag{6.16b}$$

where $M_{r,j}$, $C_{r,j}$, $K_{r,j}$, $F_{r,j}(t)$ are the modal mass, damping, stiffness, and force and $y_j(t)$ is the modal coordinate. $\theta(t)$ is the rotation of the auxiliary system, with auxiliary mass, damping, and stiffness given by m_a, c_a, and k_a, respectively. The pendulum length is L and g is the acceleration due to gravity. Selecting an input of the form $F(t) = e^{i\omega t}$ in order to calculate the complex frequency response functions $H_y(i\omega)$ and $H_\theta(i\omega)$. The responses are then

$$y_j(t) = H_y(i\omega)\frac{F_{r,j}(t)}{K_{r,j}} \tag{6.17a}$$

$$\theta(t) = H_\theta(i\omega)\frac{F_{r,j}(t)}{K_{r,j}L} \tag{6.17b}$$

Eqs. 6.17a and 6.17b are substituted into Eqs. 6.16a and 6.16b and are rewritten in matrix form as

$$\begin{bmatrix} -\omega^2\left(M_{r,j}+m_a\right) + i\omega C_{r,j} + K_{r,j} & -\omega^2 m_aL \\ -\omega^2 m_aL & -\omega^2 m_aL^2 + i\omega c_ah^2 + k_ah^2 \end{bmatrix} \begin{Bmatrix} H_y/K_{r,j} \\ H_\theta/K_{r,j}L \end{Bmatrix} = \begin{Bmatrix} 1 \\ 0 \end{Bmatrix} \tag{6.18}$$

A forcing frequency ratio, ϕ, is introduced, given by

$$\phi = \frac{\omega}{\omega_n} \tag{6.19}$$

where ω is the forcing frequency and ω_n is the circular natural frequency of the oscillator. Eq. 6.18 is solved simultaneously for the complex frequency response functions $H_y(i\omega)$ and $H_\theta(i\omega)$ in terms of the non-dimensional auxiliary to main frequency ratio f_r, auxiliary to main mass ratio μ, and the main and auxiliary damping ratios ζ and ζ_a, first introduced in

Chapter 2. The results are given in Table 6.9. The mean square response of the processes, $y_j(t)$ and $\theta(t)$, are given by [26]

$$E\left[y_j(t)^2\right] = \frac{\omega_n S_0}{K_{r,j}^2} \int_0^\infty \left|H_y\left(i\phi\right)\right|^2 d\phi \tag{6.20a}$$

$$E\left[\theta(t)^2\right] = \frac{\omega_n S_0}{\left(K_{r,j}L\right)^2} \int_0^\infty \left|H_\theta\left(i\phi\right)\right|^2 d\phi \tag{6.20b}$$

for the case of white noise excitation with constant spectral density, S_0. For a SDOF oscillator operating at the same frequency with damping ratio ζ_e, the mean square response is given by [15]

$$E\left[y_j(t)^2\right] = \frac{\omega_n^2 S_0}{2K_{r,j}^2 \zeta_e} \tag{6.21}$$

Substituting Eq. 6.20a into Eq. 6.21, rearranging to solve for ζ_e, and performing the integrations results in the effective damping provided in Table 6.9. A similar process can be performed for a translational-type TMD; the effective damping result in terms of the non-dimensional parameters f_r, ζ, ζ_a, μ, and ϕ is the same.

6.3.2 Estimating effective damping using extended Kalman filter

The approach for calculating the effective damping introduced by a TMD is quite simple, and is easily theoretically demonstrated in Eq. 6.21. However, it requires knowledge of the RMS displacement responses of the primary system, which are not directly available from acceleration response measurements. EKF modal identification is proposed to overcome this challenge. The measured TMD-attenuated response data is fit to a model of a SDOF system using the concept of EKF presented in Sec. 5.1.2. In the simplest case, the natural frequency of the main structure is known and is a fixed model parameter; the only unknown parameter is the damping ratio, which is appended to the state vector and estimated. This estimated parameter is essentially the effective damping, ζ_e, of the combined main and TMD system. For the present study, only PTMDs are considered. However, the concept can easily be extended for conventional TMDs. A simple case is demonstrated first, for a SDOF system with a PTMD with known underlying structural frequency. Next,

Table 6.9: Complex frequency response and effective viscous damping for a PTMD-equipped structure

$$H_y(i\omega) = \frac{-\phi^2 + 2i\phi f_r \zeta_a + f_r^2}{\phi^4 - i\phi^3(2\zeta + 2f_r\zeta_a + 2f_r\zeta_a\mu) - \phi^2(1 + f_r^2 + f_r^2\mu + 4f_r\zeta\zeta_a) + 2i\phi(f_r^2\zeta + f_r\zeta_a) + f_r^2}$$

$$H_\theta(i\omega) = \frac{\phi^2}{\phi^4 - i\phi^3(2\zeta + 2f_r\zeta_a + 2f_r\zeta_a\mu) - \phi^2(1 + f_r^2 + f_r^2\mu + 4f_r\zeta\zeta_a) + 2i\phi(f_r^2\zeta + f_r\zeta_a) + f_r^2}$$

$$\zeta_e = \frac{\left(\zeta f_r^2 + \zeta_a f_r\right)\left\{\left[1 + (1+\mu) f_r^2 + 4\zeta\zeta_a f_r\right][\zeta + \zeta_a(1+\mu) f_r] - \left(\zeta f_r^2 + \zeta_a f_r\right)\right\} - f_r^2[\zeta + \zeta_a(1+\mu) f_r]^2}{f_r^2\left\{[1 + (1+\mu) f_r^2 + 4\zeta\zeta_a f_r][\zeta + (1+\mu)\zeta_a f_r] - (\zeta f_r^2 + \zeta_a f_r) + 2[\zeta + \zeta_a(1+\mu) f_r](2\zeta_a^2 - 1)\right\} + \zeta f_r^2 + \zeta_a f_r}$$

the effective damping added by the PTMD for the system first presented in Sec. 6.2 is considered.

6.3.3 Effective damping for a known PTMD-equipped SDOF system

A simple SDOF is considered first, where the structural properties of the main system and the auxiliary damper parameters are known. The equations of motion for a PTMD equipped SDOF oscillator (Eq. 2.10 and 2.11) are recast in the state-space form. The main structure displacement and velocity, as well as the auxiliary system rotation and angular velocity, are the states.

$$\mathbf{x}(t) = \begin{bmatrix} u(t) & \theta(t) & \dot{u}(t) & \dot{\theta}(t) \end{bmatrix}^T \tag{6.22}$$

Selecting the acceleration response of the main system and the horizontal acceleration of the auxiliary mass as the measurements, the state matrices are given in Table 6.10. These system matrices are used to generate synthetic data for the estimation of the effective damping.

Since the identification of the effective damping is in the modal domain, the measurements are fit to a SDOF model expressed in modal coordinates. The states of the system are the modal displacement and velocity, $\mathbf{x}(t) = \begin{bmatrix} y(t) & \dot{y}(t) \end{bmatrix}$. The unknown modal damping ratio or effective damping is appended to the state vector ($x_3(t) = \zeta_e$) and a constant transition is assumed. After discretization, the nonlinear transition equations are

$$x_1[k+1] = x_1[k] + x_2[k]T + w_1[k] \tag{6.23a}$$

$$x_2[k+1] = -\frac{k}{m}Tx_1[k] + \left(1 - 2\sqrt{\frac{k}{m}}x_3[k]T\right)x_2[k] + \frac{1}{m}Td[k] + w_2[k] \tag{6.23b}$$

$$x_3[k+1] = x_3[k] + w_3[k] \tag{6.23c}$$

where $\mathbf{w}_k = \begin{bmatrix} w_1[k] & w_2[k] & w_3[k] \end{bmatrix}^T$ are the additive process noise terms with covariance

$\mathbf{Q}_k$ and $d[k]$ is the discrete time unknown input, which is treated as a stochastic noise process with covariance S_k. The nonlinear measurement equation is

$$z_1[k] = -\frac{k}{m}x_1[k] - 2\sqrt{\frac{k}{m}}x_3[k]x_2[k] + \frac{1}{m}d[k] + v[k] \tag{6.24}$$

where $v[k]$ is the additive measurement noise with covariance R_k.

Table 6.10: Continuous time state matrices for uniaxial SDOF system with planar PTMD

$$\mathbf{A}_c = \begin{bmatrix} 0 & 0 & 1 & 0 \\ 0 & 0 & 0 & 1 \\ -\frac{k}{m} & \frac{m_a g L + k_a h^2}{mL} & -\frac{c}{m} & \frac{c_a h^2}{mL} \\ \frac{k}{mL} & -\frac{(m+m_a)\left(m_a g L + k_a h^2\right)}{m m_a L^2} & -\frac{c}{mL} & -\frac{(m+m_a)c_a h^2}{m m_a L^2} \end{bmatrix}$$

$$\mathbf{E}_c = \begin{bmatrix} 0 \\ 0 \\ \frac{1}{m} \\ -\frac{1}{mL} \end{bmatrix}$$

$$\mathbf{C}_c = \begin{bmatrix} -\frac{k}{m} & \frac{m_a g L + k_a h^2}{mL} & -\frac{c}{m} & \frac{c_a h^2}{mL} \\ \frac{k}{mL} & -\frac{(m+m_a)\left(m_a g L + k_a h^2\right)}{m m_a L^2} & -\frac{c}{mL} & -\frac{(m+m_a)c_a h^2}{m m_a L^2} \end{bmatrix}$$

$$\mathbf{F}_c = \begin{bmatrix} \frac{1}{m} \\ -\frac{1}{mL} \end{bmatrix}$$

A simple numerical example is considered to demonstrate the ability to estimate the effective damping introduced by the PTMD using the EKF. The main and auxiliary masses are $m = 100$ kg and $m_a = 1$ kg, respectively. The main system stiffness is $k = 1000$ N/m, resulting in a natural frequency of $f_n = 0.50$ Hz ($\omega_n = 3.16$ rad/s). The damping coefficient was selected based on a modal damping ratio of $\zeta = 0.01$. The frequency ratio is $f_r = 0.9926$, resulting in a pendulum length of $L = 0.995$ m for the case of no auxiliary spring ($k_a = 0$). The auxiliary damping ratio was $\zeta_a = 0.0498$. The theoretical effective damping was found to be $\zeta_e = 0.0328$ using the equation given in Table 6.9. The

acceleration response of the main system was measured and additive noise with a SNR of 20 was introduced.

A total of 100 realizations of the filter were run. The initial estimate of the appended parameter $\hat{\zeta}_{e,0} = 0.01$. The initial state estimate error covariance was selected as 1% of the initial parameter estimate. The averaged parameter results are plotted in Fig. 6.9. The final estimate after a 600 s filter length was $\hat{\zeta}_e = 0.0332$ with a coefficient of variation (COV) of $\hat{c}_v = 9.55\%$; this represents a 1.31% error based on the theoretical value of $\zeta_e = 0.0328$. These results demonstrate that the EKF is capable of accurately estimating the effective damping introduced by a TMD, by fitting the measurement data to a SDOF oscillator with known natural frequency. The methodology is now extended to a MDOF uniaxial system with a PTMD.

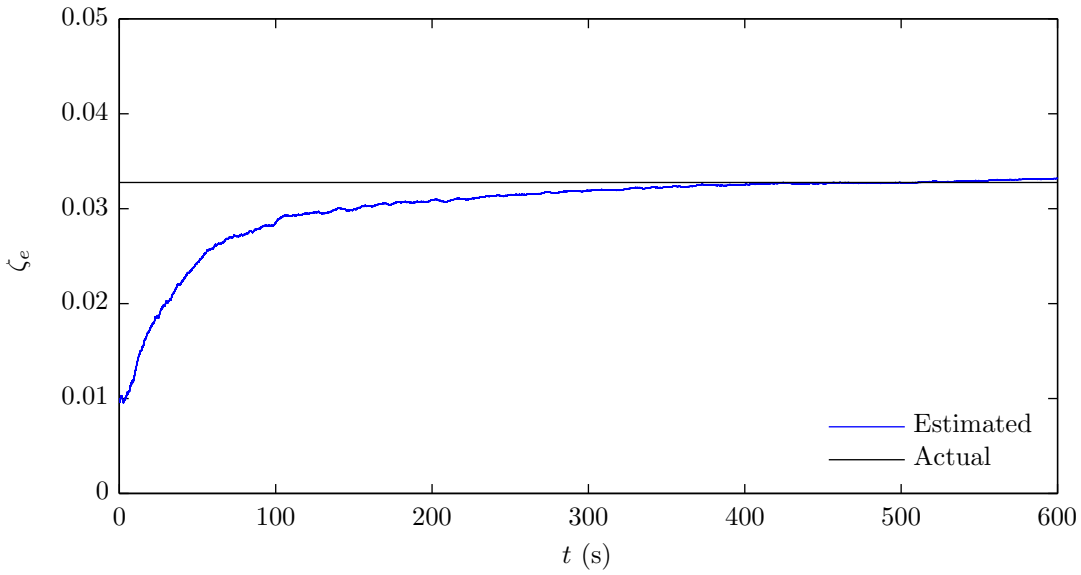

Figure 6.9: Effective damping estimate for a PTMD-equipped SDOF system by EKF identification

6.3.4 Effective damping for an unknown PTMD-equipped MDOF system

The uniaxial MDOF system equipped with a PTMD, presented in Sec. 6.2, is considered next to demonstrate the potential of using EKF identification to estimate the effective damping for the system. The case of unknown main mass excitation with unknown noise covariances is considered. The added complication of this model is a greater number of DOFs, and subsequently, high order modes of vibration. In addition to this, the natural frequency for the controlled mode is not known *a priori*. There are approaches that can be used. Firstly, the underlying structural modal properties can be estimated in advance; then, using the final estimate of the underlying structure's natural frequency for the controlled mode, the effective damping can be estimated using the approach described in the previous section. Alternatively, since the natural frequency is known to converge relatively quickly, the filters can be run simultaneously, with the effective damping estimation filter using the updated estimate of the underlying structure's natural frequency. The latter approach is considered here.

The initialization of the noise covariance matrices for the filter was based on the results of the noise covariance estimation filter, demonstrated in Sec. 6.1.2. The parameter estimation filter proceeds exactly as described in Sec. 6.2. Simultaneously, a second filter is run using the same measurement data and fitting it to the SDOF system with effective damping ratio ζ_e. At each time step k, the modal parameters, namely the circular natural frequency $\omega_{n,j}$ and mode shape vector for the controlled mode ϕ_j, are updated within the system matrices. The only unknown parameter in the second model is the effective damping ratio. The noise covariances matrices, $\mathbf{S}_k$, $\mathbf{Q}_k$, and $\mathbf{R}_k$ are the same as the parameter filter. The transition equation for the effective damping estimation filter are modified

slightly to account for the inputs at all measured DOFs.

$$x_1[k+1] = x_1[k] + x_2[k]T + w_1[k] \tag{6.25a}$$

$$x_2[k+1] = -\omega_{n,j}^2 T x_1[k] + \left(1 - 2\omega_{n,j} x_3[k] T\right) x_2[k] + \frac{1}{M_{r,j}} \phi_j^T \mathbf{d}_k T + w_2[k] \tag{6.25b}$$

$$x_3[k+1] = x_3[k] + w_3[k] \tag{6.25c}$$

Since the responses at all measured DOFs are available, the measurement equation is the transformation of the controlled mode back into the physical coordinates using the mode shape vector, as follows:

$$\mathbf{z}_k = \phi_j \left(-\omega_{n,j}^2 x_1[k] - 2\omega_{n,j} x_3[k] x_2[k]\right) + \phi_j \frac{1}{M_{r,j}} \phi_j^T \mathbf{d}_k + \mathbf{v}_k \tag{6.26}$$

The tuned and detuned auxiliary system are both considered. The effective damping estimation filter is run alongside the 100 realizations of the filter presented in Sec. 6.2, using the estimated $\mathbf{S}_k$ and $\mathbf{R}_k$ from the noise covariance estimation step. The initial estimate of the effective damping is $\hat{\zeta}_{e,0} = 0.01$ in both instances; the initial state estimation error covariance corresponding to the appended parameter is 2.5% and 1% of the initial parameter estimate, for the tuned and detuned systems, respectively. The theoretical values (from Table 6.9) are compared with the initial estimate and the final converged estimates in Table 6.11. The averaged effective damping estimates for the tuned and detuned cases are plotted in Fig. 6.10.

Table 6.11: Comparison of effective damping ratio identification results between a tuned and detuned auxiliary system for 5-DOF system equipped with a PTMD for unknown external excitation and unknown noise statistics

	Tuned	Detuned
Actual	0.0333	0.0244
Initial	0.01	0.01
Error (%)	70.0	59.9
Estimate	0.0356	0.0276
Error (%)	6.78	13.3
$\hat{c}_v$ (%)	12.2	15.7

As expected, the detuned auxiliary system produces a lower effective damping for the combined main-auxiliary system. There is close identification of the effective modal damping, particularly for the tuned auxiliary system. The reduced performance over the SDOF example presented in the previous section is caused by the increased dimensionality of the model and a lack of availability of precise knowledge of the natural frequency of the controlled mode. Recall that this parameter is being simultaneously estimated.

Having demonstrated the application of the EKF for estimating effective damping, the EKF modal identification algorithm is subsequently verified based on lab-scale experiments of a simple structure with and adaptive PTMD mechanism. The method is also applied on full-scale measurement data from a PTMD-equipped structure with measured auxiliary parameters.

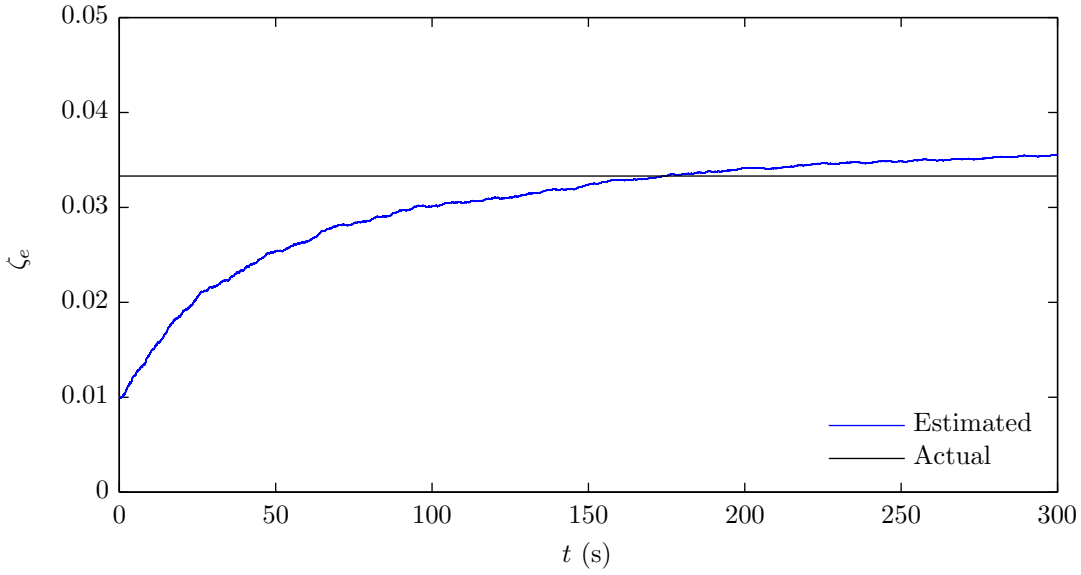

(a)

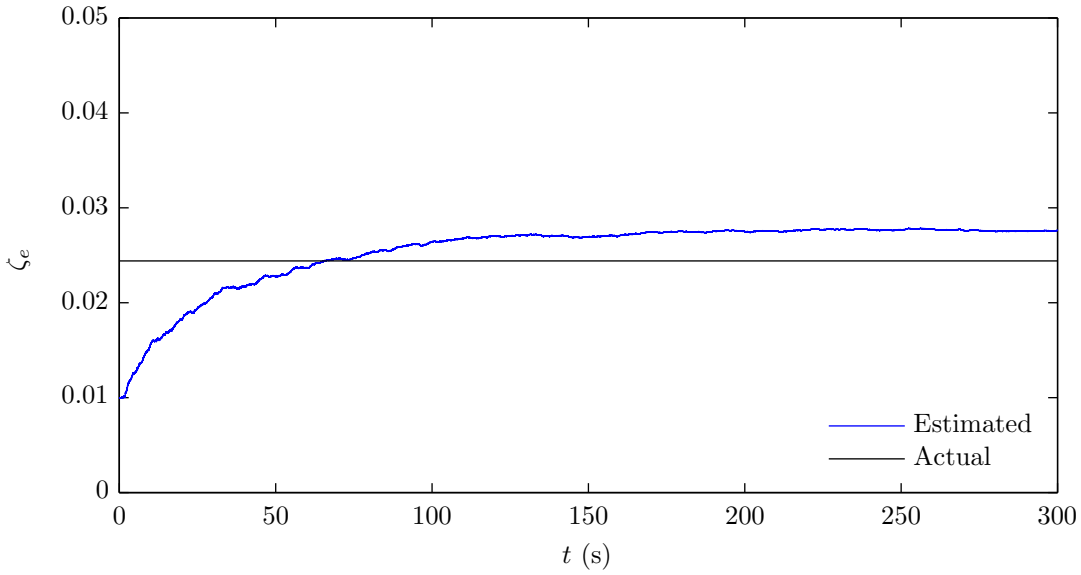

(b)

Figure 6.10: Effective damping estimate for a (a) tuned and (b) detuned PTMD-equipped 5DOF system by EKF identification for the case where the underlying structural modal properties are simultaneously estimated

Chapter 7

Experimental studies for condition assessment and key results

Having demonstrated that the combined state and noise covariance filter followed by the state and parameters estimation filter identifies the modal properties of the structure, attention is focused on demonstrating the effectiveness of the algorithm using experimentally generated data. A bench-scale laboratory model with a pendulum-type adaptive passive tuned mass damper (APTMD) is considered first, where an external broadband excitation is exerted on a two storey structure and the main structural acceleration and auxiliary horizontal displacement responses are measured. Second, the Apron Tower structure at Toronto Pearson International Airport, which is a structure equipped with a pendulum tuned mass damper (PTMD), is considered. A limited number of measurements are available, and only the first few modes of vibration are of interest; therefore, a reduced order model of the system is presented. In both instances, a precise measurement of the pendulum length is measured and assumed known throughout the filter operation. An equivalent linear damping coefficient is used to model the energy dissipation of the auxiliary system. Subsequently, an updated numerical model of the structure is used to predict the response using inputs generated from wind tunnel studies. Finally, the effective damping introduced by the PTMD is estimated using the method presented in Sec. 6.3.

7.1 EKF modal identification of a bench-scale laboratory model with PTMD

A bench-scale laboratory model is considered (Fig. 7.1), which consists of two rigid floor masses, each weighing 13.7 kg. Flexural stiffness is provided by four 12.7 mm (0.5 in) aluminum equal angles, 137.5 cm tall and 1.6 mm ($\frac{1}{16}$ in) thick. The columns are continuous from the base to the top of the structure; the connection at the base creates a near-fixed condition. A neoprene mat inserted between the base and the floor is used to dampen undesirable vibrations which may be transmitted to the structure. The inter-storey height is 68.5 cm. The structure is equipped with a pendulum-type APTMD, capable of both auxiliary frequency and damping adjustment. Frequency adjustment is accomplished by a tuning frame positioned by a stepper motor; damping adjustment is provided in each lateral direction using two air dampers with valve adjustment. The details of the adaptive mechanisms are documented elsewhere [78]. The auxiliary mass is $m_a = 1.47$ kg, and for the purpose of verifying the identification algorithm presented, the pendulum length and auxiliary damping are fixed at $L = 56.6$ mm ($k_a = 0$) and $c_a = 5.56$ N s/m, respectively. Note that the actual damping is frequency dependant [78], so a value corresponding to the estimated natural frequency of the main structure was assumed and fixed for the duration of the identification.

In order to establish an initial estimate of the modal properties, an uniaxial finite element model of the structure was constructed, assuming rigid diaphragm action at the floor masses. The lateral natural frequencies were estimated as 2.45 Hz and 6.44 Hz. The finite element model did not accommodate the considerable mass introduced by the APTMD apparatus, and is therefore considered to be a crude estimate of the actual natural frequencies.

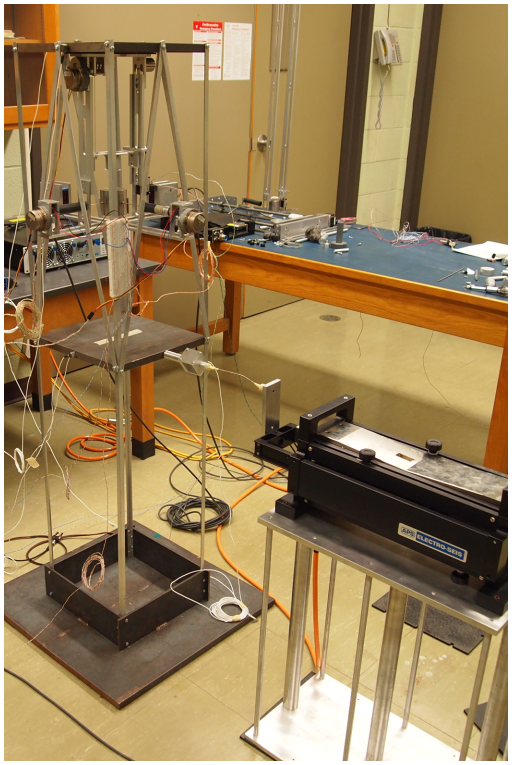

(a)

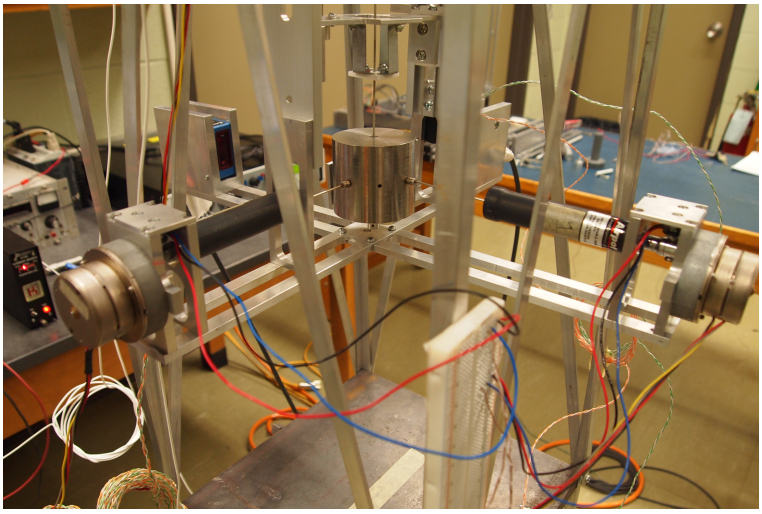

(b)

Figure 7.1: (a) Bench scale laboratory model for experimental verification (b) APTMD apparatus with pendulum mass, tuning frame, and adjustable dampers

The acceleration responses are measured at each floor using two low-frequency accelerometers. The horizontal projection of the auxiliary mass rotation (relative horizontal displacement) is measured using a displacement (laser) transducer. The measurement matrices in Table 6.1 are modified slightly to replace the auxiliary acceleration response measurement with a displacement response measurement. The system is excited by broadband main mass forcing using an APS 113-AB shaker, with a frequency range of 0 Hz to 200 Hz, at the lower floor location only. The shaker is connected to the floor mass with a stinger to limit the coupled dynamics between the shaker and structure. The response measurements were collected using a dSpace DS1104 R&D Controller Board with a sampling rate of 400 Hz. A total of 100 data sets were collected, each with a duration of 90 s.

7.1.1 Noise covariance estimation

The state and noise covariance estimation filter is initialized as follows. The system matrices are assumed known and are based on the output of the finite element model. The damping ratios for the first and second mode are assumed to be 1% and 3%, respectively. The initial unknown disturbance noise and measurement noise covariance are selected as $\hat{\mathbf{S}}_0 = \texttt{diag}\left[\begin{array}{cc} 0 & 0.15 \end{array}\right]$ and $\hat{\mathbf{R}}_0 = \texttt{diag}\left[\begin{array}{ccc} 1\times10^{-5} & 1\times10^{-5} & 1\times10^{-7} \end{array}\right]$, respectively. The noise covariances are assembled as in Eqs. 5.157 and 5.158. Since the structure is known to only be excited at the lower floor, a total of three measurement noise covariance parameters and one external feedthrough process noise parameter is sought. The mean estimates of the noise covariance estimation algorithm described in Eqs. 5.156 through 5.158 are summarized in Table 7.1, including the coefficient of variation (COV).

Despite low confidence in the final noise covariances estimates, particularly for the feedthrough process noise covariance, the combined state and parameter estimation is pursued next using the assembled identified noise covariance matrices as $\hat{\mathbf{S}} = \texttt{diag}\left[\begin{array}{cc} 0 & 13.27 \end{array}\right]$ and $\hat{\mathbf{R}} = \texttt{diag}\left[\begin{array}{ccc} 1.99\times10^{-3} & 11.0\times10^{-3} & 0.180\times10^{-6} \end{array}\right]$.

Table 7.1: Noise covariance parameter α_i estimates for $\mathbf{S}_k$ and $\mathbf{R}_k$ bench-scale laboratory model

Index	Estimate	
	$\hat{\alpha}_i$	$\hat{c}_v$
		%
$\mathbf{S}_k$		
1	36.76	614
$\mathbf{R}_k$		
2	203.5	120
3	1086	45.7
4	1.802	33.9

7.1.2 Combined state and parameter estimation

The combined state and parameter estimation was initialized as follows. The initial state estimates were set to zero, and the initial appended parameters (model properties to be estimated) were based on the finite element model, summarized in Table 7.2. The initial state estimation error covariance, $\mathbf{P}_0$, was approximately selected based on the measured variance of the state estimates in the state-noise covariance estimation filter; for the appended parameters, the initial state estimate error covariance was based on a 15% standard deviation of the initial estimates for the natural frequencies, 0.5% standard deviation for the damping ratios, and 2.5% standard deviation of the initial estimates for the mode shape coefficients. The unknown external disturbance noise covariance $\mathbf{S}_k$ and measurement noise covariance $\mathbf{R}_k$ are based on the output of the noise covariance estimation step. A small level or process noise covariance was introduced at the appended states, on the order of 0.01% of the initial estimate, to account for model uncertainty. The mean results of the parameter estimation are summarized in Table 7.2, together with their COVs ($\hat{c}_v$). These results are compared with identification results of the bare model (PTMD removed) using Blind Source Separation (BSS); the details of the aforementioned system identification approach are beyond the scope of the present work and the reader is referred elsewhere

[31, 81].

Table 7.2: Experimental investigation parameter estimate results

Mode	Natural frequencies			Modal damping ratios			Mode shapes		
	f_n	$\hat{f}_n$	$\hat{c}_v$	ζ_0	$\hat{\zeta}$	$\hat{c}_v$	ϕ_{2j}	$\hat{\phi}_{2j}$	$\hat{c}_v$
	Hz	Hz	%			%			%
1	1.73	1.68	6.75	0.022	0.020	68.5	0.60	0.62	3.22
2	4.78	4.77	1.11	0.056	0.054	3.95	-1.89	-1.76	-3.16

The results demonstrate good performance of the identification when compared with the results obtained by BSS. The first mode natural frequencies is slightly underestimated (2.9% error). Several possible sources of error in the experiment were identified. First, in addition to the rotation of the PTMD about the suspension point, a rocking motion about its own centroid was observed, which would not be modelled in a point-mass PTMD assumption. This cannot easily be accommodated by increasing the level measurement noise due the non-white nature of this additional vibration mode. Second, the auxiliary dashpot dampers were assumed to have a constant level of linear viscous damping, when in reality their damping is depending on the frequency of the damping force. Third, a small amount of rotation of the mass about the vertical contributed to the level of error in the auxiliary mass position measurement. The averaged parameter identification results as they vary with time are illustrated in Figs. 7.2 (natural frequency) and 7.3 (damping ratio).

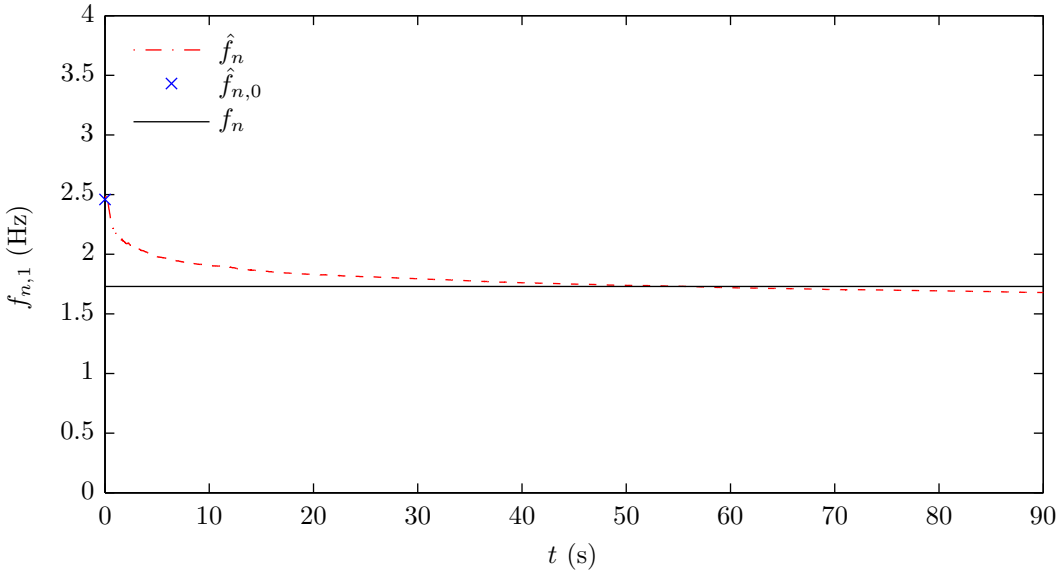

(a)

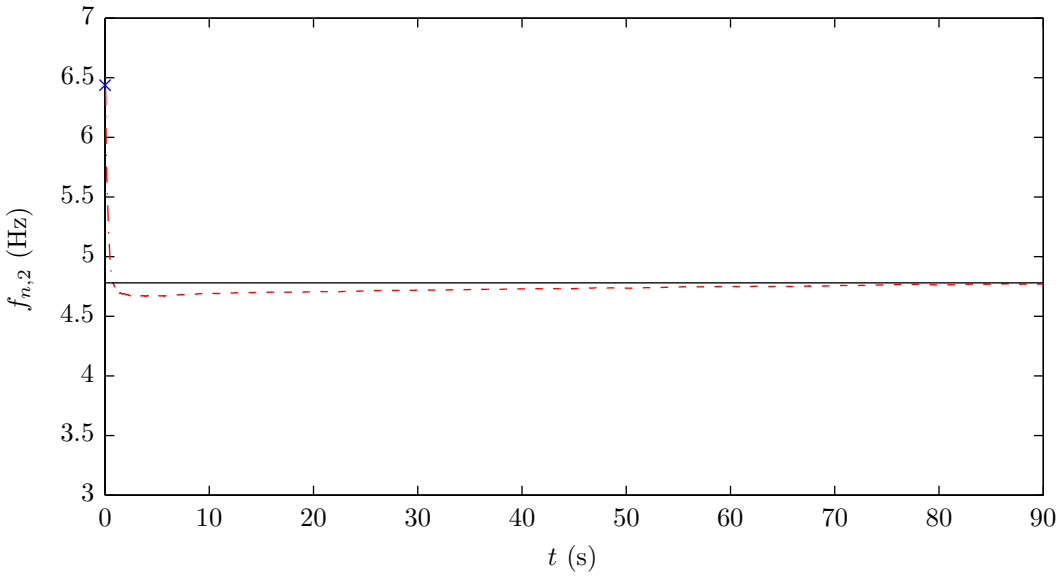

(b)

Figure 7.2: Natural frequency estimates from EKF estimation of the PTMD attenuated response data compared with results from BSS identification of the bare structure for the (a) first and (b) second modes

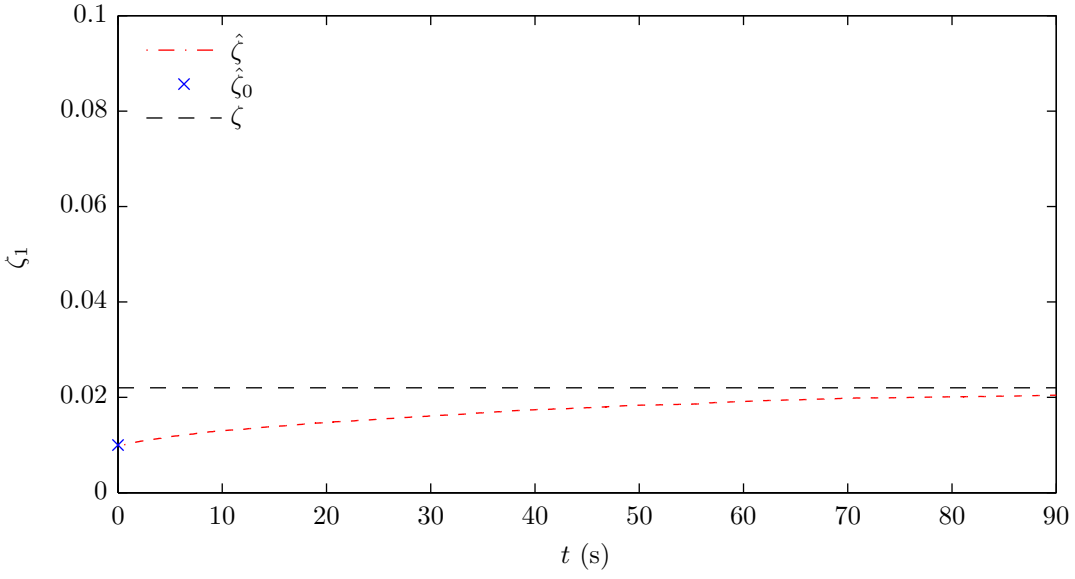

(a)

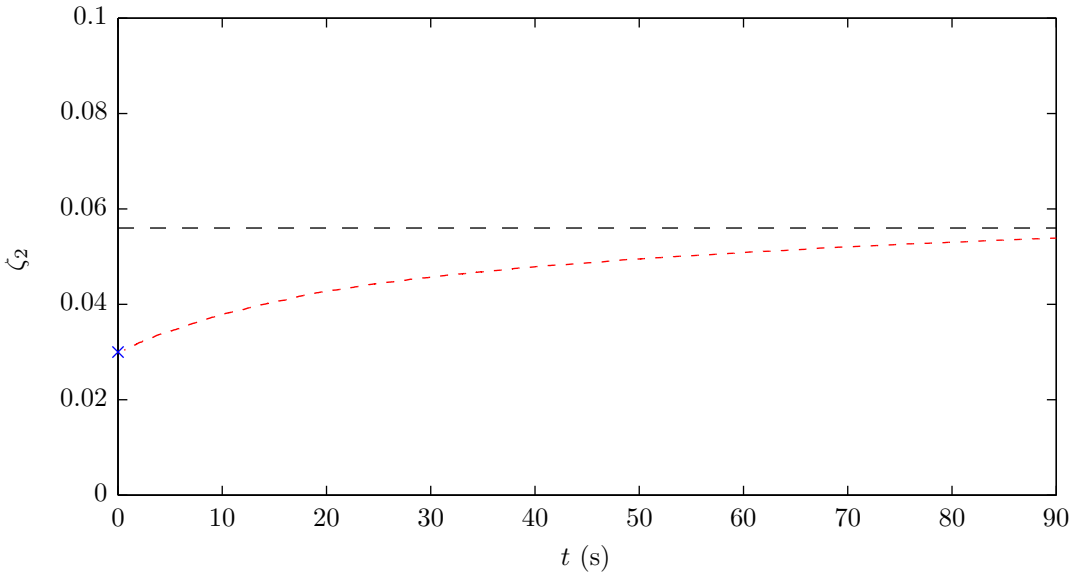

(b)

Figure 7.3: Modal damping ratio estimates from EKF estimation of the PTMD attenuated response data compared with results from BSS identification of the bare structure for the (a) first and (b) second modes

Despite the aforementioned sources of error in the experiment, the performance of the natural frequency damping ratio estimation is comparable to the results of the bare structure BSS identification. The initial estimate and mean final estimates of the mode shape vectors are plotted in Fig. 7.4. Note that the mode shapes are normalized with respect to the top floor.

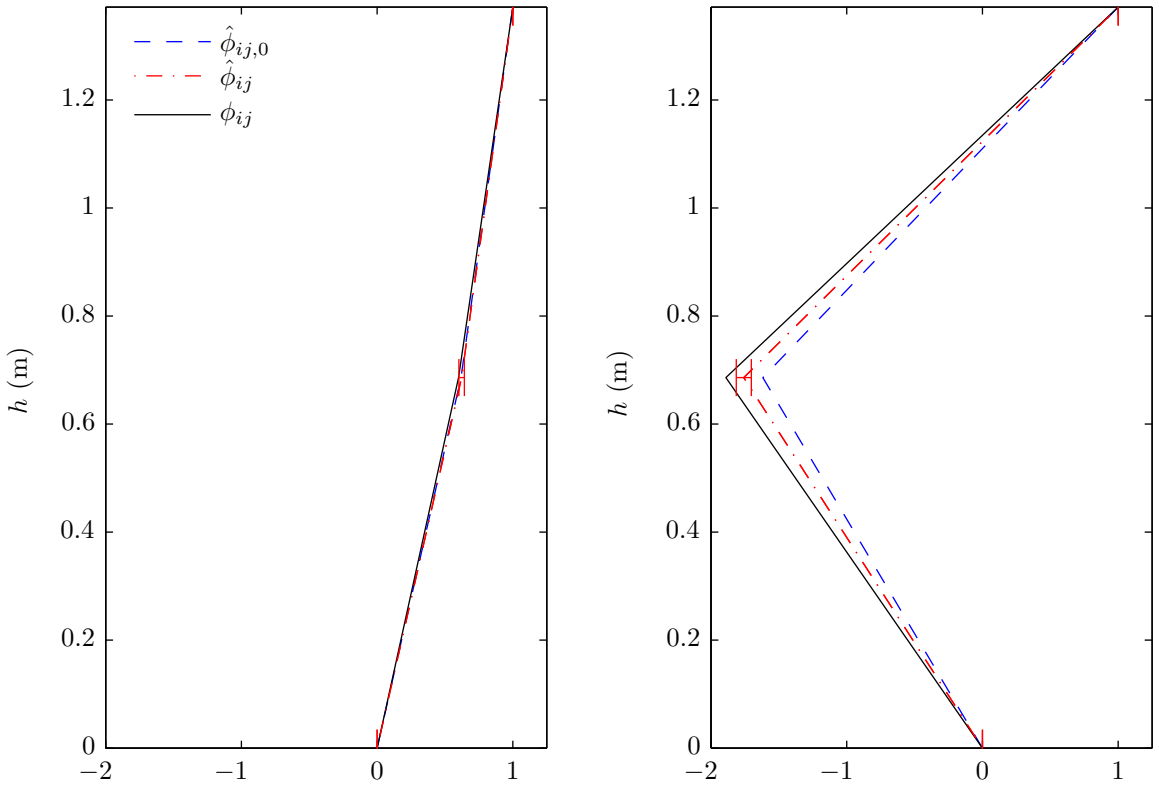

(a) 1st Mode

(b) 2nd Mode

Figure 7.4: Initial estimate and final estimate of the mode shape vectors from experimental verification

The mode shape vector estimation performed well, with fairly consistent convergence.

The final coefficients of variation for the first and second mode were $\hat{c}_{v,1} = 3.22\%$ and $\hat{c}_{v,2} = -3.16\%$, respectively.

7.2 Full-scale modal identification from attenuated response data

For most full-scale applications of the extended Kalman filter (EKF) modal identification algorithm presented in Chapters 5 and 6, it is not reasonable to assume that all measurements are available. Also, for structures with many degrees-of-freedom (DOFs), estimating all the modal characteristics is generally unnecessary and can become computationally expensive. Particularly for the application of identifying underlying modes for the purpose of retuning tuned mass dampers (TMDs), generally, the controlled mode of vibration is of interest. Therefore, the case where only a subset of the DOFs are measured and only a few modes of vibration are of interest is considered here.

If acceleration response measurements at all DOFs are available, then a reduced order model can be developed that truncates the modes no longer of interest but retains all DOFs, recognizing that most of the response is contributed by a few lower order modes. This has the effect of dramatically reducing the computational effort with no loss of input information. The more general case is subsequently considered, where a fewer number of measurements are available and a limited number of modes are considered in the response. Note there must be at least as many measurements as there are modes considered in the response.

7.2.1 Reduced-order model

There are two motivations in the proposed research for implementing dynamic model reduction methods.

- A considerable amount of computation time is required to perform the state and noise covariance estimation filter followed by the combined state and parameter estimation

filter when all DOFs and modes are retained, particularly for large systems. Since it is well known that only a few of the lower order modes contribute to the majority of the response, reducing the number of modes results in substantially fewer states and parameters that need to be estimated.

- It is difficult and costly to simultaneously measure every location on a structure; therefore, only a small number of DOFs are actually measured. It is desirable to reduce the number of DOFs of the analytical model so that valid comparisons between analytical and actual values can be made.

Several model reduction techniques exist, including Guyan or static reduction, dynamic reduction [12], Improved Reduction System (IRS) [23], Iterated IRS [24], and the System Equivalent Reduction Expansion Process (SEREP) [71]. The latter is explored more closely for the present study, as it retains the dynamic characteristics of the system for the modes of interest and does not require repeated iterations before convergence to the reduced order system matrices.

Consider the equations of motion for the uniaxial multi-degree-of-freedom (MDOF) system equipped with a planar PTMD, by substituting

$$L\ddot{\theta}(t) + \ddot{u}_1(t) = -\frac{m_a g L + k_a h^2}{m_a L}\theta(t) - \frac{c_a h^2}{m_a L}\dot{\theta}(t) \tag{7.1}$$

into Eq. 6.2.

$$\mathbf{M}\ddot{\mathbf{u}}(t) + \mathbf{C}\dot{\mathbf{u}}(t) + \mathbf{K}u(t) = \mathbf{P}(t) + \mathbf{\Gamma}\left[\frac{m_a g L + k_a h^2}{L}\theta(t) + \frac{c_a h^2}{L}\dot{\theta}(t)\right] \tag{7.2}$$

Partition the coordinate vector into retained and truncated DOFs

$$\mathbf{u}(t) = \left\{ \begin{array}{c} \mathbf{u}_r(t) \\ \mathbf{u}_t(t) \end{array} \right\} \tag{7.3}$$

where $\mathbf{u}_r(t)$ are the retained displacement responses (with corresponding velocities, $\dot{\mathbf{u}}_r(t)$, and accelerations, $\ddot{\mathbf{u}}_r(t)$) and $\mathbf{u}_t(t)$ are the truncated displacement responses (with corre-

sponding velocities, $\dot{\mathbf{u}}_t(t)$, and accelerations, $\ddot{\mathbf{u}}_t(t)$). The auxiliary system must be located at a retained DOF. Eq. 7.1 can be rewritten using partitioned mass, damping, and stiffness matrices and assuming that no external force is applied to the truncated DOFs.

$$\begin{aligned}&\begin{bmatrix} \mathbf{M}_{rr} & \mathbf{M}_{rt} \\ \mathbf{M}_{tr} & \mathbf{M}_{tt} \end{bmatrix} \begin{Bmatrix} \ddot{\mathbf{u}}_r(t) \\ \ddot{\mathbf{u}}_t(t) \end{Bmatrix} + \begin{bmatrix} \mathbf{C}_{rr} & \mathbf{C}_{rt} \\ \mathbf{C}_{tr} & \mathbf{C}_{tt} \end{bmatrix} \begin{Bmatrix} \dot{\mathbf{u}}_r(t) \\ \dot{\mathbf{u}}_t(t) \end{Bmatrix} + \begin{bmatrix} \mathbf{K}_{rr} & \mathbf{K}_{rt} \\ \mathbf{K}_{tr} & \mathbf{K}_{tt} \end{bmatrix} \begin{Bmatrix} \mathbf{u}_r(t) \\ \mathbf{u}_t(t) \end{Bmatrix} \\ &\quad = \begin{Bmatrix} \mathbf{P}_r(t) \\ \mathbf{0} \end{Bmatrix} + \mathbf{\Gamma} \left[\frac{m_a g L + k_a h^2}{L} \theta(t) + \frac{c_a h^2}{L} \dot{\theta}(t) \right]\end{aligned} \tag{7.4}$$

Using the modal matrix, which is now described in terms of retained and truncated modal responses, $\mathbf{y}_r(t)$ and $\mathbf{y}_t(t)$, respectively,

$$\mathbf{u}(t) = \mathbf{\Phi}\mathbf{y}(t) = \begin{Bmatrix} \mathbf{u}_r(t) \\ \mathbf{u}_t(t) \end{Bmatrix} = \begin{bmatrix} \mathbf{\Phi}_{rr} & \mathbf{\Phi}_{rt} \\ \mathbf{\Phi}_{tr} & \mathbf{\Phi}_{tt} \end{bmatrix} \begin{Bmatrix} \mathbf{y}_r(t) \\ \mathbf{y}_t(t) \end{Bmatrix} \tag{7.5}$$

and premultiplying by $\mathbf{\Phi}^T$ gives

$$\begin{aligned}&\begin{bmatrix} \mathbf{M}_{r,r} & \mathbf{0} \\ \mathbf{0} & \mathbf{M}_{r,t} \end{bmatrix} \begin{Bmatrix} \ddot{\mathbf{y}}_r(t) \\ \ddot{\mathbf{y}}_t(t) \end{Bmatrix} + \begin{bmatrix} \mathbf{M}_{r,r} & \mathbf{0} \\ \mathbf{0} & \mathbf{M}_{r,t} \end{bmatrix} \begin{bmatrix} \hat{\mathbf{C}}_{r,r} & \mathbf{0} \\ \mathbf{0} & \hat{\mathbf{C}}_{r,t} \end{bmatrix} \begin{Bmatrix} \dot{\mathbf{y}}_r(t) \\ \dot{\mathbf{y}}_t(t) \end{Bmatrix} \\ &\quad + \begin{bmatrix} \mathbf{M}_{r,r} & \mathbf{0} \\ \mathbf{0} & \mathbf{M}_{r,t} \end{bmatrix} \begin{bmatrix} \mathbf{\Lambda}_{r,r} & \mathbf{0} \\ \mathbf{0} & \mathbf{\Lambda}_{r,t} \end{bmatrix} \begin{Bmatrix} \mathbf{y}_r(t) \\ \mathbf{y}_t(t) \end{Bmatrix} \\ &\quad \begin{bmatrix} \mathbf{\Phi}_{rr} & \mathbf{\Phi}_{rt} \\ \mathbf{\Phi}_{tr} & \mathbf{\Phi}_{tt} \end{bmatrix}^T \begin{Bmatrix} \mathbf{P}_r(t) \\ \mathbf{0} \end{Bmatrix} + \begin{bmatrix} \mathbf{\Phi}_{rr} & \mathbf{\Phi}_{rt} \\ \mathbf{\Phi}_{tr} & \mathbf{\Phi}_{tt} \end{bmatrix} \mathbf{\Gamma} \left[\frac{m_a g L + k_a h^2}{L} \theta(t) + \frac{c_a h^2}{L} \dot{\theta}(t) \right]\end{aligned} \tag{7.6}$$

where $\mathbf{M}_r$, $\hat{\mathbf{C}}$, and $\mathbf{\Lambda}$ are the modal mass matrix, classical modal damping matrix, and spectral matrix, respectively. The subscripts r and t of $\mathbf{\Phi}_{rr}$, $\mathbf{\Phi}_{rt}$, $\mathbf{\Phi}_{tr}$, and $\mathbf{\Phi}_{tt}$ correspond to the retained and truncated DOFs and modes, respectively. Truncate the modal vector

by assuming $\mathbf{y}_t(t) = \mathbf{0}$. Eq. 7.6 becomes

$$\begin{aligned}
&\mathbf{M}_{r,r}\ddot{\mathbf{y}}_r(t) + \mathbf{M}_{r,r}\hat{\mathbf{C}}_r\dot{\mathbf{y}}_r(t) + \mathbf{M}_{r,r}\mathbf{\Lambda}_r\mathbf{y}_r(t) \\
&\quad = \left\{ \begin{array}{c} \mathbf{\Phi}_{rr} \\ \mathbf{\Phi}_{rt} \end{array} \right\}^T \left\{ \begin{array}{c} \mathbf{P}_r(t) \\ \mathbf{0} \end{array} \right\} + \left\{ \begin{array}{c} \mathbf{\Phi}_{rr} \\ \mathbf{\Phi}_{rt} \end{array} \right\}^T \mathbf{\Gamma} \left[\frac{m_a g L + k_a h^2}{L}\theta(t) + \frac{c_a h^2}{L}\dot{\theta}(t) \right]
\end{aligned} \tag{7.7}$$

From Eq. 7.5, $\mathbf{u}_r(t) = \mathbf{\Phi}_{rr}\mathbf{y}_r(t)$; therefore, $\mathbf{y}_r(t) = \mathbf{\Phi}_{rr}^{+}\mathbf{u}_r(t)$ where $\mathbf{\Phi}_{rr}^{+}$ is the pseudoinverse of $\mathbf{\Phi}_{rr}$ given by

$$\mathbf{\Phi}_{rr}^{+} = \left(\mathbf{\Phi}_{rr}^T\mathbf{\Phi}_{rr}\right)^{-1}\mathbf{\Phi}_{rr}^T \tag{7.8}$$

Transforming from modal coordinates using $\mathbf{y}_r(t) = \mathbf{\Phi}_{rr}^{+}\mathbf{u}_r(t)$ and premultiplying Eq. 7.6 by $\mathbf{\Phi}_{rr}^{+T}$ gives

$$\begin{aligned}
&\mathbf{\Phi}_{rr}^{+T}\left\{ \begin{array}{c} \mathbf{\Phi}_{rr} \\ \mathbf{\Phi}_{tr} \end{array} \right\}^T \mathbf{M} \left\{ \begin{array}{c} \mathbf{\Phi}_{rr} \\ \mathbf{\Phi}_{tr} \end{array} \right\} \mathbf{\Phi}_{rr}^{+}\ddot{\mathbf{u}}_r(t) + \mathbf{\Phi}_{rr}^{+T}\left\{ \begin{array}{c} \mathbf{\Phi}_{rr} \\ \mathbf{\Phi}_{tr} \end{array} \right\}^T \mathbf{C} \left\{ \begin{array}{c} \mathbf{\Phi}_{rr} \\ \mathbf{\Phi}_{tr} \end{array} \right\} \mathbf{\Phi}_{rr}^{+}\dot{\mathbf{u}}_r(t) \\
&\quad + \mathbf{\Phi}_{rr}^{+T}\left\{ \begin{array}{c} \mathbf{\Phi}_{rr} \\ \mathbf{\Phi}_{tr} \end{array} \right\}^T \mathbf{K} \left\{ \begin{array}{c} \mathbf{\Phi}_{rr} \\ \mathbf{\Phi}_{tr} \end{array} \right\} \mathbf{\Phi}_{rr}^{+}\mathbf{u}_r(t) = \mathbf{\Phi}_{rr}^{+T}\left\{ \begin{array}{c} \mathbf{\Phi}_{rr} \\ \mathbf{\Phi}_{tr} \end{array} \right\}^T \left\{ \begin{array}{c} \mathbf{P}_r(t) \\ \mathbf{0} \end{array} \right\} \\
&\quad + \mathbf{\Phi}_{rr}^{+T}\left\{ \begin{array}{c} \mathbf{\Phi}_{rr} \\ \mathbf{\Phi}_{tr} \end{array} \right\}^T \mathbf{\Gamma} \left[\frac{m_a g L + k_a h^2}{L}\theta(t) + \frac{c_a h^2}{L}\dot{\theta}(t) \right]
\end{aligned} \tag{7.9}$$

Defining the following transformation

$$\mathbf{T} = \left\{ \begin{array}{c} \mathbf{\Phi}_{rr} \\ \mathbf{\Phi}_{tr} \end{array} \right\} \mathbf{\Phi}_{rr}^{+} \tag{7.10}$$

Eq. 7.9 can be rewritten in physical coordinates as

$$\tilde{\mathbf{M}}\ddot{\mathbf{u}}_r(t) + \tilde{\mathbf{C}}\dot{\mathbf{u}}_r(t) + \tilde{\mathbf{K}}\mathbf{u}_r(t) = \mathbf{T}^T \left\{ \begin{array}{c} \mathbf{P}_r(t) \\ \mathbf{0} \end{array} \right\} + \mathbf{T}^T\mathbf{\Gamma} \left[\frac{m_a g L + k_a h^2}{L}\theta(t) + \frac{c_a h^2}{L}\dot{\theta}(t) \right] \tag{7.11}$$

where

$$\tilde{\mathbf{M}} = \mathbf{T}^T\mathbf{M}\mathbf{T} \tag{7.12a}$$

$$\tilde{\mathbf{C}} = \mathbf{T}^T\mathbf{C}\mathbf{T} \tag{7.12b}$$

$$\tilde{\mathbf{K}} = \mathbf{T}^T\mathbf{K}\mathbf{T} \tag{7.12c}$$

are the non-diagonal reduced order mass, damping, and stiffness matrices in the physical coordinates. Using the modal transformation $\mathbf{u}_r(t) = \mathbf{\Phi}_{rr}\mathbf{y}_r(t)$ and premultiplying by $\mathbf{\Phi}_{rr}^T$, Eq. 7.11 can be transformed back into modal coordinates, producing the same modal masses, damping ratios, and natural frequencies as the full structure, but only for the modes of interest. Since a single transformation matrix is used, the operation is reversible and can also form the basis for modal expansion. Friswell showed that the transformation matrix found using the Iterated IRS method will converge to the transformation matrix found using SEREP [24].

For the identification algorithm, the reduced order natural frequencies, damping ratios, and mode shapes are appended to the state vector and estimated. Specifically, the mode shape coefficients corresponding to the modes of interest and the measured or retained DOFs are identified. However, the transformation between the full order model to the reduced order model requires knowledge of the mode shape coefficients corresponding to the truncated DOF as well as the full mass matrix in order to produce the same modal masses as the full order model. As before, the mass matrix from the finite element model is assumed to be exact and used to calculate the modal mass for the purpose of parameter estimation. In addition to this, the mode shape coefficients at the truncated DOFs for the retained modes, $\mathbf{\Phi}_{tr}$, from the initial estimate model are used throughout the operation of the filter in order to determine the modal mass, $\mathbf{M}_r$. The mode shape coefficients corresponding to the retained modes and DOFs are appended to the state vector and estimated, subsequently used at each time step of the filter to revise the modal mass

estimate. The modal mass is found by

$$\begin{aligned}\mathbf{M}_{r,r} &= \boldsymbol{\Phi}_{rr}^T \mathbf{T}^T \mathbf{M} \mathbf{T} \boldsymbol{\Phi}_{rr} \\ &= \boldsymbol{\Phi}_{rr}^T \boldsymbol{\Phi}_{rr} \left(\boldsymbol{\Phi}_{rr}^T \boldsymbol{\Phi}_{rr}\right)^{-1} \left\{ \begin{array}{c} \boldsymbol{\Phi}_{rr} \\ \boldsymbol{\Phi}_{tr} \end{array} \right\}^T \mathbf{M} \left\{ \begin{array}{c} \boldsymbol{\Phi}_{rr} \\ \boldsymbol{\Phi}_{tr} \end{array} \right\} \left(\boldsymbol{\Phi}_{rr}^T \boldsymbol{\Phi}_{rr}\right)^{-1} \boldsymbol{\Phi}_{rr}^T \boldsymbol{\Phi}_{rr} \\ &= \left\{ \begin{array}{c} \boldsymbol{\Phi}_{rr} \\ \boldsymbol{\Phi}_{tr} \end{array} \right\}^T \mathbf{M} \left\{ \begin{array}{c} \boldsymbol{\Phi}_{rr} \\ \boldsymbol{\Phi}_{tr} \end{array} \right\}\end{aligned} \tag{7.13}$$

It is apparent from Eq. 7.13 that the mode shape vectors $\boldsymbol{\Phi}_{tr}$ are required to determine the modal mass matrix for the reduced order model. The equations of motion are transformed into the modal domain, where $\hat{n}$ modes of vibration are retained, and $\bar{n}$ DOFs are measured. The total number of states in the reduced order model system are $\tilde{n} = 2\hat{n} + 2$ and the number of outputs is $p = \bar{n} + 1$. The continuous time system matrices are given in Table 7.3. Note that

$$\boldsymbol{\Phi}_{rr} \mathbf{T}^T \left\{ \begin{array}{c} \mathbf{P}_r(t) \\ \mathbf{0} \end{array} \right\} = \boldsymbol{\Phi}_{rr}^T \mathbf{P}_r(t) \tag{7.14}$$

and

$$\boldsymbol{\Phi}_{rr} \mathbf{T}^T \boldsymbol{\Gamma} = \boldsymbol{\Phi}_{rr} \boldsymbol{\Gamma}_r \tag{7.15}$$

where $\boldsymbol{\Gamma}_r$ is an influence vector that assigns the control force from the PTMD to the DOF where the the damper is located, but only contains the locations for the retained DOFs.

7.2.2 Full-scale application of EKF modal identification

To validate the algorithm presented for the identification of the underlying structure's modal properties from TMD attenuated response data, the Apron Control Tower at Greater Toronto Airports Authority (GTAA) Toronto Pearson International Airport in Mississauga, Ontario, is considered as the testbed. The tower, shown in Fig. 7.5, is a 49 m tall structure rising above the fourth level of Terminal 1. The total height of the structure above grade is 68.5 m.

Table 7.3: Continuous time state matrices for the reduced order uniaxial MDOF system with planar PTMD

$$\mathbf{A}_c = \begin{bmatrix} \mathbf{0} & & \\ -\mathbf{\Lambda}_r & \mathbf{M}_{r,r}^{-1}\mathbf{\Phi}_{rr}^T\mathbf{\Gamma}_r\dfrac{m_agL+k_ah^2}{L} & \\ \frac{1}{L}\mathbf{\Gamma}_r^T\mathbf{\Phi}_{rr}\mathbf{\Lambda}_r & -\left(1+m_a\mathbf{\Gamma}_r^T\mathbf{\Phi}_{rr}\mathbf{M}_{r,r}^{-1}\mathbf{\Phi}_{rr}^T\mathbf{\Gamma}_r\right)\dfrac{m_agL+k_ah^2}{m_aL^2} & \\ & \mathbf{I} & \\ -\hat{\mathbf{C}}_r & \mathbf{M}_{r,r}^{-1}\mathbf{\Phi}_{rr}^T\mathbf{\Gamma}_r\dfrac{c_ah^2}{L} & \\ \dfrac{1}{L}\mathbf{\Gamma}_r^T\mathbf{\Phi}_{rr}\hat{\mathbf{C}}_r & -\left(1+m_a\mathbf{\Gamma}_r^T\mathbf{\Phi}_{rr}\mathbf{M}_{r,r}^{-1}\mathbf{\Phi}_{rr}^T\mathbf{\Gamma}_r\right)\dfrac{c_ah^2}{m_aL^2} & \end{bmatrix}$$

$$\mathbf{E}_c = \begin{bmatrix} \mathbf{0} \\ \mathbf{M}_{r,r}^{-1}\mathbf{\Phi}_{rr}^T \\ -\frac{1}{L}\mathbf{\Gamma}_r^T\mathbf{\Phi}_{rr}\mathbf{M}_{r,r}^{-1}\mathbf{\Phi}_{rr}^T \end{bmatrix}$$

$$\mathbf{C}_c = \begin{bmatrix} -\mathbf{\Phi}_{rr}\mathbf{\Lambda}_r & \mathbf{\Phi}_{rr}\mathbf{M}_{r,r}^{-1}\mathbf{\Phi}_{rr}^T\mathbf{\Gamma}_r\dfrac{m_agL+k_ah^2}{L} & -\mathbf{\Phi}_{rr}\hat{\mathbf{C}}_r & \mathbf{\Phi}_{rr}\mathbf{M}_{r,r}^{-1}\mathbf{\Phi}_{rr}^T\mathbf{\Gamma}_r\dfrac{c_ah^2}{L} \\ \mathbf{0} & -\dfrac{1}{m_a}\dfrac{m_agL+k_ah^2}{L} & \mathbf{0} & -\dfrac{1}{m_a}\dfrac{c_ah^2}{L} \end{bmatrix}$$

$$\mathbf{F}_c = \begin{bmatrix} \mathbf{\Phi}_{rr}\mathbf{M}_{r,r}^{-1}\mathbf{\Phi}_{rr}^T \\ \mathbf{0} \end{bmatrix}$$

Figure 7.5: Toronto Pearson International Airport Terminal 1 Apron Tower

The tower is a steel structure with composite steel deck and concrete floors providing a rigid diaphragm at each level. The tower has 10 core levels, consisting mainly of a scissor stairwell, elevator and service shafts. Above the core levels are five service levels, used for apron control operators, mechanical, electrical and communications services, and administrative office space. The structure is supported by six main steel columns resting on large transfer girders at the terminal roof level. Lateral loads are resisted by a combination of braced and moment frames.

7.2.3 Description of the pendulum tuned mass dampers

Due to the structure's inherent flexibility and susceptibility to wind loads, and in order to reduce the user discomfort during high wind events, the structure is equipped with two passive PTMDs located within the truss roof structure. Each mass is 25, 000 kg, comprised

of 24 50 mm thick stacked steel plates, for a total auxiliary mass of 50 tonnes. The auxiliary mass represents a mass ratio of $\mu = 12.4\%$. The arrangement of the PTMDs are shown in Fig. 7.6.

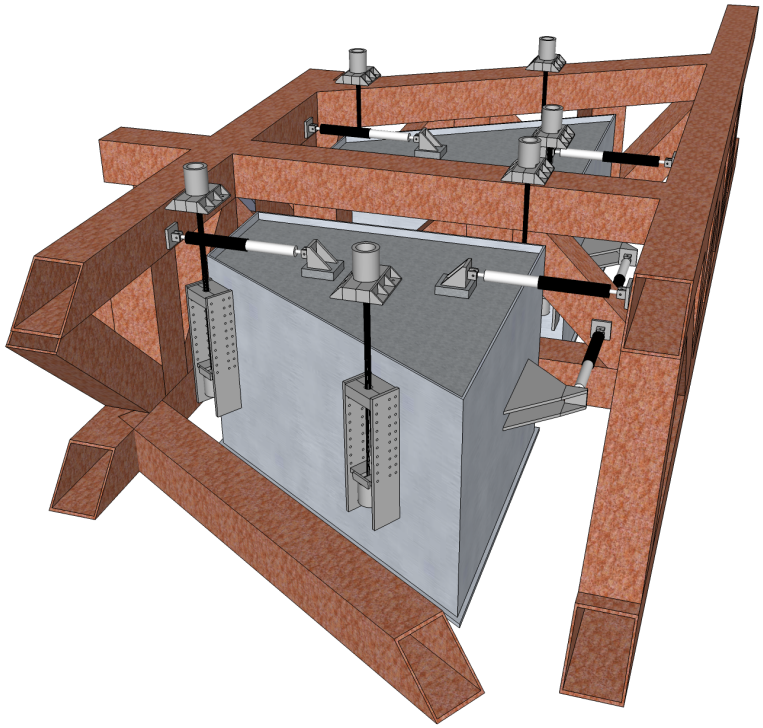

Figure 7.6: Isometric view of pendulum tuned mass damper installed in the roof structure of GTAA Toronto Pearson International Airport Apron Tower

Each mass is supported by three cables suspended from the structural steel above (not shown in Fig. 7.6). The cables are connected to the bottom of an adjustable tuning frame housing affixed to the outside of the mass blocks. Along the side of the tuning frame housing are a series of holes which will accept an adjustable tuning plate. The tuning plate does not support the gravity load of the mass; instead, it simply changes the location along the length of the cables that the mass pivots, effectively adjusting the pendulum length and the tuning frequency of the auxiliary damping device. The adjustable tuning frame housing based has a maximum tuning frequency of 0.659 Hz and a minimum tuning

frequency of 0.491 Hz.

It is generally difficult to predict the actual frequencies of the primary structure to the degree of accuracy necessary to tune a TMD. Therefore, the aforementioned adjustment frame is necessary to allow for fine frequency adjustment during the commissioning of the PTMDs after the primary structure's frequencies have been identified. Also, it facilitates simple retuning of the structure during maintenance when it is determined that the primary structural frequencies have changed. Since the cables are perfectly vertical, a rocking response of the PTMD is not present, and the mass behaves as a simple point mass, where the frequency length is measured from the suspension point to the location of the pivot block within the adjustable tuning frame housing. The measured pendulum length was $L = 0.572$ m; this measure is fixed for the duration of the filters.

Each mass is also equipped with four (two in each horizontal direction) double-acting fluid viscous dampers with a peak damping force of 31.1 kN (7000 lbf) and a maximum stroke of 178 mm (7 in). The damping force is velocity-squared proportional. The viscous dampers are the primary energy dissipation devices in the auxiliary damping system, converting mechanical energy into heat. For each viscous damper in the Apron Tower, $c_\alpha = 895 \times 10^3$ N s^2 m^{-2} (129.81 lbf s^2 in^{-2}) and $\dot{x}_0 = 0.1865$ m/s (7.343 in/s). For $\alpha = 2$, the equivalent linear viscous damping coefficient for each damper on the auxiliary damping device is $c_{eq} = 111.3 \times 10^3$ N m/s according to the equivalent linear viscous damping Eq. 3.47 in Sec. 3.5.2. This level of damping is fixed for the duration of the filters.

7.2.4 Instrumentation

From August to December, 2009, an extensive measurement program was conducted at the GTAA Toronto Pearson International Airport Apron Tower, where the structure was instrumented with 12 seismic accelerometers along the height. Structural vibration measurements were obtained under wind loading and ambient excitations, including several significant wind events during which high-fidelity measurements were obtained containing energies in several dominant modes.

The structure was instrumented using PCB Piezotronics high sensitivity seismic ceramic flexural ICP accelerometers. The accelerometers have a frequency range 0.07 to 300 Hz, sensitivity of 10.0 V/g, a measurement range of 0.5g (4.9 m/s^2), and a resolution of 1 μ-g (g = 9.807m/s^2) root mean squared (RMS). These sensors are ideal for low-level, low-frequency vibrations typical in building vibration monitoring and provide strong output signals with lower noise due to their size. The sensor's signal output was continuously recorded at a sampling rate of 200 Hz. Data was collected using a 12 channel data acquisition system with a 16-bit resolution.

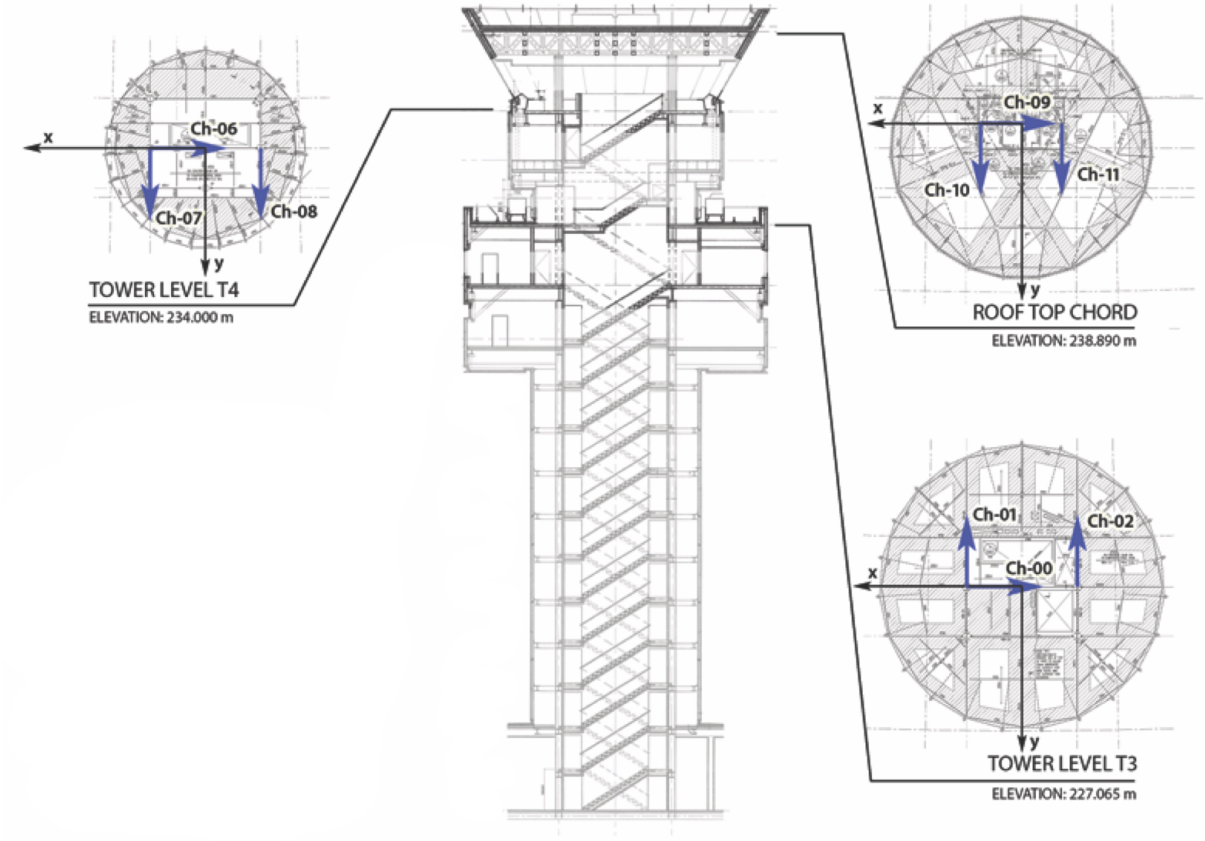

Figure 7.7: Location of siesmic accelerometers on the Toronto Pearson Internation Airport Apron Tower

A total of 9 sensors were installed horizontally on the third and first uppermost floors of the Apron Tower as well as in the top chord of the roof truss structure (Fig. 7.7). Two sensors were installed in the north-south (y-) direction on each floor. A third sensor was installed in the east-west (x-) direction. Data collected in the east-west direction on the third uppermost floor was corrupted and was not used in the subsequent analysis. Two sensors were installed measuring the lateral acceleration responses of one of the PTMD masses. Approximately 3 hours and 20 minutes of data was collected in this configuration on December 11, 2009 beginning at 12:24 pm.

The responses for three DOFs were considered at each level. In the east-west direction (x-DOF), one sensor was sufficient to provide this information at it was installed along the selected reference line corresponding to the centre of mass in north-south direction. In order to capture both the north-south direction (y-DOF) and torsion (θ-DOF), two sensors were mounted on each floor along the selected reference line away from the centre of mass in the east-west direction. The y-DOF signal was found by averaging the response of the two sensors.

$$\ddot{y}(t) = \frac{\ddot{y}_E(t) + \ddot{y}_W(t)}{2} \tag{7.16}$$

$\ddot{y}_E(t)$ and $\ddot{y}_W(t)$ are the acceleration response signals measured in the y-direction (north-south) on the east and west side of the structure, respectively. The θ-DOF signal was calculated by finding the difference between the signals and dividing it by the perpendicular distance between the mounting locations.

$$\ddot{\theta} = \frac{\ddot{y}_E(t) + \ddot{y}_W(t)}{r_E^x - r_W^x} \tag{7.17}$$

r_E^x and r_W^x are the perpendicular distances to the centre of mass (coordinate locations) of the structure from the sensors located on the east and west side of the structure, respectively. In several instances physical constraints at the sensor locations necessitated installing the accelerometers backwards; the signals are simply transformed by multiplying them by -1.

The data was collected during a significant wind event while the auxiliary damping

system was online. The results of the subsequent analysis are compared with the identification results on data collected during a similar wind event where the motion of the PTMD was restrained. The response of the structure while the PTMD motion is restrained is of particular interest, as the structural modes of the main system are more readily available without the effect of the auxiliary system. That study used a non-parametric modal identification method known as the modified cross-correlation method; however, the findings of that study are beyond the scope of the present work and are simply used here for comparison [32, 31].

7.2.5 Finite element model

In order to establish an initial estimate for the model parameters to initialize the EKF modal identification filter, a finite element model was developed using using a commercially available finite element software package, SAP2000 [14] (Fig. 7.8), excluding the auxiliary damping system. A portion of the supporting terminal substructure was modelled to limit the effects of the selection of boundary conditions, though this remained a source of uncertainty for the model. Transfer girders are used to transfer the loads from the tower into the lower terminal structure. The liner roof was modelled and the joints translations and rotations were restrained (fixed support condition). The geometry, materials, and sections were determined using as-recorded drawings. The model contains 1208 joints, 2387 frame elements, and 2387 stiffness DOFs. A rigid diaphragm assumption was made for the floor levels, and the x-, y- and θ-DOF were retained at each level. The result was a 42-DOF finite element representation of the structure. A modal analysis was performed in order to find the frequencies and mode shapes of the structure.

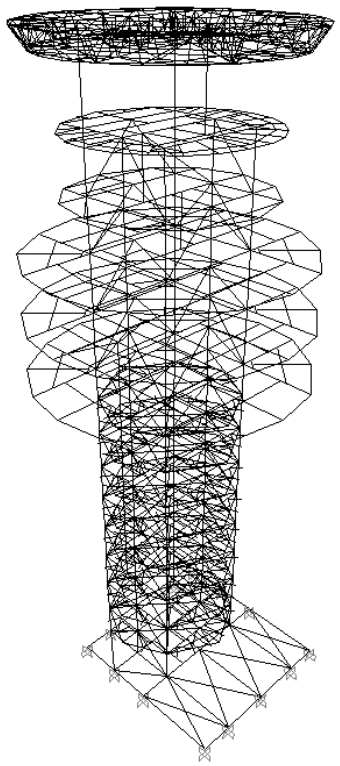

Figure 7.8: GTAA Toronto Pearson International Airport Apron Tower finite element model created in SAP2000

The results from the modal analysis are plotted in Fig. 7.9 for the first three modes of vibration. The first three natural frequencies are 0.656 Hz, 0.919 Hz, and 1.40 Hz, and correspond to a y-direction lateral mode, x-direction lateral mode, and torsional mode, respectively. For filter implementation, each direction is considered independently. For the rotation of the floor masses (θ_z-DOF), it is assumed that there is no coupling between the auxiliary mass and the main structure in order to simplify the EKF modal identification, despite the expectation that the PTMDs will also attenuate the torsional response of the structure.

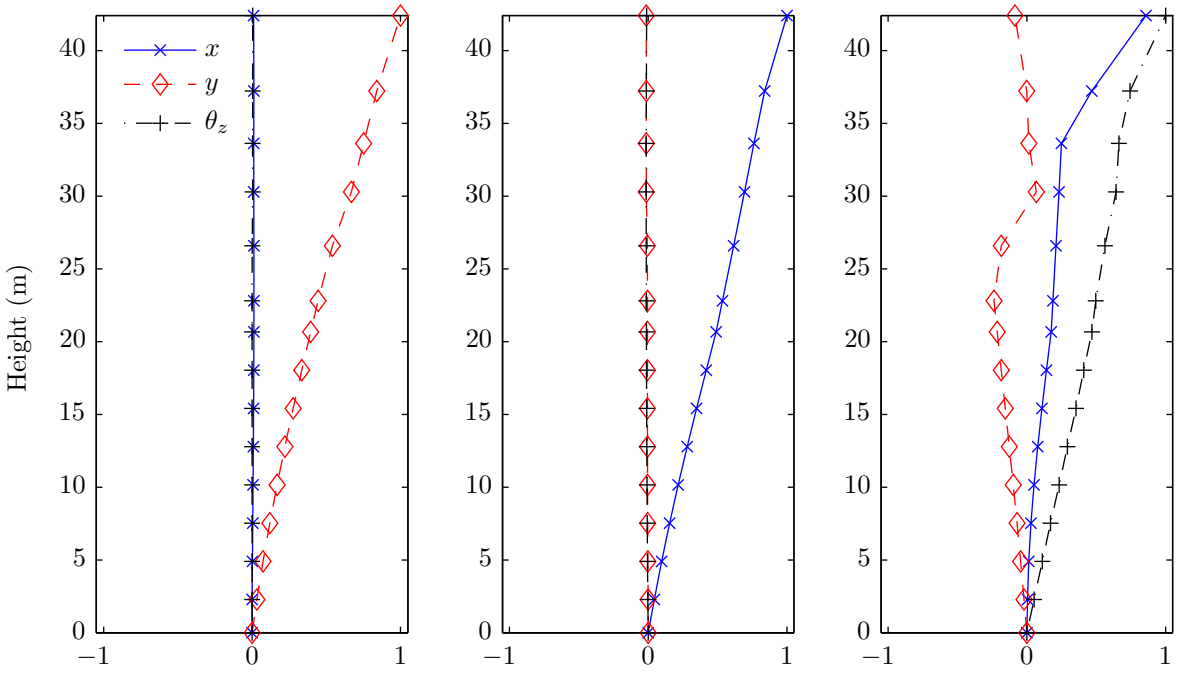

(a) $\hat{f}_{n,1} = 0.656$ Hz (b) $\hat{f}_{n,2} = 0.919$ Hz (c) $\hat{f}_{n,3} = 1.40$ Hz

Figure 7.9: Apron tower finite element model natural frequencies and mode shapes for the (a) first, (b) second, and (c) third mode of vibration.

7.2.6 Lateral mode identification results

The EKF modal identification for each lateral mode was performed by considering the response data for each direction, after transformation, separately. The y-direction (north-south) response is considered first. The first two lateral modes in the y-direction are included as parameters to be estimated (corresponding to the first and fifth mode of the overall system); however, convergence of the higher order modes was not consistent and the results are not presented. The noise covariance estimation was performed first, using the numerical model as an initial estimate of the natural frequencies and mode shapes. The

initial estimate of the damping ratio for the first mode was $\hat{\zeta}_{1,0} = 0.025$ and $\hat{\zeta}_{5,0} = 0.05$. The initial external disturbance and measurement noise covariances were selected as

$$\hat{\mathbf{S}}_0 = \texttt{diag}\left[\begin{array}{ccc} 5 \times 10^6 & 5 \times 10^7 & 5 \times 10^7 \end{array}\right] \tag{7.18}$$

and

$$\hat{\mathbf{R}}_0 = \texttt{diag}\left[\begin{array}{cccc} 1 \times 10^{-3} & 1 \times 10^{-3} & 1 \times 10^{-3} & 1 \times 10^{-2} \end{array}\right] \tag{7.19}$$

There are a total of $p = \bar{n} + 1 = 4$ measurements, where the horizontal acceleration of the auxiliary mass is measured as well as the acceleration of the roof, uppermost and third uppermost floors are included. The data is split into 20 non-overlapping windows with a total data length of 10 minutes. Each data set was resampled at 400 Hz in order to limit the effect of the approximation introduced by the discretization procedure described in Sec. 5.1.3. Following the noise covariance estimation step, the updated process and measurement noise covariance matrices were found to be

$$\hat{\mathbf{S}}_k = \texttt{diag}\left[\begin{array}{ccc} 2.67 \times 10^6 & 2.00 \times 10^7 & 3.90 \times 10^7 \end{array}\right] \tag{7.20}$$

and

$$\hat{\mathbf{R}}_k = \texttt{diag}\left[\begin{array}{cccc} 2.15 \times 10^{-5} & 7.15 \times 10^{-5} & 3.07 \times 10^{-5} & 1.65 \times 10^{-4} \end{array}\right] \tag{7.21}$$

after averaging the results for the 20 realizations of the filter. The noise covariance parameter α is given in Table 7.4, together with the COV of the parameter estimate ($\hat{c}_v$).

Table 7.4: Apron tower y-lateral mode noise covariance parameter α mean estimate and coefficient of variation.

Index	$\hat{\alpha}_i$	$\hat{c}_v$ %
$\mathbf{S}_k$		
1	0.533	58.7
2	0.401	71.3
3	0.779	79.6
$\mathbf{R}_k$		
1	0.0215	70.1
2	0.0715	24.3
3	0.0307	42.7
4	0.0165	46.2

The noise covariance estimates were then used for parameter estimation step. The initial estimate of the parameters were based on the finite element model, with the damping ratios as selected for noise covariance estimation. The initial state estimate error covariance for the states (displacement and velocities of the main and auxiliary systems) was based on the state estimation results for the noise covariance estimation filter; for the appended states (parameters), a variance of 20%, 2.5%, and 1% of the initial estimate of the natural frequencies, damping ratios, and mode shape coefficients, respectively, were selected to initialize the filter. A small amount of additive process noise covariance, equal to 1×10^{-6} times the initial state estimate error covariance for the states (displacement and velocities) was introduced to adjust the level of confidence in the model. The first mode natural frequency and damping ratio estimates as they varied with time, averaged over 20 realizations of the filter, are given in Fig. 7.10.

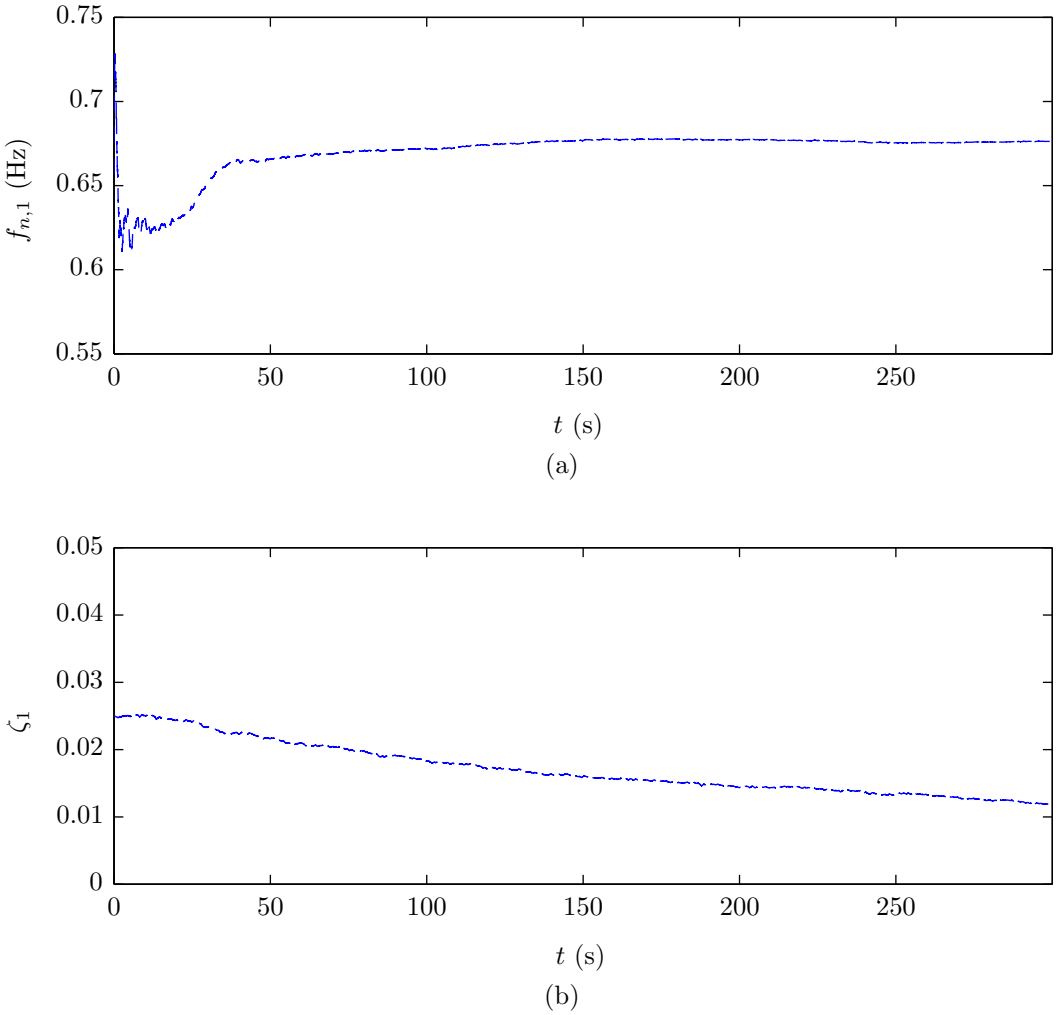

Figure 7.10: (a) Natural frequency and (b) modal damping ratio for the Apron Tower equipped with a PTMD for the first y-direction lateral mode (first mode)

The final estimate of the natural frequency is 0.676 Hz with a high level of confidence in the final estimate ($\hat{c}_v = 0.98\%$) and reasonably fast convergence. Convergence for the damping estimate was considerably slower than the natural frequency and with a lower level of confidence ($\hat{c}_v = 26.7\%$), as was the case for the numerical examples presented in Chapter 6.

The x-direction response measurements were used to determine the second mode, which corresponds to the first lateral mode in the east-west direction, following the same approach. Only two measurements of the main response of the structure were available ($\bar{n} = 2$), since the measurement at the third uppermost floor was corrupted. Therefore, $p = \bar{n} + 1 = 3$. The first two lateral modes in the x-direction (modes two and six, overall) were sought together with their modal damping ratios and mode shapes. The initial estimate of the natural frequencies and mode shapes were based on the finite element model and the initial modal damping ratios were selected as $\hat{\zeta}_{2,0} = 0.05$ and $\hat{\zeta}_{6,0} = 0.1$. The initial external disturbance and measurement noise covariances were selected as

$$\hat{\mathbf{S}}_0 = \texttt{diag}\left[\begin{array}{cc} 5 \times 10^7 & 1 \times 10^8 \end{array}\right] \tag{7.22}$$

and

$$\hat{\mathbf{R}}_0 = \texttt{diag}\left[\begin{array}{ccc} 5 \times 10^{-4} & 5 \times 10^{-4} & 5 \times 10^{-6} \end{array}\right] \tag{7.23}$$

The noise covariance estimation filter was run on each set of data. The final noise covariance matrix estimates were

$$\hat{\mathbf{S}}_k = \texttt{diag}\left[\begin{array}{cc} 1.36 \times 10^7 & 5.10 \times 10^7 \end{array}\right] \tag{7.24}$$

and

$$\hat{\mathbf{R}}_k = \texttt{diag}\left[\begin{array}{ccc} 2.68 \times 10^{-4} & 3.67 \times 10^{-4} & 2.39 \times 10^{-6} \end{array}\right] \tag{7.25}$$

The mean noise covariance parameter estimates and coefficients of variation ($\hat{c}_v$) are given in Table 7.5.

Table 7.5: Apron tower x-lateral mode noise covariance parameter α mean estimate and coefficient of variation.

Index	$\hat{\alpha}_i$	$\hat{c}_v$ %
$\mathbf{S}_k$		
1	0.255	90.9
2	0.472	66.0
$\mathbf{R}_k$		
3	0.460	98.2
4	0.061	92.5
5	0.459	32.2

Subsequently, the noise covariance estimates are used to estimate the modal parameters for the x-direction lateral mode. The natural frequency and modal damping ratio results are illustrated in Fig. 7.11 averaged over the 20 realizations of the filters. The convergence of the natural frequency is quite fast, similar to the result for the first y-direction lateral mode, with a high level of confidence in the final estimate ($\hat{c}_v = 1.01\%$). Once again, the damping estimate converges much more slowly, with less confidence in the final estimate ($\hat{c}_v = 33.8\%$).

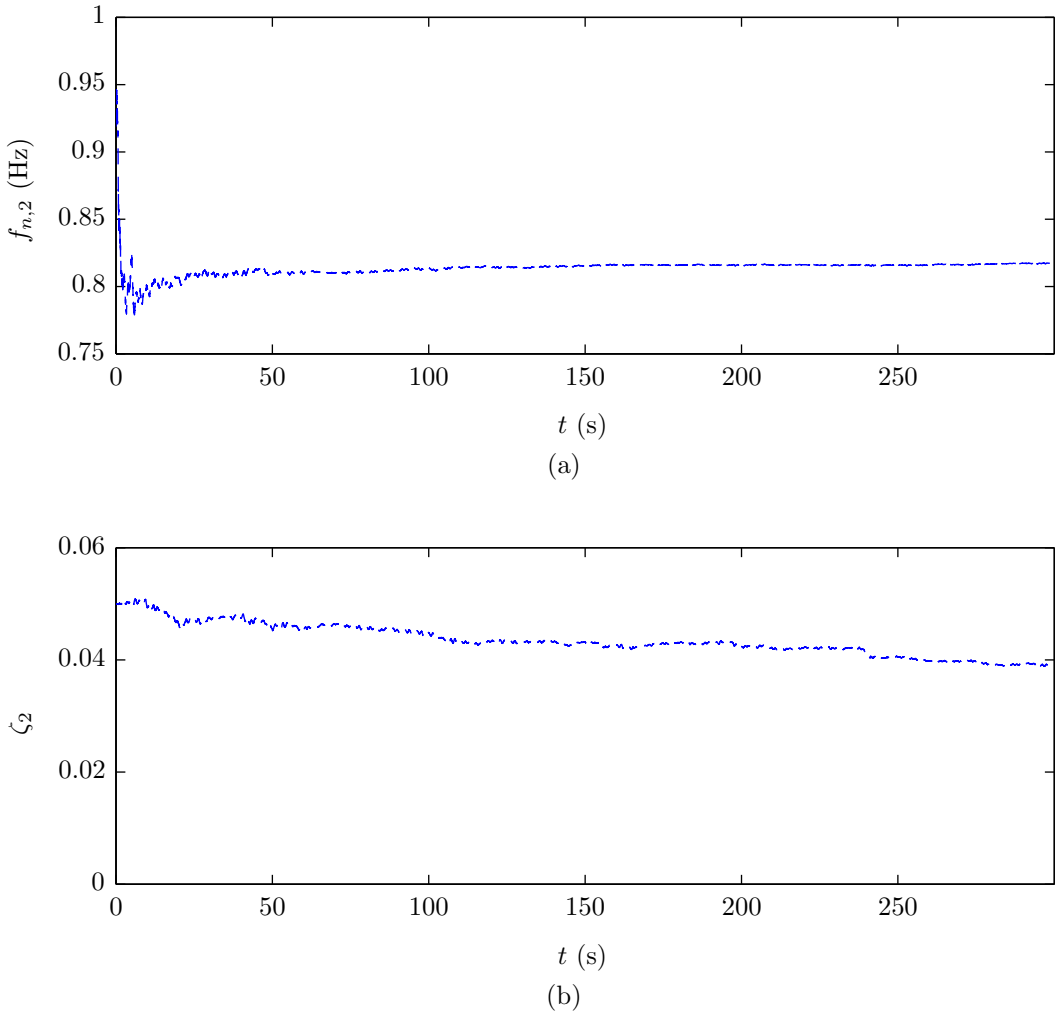

Figure 7.11: (a) Natural frequency and (b) modal damping ratio for the Apron Tower equipped with a PTMD for the first x-direction lateral mode (second mode)

7.2.7 Torsional mode identification results

For the identification of the first two torsional modes of vibration (third and fourth overall modes), the PTMDs are assumed not to impact the torsional response of the structure. Therefore, the system matrices need to be modified to no longer include the PTMD. The

displacements and velocities of the main structure are selected as states, and the modal parameters to be identified are appended. The continuous time system matrices for the reduced order system without the PTMD are

$$\mathbf{A}_c = \begin{bmatrix} \mathbf{0} & \mathbf{I} \\ -\mathbf{\Lambda}_r & -\hat{\mathbf{C}}_r \end{bmatrix} \tag{7.26a}$$

$$\mathbf{E}_c = \begin{bmatrix} \mathbf{0} \\ \mathbf{M}_{r,r}^{-1}\mathbf{\Phi}_{rr}^T \end{bmatrix} \tag{7.26b}$$

$$\mathbf{C}_c = \begin{bmatrix} -\mathbf{\Phi}_{rr}\mathbf{\Lambda}_r & -\mathbf{\Phi}_{rr}\hat{\mathbf{C}}_r \end{bmatrix} \tag{7.26c}$$

$$\mathbf{F}_c = \begin{bmatrix} \mathbf{\Phi}_{rr}\mathbf{M}_{r,r}^{-1}\mathbf{\Phi}_{rr}^T \end{bmatrix} \tag{7.26d}$$

The roof, first and third uppermost floors are measured, according to the transformation in Eq. 7.17 ($p = \bar{n} = 3$). First, the noise covariance estimation filter is run, using the following initial estimates of the process and measurement noise covariances:

$$\hat{\mathbf{S}}_0 = \mathtt{diag}\begin{bmatrix} 5\times10^7 & 5\times10^8 & 5\times10^8 \end{bmatrix} \tag{7.27}$$

and

$$\hat{\mathbf{R}}_0 = \mathtt{diag}\begin{bmatrix} 1 & 1 & 1 \end{bmatrix} \times 10^{-5} \tag{7.28}$$

The results of the noise covariance estimation are averaged over the 20 realizations of the filter and used as the noise covariances matrices for the combined state and parameter estimation filter. The final estimate of the feedthrough process noise covariance matrix is

$$\hat{\mathbf{S}}_k = \mathtt{diag}\begin{bmatrix} 6.91\times10^7 & 4.00\times10^8 & 5.29\times10^8 \end{bmatrix} \tag{7.29}$$

The final estimate for the measurement noise covariance matrix is

$$\hat{\mathbf{R}}_k = \mathtt{diag}\begin{bmatrix} 9.75\times10^{-7} & 7.04\times10^{-6} & 4.09\times10^{-6} \end{bmatrix} \tag{7.30}$$

The noise covariance parameter α mean estimate and COV are given in Table 7.6.

Table 7.6: Apron tower θ_z-torsional mode noise covariance parameter α mean estimate and coefficient of variation.

Index	$\hat{\alpha}_i$	$\hat{c}_v$ %
$\mathbf{S}_k$		
1	1.383	44.7
2	0.800	29.9
3	1.058	26.5
$\mathbf{R}_k$		
4	0.098	64.4
5	0.704	5.46
6	0.409	15.2

The initial estimates for the modal damping ratios for the torsional modes are $\hat{\zeta}_{3,0} = 0.05$ and $\hat{\zeta}_{4,0} = 0.1$. The initial estimate of the state estimation error covariance, $\mathbf{P}_{k|k}$, and the additive process noise covariance, $\mathbf{Q}_k$, are selected similar to the lateral mode identification described earlier. The results for the natural frequency and modal damping ratio for the third mode (first torsional mode) are shown in Fig. 7.12.

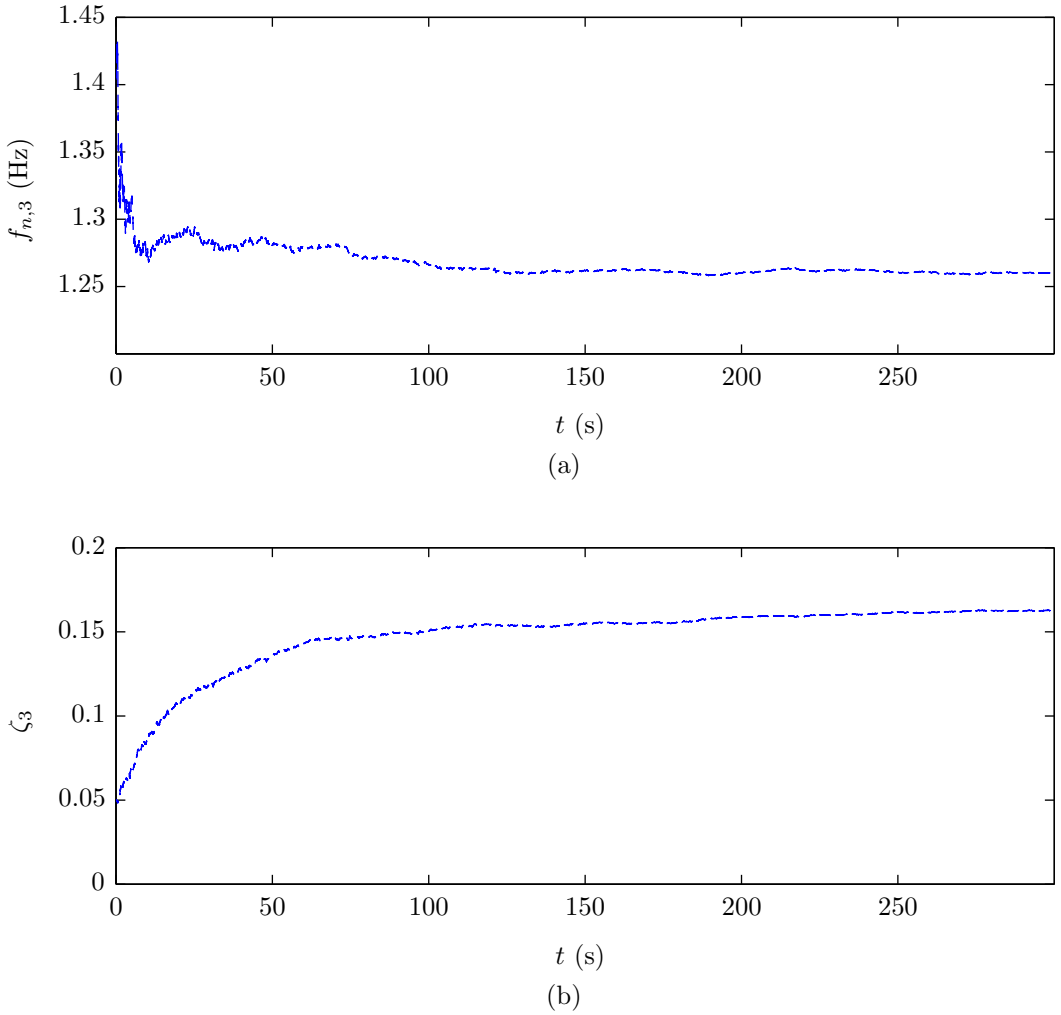

Figure 7.12: (a) Natural frequency and (b) modal damping ratio for the Apron Tower equipped with a PTMD for the first θ_z-direction torsional mode (third mode)

The convergence of the first torsional natural frequency is slower than the lateral modes, but still well before the end of the 10 minute segments; there is less confidence in the final estimate, with a COV of $\hat{c}_v = 9.85\%$. The modal damping is significantly higher than the lateral modes, but the convergence is much quicker with a considerably higher level of confidence ($\hat{c}_v = 9.87\%$).

7.3 Performance of EKF modal identification with full-scale measurement data

The final mean converged value for the natural frequency and modal damping ratio estimates as well the COV are given in Table 7.7. These results are compared with those presented by Hazra *et al* for the same structure using the modified cross-correlation method for modal identification while the PTMDs were restrained [32].

Table 7.7: Mean and coefficient of variation of the natural frequency and modal damping ratio estimates for the EKF modal identification compared with nonparameteric identification of the Apron Tower structure with the PTMDs restrained.

Mode	Natural Frequency					Modal Damping Ratio				
	Initial	Unrestrained		Restrained [32]		Initial	Unrestrained		Restrained [32]	
	$\hat{f}_{n,j,0}$	$\hat{f}_{n,j}$	$\hat{c}_v$	$\hat{f}_{n,j}$	$\hat{c}_v$	$\hat{\zeta}_{j,0}$	$\hat{\zeta}_j$	$\hat{c}_v$	$\hat{\zeta}_j$	$\hat{c}_v$
	Hz	Hz	%	Hz	%			%		%
1	0.656	0.676	0.979	0.68	1.30	0.025	0.0118	26.7	0.0084	23.0
2	0.919	0.818	1.01	0.86	3.50	0.050	0.0392	33.8	0.0198	19.0
3	1.40	1.26	9.85	1.50	1.90	0.050	0.163	9.87	0.0291	21.0

The natural frequency estimates are closely similar to those presented by Hazra *et al* for the lateral modes, for the same structure with the PTMDs restrained. The finite element model closely predicted the first mode (2.96% error); the error in the prediction of the second and third modes was 12.3% and 11.1%, respectively. There is a high level of confidence in the natural frequency estimates for the lateral modes, characterized by the small COV. There is a greater level of uncertainty in the frequency identification performance of the torsional mode ($\hat{c}_v = 9.85\%$). The modal damping ratios for the lateral modes are reasonably similar to those presented for the unrestrained PTMDs case, with a similar level of confidence in the final converged estimates. The EKF modal identification approach found a considerably higher level of damping in the torsional mode. The final mode shape coefficient estimates are plotted in Fig. 7.13 for the three modes of vibration

considered, together with the initial estimate of the mode shapes based on the finite element model output.

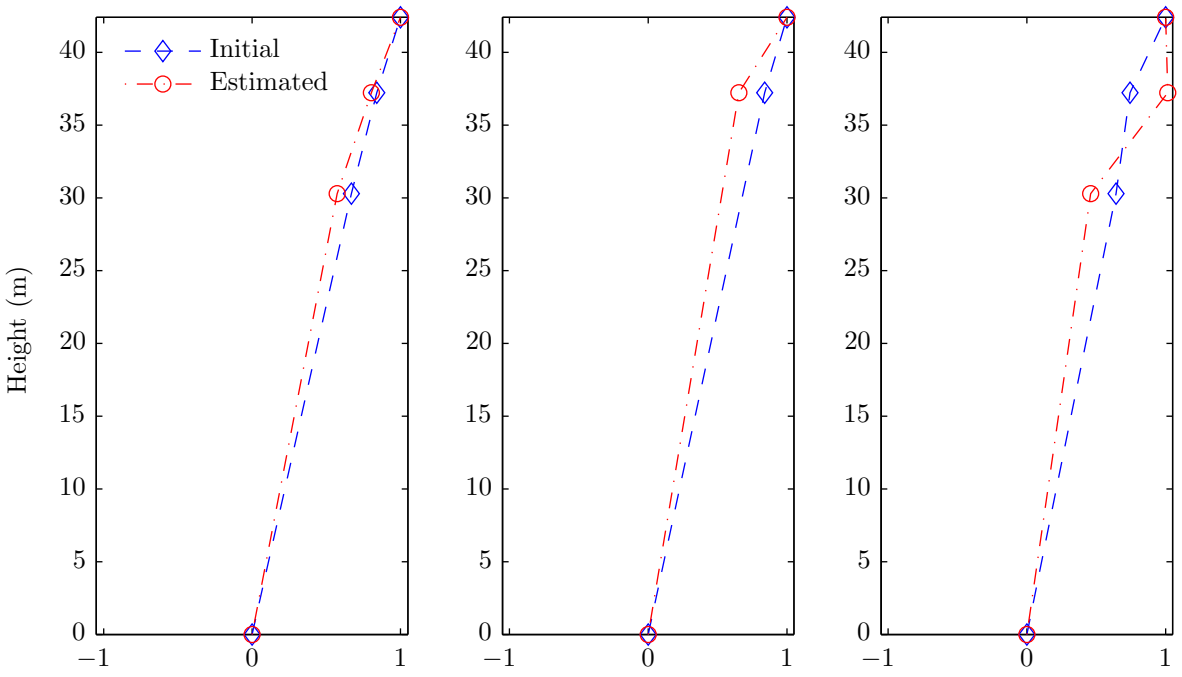

(a) $f_{n,1} = 0.676$ Hz (b) $f_{n,2} = 0.818$ Hz (c) $f_{n,3} = 1.26$ Hz

Figure 7.13: Apron tower final mean estimates of the natural frequencies and mode shapes for the (a) first, (b) second, and (c) third mode of vibration using EKF modal identification.

There are a variety of sources of error in the identification of the underlying structural modal properties for the PTMD attenuated response data from the Apron Tower.

- The presence of an auxiliary mass that does not significantly impact the mode shapes is a fundamental assumption in the development of the system of equations for the combined main and auxiliary system (Sec. 6.1). This is a reasonable assumption for relatively lightweight auxiliary masses, which are typical of TMD installations in tall

structures [26]. The Apron Tower is equipped with a large ($\mu = 12.4\%$) tuned mass in comparison to most TMDs (generally less than 2%). The response time histories for the DOFs measured were investigated and compared with the case where the PTMDs were restrained, and anecdotal evidence supports the conclusion that the large auxiliary mass has significantly impacted the mode shapes.

- The analysis has assumed that only one PTMD is present on the structure, and has lumped the mass and damping properties from the two PTMDs. Additionally, since the PTMDs on the tower are located away from the centre of rotation, it is expected that they would also attenuate the torsion response of the structure. This effect has been neglected in the analysis.

- A total of 3 hours and 20 minutes of data were collected; since approximately 10 minutes of data is required for convergence of the damping ratio estimates, this only allowed for 20 data sets to be analysed. A more meaningful analysis could have been performed with a larger data set.

- The lack of measurement data near the DOFs proximate to the maximum deflection of the second lateral modes prevented the EKF modal identification from adequately identifying the second lateral mode properties (fifth and sixth overall modes).

Despite these shortcomings, there is good performance of the identification for the first three modes. For the purpose of retuning TMDs, only the controlled mode is of interest. In the subsequent chapter, a method is presented which combines the identification results of the underlying structure's modal properties with high frequency base balance (HFBB) measurements from a boundary layer wind tunnel analysis to perform a condition assessment of the TMD. Only the first mode lateral mode in each horizontal direction as well as the first torsional mode are necessary for the HFBB method; therefore, sufficient information has been extracted using EKF modal identification to complete the condition assessment.

7.4 Condition assessment of an in-service PTMD

Little work has been published in the area of assessing the performance of full-scale in-service PTMDs [51]. The inability to accurately quantify the performance improvement for the same excitation time history is an inherent shortcoming of full-scale measurement studies of structures equipped with TMDs. It is also improbable that measurements are available for the design event with the TMD motion restrained, as gathering this data would come at the expense of occupant comfort and possibly structural damage. Generally full-scale performance of TMDs is quantified over longer periods and across various events. Therefore, much of the work in studying the ability of TMDs to attenuate wind-induced vibrations have been on numerical models excited by harmonic inputs [75] or white noise [3, 28]. Studies using synthetic wind excitation are limited [77, 105] and have demonstrated modelling wind excitation by the aforementioned conventional approaches generally overstates their performance. Therefore, there is a need to accurately compare the response of the TMD-equipped structure to the same design event. A couple studies have equipped wind tunnels models with TMDs and assessed their performance [88, 104], but there are inherent scale issues associated with that approach.

This section discusses a hybrid approach, where the bare structural properties of the actual full-scale structure identified through ambient vibration measurements (Chapters 5 and 6) are used to update the numerical model of the structure equipped with the PTMD (Chapter 3). The numerical model is excited using HFBB measurements gathered from boundary layer wind tunnel studies for a specific design event. The auxiliary damper parameters (damping coefficient and pendulum length) are readily available from field measurements, and therefore do not need to be estimated from the response data. Using equations for optimal auxiliary parameters or by a numerical search approach (Chapter 4), the optimal damper parameters for the specific application can be determined and the performance improvement can be directly quantified.

The Apron Tower at the Toronto Pearson International Airport is considered for this study. It is equipped with a pair of PTMDs and has been extensively monitored. The corresponding mass ratios in the first two lateral modes are 12.4% and 11.1% for the

auxiliary mass of 50,000 kg. In addition to the actual mass ratio, one hypothetical case of a 4,022 kg tuned mass is also selected in order to better understand the performance of lower mass ratios, corresponding to a 1.00% and 0.89% mass ratio in the two lateral modes.

7.5 Boundary layer wind tunnel study

In order to estimate the generalized forces, a scale model of the Apron Tower was built and tested in the Rowan Williams Davies and Irwin Inc. boundary layer wind tunnel facility in Guelph, Ontario, Canada. The experimental setup is shown in Fig. 7.14. The generalized forces calculated are used subsequently in the numerical simulations described in Sec. 3.6. The results of the EKF modal identification presented in Sec. 7.3 are used to update the finite element model of the Apron Tower structure. The identified natural frequencies, modal damping ratios, and mode shapes were used as inputs to the HFBB method, subsequently. The three lowest frequencies identified were 0.676 Hz, 0.818 Hz, and 1.26 Hz, and the corresponding damping ratios are 1.18%, 3.92%, and 16.3% critical (Table 7.7). The mode shapes obtained from the finite element model of the tower are fit to those coefficients identified and are used for the analysis.

Only the one-year return period event was provided to be considered for the present study. The reference wind velocity corresponding to each direction is given in Table 7.9. The 0° (also 360°) degree wind direction corresponds to a wind coming from the north. The direction proceeds clockwise, so a 90° heading is a east wind.

7.6 Comparison of the optimal PTMD parameters between various methods

To investigate which approach best predicts the optimal auxiliary parameters, $f_{r,opt}$ and $\zeta_{a,opt}$ are evaluated using the three approaches described in Chapter 4: the closed-form

Figure 7.14: High frequency base balance wind tunnel study model of Pearson International Airport Apron Tower (Courtesy Rowan Williams Davies and Irwin Inc.)

equations in Eq. 4.8 and 4.9 (closed-form) [26], the design equations in Eqs. 4.10a and 4.10b which were found using a numerical search approach of a planar PTMD excited using Gaussian white noise (planar), and the design equations in Eqs. 4.11a and 4.11b found by numerical search of the planar-spherical PTMD model, also excited using Gaussian white noise (planar-spherical). Table 7.8 shows the predicted optimal frequency ratio $f_{r,opt}$ and damping ratio $\zeta_{a,opt}$ as well as the optimal pendulum length and auxiliary damping coefficient found using Eqs. 4.12 and 4.13 for both the current in-service mass ratio of 12.4%, and the theoretical 1% mass ratio.

Table 7.8: Optimal frequency ratio, damping ratio, pendulum length, and auxiliary damping coefficient for Apron Tower from design equations for 1% and 12.4% tuned mass

Optimal Parameter		Closed-form	Planar	Planar-spherical	Measured
Parameter	Units	Eqs. 4.8/4.9	Eqs. 4.10a/4.10b	Eqs. 4.11a/4.11b	
$\mu = 1\%$					
$f_{r,opt}$		0.993	0.985	0.989	-
$\zeta_{a,opt}$		0.0498	0.0364	0.0609	-
L_{opt}	m	0.551	0.560	0.555	-
$c_{d,opt}$	N s/m	1.69×10^3	1.23×10^3	2.06×10^3	-
$\mu = 12.4\%$					
$f_{r,opt}$		0.917	0.913	0.977	0.975
$\zeta_{a,opt}$		0.169	0.178	0.204	1.075
L_{opt}	m	0.646	0.652	0.569	0.572
$c_{d,opt}$	N s/m	65.7×10^3	69.0×10^3	84.9×10^3	445.2×10^3

Each method predicts slightly varying pendulum lengths when a full-scale structure equipped with a PTMD is considered. For the 1% mass ratio, the variation is a nominal 0.9 cm. For the 12.4% mass ratio, the difference is 8.3 cm; however, this is expected to have a limited effect on the actual response since it has been demonstrated that the sensitivity to detuning is less pronounced for higher mass ratios. Due to the varying nature of the wind excitation, the performance of the PTMD will change depending on the wind direction. A numerical search was performed for each wind direction to find the optimal auxiliary parameters. The optimal pendulum length and auxiliary damping coefficient for each wind direction are presented in Table 7.9; the results are averaged and the COVs are provided. For the sake of brevity, only the critical wind direction results are considered.

Table 7.9: Apron tower optimal damper parameters found by numerical search of a model excited using HFBB

Wind direction	Reference Wind Velocity	Optimal Damper Parameters			
		$\mu = 1.00\%$		$\mu = 12.4\%$	
		L_a	c_a	L_a	c_a
	km/hr	m	$\times 10^3$ N s/m	m	$\times 10^3$ N s/m
260°	129	0.539	1.96	0.530	76.0
270°	129	0.536	2.02	0.522	73.6
280°	126	0.530	1.84	0.518	77.5
290°	122	0.540	2.05	0.520	83.7
300°	116	0.551	1.27	0.527	80.9
Mean		0.539	1.83	0.523	78.4
COV (%)		1.39	17.6	0.926	5.1

From Table 7.9, a greater variation in the damper parameters for the lower mass ratio is observed. The optimal pendulum length varies by approximately 2.1 cm for the 1% mass ratio and 1.2 cm for the 12.4% mass ratio. There is a relatively insignificant difference in the average optimal pendulum lengths between the two mass ratios (1.6 cm), which verifies the results for the optimal frequency ratio given in Fig. 4.7. The planar-spherical prediction approach best captured the negligible difference in optimal pendulum length for the two mass ratios. The actual optimal pendulum length (by numerical search using HFBB excited model) is 3% and 9% less than than the best prediction in Table 7.8, for $\mu = 1\%$ and 12.4% respectively. This is likely due to the higher damping ratio in the x-direction lateral mode; from Fig. 4.7, a higher damping ratio results in greater frequency ratio and subsequently, shorter suspended length. The parametric study assumed equal damping in each horizontal direction.

The optimal auxiliary damping coefficient varied considerably for both mass ratios, for the comparative excitation cases in Tables 7.8 and 7.9. The auxiliary damping coefficient must be selected in order to provide the best statistical performance over a variety of excitations due to the variation in performance for different events. The planar-spherical

prediction approach best predicted the optimal auxiliary damping compared to the numerical search results using the HFBB method; the optimal damping coefficient was 12% greater than the best prediction for the 1% mass ratio and 15% less for the 12.4% mass ratio. It is hypothesized that the assumption of equal lateral natural frequencies in the orthogonal directions results in an uncertain estimate of the auxiliary damping coefficients. The effect of lateral frequency ratio on the optimal parameter estimates needs to be investigated further.

To evaluate the performance of the parameter prediction methods, the responses are calculated using the HFBB approach for all three auxiliary parameter settings for each wind direction. The wind time histories for each angle are scaled to a one-year mean recurrence interval. The RMS response for each wind direction, together with the corresponding reduction when compared to the bare structural system lacking the TMD are provided. The results for the responses in the north-south (y) direction for a 1% tuned mass are provided in Table 7.10; the responses in the east-west (x) direction are provided in Table 7.11. Note that only the data for the critical wind directions (260° to 300°) are shown for the sake of brevity. The numerical search to find the optimal auxiliary parameters seeks to minimize the RMS response in both the x- and y-directions simultaneously; therefore, occasionally it may not always results in the smallest RMS response when the directions are considered separately.

Table 7.10: Roof RMS acceleration response in the y-direction and corresponding reduction for the Apron Tower equipped with a PTMD tuned to $\mu = 1\%$ for the critical wind directions

Wind direction	RMS Acceleration Response in y-direction								
	Without PTMD	With PTMD tuned using method						Optimally Tuned	
		Closed-form		Planar		Planar-spherical			
	milli-g	milli-g	%	milli-g	%	milli-g	%	milli-g	%
260°	9.80	6.23	36.4	6.43	34.4	6.25	36.2	6.19	36.8
270°	9.35	6.23	33.3	6.44	31.1	6.22	33.5	6.17	34.0
280°	9.54	6.10	36.0	6.30	33.9	6.13	35.7	6.04	36.7
290°	8.38	5.30	36.8	5.47	34.7	5.30	36.7	5.26	37.2
300°	9.24	4.72	48.9	4.67	49.5	4.82	47.8	4.66	49.5

Table 7.11: Roof RMS acceleration response in the x-direction and corresponding reduction for the Apron Tower equipped with a PTMD tuned to $\mu = 1\%$ for the critical wind directions

Wind direction	RMS Acceleration Response in x-direction								
	Without PTMD	With PTMD tuned using method						Optimally Tuned	
		Closed-form		Planar		Planar-spherical			
	milli-g	milli-g	%	milli-g	%	milli-g	%	milli-g	%
260°	4.97	4.76	4.19	4.80	3.50	4.75	4.46	4.74	4.72
270°	5.11	4.87	4.71	4.90	4.03	4.85	4.95	4.83	5.42
280°	5.08	4.89	3.75	4.93	3.04	4.87	4.07	4.85	4.45
290°	4.51	4.38	3.00	4.41	2.33	4.36	3.31	4.35	3.59
300°	4.31	4.25	1.26	4.29	0.362	4.23	1.77	4.29	0.538

From Tables 7.10 and 7.11, the 260° wind direction produces the critical response in the y-direction for the uncontrolled system. The 270° wind direction produces the critical response of the x-direction motion. The various design formulae for predicting optimal parameters produce negligible difference in the response values; this result is expected as the

optimal frequency and damping ratios do not vary considerably between the methodologies for low mass ratios. Also, the performance of each design equation is close to optimal (as determined by numerical search using the HFBB excitation).

In general, the optimal parameters obtained by the planar-spherical prediction model resulted in marginally better results for the x-direction response, when tuned to the y-direction lateral mode. Therefore, the reduced effect of the PTMD on the x-direction responses shown in Table 7.11 is expected. The performance improvement for the lateral mode orthogonal to the controlled mode is small for the 1% tuned mass; the potential for a performance degradation is possible and the RMS attenuated responses in the x-direction are approaching the same level as the attenuated y-direction. This highlights a critical weakness in a PTMD with a low auxiliary to main mass ratio when the orthogonal lateral frequencies of the primary structure are well-separated. The auxiliary damper parameters, particularly the pendulum length, are tuned to the fundamental mode and provide little improvement, and in some cases, have the potential to degrade the performance, in the other lateral direction. It is important to note that there is a potential for the critical response to switch from one direction in the uncontrolled system to the other direction in the controlled structure. Note that the optimally tuned results are found by numerical search based on a cost function of reducing the combined x- and y-direction RMS response; therefore, a greater x-direction response occurs in the 300° direction when the lateral responses are considered separately.

A means of overcoming this inherent weakness in PTMD design is to increase the mass ratio, μ. As discussed earlier, an increased mass ratio decreases the overall RMS response of the main system. Also, from Figs. 4.3 and 4.4, the sensitivity to detuning for higher mass ratios is reduced. Therefore, it is expected that the x-direction response will experience an improved RMS response when equipped with the as-constructed 12.4% tuned mass due to the reduced sensitivity to detuning, despite being PTMD is tuned to the first lateral mode in the y-direction. The north-south (y) direction roof RMS acceleration responses for the structure without the PTMD are compared with the structure equipped with a 12.4% tuned mass. Additionally, various parameters prediction approaches together with the optimal auxiliary parameters are presented in Tables 7.12. The results for the east-west

(x-) direction responses are given in Table 7.13.

Table 7.12: Roof RMS acceleration response in the y-direction and corresponding reduction for the Apron Tower equipped with a PTMD tuned to $\mu = 12.4\%$ for the critical wind directions

Wind direction	RMS Acceleration Response in y-direction								
	Without PTMD	With PTMD tuned using method						Optimally Tuned	
		Closed-form		Planar		Planar-spherical			
	milli-g	milli-g	%	milli-g	%	milli-g	%	milli-g	%
260°	9.80	3.81	61.1	3.81	61.1	3.66	62.6	3.64	62.9
270°	9.35	3.84	58.9	3.85	58.8	3.69	60.6	3.66	60.9
280°	9.54	3.78	60.3	3.79	60.3	3.61	62.1	3.58	62.5
290°	8.38	3.29	60.7	3.29	60.7	3.16	62.3	3.14	62.6
300°	9.24	2.99	67.7	2.99	67.7	2.88	68.8	2.87	68.9

Table 7.13: Roof RMS acceleration response in the x-direction and corresponding reduction for the Apron Tower equipped with a PTMD tuned to $\mu = 12.4\%$ for the critical wind directions

Wind direction	RMS Acceleration Response in x-direction								
	Without PTMD	With PTMD tuned using method						Optimally Tuned	
		Closed-form		Planar		Planar-spherical			
	milli-g	milli-g	%	milli-g	%	milli-g	%	milli-g	%
260°	4.97	3.86	22.4	3.84	22.8	3.62	27.2	3.60	27.6
270°	5.11	3.88	24.1	3.86	24.4	3.65	28.6	3.63	28.9
280°	5.08	3.89	23.3	3.87	23.7	3.63	28.5	3.57	29.8
290°	4.51	3.44	23.8	3.42	24.2	3.20	29.0	3.12	30.8
300°	4.31	3.03	29.6	3.03	29.8	2.84	34.1	2.78	35.5

For all wind directions, an increased reduction in the roof RMS acceleration response was experienced for y-direction motion when compared with the 1% tuned mass. On average this reduction was 28% in the vicinity of the critical wind directions.

There is a significant performance improvement for the 12.4% tuned mass in the x-direction when compared with the 1% tuned mass (40% reduction) in the vicinity of the critical wind directions. The performance improvement is twofold. First, PTMD performance increases with larger mass ratios. Second, the increased mass ratio results in a reduced sensitivity to detuning; therefore, a significant improvement was realized in the x-direction response despite the PTMDs being tuned to the first lateral mode in the y-direction.

As was observed for the 1% tuned mass, the evaluation of the various parameter prediction approaches finds nominal performance improvement of the planar-spherical over the closed-form prediction or planar prediction model for the y-direction response. This is of particular interest, as the different methods predict relatively different auxiliary frequency ratios ($f_{r,opt} = 0.917$ to 0.977). This underscores that increasing the mass ratio dramatically reduces the sensitivity of the system to detuning. For the x-direction responses, the planar-spherical model better predicts the optimal auxiliary parameters when compared with the 1% mass ratio, demonstrating an increasing lateral coupling effect for higher mass ratios. In conclusion, using the planar-spherical design equations offer little benefit for low mass ratio and when considering the situation of closely-spaced lateral modes or only the controlled mode for higher mass ratios. However, if a high mass ratio is being considered for the purpose of improving the performance of the structure in both horizontal directions with well separated modes, the planar-spherical design equations (Eqs. 4.11a & 4.11b) can be relied on to consistently produce better performance in the direction orthogonal to the controlled lateral mode.

7.7 Condition assessment

The performance of the combined main and auxiliary system for the in-service Apron Tower structure is of interest. Once the bare modal properties have been extracted, the numerical model is updated. The auxiliary system parameters are measured (in the case of the suspended length) or based on manufacturer's specification (for the auxiliary dampers).

The pendulum length was measured to be 0.572 m. The PTMDs each are equipped with two velocity-squared proportional damping auxiliary viscous dampers in each direction with an equivalent linear viscous damping coefficient of $c_a = 111.3 \times 10^3$ N s/m. The in-service measured auxiliary parameters are also given in Table 7.8. The frequency and damping ratios are calculated based on the identified modal properties by rearranging Eqs. 4.12 and 4.13 and using the identified circular natural frequency for the controlled mode of $\omega_n = 4.247$ rad/s.

The roof RMS acceleration responses are found by simulating the updated numerical model using the HFBB measurements for the one year return period event. The results are presented in Table 7.14 and compared the response using optimal auxiliary parameters (repeated from Tables 7.10 and 7.11). A more comprehensive condition assessment could be performed for various return period events using the same approach; however, only the one year recurrence interval data was available for the present study.

Table 7.14: Comparison with as-measured and optimal auxiliary damper parameters of the roof RMS acceleration response for the Apron Tower equipped with a $\mu = 12.4\%$ tuned mass

Wind direction	Without PTMD		As-measured				Optimal			
	x	y	x		y		x		y	
	milli-g	milli-g	milli-g	%	milli-g	%	milli-g	%	milli-g	%
260°	4.97	9.80	3.74	24.8	5.22	46.7	3.60	27.6	3.64	62.9
270°	5.11	9.35	3.83	25.1	5.14	45.1	3.63	28.9	3.66	60.9
280°	5.08	9.54	3.80	25.2	5.12	46.4	3.57	29.8	3.58	62.5
290°	4.51	8.38	3.38	25.1	4.44	47.1	3.12	30.8	3.14	62.6
300°	4.31	9.24	3.12	27.6	4.35	53.0	2.78	35.5	2.87	68.9

The results in Table 7.14 demonstrate that considerable improvement is possible by selecting more optimal auxiliary parameters; specifically, a mode reduction in the pendulum length and considerably smaller auxiliary damping coefficients. A further reduction in the RMS acceleration response of 11% and 34%, for the x- and y-directions, respectively, could

have been realized. There are three reasons why a greater than optimal auxiliary damping coefficient may have been selected.

- The auxiliary damping coefficients used for the model are based on linearized equivalent viscous dampers; for shorter return period events, the damper motion is considerably less and the as-measured value in Table 7.8 is likely overstated. A more robust analysis could be performed by modelling the velocity-squared proportional damping (see Sec. 3.5); this is beyond the scope of the present work.
- Reducing the stroke of the PTMDs is likely why a greater than optimal damping coefficient was selected. The are space constraints within the roof truss structure for locating the PTMDs, and it is often desirable to reduce the auxiliary damper motion.
- As was shown in Fig. 4.4, selecting an auxiliary damping coefficient greater than optimal has less impact on the performance than an equivalent level of suboptimal damping, particularly for high mass ratios. If there is a level of uncertainty in the main structure's modal properties, increasing the auxiliary damping coefficient will still guarantee adequate performance for the case where there are uncertain estimates of the main structure's modal properties.

7.7.1 Effective viscous damping using full-scale measurements

The effective damping introduced by the PTMD, ζ_e, is another means of quantifying TMD performance. The measure can be readily ascertained by fitting the acceleration response measurements to a single-degree-of-freedom (SDOF) system operating at the same natural frequency as the underlying structure using EKF. The advantage over the approach described in the previous step is that the result is a direct output of the filter, and further simulation of the structural response is not required.

The effective damping introduced by the PTMD is averaged over the 20 realizations and plotted in Fig. 7.15. The mean estimate is $\zeta_e = 0.0306$ with a COV of $\hat{c}_v = 18.1\%$. The identified damping ratio for the underlying structure was $\zeta_1 = 0.0118$; therefore, the

PTMDs increased the damping in the structure by $\Delta\zeta_1 = 0.0188$. The results are within the range of expected performance cited in the literature [80].

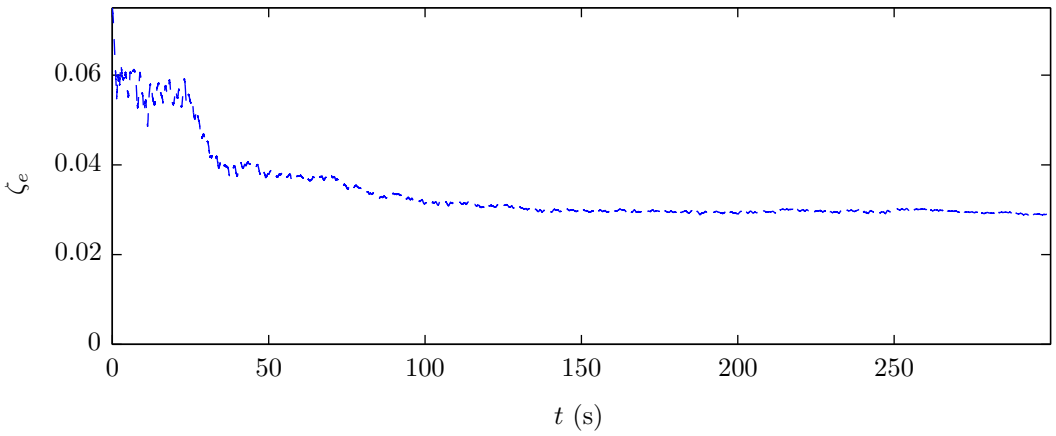

Figure 7.15: Effective viscous damping for the controlled mode of vibration for the Apron Tower

The effective damping is not an instantaneous measure; final estimation convergence occurred after approximately 150 s. There is some variation in the final converged estimate, likely due to damping widely believed to be dependent on the level and nature of the excitation. Though linear viscous damping is independent of amplitude [50], it is simply being used in this case to model an inherently more complex phenomena due to its simplicity. Therefore, this measure is only useful for quantifying the performance of the PTMDs for the particular event experienced while the data was being collected, and can be expected to vary for different return period wind events. A comprehensive condition assessment would included quantifying the effective damping as well as the response reduction when compared with the uncontrolled structure, described earlier, for a series of increasing return periods.

7.8 Comparison of planar and planar-spherical model RMS acceleration responses

The effect of using the more simplified linearize planar PTMD model for predicting optimal parameters has already been explored. Next, the ability to predict the structural responses using the model described in Chapter 3, where the coupled planar and spherical PTMD motion is included, is considered.

Table 7.15 outlines the RMS acceleration of the roof for the critical wind directions, evaluated by combining the planar PTMD (with 1.00% tuned mass) model coupled with the effective modal mass, stiffness, and damping for the main system for each mode of vibration. The input excitation is the generalized force for each mode, directly measured from the HFBB model. The RMS response of the planar model is compared with the planar-spherical HFBB model described earlier. The auxiliary damper parameters are set to their optimal values, given previously in Table 7.9.

Table 7.15: Comparison of roof RMS acceleration response predictions and corresponding reduction for the Apron Tower equipped with a PTMD tuned to $\mu = 1\%$ using a planar-spherical model and planar model for the critical wind directions

Wind direction	Without PTMD		Planar-spherical PTMD				Planar PTMD			
	x	y	x		y		x		y	
	milli-g	milli-g	milli-g	%	milli-g	%	milli-g	%	milli-g	%
260°	4.97	9.80	4.73	4.73	6.19	36.8	4.67	6.10	6.11	37.6
270°	5.11	9.35	4.83	5.42	6.17	34	4.79	6.25	6.09	34.8
280°	5.08	9.54	4.85	4.45	6.04	36.7	4.8	5.57	5.98	37.3
290°	4.51	8.38	4.35	3.59	5.26	37.2	4.27	5.33	5.19	38.0
300°	4.31	9.24	4.29	0.537	4.66	49.5	4.21	2.22	4.65	49.7

There is little discrepancy (less than 2%) in the roof RMS responses between the two methods, with the more simplistic model predicting greater reductions in RMS responses.

The results for a 12.4% mass ratio are presented in Table 7.16 for the critical wind directions.

Table 7.16: Comparison of roof RMS acceleration response predictions and corresponding reduction for the Apron Tower equipped with a PTMD tuned to $\mu = 12.4\%$ using a planar-spherical model and planar model for the critical wind directions

Wind direction	Without PTMD		Planar-spherical PTMD				Planar PTMD			
	x	y	x		y		x		y	
	milli-g	milli-g	milli-g	%	milli-g	%	milli-g	%	milli-g	%
260°	4.97	9.80	3.60	27.6	3.64	62.9	3.40	31.7	3.86	60.6
270°	5.11	9.35	3.63	28.9	3.66	60.9	3.45	32.5	3.86	58.7
280°	5.08	9.54	3.57	29.8	3.58	62.5	3.39	33.2	3.74	60.8
290°	4.51	8.38	3.12	30.8	3.14	62.6	2.99	33.8	3.26	61.1
300°	4.31	9.24	2.78	35.5	2.87	68.9	2.69	37.6	2.90	68.6

The performance of the planar model for predicting the RMS response of the structure equipped with a 12.4% tuned mass is poorer than for the 1% tuned mass, with up to 6.1% difference in RMS response predictions (5.1% unconservatively). For the larger auxiliary mass, the coupling effect of the PTMD on the main structural response is more pronounced. Though the performance for this particular example is relatively insignificant, this is an important conclusion that has implications with respect to the design of PTMDs. Specifically, for the higher modes, the acceptance threshold for occupant comfort decreases with increasing frequency within the 0-1 Hz range (ISO 6897) [56]. Hence, it is important to quantify the effect of TMD tuned to the dominant mode on higher modes, as they may not meet the performance requirements. For the case of well separated first lateral modes within the 0-1 Hz range, there may be substantial attenuation in the controlled mode (first mode) response, resulting in the first lateral mode in the orthogonal direction (second mode) dominating the response and potentially exceeding acceptable limits.

Chapter 8

Conclusions and recommendations

A comprehensive approach to performing condition assessment of in-service pendulum tuned mass dampers (PTMDs) has been undertaken in this dissertation. A general framework including online estimation algorithms and measures to perform condition assessment have been developed. Both numerical and full-scale experiments have been conducted and used to demonstrate the procedures to be employed for condition assessment of in-service PTMD equipped structures. This chapter highlights the significant contributions, key conclusions, and recommendations for future work.

8.1 Significant contributions

The present work has led to several important contributions, summarized below:

1. A broader understanding of the coupled biaxial behaviour of pendulum-type tuned mass dampers (TMDs) now exists. Specifically, increasing the mass ratio has a less significant impact on the optimal frequency ratio than what is predicted by closed-form or numerical search solutions using a linearized planar PTMD. For higher mass ratio systems, a greater optimal auxiliary damping ratio is predicted as well. This is due to the increased coupling effect for higher auxiliary masses. However, it has

been demonstrated that due to the reduced sensitivity to detuning for high auxiliary masses, selecting optimal parameters based on conventional approaches has a minor negative impact on the performance of the PTMD.

2. A time-domain parametric identification algorithm using extended Kalman filter (EKF) has been demonstrated as an effective approach for estimating the underlying structure's natural frequencies, modal damping ratios, and mode shapes while the TMD is still in service. This is a difficult undertaking, as the presence of the TMD changes the dynamic characteristics of the response. The methodology overcomes traditional manual approaches, where the TMD motion is arrested in order to perform the identification. Unlike other approaches attempted in the literature, it requires no *a priori* knowledge of the degree of detuning present in the system; the auxiliary parameters are simply measured and used within the system model. The proposed algorithm is also readily amenable to online implementation within feedback control systems.

3. Despite relatively wide use of parametric identification using Kalman filtering approaches, two issues have generally been overlooked thus far. The first issue is the presence of feedthrough of the disturbance input for the case of a main mass excited system with only acceleration response measurements available (no direct measurements of the states). The present work has accounted for this by treating the noise processes present in the measurement equations as correlated to those present in the transition equations, and adapted the Kalman filter equations to eliminate this correlation using a one-step predictor gain matrix. This was subsequently extended for the application of combined state and parameter estimation, an inherently nonlinear problem addressed by EKF. The second issue is that most applications of Kalman filtering for structural system identification have assumed knowledge of the noise covariance matrices and known inputs. In the current research, this issue has been systematically addressed by introducing a noise covariance estimation step; by setting the covariance matrices as a linear combination of a set of parameters, the covariance of the residual sequence is linear in the same set of parameters. This has

been exploited by measuring the actual correlation of the residual sequence and using a weighted least-squares fit to estimate these parameters, and subsequently the noise covariance matrices.

4. The concept of effective damping due to the presence of a TMD has not received widespread application to condition assessment of in-service TMDs, since its theoretical calculation requires *a priori* knowledge of the structure's natural frequency (without the TMD) and the ability to measure or accurately estimate the root mean squared (RMS) displacement response. Applying a similar approach to fit the acceleration response measurements to a single-degree-of-freedom (SDOF) system operating at the same frequency of the main bare structure (estimated using EKF modal identification), the effective damping parameter is appended to the state vector and estimated. This method was demonstrated to produce reliable results based on numerical simulations and verified using PTMD attenuated acceleration ambient response measurements.

5. A comprehensive framework to undertake condition assessment has been presented. The methodology integrates the modal parameter data obtained from measurements into an assessment framework that enables one to arrive at conclusions regarding the condition of the in-service PTMD.

8.2 Conclusions

Having highlighted the significant findings of the present work, the primary conclusions are summarized below.

1. Key conclusions from the parametric study of the three-dimensional model are as follows. The effect of detuning was considered for various levels of frequency and damping detuning. It was found that errors of 15% in the initial mass and stiffness estimates of the bare structure could result in nearly 30% reduced frequency response performance of the system. For auxiliary damping detuning, using a greater

than optimal auxiliary damping was less detrimental to the performance than a corresponding level of suboptimal damping. Studies into the effect of the mass ratio confirmed the findings of other researchers that a heavier auxiliary mass not only improved the TMD performance, but also reduced the sensitivity of the system to detuning.

2. The design formulae generally corresponded to the ones available in the literatures for low mass ratios. For optimal frequency ratio, a reduced sensitivity to increasing mass ratio was observed; conventional closed-form solutions or those designs based on numerical search (necessary for the case of main-mass damping) of linearized planar models predicted considerably lower optimal frequency ratios for higher mass ratios. The optimal auxiliary damping predicted by the proposed model was higher than the closed-form case, with greater disparity as the mass ratio increased.

3. The effect of predicting the responses using the simplified planar PTMD model were considered. It was found that there was little prediction error in the responses for low mass ratios. For the higher mass ratio considered, the coupling effect of the PTMD became more substantial. In some cases, the planar model unconservatively predicted better performance than the more accurate planar-spherical auxiliary system model. For higher mass ratios, there is a potential that the lateral response orthogonal to the controlled response becomes the dominant response; therefore, it has been concluded that it is important to quantify the effect the PTMD may have on higher-order modes, particularly in ensuring comfort criteria are met.

4. The EKF proved to be an effective means of identifying the underlying structure's modal properties from PTMD attenuated acceleration response measurements. The presence of feedthrough of the disturbance noise in the measurement equation was accounted for by modifying the Kalman filter equations to first eliminate the correlation between the process and measurement equations. For the application of wind excitation, the input is modelled as an unknown disturbance noise with unknown noise covariance matrix. The natural frequency estimates were precise and converged quickly. It was noted that these are of primary interest for the purpose

of retuning TMDs, particularly for the controlled mode. The damping estimation was deemed adequate for the application of selecting TMD parameters and condition assessment. Convergence of damping estimates was considerably slower, and estimating the damping ratio for the controlled mode proved to be more difficult. For the case where the PTMD was detuned, the damping estimate for the controlled mode was improved. The mode shape estimation also demonstrated good performance, particularly for lower order modes.

5. The correlation method presented for estimating the noise covariance matrices demonstrated outstanding performance for the case where the model parameters were known. For the more practical case of unknown model parameters, an initial estimate of the model parameter was used instead. This lead to an increase in the error for the noise covariance estimation step, but resulted in no noticeable performance degradation in the final parameter estimates.

6. The EKF can readily be applied to the problem of estimating the effective damping of the PTMD, unencumbered by the lack of availability of displacement response measurements. The natural frequency of the controlled mode is simultaneously estimated using EKF modal identification. The investigation on the numerical model produced results similar to the theoretical values. The methodology was confirmed to produce realistic results for the measured data from the full-scale structure considered.

7. The online estimation algorithm demonstrated excellent performance in terms of the parameter estimates from the PTMD contaminated response measurements for the bench-scale laboratory model, when compared to estimating the modal parameters using Blind Source Separation (BSS) with the adaptive passive tuned mass damper (APTMD) apparatus removed.

8. The EKF modal identification approach was demonstrated using full-scale response measurements from the Apron Tower at Toronto Pearson International Airport. The results were similar to other published findings for the same structure; in that case, the motion of the PTMD had to be restrained for the identification to proceed.

8.3 Recommendations for future work

There are several possible extensions of the present work to enhance the understanding and assessing the performance of PTMDs.

1. The numerical aspect of this work can be extended through more parameteric studies. For example, design equations for a wider range of orthogonal lateral frequency ratios can be developed.

2. The EKF has been considered for the present work, due to its classic application to nonlinear Kalman estimation and numerous successful implementations, including structural system identification. A key step in applying EKF is determining the Jacobian matrices of partial derivatives of the nonlinear transition and measurement equations, with respect to the state or stochastic input variable, evaluated at the current state estimate. This proved to be an onerous task and prone to human error. The unscented Kalman filter (UKF) is an improvement over the EKF, where the unscented transform is used to select a minimum number of sample points about the mean, which are subsequently propagated through the nonlinear transition equation, from which the statistics are measured [85]. This circumvents the need to linearize the equations for the sake of propagating the covariance matrices to the next time step, and eliminates the error introduced by the linearization process. It has been demonstrated that the UKF results in an improved performance for structural system identification [102], though not substantially, since nonlinearities introduced by appending the parameters are not considerable. It is worth noting that the primary contribution of the present work was not in applying the EKF, but rather in developing an approach to estimate the underlying structural properties, addressing the issues of feedthrough process noise in the measurement equation, and estimating the statistics of the unknown input and measurement noises. Aside from the aforementioned difference between the filtering methods, the remaining equations proceed similarly, and the issues of unknown noise statistics and feedthrough disturbance remain.

3. It was established that the EKF modal identification approach was fundamentally based on the assumption that the mode shape vectors were not significantly impacted by the presence of the auxiliary mass. This is true for low auxiliary mass systems; however, reasonable performance was demonstrated for the full-scale structure with a 12.4% tuned mass. Further analysis considering large mass ratios would shed more light on this issue.

4. The identification algorithms can be used to develop a prototype APTMD or semi-active tuned mass damper (STMD). This can be achieved through little or no modification to the estimation algorithm developed in this thesis and through the choice of proper control hardware.

APPENDICES

Appendix A

Auxiliary system described in Cartesian coordinates

Selecting the suspension point of the auxiliary mass as the origin of the system (as before), and defining three new quantities, $u_a(t)$, $v_a(t)$, and $w_a(t)$ as the distance of the auxiliary mass away from its at-rest position in the x-, y-, and z-directions. The position of the auxiliary mass is then

$$\mathbf{r}(t) = \left\{ \begin{array}{c} u(t) + u_a(t) \\ v(t) + v_a(t) \\ w(t) - L + w_a(t) \end{array} \right\} \tag{A.1}$$

The velocity of the auxiliary mass is

$$\mathbf{v}(t) = \left\{ \begin{array}{c} \dot{u}(t) + \dot{u}_a(t) \\ \dot{v}(t) + \dot{v}_a(t) \\ \dot{w}(t) + \dot{w}_a(t) \end{array} \right\} \tag{A.2}$$

The relative motion of the attachment point, a distance h_x or h_y along the pendulum

length L is given by (assuming the auxiliary damper and spring remain horizontal)

$$r_{p,x} = \frac{h_x}{L} u_a(t) \tag{A.3a}$$

$$r_{p,y} = \frac{h_y}{L} v_a(t) \tag{A.3b}$$

The relative velocity of the attachment point is

$$v_{p,x} = \frac{h_x}{L} \dot{u}_a(t) \tag{A.4a}$$

$$v_{p,y} = \frac{h_y}{L} \dot{v}_a(t) \tag{A.4b}$$

The kinetic energy of the auxiliary mass, dropping the (t) notation for convenience, is

$$\begin{aligned} \mathcal{T}_a = \frac{1}{2} \mathbf{v} m_a \mathbf{v}^T &= \frac{1}{2} m_a \left(\dot{u} + \dot{u}_a\right)^2 + \left(\dot{v} + \dot{v}_a\right)^2 + \left(\dot{w} + \dot{w}_a\right)^2 \\ &= \frac{1}{2} m_a \left(\dot{u}^2 + 2\dot{u}\dot{u}_a + \dot{u}_a^2 + \dot{v}^2 + 2\dot{v}\dot{v}_a + \dot{v}_a^2 + \dot{w}^2 + 2\dot{w}\dot{w}_a + \dot{w}_a^2\right) \end{aligned} \tag{A.5}$$

The potential energy of the auxiliary mass is

$$\begin{aligned} \mathcal{V}_a &= m_a g \left(w - L + w_a\right) + \frac{1}{2} k_x r_{p,x}^2 + \frac{1}{2} k_y r_{p,y}^2 \\ &= m_a g \left(w - L + w_a\right) + \frac{1}{2} \frac{k_x h_x^2}{L^2} u_a^2 + \frac{1}{2} \frac{k_y h y^2}{L^2} v_a^2 \end{aligned} \tag{A.6}$$

The Raleigh dissipation function for the auxiliary mass is

$$\begin{aligned} \mathcal{F}_a &= \frac{1}{2} c_x v_{p,x}^2 + \frac{1}{2} c_y v_{p,y}^2 \\ &= \frac{1}{2} \frac{c_x h_x^2}{L^2} \dot{u}_a^2 + \frac{1}{2} \frac{c_y h_y^2}{L^2} \dot{v}_a^2 \end{aligned} \tag{A.7}$$

The kinetic energy, potential (strain) energy, and Raleigh dissipation function for the main structure are given in Eqs. 3.20, 3.21, and 3.22.

To reduce the dimensionality of the problem, a relationship is developed to relate w_a in terms of u_a, v_a, and the pendulum length L.

$$\begin{aligned} L^2 &= u_a^2 + v_a^2 + (L - w_a)^2 \\ &= u_a^2 + v_a^2 + L^2 - 2Lw_a + w_a^2 \end{aligned} \tag{A.8}$$

Solving the quadratic in terms of w_a,

$$w_a = L - \sqrt{L^2 - u_a^2 - v_a^2} \tag{A.9}$$

It follows that

$$w_a^2 = 2L^2 - 2L\sqrt{L^2 - u_a^2 - v_a^2} - u_a^2 - v_a^2 \tag{A.10}$$

The first derivative of w_a with respect to time is

$$\dot{w}_a = \frac{u_a\dot{u}_a + v_a\dot{v}_a}{\sqrt{L^2 - u_a^2 - v_a^2}} \tag{A.11}$$

and

$$\dot{w}_a^2 = \frac{u_a^2\dot{u}_a^2 + 2u_a\dot{u}_a v_a\dot{v}_a + v_a^2\dot{v}_a^2}{L^2 - u_a^2 - v_a^2} \tag{A.12}$$

The second time derivative is

$$\begin{aligned} \ddot{w}_a = &\frac{u_a\ddot{u}_a}{\sqrt{L^2 - u_a^2 - v_a^2}} + \frac{v_a\ddot{v}_a}{\sqrt{L^2 - u_a^2 - v_a^2}} + \frac{\dot{u}_a^2}{\sqrt{L^2 - u_a^2 - v_a^2}} + \frac{\dot{v}_a^2}{\sqrt{L^2 - u_a^2 - v_a^2}} \\ &+ \frac{u_a^2\dot{u}_a^2}{(L^2 - u_a^2 - v_a^2)^{\frac{3}{2}}} + \frac{2u_a\dot{u}_a v_a\dot{v}_a}{(L^2 - u_a^2 - v_a^2)^{\frac{3}{2}}} + \frac{v_a^2\dot{v}_a^2}{(L^2 - u_a^2 - v_a^2)^{\frac{3}{2}}} \end{aligned} \tag{A.13}$$

The kinetic energy of the auxiliary mass (Eq. A.5) becomes

$$\begin{aligned} \mathcal{T}_a = \frac{1}{2}m_a \Bigg(&\dot{u}^2 + 2\dot{u}\dot{u}_a + \dot{u}_a^2 + \dot{v}^2 + 2\dot{v}\dot{v}_a + \dot{v}_a^2 + \dot{w}^2 + 2\dot{w}\frac{u_a\dot{u}_a + v_a\dot{v}_a}{\sqrt{L^2 - u_a^2 - v_a^2}} \\ &+ \frac{u_a^2\dot{u}_a^2 + 2u_a\dot{u}_a v_a\dot{v}_a + v_a^2\dot{v}_a^2}{L^2 - u_a^2 - v_a^2} \Bigg) \end{aligned} \tag{A.14}$$

The potential energy of the auxiliary mass (Eq. A.6) becomes

$$\mathcal{V}_a = m_a g\left(w - \sqrt{L^2 - u_a^2 - v_a^2}\right) + \frac{1}{2}\frac{k_x h_x^2}{L^2}u_a^2 + \frac{1}{2}\frac{k_y h y^2}{L^2}v_a^2 \tag{A.15}$$

The kinetic energy, potential energy, and dissipation function for the combined system are given in Eqs. 3.8 and 3.17. Lagrange's equation is given by Eq. 3.23. The generalized displacements of the system are selected as u, v, w, $\mathbf{\Delta}$, u_a, and v_a and the generalized velocities are $\dot{u}$, $\dot{v}$, $\dot{w}$, $\dot{\mathbf{\Delta}}$, $\dot{u}_a$, and $\dot{v}_a$. The generalized forces are $\mathbf{Q} = \begin{bmatrix} P_u & P_v & P_w & \mathbf{P}_r & 0 & 0 \end{bmatrix}$.

The equations of motion are

$$\begin{aligned}\left[\mathbf{M} + \begin{bmatrix} m_a & 0 & 0 & \mathbf{0} \\ 0 & m_a & 0 & \mathbf{0} \\ 0 & 0 & m_a & \mathbf{0} \\ \mathbf{0} & \mathbf{0} & \mathbf{0} & \mathbf{0} \end{bmatrix}\right]\begin{Bmatrix} \ddot{u} \\ \ddot{v} \\ \ddot{w} \\ \ddot{\mathbf{\Delta}}_r \end{Bmatrix} + \mathbf{C}\begin{Bmatrix} \dot{u} \\ \dot{v} \\ \dot{w} \\ \dot{\mathbf{\Delta}}_r \end{Bmatrix} + \mathbf{K}\begin{Bmatrix} u \\ v \\ w \\ \mathbf{\Delta}_r \end{Bmatrix} \\ = \begin{Bmatrix} -m_a\ddot{u}_a \\ -m_a\ddot{v}_a \\ -m_a\left(\ddot{w}_a + g\right) \\ 0 \end{Bmatrix} + \begin{Bmatrix} P_u \\ P_v \\ P_w \\ \mathbf{P}_r \end{Bmatrix}\end{aligned} \tag{A.16}$$

where $\ddot{w}_a$ is given in Eq. A.13. The remaining equations of motion corresponding to the auxiliary degree-of-freedom (DOF) are

$$0 = m_a\left(\ddot{u} + \ddot{u}_a\right) + m_a u_a \Lambda_a + k_x\frac{h_x^2}{L^2}u_a + c_x\frac{h_x^2}{L^2}\dot{u}_a \tag{A.17a}$$

$$0 = m_a\left(\ddot{v} + \ddot{v}_a\right) + m_a v_a \Lambda_a + k_y\frac{h_y^2}{L^2}v_a + c_y\frac{h_x^2}{L^2}\dot{v}_a \tag{A.17b}$$

where

$$\Lambda_a = \frac{\ddot{w} + g}{\sqrt{L^2 - u_a^2 - v_a^2}} + \frac{\dot{u}_a^2 + \dot{v}_a^2}{L^2 - u_a^2 - v_a^2} + \frac{u_a\ddot{u}_a + v_a\ddot{v}_a}{L^2 - u_a^2 - v_a^2} + \frac{\left(u_a\dot{u}_a + v_a\dot{v}_a\right)^2}{\left(L^2 - u_a^2 - v_a^2\right)^2} \tag{A.18}$$

References

[1] M. Abe and Y. Fujino. Dynamic characterization of multiple tuned mass dampers and some design formulas. *Earthquake Engineering and Structural Dynamics*, 23:813–835, 1994.

[2] B.D.O. Anderson and J.B. Moore. *Optimal Filtering*. Dover Books on Engineering. Dover Publications, 2005.

[3] S. V. Bakre and R. S. Jangid. Optimum parameters of tuned mass damper for damped main system. *Structural Control and Health Monitoring*, 14(3):448–470, 2007.

[4] P. R. Bélanger. Estimation of noise covariance matrices for a linear time-varying stochastic process. *Automatica*, 10(3):267–275, 1974.

[5] Compute/Calcul Canada. Shared Hierarchical Academic Research Computing Network (SHARCNET), 2012.

[6] G. Chen and Q. Chen. *Approximate Kalman Filtering*. Series in approximations and decompositions. World Scientific, 1993.

[7] G. Chen and J. Wu. Experimental study on multiple tuned mass dampers to reduce seismic responses of a three-storey building structure. *Earthquake Engineering and Structural Dynamics*, 32(5):793–810, 2003.

[8] X. Chen and A. Kareem. Coupled dynamic analysis and equivalent static wind loads on buildings with three-dimensional modes. *Journal of Structural Engineering*, 131(7):1071–1082, 2005.

[9] M. Chey, J. G. Chase, J. B. Mander, and A. J. Carr. Semi-active tuned mass damper building systems: Application. *Earthquake Engineeringand Structural Dynamics*, 39(1):69–89, 2010.

[10] M. Chey, J. G. Chase, J. B. Mander, and A. J. Carr. Semi-active tuned mass damper building systems: Design. *Earthquake Engineering and Structural Dynamics*, 39(2):119–139, 2010.

[11] C. Chin, A.H. Nayfeh, and E. Abdel-Rahman. Nonlinear dynamics of a boom crane. *Journal of Vibration and Control*, 7:199–220, 2001.

[12] A. K. Chopra. *Dynamics of Structures: Theory and Applications to Earthquake Engineering*. Prentice Hall, Englewood Cliffs, N.J., 1995.

[13] A. J. Clark. Multiple passive tuned mass damper for reducing earthquake induced building motion. In *Proceeding of the 9th World Conference on Earthquake Engineering*, volume 5, pages 779–784, 1998.

[14] Computers and Structures Inc. SAP2000, Vers. 11.0.8, 2008.

[15] S.H. Crandall and W.D. Mark. *Random Vibration in Mechanical Systems*. Academic Press, 1963.

[16] M De Angelis, S Perno, and A Reggio. Dynamic response and optimal design of structures with large mass ratio TMD. *Earthquake Engineering and Structural Dynamics*, 41(1):41–60, 2012.

[17] R.A. DeCarlo. *Linear systems: a state variable approach with numerical implementation*. Prentice Hall, 1989.

[18] D. B. den Hartog. *Mechanical Vibrations*. McGraw-Hill, New York, 4th edition, 1956.

[19] G.A. Einicke and L.B. White. Robust extended kalman filtering. *IEEE Transactions on Signal Processing*, 47(9):2596–2599, 1999.

[20] K. C. Falcon, B. J. Stone, W. D. Simcock, and C. Andrew. Optimization of vibration absorbers: a graphical method for us on idealized systems with restricted damping. *Journal of Engineering Mechanics*, 9:374–381, 1967.

[21] M. Q. Feng and A. Mita. Vibration control of tall buildings using mega subconfiguration. *Journal of Engineering Mechanics*, 121(10):1082–1088, 1995.

[22] H. Frahm. Device for damping vibrations of bodies, 1909.

[23] M. I. Friswell. *Finite Element Model Updating in Structural Dynamics*. 1995.

[24] M. I. Friswell. The convergence of the iterated IRS method. *Journal of Sound and Vibration*, 211(1):123, 1998.

[25] R. R. Gerges and B. J. Vickery. Parametric experimental study of wire rope spring tuned mass dampers. *Journal of Wind Engineering and Industrial Aerodynamics*, 91(12-15):1363–1385, 2003.

[26] R. R. Gerges and B. J. Vickery. Optimum design of pendulum-type tuned mass dampers. *The Structural Design of Tall and Special Buildings*, 14(4):353–368, 2005.

[27] R. Ghanem and M. Shinozuka. Structural-system identification. I: Theory. *Journal of Engineering Mechanics*, 121(2):255–264, 1995.

[28] A. Ghosh and B. Basu. A closed-form optimal tuning criterion for TMD in damped structures. *Structural Control and Health Monitoring*, 14(4):681–692, 2007.

[29] T. Hasket, B. Breukelman, J. Robinson, and J. Kottelenburg. Tuned mass dampers under excessive structural excitation. In *Response of Structures to Extreme Loading*, pages 37–43, August 2003.

[30] B. Hazra, A. Sadhu, R. Lourenco, and S. Narasimhan. Re-tuning tuned mass dampers using ambient vibration measurements. *Smart Materials and Structures*, 19(11):115002, 2010.

[31] B. Hazra, A. Sadhu, A. J. Roffel, and S. Narasimhan. Hybrid time-frequency blind source separation towards ambient system identification of structures. *Computer-Aided Civil and Infrastructure Engineering*, 27(5):314–332, 2012.

[32] B. Hazra, A. Sadhu, A. J. Roffel, P. E. Paquet, and S. Narasimhan. Underdetermined blind identification of structures by using the modified cross-correlation method. *Journal of Engineering Mechanics*, 138(4):327–337, 2012.

[33] N. Hoang and P. Warnitchai. Design of multiple tuned mass dampers by using a numerical optimizer. *Earthquake Engineering and Structural Dynamics*, 34(2):125–144, 2004.

[34] J. D. Holmes. Mode shape corrections for dynamic response to wind. *Engineering Structures*, 9(3):210–212, 198707 1987.

[35] J. D. Holmes. Listing of installations. *Engineering Structures*, 17(9):676–678, 1995.

[36] M. Hoshiya and E. Saito. Structural identification by extended Kalman filter. *Journal of Engineering Mechanics*, 110(12):1757–1770, 1984.

[37] D. Hrovat, P. Barak, and M. Rabins. Semi-active versus passive or active tuned mass dampers for structural control. *Journal of Engineering Mechanics*, 109(3):691–705, 1983.

[38] J. Hwang, A. Kareem, and H. Kim. Wind load identification using wind tunnel test data by inverse analysis. *Journal of Wind Engineering and Industrial Aerodynamics*, 99(1):18 – 26, 2011.

[39] J. Hwang, A. Kareem, and W. Kim. Estimation of modal loads using structural response. *Journal of Sound and Vibration*, 326(3-5):522–539, 2009.

[40] The MathWorks Inc. Matlab, Vers. 7.14.0.739 (R2012a), 2012.

[41] T. Ioi and K. Ikeda. On the dynamic vibration damped absorber of the vibration system. *Japanses Society of Mechanical Engineering Bulletin*, 21:64–71, January 1978.

[42] P. A. Irwin and B. Breukelman. Recent applications of damping systems for wind response. In *Proceedings of the 6th World Congress of the Council on Tall Buildings and Urban Habitat*, 2001.

[43] N. Isyumov, F. Knoll, J. Mardukhi, and D. P. Morrish. Cn tower–revisit of antenna performance under wind action. In *Proceedings of the 3rd Structural Specialty Conference of the Canadian Society of Civil Engineers*, pages 311–319. CSCE, 2000.

[44] F. Ju, Y. S. Choo, and F. S. Cui. Dynamic response of tower crane induced by the pendulum motion of the payload. *International Journal of Solids and Structures*, 43(2):376–389, 2006.

[45] R. E. Kalman. A new approach to linear filtering and prediction problems. *Transactions of the ASME Journal of Basic Engineering*, 82(Series D):35–45, 1960.

[46] E. W. Kamen and J. Su. *Introduction to optimal estimation*. Springer, 1999.

[47] N. Kang, H. Kim, S. Choi, S. Jo, J. Hwang, and E. Yu. Performance evaluation of TMD under typhoon using system identification and inverse wind load estimation. *Computer-Aided Civil and Infrastructure Engineering*, 2012.

[48] A. Kareem. Mitigation of wind induced motion of tall buildings. *Journal of Wind Engineering and Industrial Aerodynamics*, 11:273, 1983.

[49] A. Kareem. Dynamic response of high-rise buildings to stochastic wind loads. *Journal of Wind Engineering and Industrial Aerodynamics*, 42(1-3):1101–1112, 1992.

[50] A. Kareem and K. Gurley. Damping in structures: its evaluation and treatment of uncertainty. *Journal of Wind Engineering and Industrial Aerodynamics*, 59(2-3):131–157, 1996.

[51] A. Kareem and T. Kijewski. Mitigation of motions of tall buildings with specific examples of recent applications. *Wind and Structures*, 2(3):201–252, 1999.

[52] A. Kareem and S. Kline. Performance of multiple mass dampers under random loading,. *Journal of Structural Engineering*, 121(2):348–361, 1995.

[53] C. G. Koh and L. M. See. Identification and uncertainty estimation of structural parameters. *Journal of Engineering Mechanics*, 120(6):1219–1236, 1994.

[54] K. C. S. Kwok and P. A. Macdonald. Full-scale measurements of wind-induced acceleration response of Sydney Tower. *Engineering Structures*, 12(3):153–162, July 1990.

[55] K. C. S. Kwok and B. Samali. Performance of tuned mass dampers under wind loads. *Engineering Structures*, 17(9):655–667, 1995.

[56] K.C.S. Kwok, P. A. Hitchcock, and M. D. Burton. Perception of vibration and occupant comfort in wind-excited tall buildings. *Journal of Wind Engineering and Industrial Aerodynamics*, 97(7–8):368–380, 2009.

[57] K.M. Lam and A. Li. Mode shape correction for wind-induced dynamic responses of tall buildings using time-domain computation and wind tunnel tests. *Journal of Sound and Vibration*, 322(4-5):740–755, 2009.

[58] C. L. Lee, Y. T. Chen, L. L. Chung, and Y. P. Wang. Optimal design theories and applications of tuned mass dampers. *Engineering Structures*, 28(1):43–53, 2006.

[59] C. C. Lin, J. F. Wang, and J. M. Ueng. Vibration control identification of seismically excited m.d.o.f. structure-ptmd systems. *Engineering Structures*, 240(1):87–115, 2001.

[60] J. Lin, R. Betti, A. W. Smyth, and R. W. Longman. On-line identification of non-linear hysteretic structural systems using a variable trace approach. *Earthquake Engineering and Structural Dynamics*, 30(9):1279–1303, 2001.

[61] J. Lin and Y. Zhang. Nonlinear structural identification using extended Kalman filter. *Computers and Structures*, 52(4):757–764, 1994.

[62] C. Loh and I. Tou. A system identification approach to the detection of changes in both linear and non-linear structural parameters. *Earthquake Engineering and Structural Dynamics*, 24(1):85–97, 1995.

[63] Chin-Hsiung Loh and Yuan-Huei Tsaur. Time domain estimation of structural parameters. *Engineering Structures*, 10(2):95–105, 1988.

[64] E. Lourens, E. Reynders, G. De Roeck, G. Degrande, and G. Lombaert. An augmented Kalman filter for force identification in structural dynamics. *Mechanical Systems and Signal Processing*, 27(0):446–460, 2012.

[65] Giuseppe Carlo Marano, Rita Greco, and Bernardino Chiaia. A comparison between different optimization criteria for tuned mass dampers design. *Journal of Sound and Vibration*, 329(23):4880–4890, 2010.

[66] R.J. McNamara. Tuned mass dampers for buildings. *ASCE Journal of Structural Division*, 103(9):1785–1798, 1977.

[67] R. Mehra. Approaches to adaptive filtering. *IEEE Transactions on Automatic Control*, 17(5):693–698, oct 1972.

[68] L. Meirovitch. *Methods of Analytical Dynamics*. McGraw-Hill, New York, 1970.

[69] S. Nagarajaiah. Adaptive passive, semiactive, smart tuned mass dampers: identification and control using empirical mode decomposition, hilbert transform, and short-term fourier transform. *Structural Control and Health Monitoring*, 16(7-8):800–841, 2009.

[70] S. Nagarajaiah and N. Varadarajan. Semi-active control of wind excited building with variable stiffness tmd using short-time fourier transform. *Journal of Engineering Structures*, 27:431–441, 2005.

[71] J. O'Callahan, P. Avitabile, and R. Riemer. System equivalent reduction expansion process (serep). Univ. Lowell, USA; Society for Experimental Mechanics (SEM); Union College Schenectady (UCS), 30 Jan - 2 Feb, 1989.

[72] J. Ormondroyd and J. P. den Hartog. The theory of the dynamic vibration absorber. *Transactions of the American Society of Mechanical Engineers*, 50(A):9–22, 1928.

[73] G. Pekcan, J. B. Mander, and S. S. Chen. Fundamental considerations for the design of non-linear viscous dampers. *Earthquake Engineering and Structural Dynamics*, 28(11):1405–1425, 1999.

[74] T. Pinkaew and Y. Fujino. Effectiveness of semi-active tuned mass dampers under harmonic excitation. *Engineering Structures*, 23(7):850–856, 2001.

[75] R. Rana and T. T. Soong. Parametric study and simplified design of tuned mass dampers. *Engineering Structures*, 20(3):193–204, 1998.

[76] Karl Johan Åström and Björn Wittenmark. *Adaptive Control*. Addison-Wesley Longman Publishing Co., Inc., Boston, MA, USA, 2nd edition, 1994.

[77] F. Ricciardelli, A. Occhiuzzi, and P. Clemente. Semi-active tuned mass damper control strategy for wind-excited structures. *Journal of Wind Engineering and Industrial Aerodynamics*, 88(1):57–74, 2000.

[78] A. J. Roffel, R. Lourenco, S. Narasimhan, and S. Yarusevych. Adaptive compensation for detuning in pendulum tuned mass dampers. *Journal of Structural Engineering*, 137(2):242–251, 2011.

[79] A. J. Roffel, S. Narasimhan, and T. Haskett. Performance of pendulum tuned mass dampers in reducing the response of flexible structure. Under review in *ASCE Journal of Structural Engineering*, 2012.

[80] M. P. Sacks and J. C. Swallow. Tuned mass dampers for towers and buildings. In *Proceedings of the Symposium on Structural Engineering in Natural Hazards Mitigation*, pages 640–645, 1993.

[81] A. Sadhu, B. Hazra, S. Narasimhan, and M. D. Pandey. Decentralized modal identification using sparse blind source separation. *Smart Materials and Structures*, 20(12):125009, 2011.

[82] I. B. Schwartz, Y. K. Wood, and I. T. Georgiou. Extreme parametric uncertainty and instant chaos in coupled structural dynamics. *Computer Physics Communications*, 121-122:425–428, 1999.

[83] M. Setareh. Application of semi-active tuned mass dampers to base-excited systems. *Earthquake Engineering & Structural Dynamics*, 30(3):449–462, 2001.

[84] M. Shinozuka and R. Ghanem. Structural system identification. II: Experimental verification. *Journal of Engineering Mechanics*, 121(2):265–273, 1995.

[85] Dan Simon. *Optimal State Estimation: Kalman, H_∞, and Nonlinear Approaches*. Wiley & Sons, August 2006.

[86] A. W. Smyth, S. F. Masri, A. G. Chassiakos, and T. K. Caughey. On-line parametric identification of MDOF nonlinear hysteretic systems. *Journal of Engineering Mechanics*, 125(2):133–142, 1999.

[87] J. Q. Sun, M. R. Jolly, and M. A. Norris. Passive, adaptive and active tuned vibration absorbers—a survey. *Journal of Vibration and Acoustics*, 117(B):234–242, 1995.

[88] H. Tanaka and C. Y. Mak. Effect of tuned mass dampers on wind induced response of tall buildings. *Journal of Wind Engineering and Industrial Aerodynamics*, 14(1-3):357–368, 12 1983.

[89] A. G. Thompson. Optimum tuning and damping of a dynamic vibration absorber applied to a force excited and damped primary system. *Journal of Sound and Vibration*, 77(3):403–415, 1981.

[90] Z. Tian, J. Qian, and L. Zhang. Slide roof system for dynamic response reduction. *Earthquake Engineering and Structural Dynamics*, 37(4):647–658, 2008.

[91] T. Tschanz and A. G. Davenport. The base balance technique for the determination of dynamic wind loads. *Journal of Wind Engineering and Industrial Aerodynamics*, 13(1-3):429–439, 1983.

[92] K. T. Tse, P. A. Hitchcock, and K. C. S. Kwok. Mode shape linearization for HFBB analysis of wind-excited complex tall buildings. *Engineering Structures*, 31:675–685, 2009.

[93] B. J. Vickery, N. Isyumov, and A. G. Davenport. The role of damping, mass and stiffness in the reduction of wind effects on structures. *Journal of Wind Engineering and Industrial Aerodynamics*, 11(3):285–294, 1983.

[94] B.J. Vickery and A.G. Davenport. *An Investigation of the Behaviour in Wind of the Proposed Centrepoint Tower in Sydney, Australia*. Engineering science research report. University of Western Ontario, Faculty of Engineering Science, 1971.

[95] D. Wang and A. Haldar. System identification with limited observations and without input. *Journal of Engineering Mechanics*, 123(5):504–511, 1997.

[96] G. B. Warburton. Optimal absorber parameters for various cobinations of response and excitation parameters. *Earthquake Engineering and Structural Dynamics*, 10(3):381–401, 1982.

[97] G. B. Warburton and E. O. Ayorinde. Optimum absorber parameters for simple systems. *Earthquake Engineering and Structural Dynamics*, 8(3):197–217, 1980.

[98] P. Watts. On a method of reducing the rolling of ships at sea. *Transactions of International of Naval Architects*, 34:90–165, 1883.

[99] B. Weber and G. Feltrin. Assessment of long-term behavior of tuned mass dampers by system identification. *Engineering Structures*, 32(11):3670 – 3682, 2010.

[100] G. Welch and G. Bishop. An introduction to the Kalman filter. *IEEE Transactions on Reliability*, 2001.

[101] K. B. Wiesner. Tuned mass dampers to reduce building wind motion. In *ASCE Convention and Exposition*, April 1979.

[102] M Wu and A. W. Smyth. Application of the unscented Kalman filter for real-time nonlinear structural system identification. *Structural Control and Health Monitoring*, 14(7):971–990, 2007.

[103] Kangming Xu and Takeru Igusa. Dynamic characteristics of multiple substructures with closely spaced frequencies. *Earthquake Engineering and Structural Dynamics*, 21(12):1059–1070, 1992.

[104] Y. L. Xu and K. C. S. Kwok. Semianalytical method for parametric study of tuned mass dampers. *Journal of Structural Engineering*, 120(3):747–764, 1994.

[105] Y.L. Xu, K.C.S. Kwok, and B. Samali. The effect of tuned mass dampers and liquid dampers on cross-wind response of tall/slender structures. *Journal of Wind Engineering and Industrial Aerodynamics*, 40(1):33–54, 1992.

[106] J. N. Yang, S. Lin, H. Huang, and L. Zhou. An adaptive extended Kalman filter for structural damage identification. *Structural Control and Health Monitoring*, 13(4):849–867, 2006.

[107] J. N. Yang, S. Lin, and L. Zhou. Identification of parametric changes for civil engineering structures using an adaptive Kalman filter. *Smart Structures and Materials 2004: Sensors and Smart Structures Technologies for Civil, Mechanical, and Aerospace Systems*, 5391(1):389–399, 2004.

[108] D. Y. N. Yip and R. G. J. Flay. A new force balance data analysis method for wind response predictions of tall buildings. *Journal of Wind Engineering and Industrial Aerodynamics*, 54-55:457–471, 1995.

[109] H. Zhang, G. C. Foliente, Y. Yang, and F. Ma. Parameter identification of inelastic structures under dynamic loads. *Earthquake Engineering & Structural Dynamics*, 31(5):1113–1130, 2002.

[110] Y. Zhou, A. Kareem, and M. Gu. Mode shape corrections for wind load effects. *Journal of Engineering Mechanics*, 128(1):15–23, 2002.

[111] M. Ziyaeifar and H. Noguchi. Partial mass isolation in tall buildings. *Earthquake Engineering and Structural Dynamics*, 27(1):49–65, 1998.